SEISMOTECTONICS OF ACTIVE FAULTS: MAGADI FAULT SYSTEM, SOUTHERN KENYA RIFT

Zacharia Njuguna Kuria

Examining committee:

prof.dr. V.G. Jetten	University of Twente, Faculty ITC
prof.dr.ir. A. Stein	University of Twente, Faculty ITC
prof.dr. J.O. Barongo	University of Nairobi, Dept. of Geology
prof.dr. J.D. van Wees	Free University Amsterdam, Earth Sciences
dr. D. Delvaux	Royal Museum for Central Africa

ITC dissertation number 194
ITC, P.O. Box 217, 7500 AE Enschede, The Netherlands

ISBN 978-90-6164-315-9
Cover designed by Benno Masselink
Printed by ITC Printing Department

SEISMOTECTONICS OF ACTIVE FAULTS: MAGADI FAULT SYSTEM, SOUTHERN KENYA RIFT

DISSERTATION

to obtain
the degree of doctor at the University of Twente,
on the authority of the Rector Magnificus,
prof.dr. H. Brinksma,
on account of the decision of the graduation committee,
to be publicly defended
on Thursday 29 September 2011 at 14.45 hrs

by

Zacharia Njuguna Kuria

born on 12 February 1971

in Nakuru, Kenya

This thesis is approved by
Prof. dr. Freek van der Meer, Promotor
Dr. Tsehaie Woldai, assistant promotor

Acknowledgements

A decade ago I was conferred MSc degree, I considered acknowledgement to be a very important part of my MSc Thesis, a notion I still hold to-date. During my PhD studies, I reckon with certainty that it is a real-training exercise in communication and expression, with unrelenting patience and consistency and perhaps most outstandingly hard work, focus and ardent commitment. Whereas I humbly accept responsibility for the work and time leading to this thesis, the contribution of many others who helped me will certainly lead to another dissertation like this one: they taught me “what is good science” and motivated me to do my best by trusting that I was able. To this end, I am deeply humbled.

Meeting Dr. Woldai (Tsehaie) during a training workshop at Regional Centre for Mapping of Resources in Kenya was whole mark turn in my scientific research and career. We discussed about my research interest – on active faults - subsequent to which application for scholarship ensued. In the end, I was accepted at ITC graduate school. Working with you has been a pleasure. Tsehaie, I am deeply indebted to you and I will always be. At department of Earth System Analysis, I met Prof. van der Meer (Freek), whose intuitive approach to science was most obvious from our first encounter. Freek, apart from the role you have played as my Promoter, I consider myself very lucky to have experienced a glimpse of your instinctive approach, creative style and effortless enthusiasm to science - a virtue attested by a total of 10 certificates and wards meticulously displayed in your back office. I admired them secretly, as I sat strategically, during our many meetings – in a nutshell they motivated me. It was a great pleasure and honour to work with you – thanks for your time, encouraging emails during my time in Kenya and most importantly the visit you paid to me in Kenya. Apart from delivering a very interesting lecture “Journey from Australia to Mars”, your countless words of support utterly encouraged and motivated me. I am indeed very thankful.

My sincere thanks goes to Vice Chancellor, University of Nairobi (UoN) Prof. Mogaha for not only approving my sandwich program between ITC and UoN but also providing “off-duty times” to study at ITC, without which this thesis would not have been completed. In the same token, I appreciate the role played by the Principal College of Biological Sciences Prof. Irungu and Director Board of Post graduate studies Prof. Kamau for their support and advice. For Prof. Mathu, Chairman Department of Geology (by then) – apart from setting the firm foundation on structural geology – he discussed every bit of my progress and as a friend, he untiringly encouraged and motivated me. “Thank you, Prof. Mathu”. Prof. Ngecu, you played a key role (that I needed most) during application for fellowship with ITC, that requires no

trumpeting, but that does not delimit my sincere appreciation. The passionate concern you had about my progress and eagerness to see me graduate was a big motivation. “I am indeed very grateful, Prof. Ngecu”. My heart felt gratitude goes to Dr. Nyamai – current Chairman, Dept. of Geology – for smooth administrative and optimal scheduling of my studies (when to teach and when to do research). Prof. Barongo – you natured me as a young geophysicist overlooking my defects and embracing my success during MSc. In my PhD research you helped me shape my line of thought, with many encouraging words. From you, I have learnt how a combination of friendly face and role model can be effective in passing knowledge to young upcoming scientists. “Thanks, Prof. Barongo”. Every member of staff at the Department of Geology has played a key and unique role in my PhD research. I salute Prof. Nyambok, Prof. Odada, Prof. Opiyo-Akech, Dr. Ichang’i, Dr. Olago, Dr. Mboya, Dr. Gichaba, Mr. Mulwa, Mrs. Kianji including all the technical staffs and secretaries for diverse and invaluable support you all accorded me. “I am indeed very grateful to you all”.

I want to recognize the invaluable support from Geothermal Development Company (GDC) through the generous support of Dr. Simiyu (Managing Director and Chief Executive officer) for financing the fieldwork in terms of equipment (MT set, TEM) camping gear, transport and a hardworking team of technicians: Mr. Waswa, Mr. Basweti, Mr. Omondi and Mr. Mukiri. Not forgetting Mr. Wambugu and Mr. Muturia for overwhelming support during the field. Certainly, Chapter 7 (this thesis) is a product of your (GDC) support. I am indeed very grateful. Dr. Macharia (Director, KARI) you supported me with Land-rover and hardworking driver (Njuguna). I am indeed very grateful for this support.

I am most grateful to Dr. Ibs-von Seht (Malte) from Hannover, Germany for providing me with raw seismograms for Magadi area and catalogues for larger Kenya seismic network. Dr. Sally Barrit you provided me with aeromagnetic data from GETECH, which has made a huge contribution in my research. I am very grateful.

Back at ITC, my sincere thanks goes to Prof. Hale (Martin) and Ms. Loes Colenbrander for utmost administration of the research project. Loes, thanks for being very patient with me particularly, when I presented last minute changes on schedule and you accommodated me unwittingly. I am greatly indebted to Dr van Dijk (Paul), who apart from playing key role in administration – having taken over from Martin - became a warm friend with time. Your humility is outstanding – a virtue that I learnt to embrace – I treasure the moments we read the bible and prayed together, God bless you

abundantly. Thanks Christie Agema for organizing my meetings and communication. I also acknowledge the contributions of staff from ESA Department for your valuable contributions during my presentations. ITC IT Department - “helpdesk” – am grateful for your support, in Particular, I salute Aiko Mulder for sarscape and geosoft – software management. I also acknowledge the contribution and support from Education Affairs department: Marie Chantal Metz, Theresa van den Boogard and Bettine Geerdink. The staff at the library department played a key role: delivering the required research papers and books, even from outside ITC library, fairly fast. In particular, my many thanks goes to Carla Gerritsen, Marga Koelen and Petry Maas-Prijs. I acknowledge Marjolein Woerlee and the warm staff of ITC Hotel for organizing my accommodation for times spent in Enschede.

During my stay at ITC, I made numerous friends, in particular other PhD candidates. It is well appreciated that I cannot exhaust the list but am indeed grateful to you all for the times we spent encouraging each and sharing common problems. However, I cannot fail to mention those we shared office: Fekerte, Abel, Mariela, Byron, Khamarrul, Sharon, Xuanmei, Roberta, and by extension Andre, Tolga and Dr. Kuriakose (Sekhar). I recognize the contribution of Kenyan PhD counterparts Dr. Ngene, Jeniffer, Jane, Vincent, Francis and Leonard, it was a pleasure to spend time together. In the same token, I thank all the Kenyan students (MSc, PM, Dipl) of my PhD tenure for being very encouraging and supportive.

I want to recognize with appreciation the MSc students from ITC that I worked with in my research: Kodikara (Sri Lanka), Woldu (Eriteria) and Akinola (Nigeria). We started research as strangers but ended up as good friends. Our fieldworks were a whole time of learning from each other: Having your theses online attest to the good science we did together. I am indeed grateful for all the time we spent learning together.

To my parents: “Although, I have not been a student in your classrooms, you will always be my most treasured teachers of life”. Together with all my family members and my in-laws, uncles and aunties you all deserve my sincere gratitude for you prayers, invaluable support and encouragement. To my family: Lilian (my wife), Lewis (son) and Mercy (daughter), thanks for being patient during my long stay out of the country. Your Love inspired me every day. In particular, am grateful Lilian for finding time to review my thesis chapters, discussions on various aspects of my project and allowing me peaceful work time - Given chance I won’t ask God for more than you are.

Lilian, Lewis, Mercy this (thesis) is the begging…..

Table of Contents

CHAPTER 1

INTRODUCTION

1.1 Research background

Characteristically, the earth surface has continental-scale rifts. These rift domains are long narrow features, predominantly asymmetrical, bounded by normal faults whose vertical displacement in a range of several kilometres results into deep rift valleys (Scholz and Contreras, 1998). Rio Grande in USA, the European Cenozoic rift system, the East African rift system and Baikal rift in Russia are examples of continental scale rift systems (Keller et al., 1991, Morgan et al., 1986, Olsen et al., 1987, Déverchère et al., 2001). Whereas these rifts are lopsided, common feature of half graben rifts, they manifest common geometrical features i.e. width and segmentation along axis that is characteristic of their region (Scholz and Contreras, 1998).

Attempts to understand initiation and evolution of the continental rift zones ascribe thermo-mechanical properties of the continental lithosphere as controlling factor to topographic relief and ultimately rift architecture (Ebinger et al., 2002). In this respect, short narrow basins with narrow uplifted flanks form young, hot, weak lithosphere with less than 15 km thick seismogenic layer. On the other hand long, wide deep basins with broad uplifted flanks result into old, cold, strong continental lithosphere with seismogenic layer thickness greater than 30 km (Ebinger et al., 2002).Whereas this approach is feasible in providing framework for fault arrays within the basin, it is limiting in identification of key processes and parameterization of individual seismogenic source. However, reliable generic classification of rifts into passive and active zones gives cognizance to tectonic processes therein: Asthenospheric upwelling in active rifts and regional based extensional forces in passive rifts are identified as driving mechanisms of the rifting process (Keller et al., 1991, Morgan, 1983, Rogers, 1993). To make the distinction even more clearer Sengor and Burke (1978) noted that prior to rifting in active rift domal uplift and volcanism mark initial phase and vice versa for passive rift, an opinion shared later by Condie (1997).

Southern Kenya rift – sinuous system consisting of a combination of normal-asymmetric grabens and monoclinally flexed depressions (Baker and Wohlenberg, 1971, Baker et al., 1972b) – is focal point of this research. It forms part of the eastern branch of the continental scale East African Rift System (EARS) series of rift zones stretching more than 3,000 Kilometres (Figure 1-1). This eastern branch stretches from Afar triple junction and straddles through Ethiopia, whilst the western branch circumvents Lake Victoria thorough Uganda, Rwanda, Burundi, Tanzania, Malawi and terminates further south into Mozambique (Chorowicz, 2005). The East African Plateau is a characteristic feature of elevated relief lying between

eastern and western rift branches and on which Lake Victoria is located (Bechtel et al., 1987). The central part of Kenya Rift (i.e. 2°N to 2°S) lies the Kenya Dome (~300 – 400 km wide topographic high) superimposed on the fringe of the plateau, an area where the rift has markedly uplifted shoulders (Baker and Wohlenberg, 1971).

The evolution of the Kenya Rift System dates back to the East African orogeny, a product of Neoproterozoic orogenesis (Stern, 1994) involving accressionary and amalgamation of east and west Gondwana (Shackleton, 1986, Shackleton, 1993, Shackleton, 1996, Stern, 1994). Among other belts, the Proterozoic Mozambique Belt is a part of this orogeny. The western margin of Mozambique Belt in southern Kenya and Northern Tanzania is bordered by Archean Tanzania Craton, a boundary along which Cenozoic rifting and magmatism evolved (Bosworth, 1987, Stern, 1994) to form part of Kenya Rift. However, the presence of crystalline rocks on both the western and eastern part of the rift (Simiyu and Keller, 2001) complicates the precise localization of the boundary between Mozambique Belt and Tanzania Craton. All in all, Chorowicz (2005) noted that the ancient tectonic patterns along which rifting kinematics was localised - a result of divergent movement - marked lines of pre-existing lithospheric weakness.

To further refine the evolution of the Kenya Rift, several models have been proposed ranging from extension of the lithosphere by pure shear (Baker and Wohlenberg, 1971), through extension by simple shear (Bosworth, 1987) to diapiric upwelling of an asthenolith (Mohr, 1987). The current geophysical data support the active model of rifting and indicate the presence of an asthenospheric diapir or plume beneath the central part of the Kenya Rift and at the base of the lithosphere which is undergoing a pure shear extension. Seismic refraction images (Green et al., 1991) show small-degree melts rising from the plume to the base of the crust as consequence of the thermal weakening of the overlying lithosphere. seismic tomography data (Anderson et al., 1992), crustal thickness variations (KRISP Working Group Party, 1991) and Moho topography (Pointing and Maguire, 1990) point to the underplating of ultramafic and mafic accumulations at the crust-mantle boundary.

The characteristic feature of these enormous previous research works is that they have focused on deep earth subsurface processes (lithospheric) that have contributed immensely to the understanding of the long term evolution of the rift basins and the related dynamic processes. Once this generalized regional framework and evolution have been better understood, investigations need to progressively focus on the recent manifestation of rifting at rift basin scale. Central to this discussion, the Kenya Rift comprises

of a series discrete internal drainage basins currently occupied by rift floor lakes i.e. Turkana, Baringo, Bogoria, Nakuru, Naivasha and Magadi and seismicity along the rift floor is variable (Hollnack and Stangl, 1998). In addition, these basins are segmented by intra-continental shear zones (Chorowicz, 2005). These evidences of both earth surface and subsurface processes, among others, support discretization of basins and parameterisation of the seismogenic sources and their driving mechanism, possibly due to heterogeneity of the crust. This change of approach from regional to discrete rift- basin scale using integrated techniques (structural geology, remote sensing, active and passive geophysical surveys) is the philosophy advanced in this research.

1.2 Problem statement

The East African Rift System has been subjected to a lot of detailed geological and geophysical investigations since its first discovery in 19th century (Suess, 1891). Despite the enormous detailed studies on crustal structure and tectonic evolution of the basins within the rift there are still key issues that have not been adequately addressed, namely;

a) Little detailed investigations have been done to understand localized active rifting process manifested in some places by earthquake swarm activities. So far, emphasis on the research work has been on the rift system as a whole. This has resulted in gap in geoscientific knowledge on the rifting process and its implication on earthquake hazard particularly for Lakes Magadi-Natron area (Figure 1-1); where the rift is terminated by the stable Tanzania Craton and also flanked by the Aswa transform faults.

b) Unresolved extensional direction in southern Kenya Rift and lack of manifestation of north-south deformational style deduced for the entire East Africa rift system.

c) Undefined spatial patterns and progress of natural hazards related to active faulting for Magadi-Natron area, particularly earthquakes.

d) Unmapped thermal regimes as possible driving mechanisms of the rifting process.

A brief description of the problems outlined above is provided in the follow section.

a) Insufficient detailed investigations at active deformation zones (active faults) within the Kenya rift

The discovery and subsequent research works along the East Africa Rift System began as early as 19th century. Since then the Kenya rift has been subjected to a lot of detailed investigations ranging from geological (Smith, 1931, McCall, 1957, Baker, 1958, Baker, 1963); intra-continental rifting (from perspective of the global tectonics) (Searle, 1970, Baker and Wohlenberg, 1971, Baker et al., 1971b, Fairhead and Girdler, 1972); rifting evolution (Bosworth, 1985, Mougenot et al., 1986, Strecker et al., 1990, Kampunzu and Mohr, 1991, KRISP Working Group Party, 1991); seismic reflection profiling (Morley et al., 1992) to seismological studies (Tobin et al., 1969, Shah, 1986, Maguire, 1988, Young et al., 1989, Tongue et al., 1992, Ibs-von Seht et al., 2001, Kianji, 2003).

The characteristic feature of these enormous previous research works is that they have focused on deep earth subsurface processes that have contributed immensely to the understanding of the long term evolution of the rift basins and the related dynamic processes. Once this general framework and evolution have been better understood, investigations need to progressively focus on the recent manifestation of rifting including the Holocene and the present ones. These studies on seismotectonics, which are part of this research project, are expected to establish and describe the active faults in this region. This will be the first step towards understanding the intertwinement of active faults and earthquakes in the realm of earthquake hazard for the Southern Kenya Rift (Lake Magadi-Natron area). It is on this premise that this research work has been proposed.

The choice for Lake Magadi-Natron area for detailed study was made because rifting process is in progress as marked by a cluster of earthquakes epicentre locations on the north eastern edge of this lake (Ibs-von Seht et al., 2001). In addition, rifting process at Magadi - Natron area is unique because its southward propagation is inhibited by Tanzania Craton and to the north the area is flanked by Aswa Nandi Loita shear zone. All these geological features affect adversely the orientation and size characteristics of the fracture and faults in this area. To advance the basic knowledge of rifting in a continental tectonic set-up was the motivation of this study.

b) Unresolved extensional direction in southern Kenya rift and lack of manifestation of north-south deformational style deduced for the entire East Africa Rift System

The East Africa Rift System is recognized as representing the incipient stages of continental break up and rifting (Fairhead and Stuart, 1982). The age of the rift initiation as well as of volcanism suggest north-south rift propagation (Baker, 1986, Smith, 1994). However, seismotectonic studies and seismicity of Magadi area indicated a cluster of earthquakes to the north east of Lake Magadi (Ibs-von Seht et al., 2001) whereas the neotectonic joints are located to the east of the Lake (Atmaoui and Hollnack, 2003). The question then is what is the trend of the crustal deformational for Magadi area?

In addition, focal mechanism solutions were determined for the northern and central parts of the Kenya Rift (Doser and Yarwood, 1991, Strecker and Bosworth, 1991) where they showed the occurrence of normal-, strike-slip and oblique-slip faulting. Strecker and Bosworth (1991) carried out structural studies in the central part of the rift and inferred a clockwise change in stress field. The extension direction interpreted to have been oriented ENE-WSW during Miocene, later rotated to E-W in early Pleistocene then to NW-SE during late Quaternary times (Bosworth et al., 1992). But later morphostructural studies on this central part of Kenya Rift do not confirm the existence of the NW-SE rotation of the extension direction (Grimaud et al., 1994). More recent structural studies at Magadi area support the Strecker and Bosworth (1991) and Bosworth et al. (1992) clockwise rotation of the extension direction (Atmaoui and Hollnack, 2003) but also proposed further collection of field data especially from Quaternary lake and fluvial sediments found along the axial rift zone to assess with confidence the recent rotation of extension direction in the southern part of the Kenya Rift. The understanding of the present stress fields will help us to infer the future trends and relate them to possible spatial distribution of the hazards (i.e. earthquakes).

c) Undefined spatial patterns and progress of natural hazards related to active faulting for Magadi-Natron area, particularly earthquakes.

Earthquake seismology has played an important role in developing the concept of plate tectonics, an overarching theory that describes the dynamics of the Earth's outer shell (Lay and Wallace, 1995). The release of strain energy of seismic events is restricted to regions where there is an inhomogeneous stress environment and where material is sufficiently strong for brittle failure (Scholz, 1990). In this respect, studies of micro-earthquakes have shown that the rift floor is seismically active (Young et al., 1991, Hollnack and Stangl, 1998, Ibs-von Seht et al., 2001). Most of the energy is released through micro-earthquakes with maximum depth about 12 km. The area south of Lake Magadi, on the other hand, is a diffuse region of

splay faults that developed as the southern end of the Kenyan Rift encountered the stable Tanzanian Craton. Dominant faults trend NE-SW and NW-SE. In this part, there is a significant increase in seismic activity that also spread out over a much wider area with focal depth range of 0 - 40 km (Rykounov et al., 1972, Bungum and Nnko, 1984, Nyblade et al., 1996). Such a depth range could suggest a thick and strong crust that can accommodate brittle failure (Shudofsky, 1985). Few large and moderate earthquakes had their focal mechanisms determined by various researchers during studies of seismicity, crustal structure, event depth or calibration of ground truth (Shudofsky, 1985). Results from these events showed that the movement was dominated by normal and strike slip. From the forgoing, it is apparent the status of the earthquakes study is mainly based on seismicity, characterization of the earthquake to possible fault movement to crustal structure. More recent studies focus on the magmatic processes and earthquake activity (Calais et al., 2008, Baer et al., 2008). However, characterization of faulting activity, and therefore the resultant earthquake hazard still remains wanting.

d) Unmapped thermal regimes as possible driving mechanisms of the rifting process.

In the study area, this active deformation is characterised by hot springs (possibly hydrothermal solutions) that indicate possibly elevated local thermal regimes and a change in mineralogy along the fracture trace. The quantification of the thermal gradients is an important ingredient to understanding its (thermal) influence on chemical reactions, physical character and mineralogy near active faults. In a more practical sense, thermal gradient provide information on geothermal resource potential, whose exploration in Kenya is considered to be at youthful stage (Omenda, 2001, Simiyu, 2010).

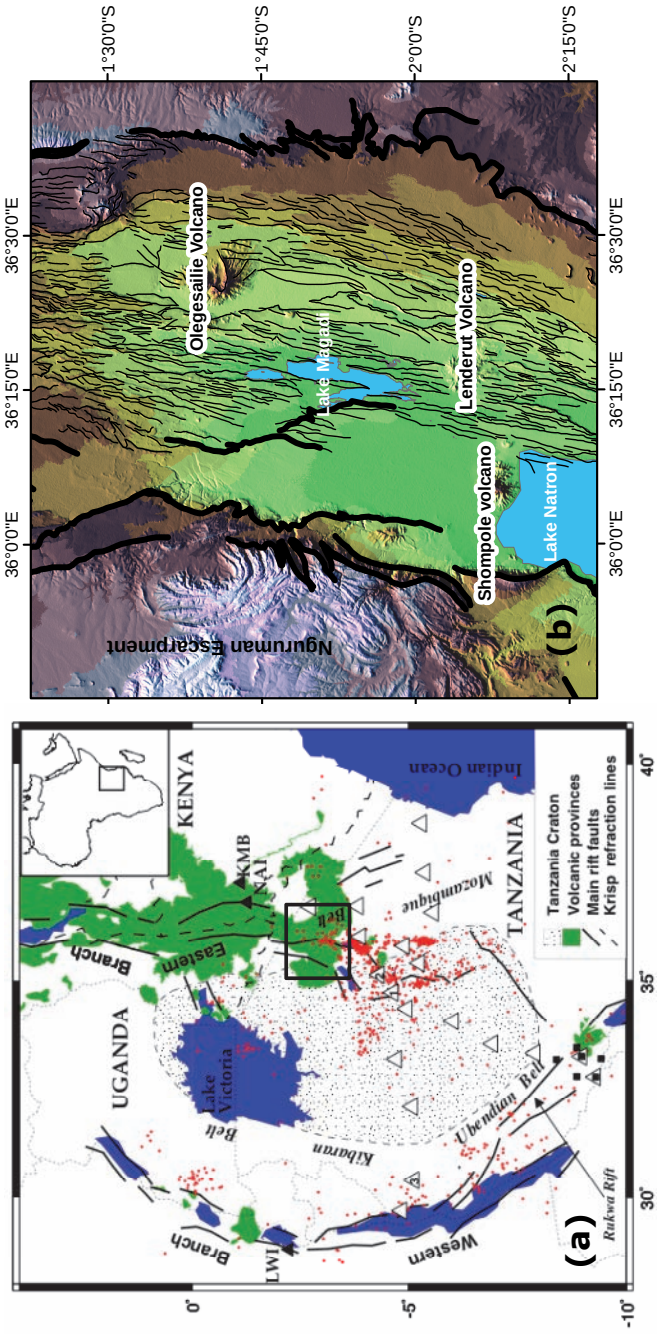

Figure1-1a. Part of the East African Rift System; showing eastern and western branches. b. location of study area marked by Lakes Magadi and Natron

1.3 Research questions

This research endeavoured to use remote sensing and geophysical techniques including field studies to examine and understand active faults and how they relate to spatial patterns and progress of natural hazards, particularly earthquakes, in Magadi-Natron area of the southern Kenya Rift.

The research questions asked below are linked directly to the four problems outlined in Section 1.2 above for ease of reference and consistency.

1.3.1 Questions related to problem 1.2a

i. What is the spatial distribution of the active/Recent extensional structures (faults, fractures) in relation to geology within the entire study area? i.e. are they located within Precambrian metamorphic rocks, the Plio-Pleistocene volcanics, and the Holocene to Recent lake and fluvial sediments or are they cutting across several formations. All these geological formations are outcropping in the study area.
ii. What is the orientation and size characteristic of active faults relative to each other and relative to other faults in the region?
iii. What is characteristic movement of these active extension structures (normal, stike-slip or oblique - slip)?
iv. Is there any control of the pre-existing discontinuities on the geometry of the recent rift patterns?

1.3.2 Questions related to problem 1.2b

i. What changes in stress field are prevalent in Magadi-Natron area? Strecker and Bosworth (1991), Atmaoui and Hollnack (2003) or Grimaud et al. (1994).
ii. Does the clockwise extension deformation deduced for the central Kenya Rift (Strecker and Bosworth, 1991) explain the deformation along the active faults?

1.3.3 Questions related to problem 1.2c

i. What is the magnitude of surface deformation from rift extension?
ii. What displacement vectors characterize active faults and how do they relate to potential earthquakes?

1.3.4 Questions related to problem 1.2d

i. What thermal gradients prevail in the study and do they influence faulting activity.
ii. What other possible factors influence the faulting process and therefore evolution of the rift basin?

s1.4 Objectives of the study

The global scientific objective was to examine and understand active faults and how they relate to spatial patterns and progress of natural hazards particularly earthquakes in Magadi-Natron Area, southern Kenya Rift.

The specific scientific objectives of the study include:

i. To establish spatial and density distribution of active extensional structures including their geometry and trends and their implication to earthquakes distribution.
ii. To determine migration and propagation of the extension throughout the Magadi rift basin and relate it to the entire Kenyan Rift.
iii. To deduce the magnitude of the surface deformation in the Magadi area (ground deformation detection) and relate it to potential earthquakes.
iv. To map and quantify the thermal gradients as possible driving mechanism of the rifting process as well as geothermal indicators.

1.5 Thesis layout

This thesis is based on a number of papers published or under review in peer reviewed international journals.

Chapter 1: Introduces the seismotectonics of a divergent rifting plate boundary, problem statements and related questions, objectives of this research and a layout structure of this thesis.

Chapter 2: Provides a description of the active fault segments: their identification from ASTER images and DEMS, followed by detailed field campaign. The active faults are correlated with earthquake data. The fault sets are described including their orientation, relative age, spatial and density distribution. The influence of pre-existing discontinuities is also elucidated. The key contribution is a new model of extension direction.

Chapter 3: Presents a characterisation of earth surface deformation from SAR interferometry and earthquake potential. 3-pass and 4-pass SAR interferometry is applied to monitor fault nucleation, growth and linkage for a period of eight months. This provides overwhelming evidence for an actively deforming fault zone and extension direction deduced above (Chapter 2) including associated earthquake potential.

Chapter 4: Analyses the subsurface characteristics of active faults through an integrated geophysical mapping of Magadi fault system. The results show

subsurface fault geometry, faulting intensity and constituents (fluids and sediments). In addition, scattering of magnetic sources is used for the first time as an index of faulting activity. The presence of fluids is inferred to affect seismicity.

Chapter 5: Investigates Curie point depths (CPD) and their spatial distribution in central to southern Kenya Rift from geomagnetic observations. An evaluation on whether the CPD are compositional boundaries or Curie isotherm is carried out. The CPD morphology together with depth-temperature and steady state geotherms are interpreted in terms of geothermal potential. These CPD and their spatial distribution were mapped for first time in the Kenya Rift.

Chapter 6: Establishes crustal thermal regime and its implication for earthquake hypocentral distribution. An interpretation of the shallow CPD as mantle plume is made, as well as their (shallow CPD) possible influence on nucleation of earthquakes. A relationship of the Curie isotherm with other geophysical models is made.

Chapter 7: Images faults from the earth surface to upper mantle using collocated transient electromagnetic (TEM) and magnetelluric (MT) soundings. It furnishes details on fault architecture and its constituents and how they influence seismicity. The results – dyke intrusion and fluidised fault zone – bridge the gap on factor controlling seismicity in southern Kenya Rift.

Chapter 8: Syntheses the results of the previous chapters by providing two integrated models along two profiles located north and south of Lake Magadi explaining the spatial variability in seismicity. The physical models incorporate topography, CPD, earthquake focal depth and Moho depths. A discussion on the earthquake nucleation process in each model is described. The short comings from this research are highlighted and future frontier recommended.

CHAPTER 2

STRUCTURAL SET-UP OF THE SEISMICALLY ACTIVE FAULTS AND THEIR DEFORMATIONAL STYLE

This chapter is based on:

Kuria, Z.N., Woldai, T., van der Meer, F.D., Barongo, J.O., 2010. Active fault segments as potential earthquake sources: Inferences from integrated geophysical mapping of the Magadi fault system, southern Kenya Rift. J. Afr. Earth. Sci. 57 (4) 345-359. Part 1.

2.1 Introduction

The Kenya Rift (also known as Gregory Rift) is considered the archetype of a continental rift in the initial stage of continental breakup (Chorowicz, 2005, Achauer and Masson, 2002). It forms part of the East African Rift System (EARS) (Figure 2-1), which comprises a series of rift zones stretching more than 3,000 km from the Afar triple junction in the North to the Zambezi river in southern Africa. The rift system bifurcates around the Tanzanian Craton, which coincides with the uplifted East African plateau. The Kenya Rift transects the Kenya Dome, which itself is superimposed on the eastern margin of the East African plateau and is located close to the boundary of the Tanzanian Craton and the Pan-African Mozambique shear belt (Baker et al., 1972b). Kenya Rift ends in Northern Tanzania, where it widens into a broad depression and becomes indistinctly defined.

The discovery and subsequent research works along the EARS began as early as 19th century. Since then, the Kenya rift has been subjected to a lot of detailed investigations ranging from geological (Smith, 1931, Baker, 1958, Baker, 1963); intra-continental rifting (Searle, 1970, Baker et al., 1971b, Fairhead and Girdler, 1972); rifting evolution (Bosworth, 1985, Mougenot et al., 1986, Strecker et al., 1990, Kampunzu and Mohr, 1991, KRISP Working Group Party, 1991);seismic reflection profiling (Morley et al., 1992) to seismological studies (Tobin et al., 1969, Young et al., 1989, Tongue et al., 1992, Ibs-von Seht et al., 2001, Ibs-von Seht et al., 2008).

Previous studies have focused on the deeper structures, giving less attention to studies on the neotectonic resulting from the shallower structures expressed by the recent high rate of seismicity, geothermal activity and volcanism. All these activities related to geodynamic activities are well displayed in the southern Kenya Rift, at Lake Magadi Area.

Molnar and Aggarwal (1971) carried out the first micro-earthquake surveys in Kenya and found the area around Lake Magadi to be seismically active section of the Kenya Rift. A subsequent temporary seismic network established in the vicinity of Lake Magadi under Kenya Rift International Seismic Project of 1994 recorded more than 200 local events in a period of the 2 weeks (Prodehl et al., 1997a). In 1997 and 1998 another denser seismic network consisting of 15 stations was installed around Lake Magadi. The network recorded approximately 10 events per day that were found to be equally distributed on the rift floor and a swarm activity with rates of more than 300 events per day (Ibs-von Seht et al., 2001). The microseismic activity observed in the southern Kenya rift valley is associated with geothermal processes (Maguire and Long, 1976), but these geothermal

manifestations do not occur on a regional scale (Martin and Morogan, 1988). The heat flow is considered an expression of focused mantle degassing (Bailey, 1983) and the unusual intensity of injections of mantle-derived magmas into the crust. From geophysical records, mantle structure beneath the Magadi trough is considered as a narrow and linear (N-S) steep-sided low-velocity channel from 80 to 200 km depth (Green et al., 1991, Achauer et al., 1992), suggesting local lithospheric thinning. Moho depth is known to be shallow from approximately 40 km beneath the unrifted domain to 35 km beneath the south Kenya rift axis (Prodehl et al., 1994a, Last et al., 1997). These deep magmatic and heat flow processes have not been linked to the surface manifestation of the geodynamic processes manifested in the southern Kenya Rift, Lake Magadi area. The intertwinement of the deep and surface earth processes in the realm of the seismotectonics is motivation of this study.

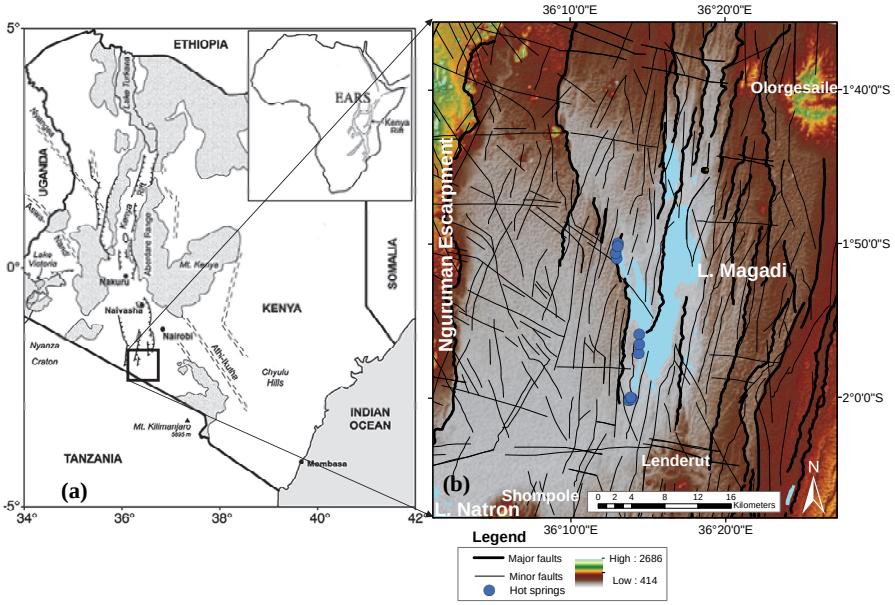

Figure 2-1a. Shows location of the Kenya Rift and key features: Aswa-Nandi-Loita shear zone and Aberdare Detachment. Insert is map of Africa showing East African Rift System (EARS). (b) Shows lineaments superimposed on shaded-relief map of Lake Magadi area developed from ASTER DEM (30 m resolution). The lineament trend N-S, dextral NW-SE, strike slip ENE-WSW and sinistral NE-SW supporting an E-W extension, bridging gap on extension direction along south Kenya rift.

2.2 Geological setting

According to Baker (1958) and (1963) geology of the Lake Magadi area is characterized by Precambrian metamorphic rocks, the Plio-Pleistocene volcanics, and the Holocene to Recent Lake and fluvial sediments. The Precambrian metamorphic rocks outcrop in the elevated area west of the Nguruman Escarpment (Figure 2-2). They underlie olivine basalts of the Kirikiti platform, which extruded between 3.1 and 2.5 Ma (Crossley, 1979) and is down-faulted to the rift floor at the Nguruman escarpment.

The area has three central volcanoes, Ologorgesailie being the most important one in size. Its lava composition shows variations of olivine basalts, alkali trachyte and nephelinite. Further, south, Lenderut volcano (2.5 Ma) has basalt to andesite lavas, while Shompole (2.0 Ma) consists of carbonatite and nephelinite rocks.

The volcanic activity in the area occurred between 1.4 and 0.7 Ma (Crossley, 1979) with the formation of the Magadi Plateau Trachyte Series. The Magadi Plateau Trachytes are closely followed by the development of ash and lava vents, and the small obsidian lava volcano. Oldoinyo Nyokie ends the volcanic formation of the southern Kenya Rift. The last geological formations of the Lakes Magadi area relates to the lacustrine and fluviatile sediments. These include Lake beds and fluviatile sediments found in the Ewaso Ngiro basin.

2.3 Structural and tectonic setting

The Lake Magadi area is situated at the southern part of the elliptically shaped Kenya Rift, where the lake occupies a narrow complex graben in the axial zone of the rift floor. The rift at the depression of Lake Magadi in the Kenya Paleogene Rift Valley follows a marked sub-meridian trend controlled by Proterozoic structures, along the margins between the Tanzanian Craton and Precambrian Mozambique Belt (Smith and Mosley, 1993, Mathu and Davies, 1996). The Magadi-Natron together with Baringo-Turkana, broad half-graben depressions as well as the Aberdare Detachment graben are sub-meridian and traversed by major antithetic tilted blocks of Late Miocene to Early Pliocene (Bosworth et al., 1986). The sub-meridian structures are separated by transverse fault structures interpreted by Smith and Mosley (1993) to have developed along areas of weaker crust caused by E-W regional extension on the major escarpments.

During Pleistocene to Recent, the faulting that dissects the rift floor obviously increased in Magadi area in comparison with the other segments of the Kenya Rift (Baker, 1986) i.e. Baringo-Turkana and Aberdare Detachment. Lake

Magadi area has been investigated using geophysical techniques such as gravity, magnetics and wide-angle seismic refraction: KRISP 85 (Henry et al., 1990) investigations along the rift axis from Lake Baringo to Lake Magadi, and KRISP 94 (Prodehl et al., 1997b) investigations across the Kenya Rift through Lake Magadi. It is interpreted that the crust in this southern part of the rift is 35 km thick where the axial zone is penetrated by feeder dikes originated probably from the upper mantle. The combined integrated interpretation of all these geophysical data (Simiyu and Keller, 2001) resulted in a geological cross-sectional model showing Magadi area as an asymmetric rift graben bordered in the western part by the high angle faults of Nguruman Escarpment. The basin fill which has a depth of 3.5 km against the Nguruman scarp to the west and 2.0 km to the east is divided into two parts by a horst structure located just beneath Lake Magadi.

On the basis of morphological, structural and volcanic signature, Smith and Mosley (1993) subdivided the Kenya rift into three segments namely; northern Baringo/Turkana, Aberdare Detachment and southern Magadi/Natron, which are separated by major NW-SE trending ductile shear zones in the underlying Precambrian basement. The southern segment, which corresponds to Lake Magadi area and extends to the northern Tanzania, is supposed to have developed on a craton type lithosphere that has been obscured by imbricated thrust slices and gravitationally collapsed nappes of the Tanzania Craton and the Mozambique Belt (Smith, 1994, Simiyu and Keller, 1998). Thus this pre-existing framework might have influenced and controlled the location and structural geometry of this part of the rift by the reactivation of the Aswa – Nandi - Loita (ANL) shear zone, which is a ductile and brittle NW - SE to NNW-SSE zone bounding Lake Magadi area at its northern limit.

2.4 Methodology

The methodology adopted in this research was dedicated to establishing the local active faults using structural data (fault/fracture system) and earthquake data. However, due to the close relationship between geology and structures, an appraisal of the rock types was deemed very necessary. For this purpose aeromagnetic data was used. In case of mapping active structures ASTER images and DEM were used coupled with earthquake data, as detailed hereafter.

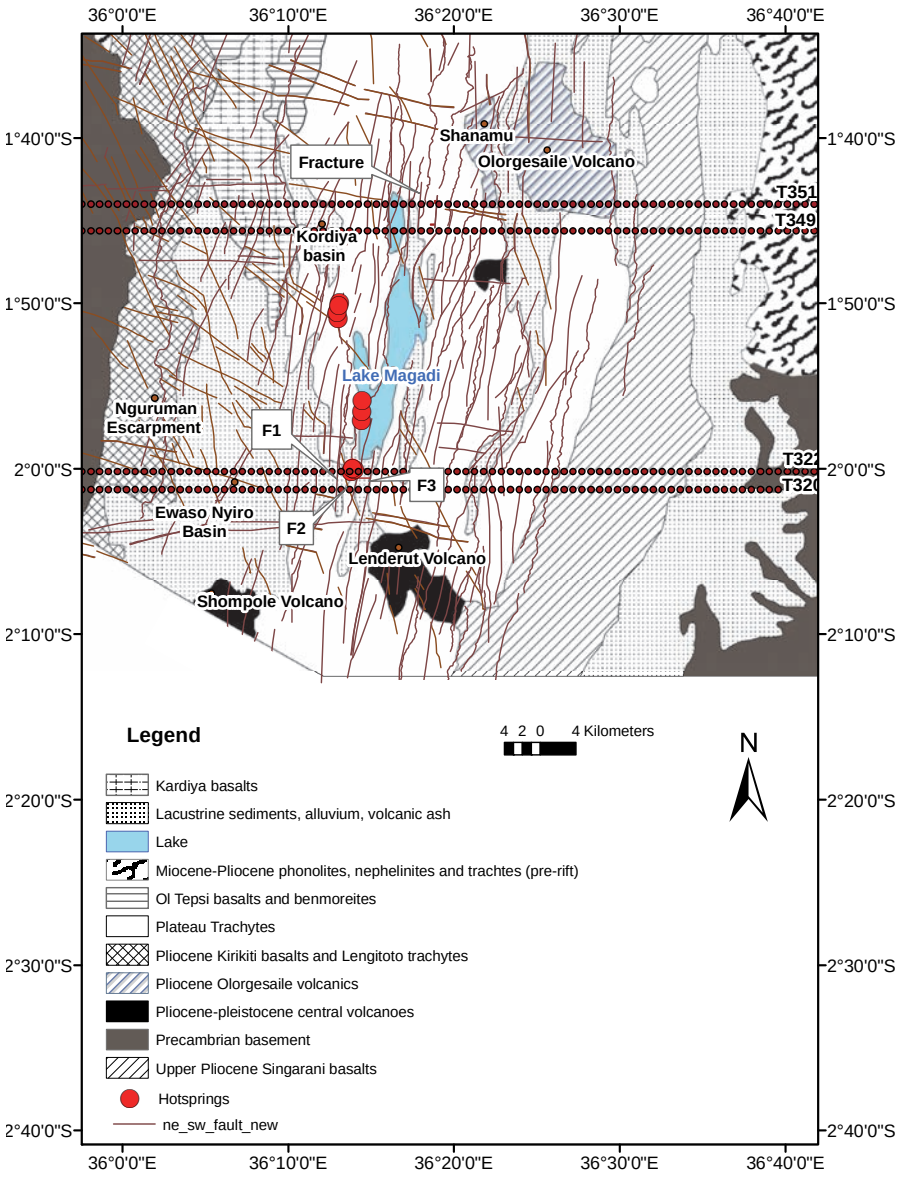

Figure 2-2. Geological map of Lake Magadi area showing the relationship between geology, faults and hot springs

2.4.1 Aeromagnetic data analysis and geological mapping

The aeromagnetic dataset used in this research is part of the African Magnetic Mapping Project (AMMP) which compiled airborne magnetic data covering most parts of Africa (Barrit, 1993). The aeromagnetic data of the study area was acquired in the year 1987 by Compagnie Générale de Géophysique, a French Seismic Acquisition and Processing Services Company with line spacing of 2 km and flight direction of 90° running in E-W direction at a flying height of 2896 m above mean sea level. Aeromagnetic data was acquired along a total of 241 flight lines (each at 2 km line spacing) and each flight line covered an average distance of about 148 km i.e. the total area covered was 148 km by 482 km. In addition, magnetic data was acquired along 16 cross over lines running in N-S direction. The magnetic data was pre-processed by AMMP that included levelling correction and regional field removal (using IGRF model of 1987 with field strength of 33383 nT, Inclination of -35.4°, declination of -1.4° to the south, and 33949 nT, Inclination of -21° declination of -0.13° to the north). It is worth noting that the regional field removal was channel based, meaning that each sampling point was corrected with respect to its geographical location. After correction the magnetic data was gridded at 1 km by 1 km cell size with a projection system of AMMP. The analytic signal of the total field (Roest et al., 1992) was used in this case because it provides alternative to reduction to the pole from low magnetic latitudes i.e. near equator. The results from analytic signals were correlated with geological maps (1:125,000) and field data.

2.4.2 Structural mapping

The structural mapping consisted of the remote sensing analysis of the structural elements in the Lake Magadi area. The fracture and fracture system were extracted from the available ASTER images, resampled at 15 m, draped over ASTER DEM with a vertical resolution of 30 m. Following the preliminary interpretation, a field campaign was organized to confirm the interpreted lineaments from Aster images and to obtain structural data such as strike and dip. The interpreted structural map was used to improve the existing lineament map of the area (Atmaoui and Hollnack, 2003). The output from this interpretation was a spatial and density distribution of the structural faults and fractures in the area (Figure 2-2). The improved structural map was used to constrain earthquake locations that are detailed below.

2.4.3 Seismotectonic studies

The delineation of the faults was followed by identification of the active faults using earthquake data. For this purpose, arrival times of seismic phases from a temporary seismic network installed and operated for 8 months (Ibs-von Seht et al., 2001) consisting of 15 stations were relocated using a SEISAN

program (Havskov, 1997). The purpose of the re-locating the earthquakes was to constrain their epicentre location using interpreted lineaments (Figure 2-1). The well located events (i.e. recorded by more than 4 stations) were used to map-out the active faults in the study area. The velocity model used for the re-location was derived from the results of the KRISP 1994 experiment (Prodehl et al., 1997b). The mean vp/vs ratio of the study area was 1.74 (Ibs-von Seht et al., 2001). The original Earthquake data in a CD were obtained from a seismological survey conducted in Magadi area between November 1997 and June 1998 courtesy of Ibs-von Seht, Hannover Germany. Additional earthquake data were obtained from the catalogues (Hollnack and Stangl, 1998).

In addition focal mechanism solutions were deduced using first motion of P-wave polarity of well-located earthquakes i.e. events recorded by more than eight seismic stations that are well distributed geographically around the epicentre. In order to characterize the fault plane orientation and direction of slip a program called FOCMEC_EXE (with first version written by Snoke et al. (1984)); a part of SEISAN was used. The program works with polarities and amplitude ratios of direct waves using the same wave types i.e. Pg and Sg. Ideally, the solutions were obtained from polarities while the amplitude ratios were used to constrain the results. The candidate earthquake for focal mechanism was selected based on the number of stations that recorded event and their geographical distribution, which should surround the earthquake epicentre. The minimum number of the seismograph stations required was set at 8. It was observed that many earthquakes fulfilled this criterion (of minimum 8 stations). However, the north western part had a poor seismograph stations configuration that resulted into fewer solutions. The number of polarity errors were selected depending on the number of data values available, in most case 2 was selected (a range between 0-5 is recommended). For maximum amplitude ratio errors, 0.1 was used, i.e. results read to within 10%. After in-putting the data the program makes an efficient and systematic grid-search for focal sphere based on defined criteria i.e. acceptable number of wrong polarities and errors of amplitude ratios. The most preferred solution is selected. The results were presented as “beachball” diagram; a representation of the P-wave radiation pattern. The interpretation of the beachballs is provided in Figure 2-6 and results (beachballs) are superimposed on the faults as shown in Figure 2-7.

2.5 Results

2.5.1 Aeromagnetic analysis and geological mapping

After calibrating the analytic signal anomalies deduced from the total aeromagnetic field with the 1:125,000 geological maps (Baker, 1958, Baker, 1963, Matheson, 1958) and field data, it was observed that the anomalies corresponded with precise location of the lithological boundaries providing a clear picture of the geology of the area, beneath the alluvium and in poorly accessed (mapped) regions (Figure 2-3).

The prominent geological formations with high magnetic intensity occur in rather four isolated locations marked largely by volcanoes such Olorgesalie (Nephelinites and a series of trachytes, augite basalts, agglomerates), Lenderut (Andesites, Tephrites, basanites) and Shompole (Tuffs and nephelinites) and the down-faulted Kiriti basalts. The Tanzania Craton is marked by very low magnetic intensity which clearly defines its boundary with the Mozambique Belt. A NW-SE trace of isolated low magnetic intensity patches located within a zone of moderate magnetic intensity, is inferred to mark the location of ANL shear zone (Mathu and Davies, 1996). Another zone of moderate magnetic intensity with very small isolated low magnetic anomalies occurs between the Tanzania Craton and Ngurumani Escarpment and provides leads to the location of reworked rocks of Mozambique Belt. This zone has equally been very challenging to define its lateral limits using gravity and seismic methods (Simiyu and Keller, 1998).

2.5.2 Structural mapping and seismotectonic studies

A lineament map (Figures 2-1, 2-2) was interpreted from ASTER image and ASTER DEM. The lineament map shows 4 distinct principal orientations that define the study area namely; normal N-S, dextral NW-SE, strike slip ENE-WSW and sinistral NE-SW trending faults. The N-S and ENE-WSW structures are easily deduced from the remote sensing data, while the NW-SE and NE-SW observed in the field are reactivation of the pre-existing structures (Figure 2-4a, b, c, d).

Cross cutting relationship amongst the different fault sets show that the N-S faults are the oldest in the area because they are cut by all the other sets of faults. The reactivated NE-NW faults are the youngest faults. A visit to area of the earthquake swarm activity revealed a fault striking N10˚E, Dip 85˚, Dip direction N86˚ and small throw 10 cm. This fault cuts N62˚E and NW-SE fracture. The small deflection noted on this fault could possibly be due to buried ENE-WSW fractures.

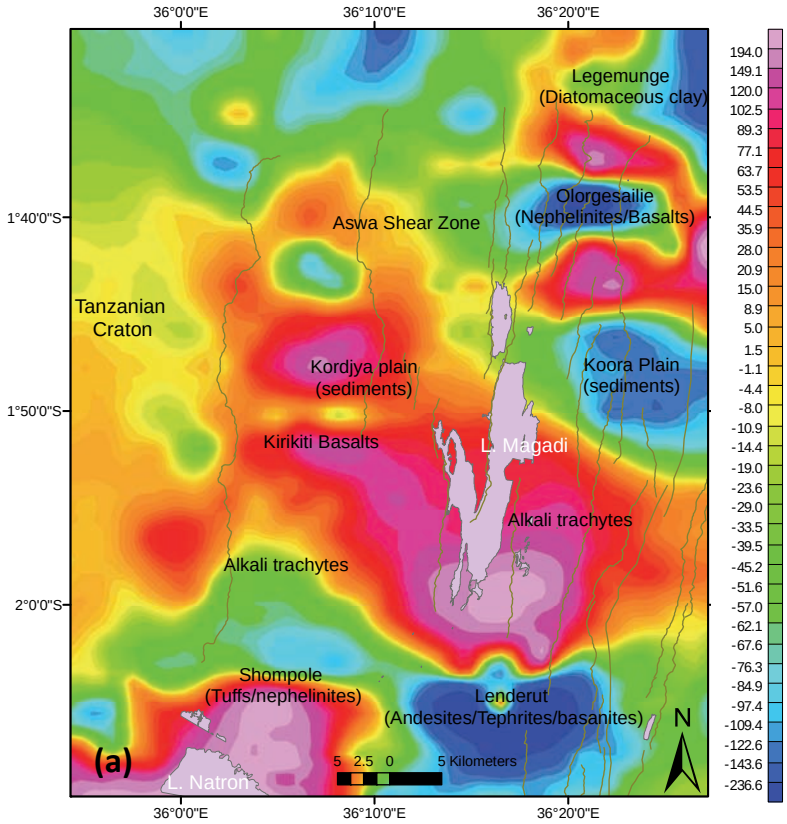

Figure 2-3a. Map of the magnetic residual anomalies (from AMMP 1 X 1 km cell size) correlated with the local geology. Largely, the magnetic anomalies depict the near surface geology. Major faults are coincident with the boundaries of the magnetic anomalies.

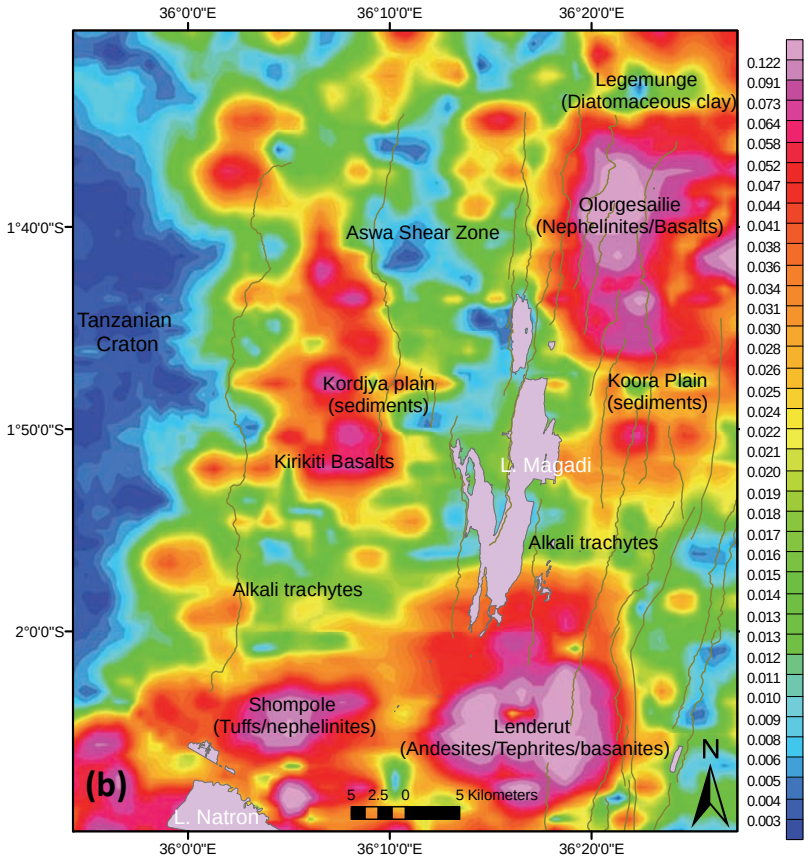

Figure 2-3b. Analytic signal map of the magnetic field representing geology beneath alluvium i.e. filtered near surface geological materials. Note the well-defined eastern boundary of Tanzania Craton, Aswa Shear Zone and the volcanoes (Shompole, Lenderut and Oloegesailie). Major faults are coincident with the boundaries of the magnetic anomalies.

The NW-SE lineaments are closely linked to ANL shear zone, which is a highly fractured zone of massive quartizitic Precambrian rocks (Figure 2-4b). The NNW striking lineaments are distributed to the north of Lake Magadi and delimited to its southern margin. The ENE – WSW lineaments are normal to the regional trend of the rift and affect the Tertiary volcanics of the rift floor and Precambrian rocks of the Nguruman region. The lineament density is high along volcanoes Oldoinyo Sambu, Shompole and Lenderut to the south of Lake Magadi. To the north the lineament density decreases between Loita hills and Ologesaile volcano.

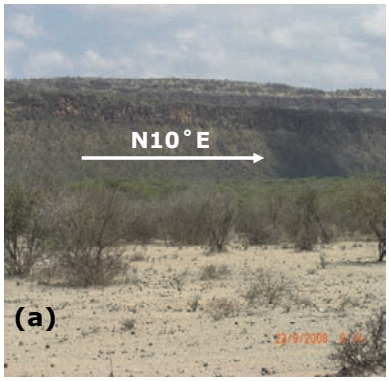

(a) N-S fault escarpment. Photo taken facing ESE.

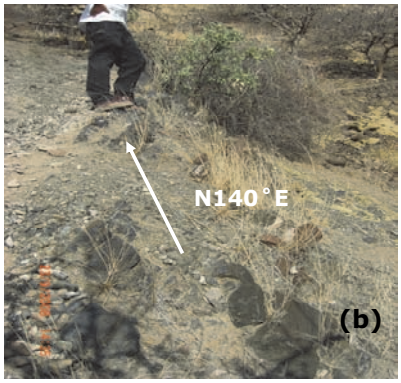

(b) NW-SE trending breccia cutting N-S fault. Photo taken facing SE.

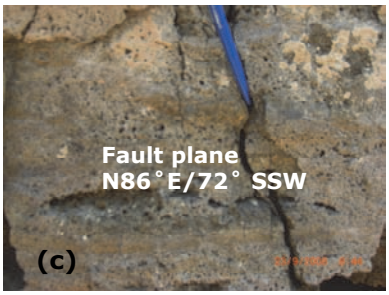

(c) ENE-WSW with horizontal slicken slides.

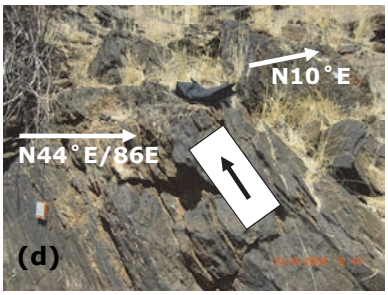

(d) NE-SW fault with slicken slides cuts N10E fault. Black arrow shows sinistral movement. Photo taken facing NW.

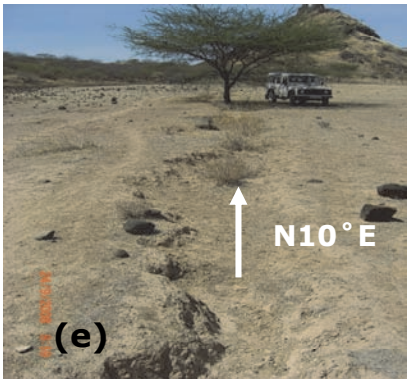

(e) North rupture zone at location of swarm earthquakes cutting through the hill to the further south. Photo taken facing south.

Figures 2-4a, b, c, d, e. Show the four sets of faults; N-S, NW-SE, ENE-WSW, NE-SW and rupture zone respectively. The fresh fault scarps marked by slicken slides indicate active deformation.

The analysis of the earthquake data from microseismic survey proves that Magadi area is seismically active. The magnitude of these earthquakes range between 0.5 and 4.3 and their focal depth vary from 1 km to 27 km. The earthquakes mainly cluster along the axial zone of the rift. However, a closer look shows that micro-earthquakes occur all over the area along the main tectonic trends (Figure 2-5). The main cluster is located north of the Lake Magadi at the intersection of all the 4 fault sets. Whereas the NE-SW active faults do not continue south of Lake Magadi, the NW-SE persist on south eastern part of the Lake Magadi possibly indicating propagation of the ANL shear zone to the further south. The focal mechanism solutions indicate an E-W normal faulting extension. Other active lineaments include the E-W fractures cutting across Lake Magadi marked by a linear E-W plot of earthquake epicenters.

The results from analysis of focal mechanism are presented as “beachballs” spread out within the study area. These are lower-hemisphere stereographic projections with two black quadrants and white quadrants separated by great arcs representing the auxiliary and fault planes. The compressional quadrants are shaded. The interpretation of the beachballs is provided in Figure 2-6 after Snoke et al. (1984)

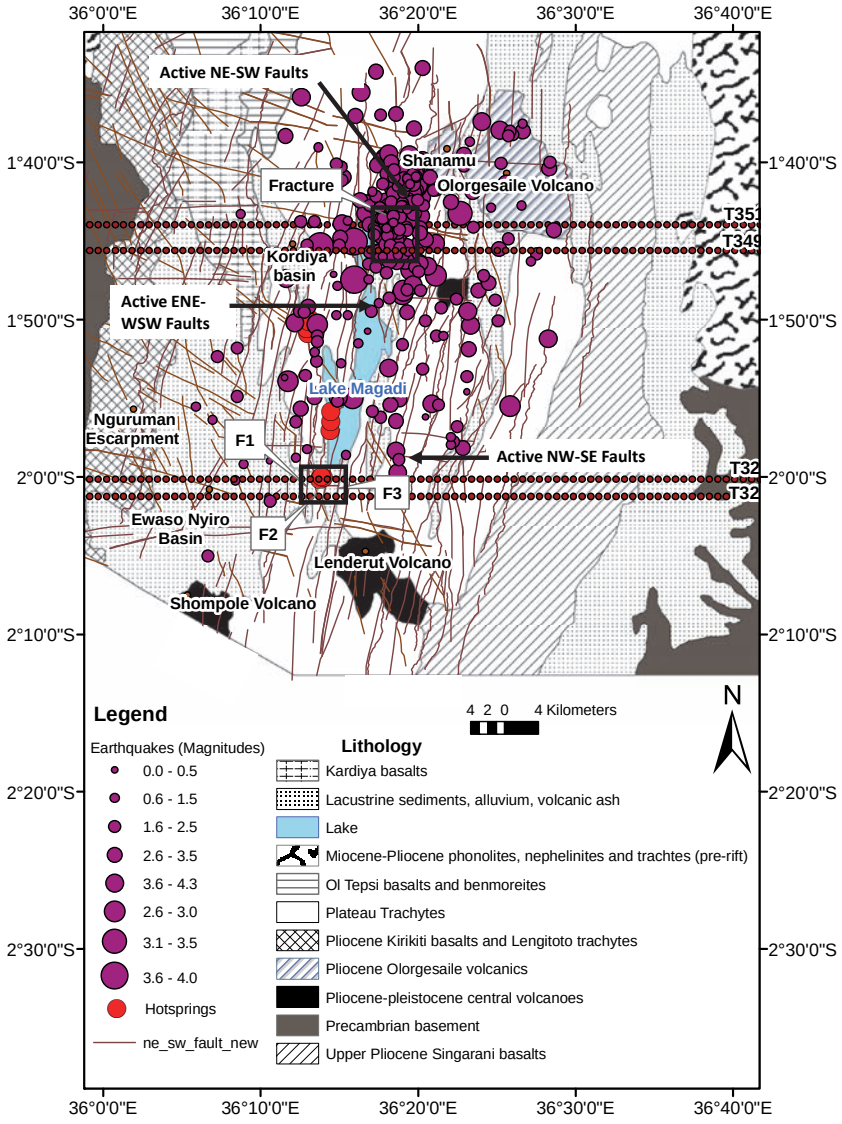

Figure 2-5. Map showing active faults (NE–SW, ENE–WSW, NW–SE) deduced from lineament map and earthquake data. These active fault sets including N–S faults intersect at the area north of Lake Magadi marked by earthquake cluster. The hot springs are confined along the south western part of Lake Magadi.

The results of focal mechanism indicate 22 beachballs (Figure 2-7) covering almost the entire axial rift floor, provide for characterization of orientation and sense of slip of the fault that ruptured during earthquake activity. A poor configuration of the seismograph stations hampered focal mechanism solutions at the rift margins (east and west) as well as north western part of the study area. Distinctly, the fault planes marked by the beachballs are oriented in N-S, NE-SW, NW-SE and E-W. These orientations match those of the faults at or in the vicinity of the beachball. The close match in orientation of fault planes indicates that faults on the rift floor are seismically active. Along the axial zone the beachballs have three quadrants with a white center which denote a pure normal dip slip. Majority of the fault planes having pure dip slip components are oriented NE-SW but for the area with swarm earthquake activity a NW-SE orientation is apparent. The beachballs showing oblique faulting mechanism i.e. a combination of the strike slip and normal dip-slip are located south of Lake Magadi and its entire western margin. In addition, the area immediately north of the swarm earthquake activity has strike-slip and normal slip faulting. The west and east of Lake Magadi is characterised by very unique beachballs with only two patches (black and white), these balls mark a vertical dip slip common to rift margin.

There were no focal mechanisms with pure strike slip or oblique faulting with reverse dip slip component. The dominant strike of the fault planes ranges between 10-20°, with steep P-axes and almost horizontal T-axes. This indicates prevalence of the normal faulting along NE-SW faults. In addition, the abundance of oblique faulting with strike slip and normal dip slip is preferentially located on the north western part of Lake Magadi.

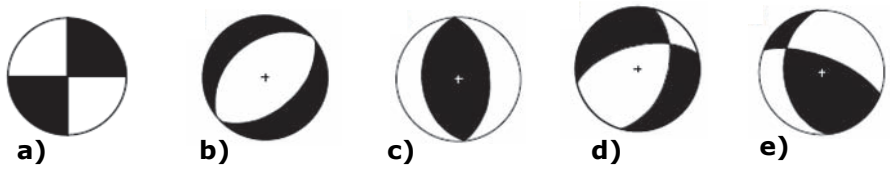

Figure 2-6. Interpretation of beachballs: a) a pure strike-slip fault, with all the four quadrants observed. b) a pure dip-slip, with normal faulting mechanism; the center of the beachball (black mark) is white with three quadrants. c) pure dip-slip, with reverse faulting mechanism; the center is black with three quadrants. d) Oblique-slip faults with strike slip and normal component of slip; the center is a white quadrant. e) oblique-slip fault with strike slip and reverse component of slip component; the center is black.

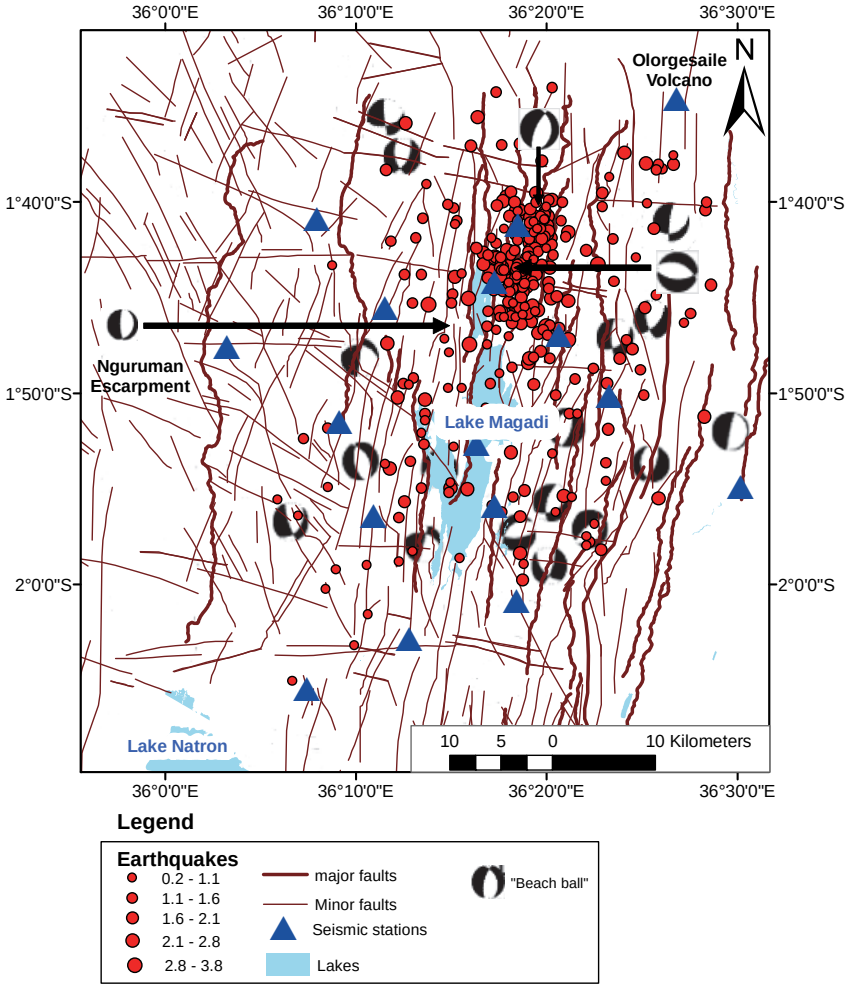

Figure 2-7. Focal mechanism solutions deduced from P-polarities of well-located earthquakes presented by "beachball" diagrams. Notably, there is a close match in orientation of the fault plane from "beachballs" and those from faults determined from DEM and ASTER image. In addition, location of the "beachballs" mark the patch of the fault that slipped therefore the entire axial rift floor is seismically active.

2.6 Discussion

Several geophysical studies have been conducted in the past to locate the suture between the Mozambique Belt and the Tanzania Craton (Nyblade and Pollack, 1992, Tesha et al., 1997, Simiyu and Keller, 1998) without much success. However, in this study the variability in magnetic signatures emanating from the diverse geological compositions of the rocks forming part of the Tanzania Craton (metasediments, metavolcanics, granitoids and other intrusives) provide a distinct boundary with the rocks of the Mozambique Belt that have a characteristic uniform magnetic signature. This provides the first step towards refining the boundary appropriately. A NW-SE trace of isolated low magnetic intensity patches located within a zone of moderate magnetic intensity, in this case, marks the location of ANL shear zone (Mathu and Davies, 1996).

The moderate magnetic intensity with very small isolated low magnetic anomalies located between the Tanzania Craton and Ngurumani Escarpment provides leads as to the location of reworked rock of Mozambique Belt. This zone has equally been very challenging to define using gravity and seismic methods (Simiyu and Keller, 1998). In addition, this study supports the interpretation from the gravity profiles across the rift valley in Kenya and Tanzania that contain a gravity low west of the rift valley, a signature from crustal thickening (approx. 5 Kilometres) associated with the suture (Nyblade and Pollack, 1992, Tesha et al., 1997, Simiyu and Keller, 1998).

The presence of four sets of faults (normal N-S, dextral NW-SE, strike slip ENE-WSW and sinistral NE-SW) of different age and deformational styles indicate geodynamic change in rift tectonics. At the onset of the rifting tectonics, the rift experienced normal faulting under E-W extension. Subsequently, the rift was subjected to a tectonic change that reactivated pre-existing structures creating dextral NW-SE, strike slip ENE-WSW and sinistral NE-SW faults under E-W extension. The recent rupture (NNE-SSW) at area of swarm activity support E-W extension. These results are in agreement with the rift development model of central Kenya Rift proposed by Le Turdu et al. (1999). Different suggestions on neo-tectonic extension of the Kenya Rift have been proposed by different authors: Bosworth and Strecker (1997) advocated a NW-SE neotectonic extension from their work in central Kenya Rift by assuming the NW-SE structures as direction of extension; Atmaoui and Hollnack (2003) argued an E-W to ESE-WNW neotectonic extension for the Lake Magadi area by assuming the NW-SE dextral movement is localized. Both views did not recognize the existence of the sinistral oblique slip NE-SW trending faults which were created under an E-W extension to counterbalance the NW-SE faults.

The results from focal mechanism indicate a unique close match in orientation of the faults planes (beachballs) and those deduced from the ASTER (DEM and image) and confirmed during the fieldwork. This close agreement indicates that the faults on the rift floor are seismically active. The prevalence of the normal faults particularly along NE-SW direction supports faulting mechanism under E-W extension, an observation further adduced by complete absence of pure strike faulting. These findings therefore, bridge the existing gap in opinion on neotectonic extension of the rift suggested by the earlier authors.

In addition, the abundance of oblique faulting with strike slip and normal dip slip, particularly on the north western part of Lake Magadi indicate the influence of ANL shear zone to N-S propagation of the rift system; an evidence of influence of pre-existing structures on the evolution of southern Kenya rift.

2.7 Conclusions

An integrated approach comprised of aeromagnetic data analysis, structural mapping and seismological data analysis has been used to elucidate the structural set-up of various active faults and refine the model of tectonic deformation. The following conclusions were drawn:

1. There are four sets of faults with different age and deformational styles. Chronologically, these faults are normal N-S; dextral NW-SE; strike slip ENE-WSW and sinistral NE-SW. The NE-SW faults were mapped for the first time.
2. The NE-SW trending faults were created to counterbalance the NW-SE faults.
3. The NW-SE and NE-SW structures are reactivation of the pre-existing structures. The NW-SE lineaments are closely linked to ANL shear zone, a highly fractured zone of massive quartizitic Precambrian rocks.
4. The faults within the axial rift floor are seismically active.
5. The dominant faulting mechanism is normal slip along fault zone.
6. Vertical dip slip characterises the major faults along rift margin i.e. boundary faults.
7. The ANL shear influences the rift evolution by inducing oblique slip component.
8. The southern Kenya rift is deforming under E-W extensional stress direction.

CHAPTER 3

CHARACTERISATION OF EARTH SURFACE DEFORMATION AS EARTHQUAKE POTENTIAL SITES USING SAR INTERFEROMETRY

This chapter is based on:

Kuria, Z.N., Woldai, T., van der Meer, F.D., Barongo, J.O., 2010. Fault growth through nucleation and interaction at Lakes Magadi-Natron area, south Kenya rift: inferences from repeat pass radar interferometry, Submitted: International Journal of Digital Earth.

Preliminary results were presented during Geological Society of Kenya (GSK) Conference, 17th – 19th March 2009.

3.1 Introduction

The characteristic feature of the normal faults within actively extending regions on the continents is that they are organized into sub-parallel systems distributed over regions of tens or hundreds of kilometres (Chorowicz, 2005). The faulting activity within these sub-parallel fault systems is not uniformly distributed over the entire period of extension. Therefore, permanent or recurrent faulting activity occurs more rapidly, shifting from one fault system to another, making resolution of their temporal evolution more difficult compared with dating in the older terranes (Goldsworthy and Jackson, 2001). These changes along the faults are of prime importance on two aspects (among others): 1) at local scale they provide clues on spatial distribution of hazards (earthquakes in particular), and 2) at regional scale they provide fundamental insights on continental dynamics that explains the intertwinement of discontinuous deformations of faults in the upper crust as a result of more continuous flow in the lower part of the lithosphere e.g. (Jackson, 1999).

Notably, the fault zone architecture is both temporally and spatially variable. To understand this variability numerous studies have been carried out relating the changes to variations in geology (Yielding et al., 1997), branching of the faults during their evolution (Childs et al., 1996), growth and linkage of the fault segments on a temporal scale (Cartwright et al., 1995) and changes in local stress environment along the fault (Sibson, 1986). Despite all these studies the understanding of strain distribution (both temporal and spatial) during faulting activity and its relationship to the regional stress field remains poorly resolved.

In order to understand the strain distribution in active fault (in the Late Quaternary) several approaches have been adopted in the past that include earthquake seismology (Ibs-von Seht et al., 2001), active geomorphology (Goldsworthy and Jackson, 2001), and relative vertical motions using GPS campaigns (Calais et al., 2008). The common one is statistical analyses applied in low strain regions e.g. Lake Magadi area where power-law scaling fits the data sets e.g. (Scholz et al., 1991) and higher strain areas where exponential law seems to describe the fault distribution e.g. (Cowie et al., 1993). In all these methods, there still remains disconnect between the spatial distribution of strain and its temporal constrain, which hampers the understanding of nucleation, growth, interaction and connection of faults to form networks. In order to ameliorate this shorting, a “snap shot” that monitors a fault nucleation and its growth (strain distribution) through a short temporal scale using three and four-pass interferometric Synthetic Aperture Radar (InSAR) observations is provided. Additionally, the resultant

deformation is modelled to determine whether it is related to regional stress field or a result of a localized phenomenon and subsequently inference is made on the earthquake potential from the deformation.

The study area is located close to the southern tip of Kenya Rift (part of Eastern African Rift System) between Lakes Magadi and Natron. The area is delimited to the north by Aswa Nandi Loita (ANL) Shear zone and to the south by Oldoinyo Gelai volcanic center (Figure 3-1). In this area the regional stress field i.e. E-W extension was recently resolved from structural studies that identified four faults sets of different age and deformational styles namely normal N-S; dextral NW-SE; strike slip ENE-WSW and sinistral NE-SW and supported by focal mechanism solutions of swarm earthquakes (Kuria et al., 2010a). The arid climate (sparsely vegetated) and minimal erosion in this region have preserved the morphology of the faults (Gloaguen et al., 2007) and provides ideal environment for InSAR, that permits mapping of the spatial pattern of deformation and evaluation of the extent and geometry of the sources of deformation characterizing an area 100 km by 100 km.

3.2 Structural and tectonic set-up

The rift at the depression of Lakes Magadi and Natron in the Kenya Paleogene Rift Valley follows a marked sub-meridian trend controlled by Proterozoic structures along the margins between the Tanzania Craton and Precambrian Mozambique Belt (Smith and Mosley, 1993). The morpho-structural set up of the Magadi-Natron rift system shows pronounced changes in the surface expression, which is a reflection of fundamental variation of the underlying crust/lithosphere structural pattern (Le Gall et al., 2008). The Magadi-Natron, a broad half graben depression, is a submeridian traversed by major antithetic and tilted blocks of Late Miocene to Early Pliocene (Bosworth et al., 1986). The sub-meridian structures are separated by traverse fault structures interpreted by Smith and Mosley (1993) to have developed along areas of weaker crust caused by E-W regional extension on the major escarpment.

The northern limit of the Lake Magadi-Natron basin is characterized by a major NW-SE trending ductile shear zone in the underlying Precambrian basement (Smith and Mosley (1993) and to the south, the rift evolves from asymmetrical graben to East facing half graben bounded to the west by a double system of normal faults (Le Gall et al., 2008).

Tectonically, Baker et al. (1972b) and Smith (1994) observed that with time there was a north to south rift propagation and a shift in volcanism from the rift margins towards the axial part of the rift floor. This trend was

accompanied by an increase in fault density and a decrease in fault length and displacement (Atmaoui and Hollnack, 2003). Therefore, the recent tectonic activity is mainly concentrated in the axial part of the southern Kenya Rift. It was on this basis that the study site was selected.

The mantle structure, constrained from geophysical survey, is marked by a narrow and linear N-S steep-sided low-velocity channel occurring between a depth of 80 and 200km (Achauer et al., 1992), signifying local lithospheric thinning. On the other hand, Moho depth is known to occur at a depth of ~40km within the unrifted domains and shallower (35 km) beneath the rift axis (Prodehl et al., 1994b).

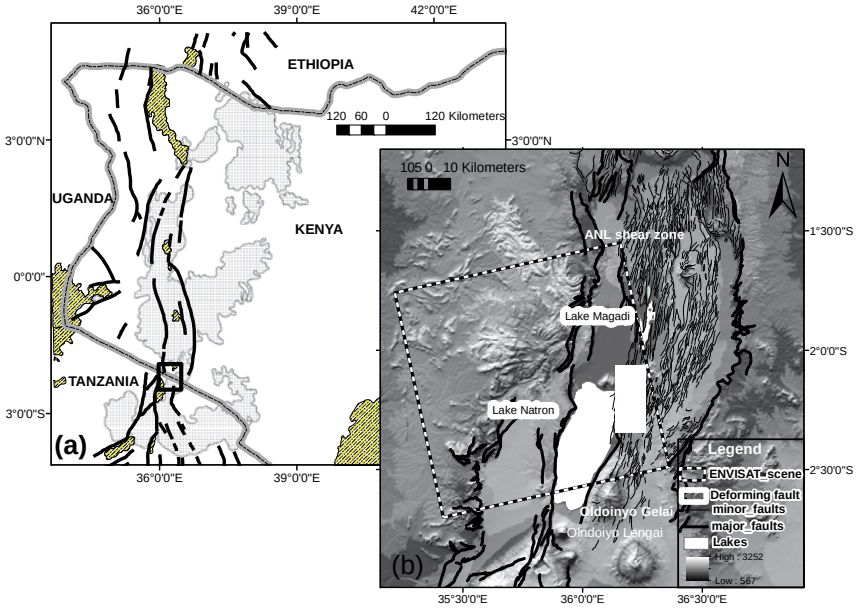

Figure 3-1. Shows regional tectonic setting of the study area. (a) Shows Kenya Rift System: the bold black lines mark the sinuous rift escarpment, grey light shaded polygons show extent of Quaternary volcanics. The small square box is location of (b) relief map showing intense rift floor faulting and the black dashed border marks outline of ENVISAT scenes (ascending) used in this study.

3.3 InSAR data processing and modelling

The following section provides a description of the methods adopted in InSAR data analysis and interpretation of results.

3.3.1 Methods

InSAR technology has evolved over the last two decades to become a widespread tool for measuring subtle ground surface displacements e.g. (Massonnet and Feigl, 1998). The study area lacked repeat GPS data and had a poor coverage of the seismological stations, in terms of number and configuration. Therefore, InSAR observations provided the only constraints for fault slip characterization and inference on source parameters for possible earthquakes prior to July-August 2007 seismic crisis. The coseismic deformation was well covered during the magma driven earthquake swarm and triggering of Oldoinyo Lengai eruption in 2007 (Baer et al., 2008) and well constrained due to fortuitous deployment of temporary broadband seismic network and GPS campaign later in 2006 (Calais et al., 2008).

In this study ENVISAT ASAR images (C-band, 5.6 cm wavelength) from the European Space Agency (ESA) acquired in the beam modes at incidence angle of 23° were used. These data sets were sourced from European Space Research Institute (ESRIN) through Tiger project. In this study the ESA radar images were provided in Single Look Complex 1 (SLC/SLCI) format. A total of 14 images were used, 2 of which spanned a period in 2003 while the rest provided a continuous series covering a period of about eight months in 2006 (i.e. January to August). The images were processed using SARscape software (Sahraoui et al., 2006). Precise orbits were provided by the Delft Institute of Earth Observation and Space Systems.

Based on estimation of baseline parameters, eleven interferometric pairs were identified as shown in Table 3.1. However, for the purpose of monitoring ground deformation, five pairs spanning a period of 6 months were selected after noting that there was no deformation for the months of July and August 2006. The deformation fields are represented by interference (phase change) fringes, with each fringe cycle corresponding to 28 mm in range along the line-of-sight (LOS) direction between the ground pixels and satellite. Notably, most interferograms allow nearly complete spatial coverage of the phase change (fully coherent), including a half phase change in January - February 2006 interferogram because of the relatively short temporal and moderate spatial baselines between the orbits.

A dual pair differential interferometry, a robust analysis tool installed in SARScape 4.2 software was used. This function is an extension of the 3-pass (Zebker et al., 1994) and 4-pass differential interferogram. The execution of 3-pass or 4-pass depends on the input files as follows: For a 3-pass a single “master file” is used together with “two slaves” as input files. When “two masters” and “two slaves” are used as input files, a 4-pass approach is

implemented. The resampling method set among the input parameters is used for coregistration of the second pair into the first one i.e. focusing of pixels for time scale images by correcting relative translation shift, rotation and scale differences. The use of "two masters" spanning a period not affected by deformation and two slaves covering the deformation provides an intrinsic validation of deformation field. In order to cancel out the noise between two acquisitions (passes), filtering algorithm of Goldstein and Werner (1998) proved useful. The results are shown in Figures 3-2 to 3-6.

Table 3.1: Interferometric pairs

Number	Codes	Dates (yymmdd)	Track	Days	Baseline (m)	Ambiguity Height (m)
1	4098-4099	031027-031201	92	35	279	33
2	4102-4103	031027-031201	92	35	300	31
3	4093-4094	060103-060207	13	35	127	59
4	4117-4118	060213-060320	92	35	159	57
5	4047-4048	060314-060523	13	70	48	155
6	4119-4104	060703-060807	92	35	75	122
7	4094-4047	060207-060314	13	35	326	23
8	4093-4047	060103-060314	13	70	208	36
9	4094-4048	060207-060523	13	105	287	26
10	4093-4048	060103-060523	13	140	174	43
11	4093-4094	060103-060207	13	35	127	59

NASA's 3 arc second Shuttle Radar Topographic Mission (SRTM) digital elevation model (DEM) was used to remove topographic phase from the phase changes due to ground displacements and to geocode the interferogram. The SRTM DEM arc 3 has absolute vertical accuracy less than 16 m and a relative vertical accuracy less than 10 m (Falorni et al., 2005). These results were useful for comparison with those of 3 pass and 4 pass interferometry.

In order to quantify the deformation zone spatially (i.e. area of influence), the geocoded unwrapped interferograms were exported into a GIS software (ArcGis 10) and the outmost area affected by deformation was outlined into polygons (i.e. delineated the outmost lobes) as shown in Figure. 3-7. The area covered by each pair of interferogram was computed i.e. polygons for January-February and those of February-March 2006. The percentage change was computed from one pair of interferogram to the next one using January-February as a bench mark (i.e. literal growth rate) as shown in Table 3.2.

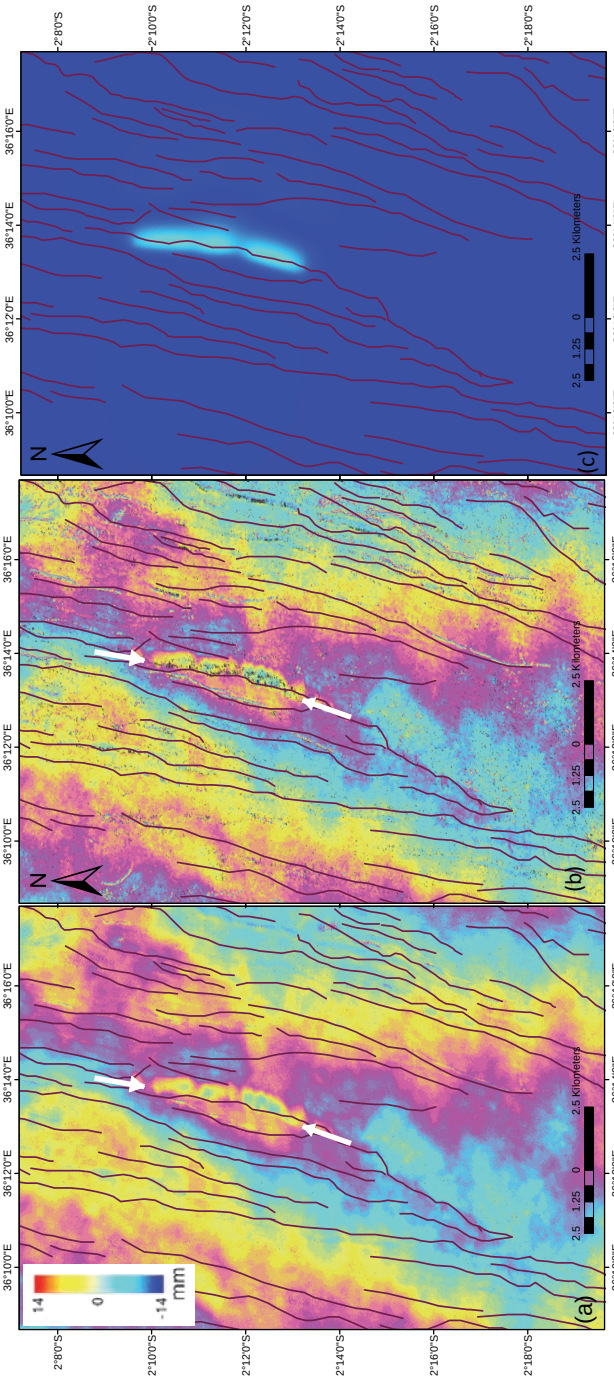

Figure 3-2. Interferogram and corresponding model results for January-February 2006: (a) Goldstein filtered. (b) Adaptive filtered. (c) Model.

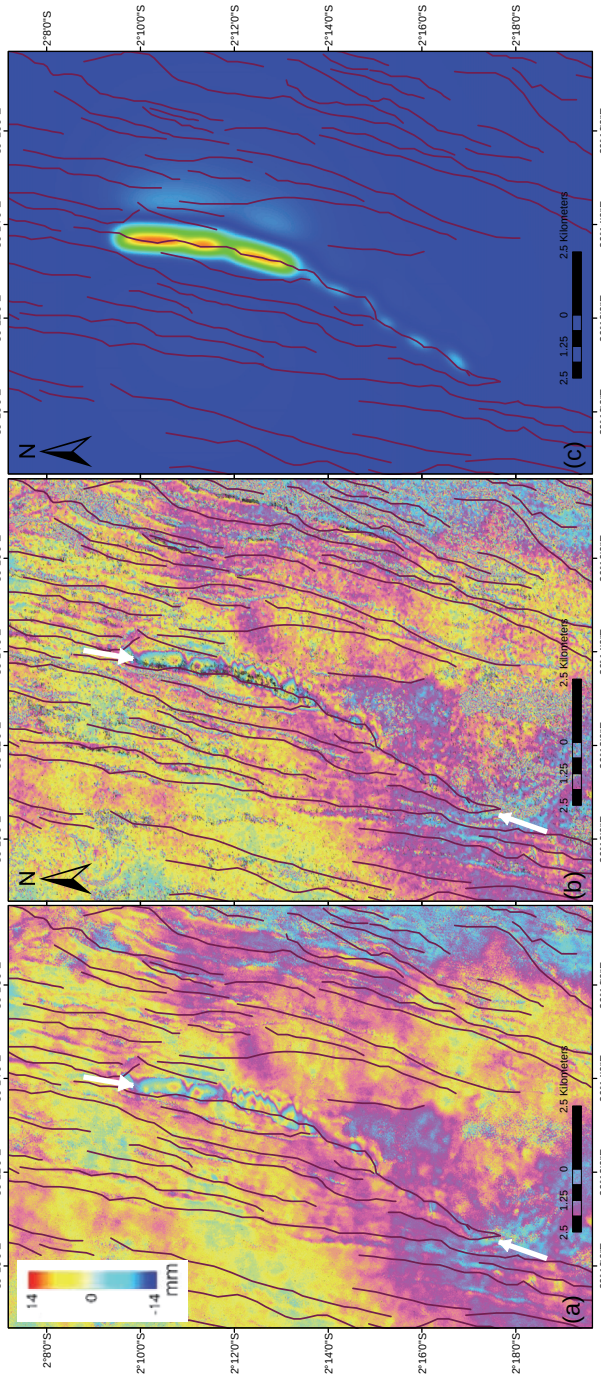

Figure 3-3. Interferogram and corresponding model results for February-March 2006: (a) Goldstein filtered. (b) Adaptive filtered. (c) Model.

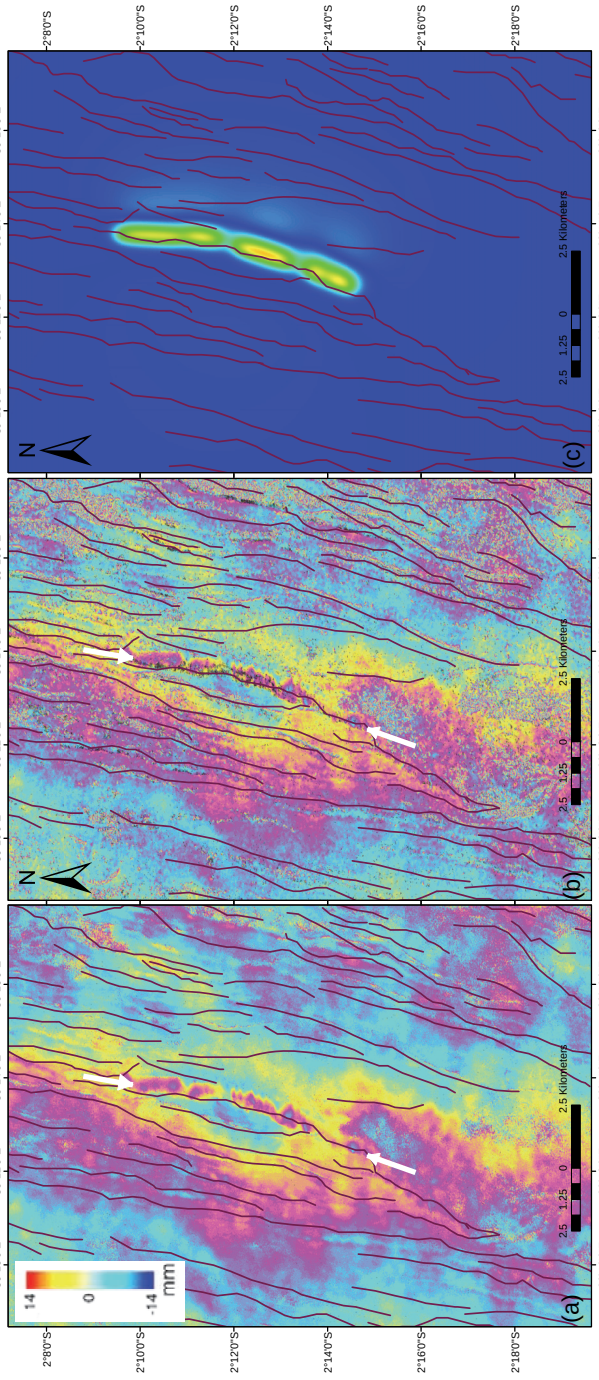

Figure 3-4. Interferogram and corresponding model results for January-March 2006: (a) Goldstein filtered. (b) Adaptive filtered. (c) Model.

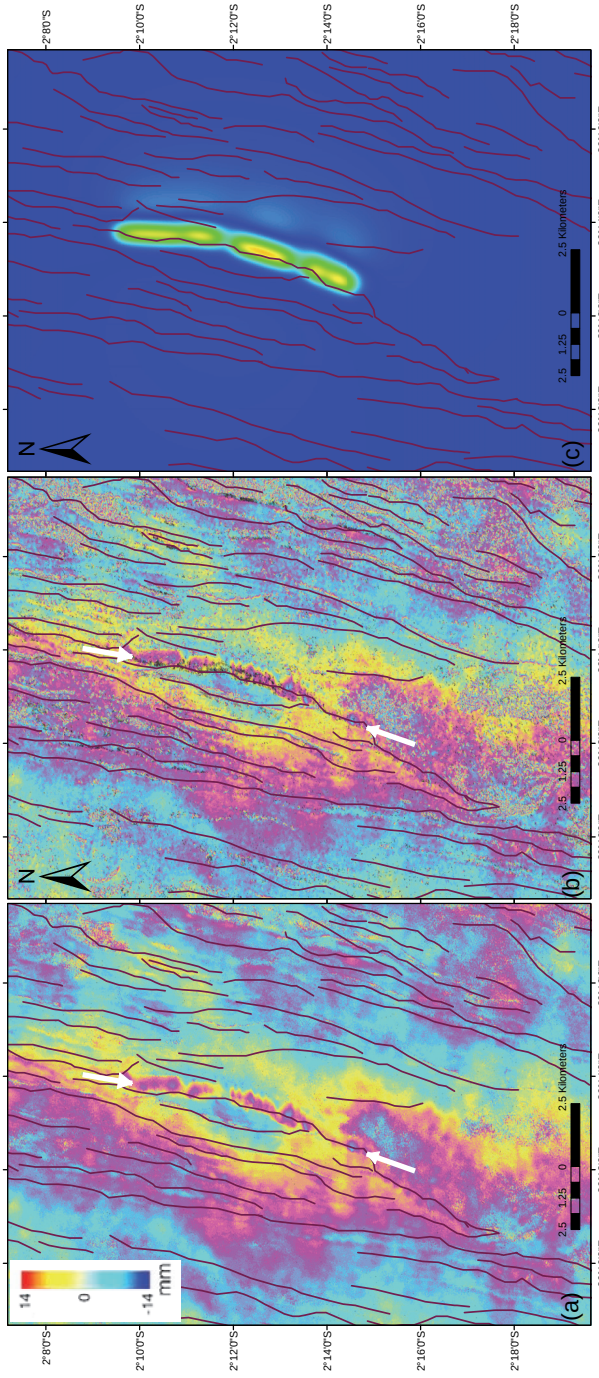

Figure 3-5. Interferogram and corresponding model results for February-May2006: (a) Goldstein filtered. (b) Adaptive filtered (b). (c) Model.

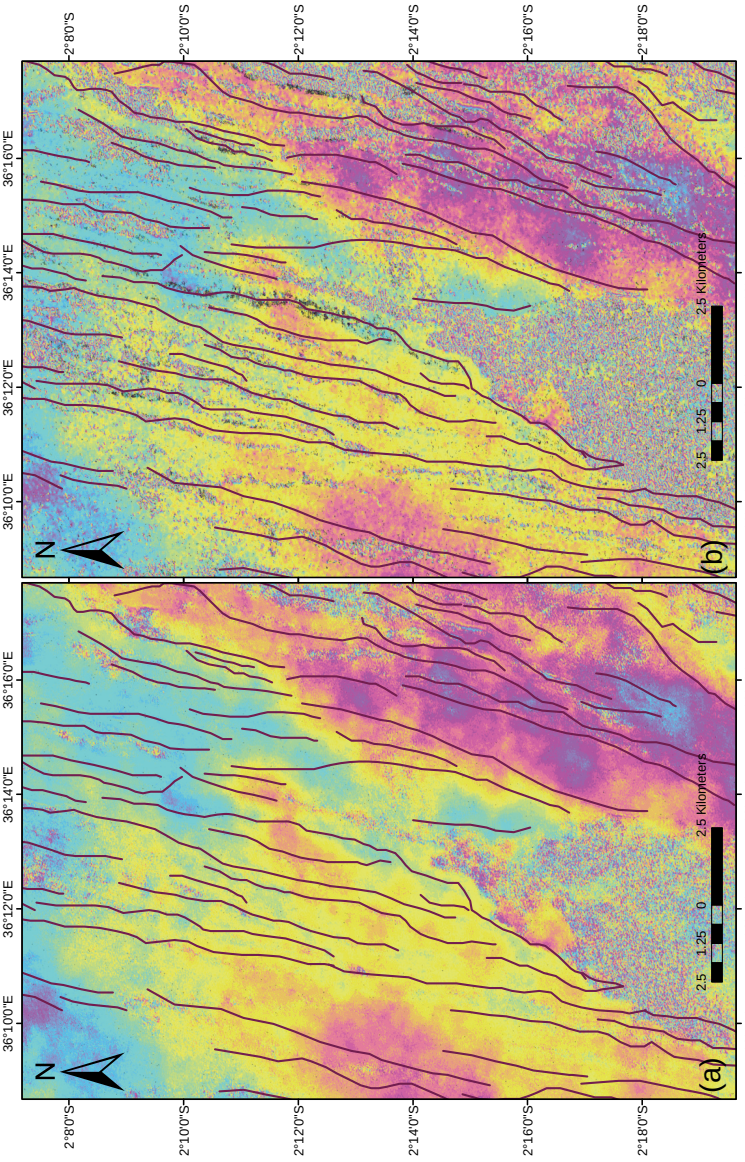

Figure 3.6. Interferogram of period not spanned by deformation i.e. March – May 2006: (a) Goldstein filtered. (b) Adaptive filtered.

Table 3.2. Areas defining deformation fields spanning the period shown (km^2)

No.	Jan-Feb	Jan-March	Jan-May	Feb-March	Feb-May
1	0.000016	0.000048	0.000045	0.000039	0.00005
	0.00001	0.000022	0.000032	0.00003	0.000023
2	0.000002	0.000053	0.000054	0.000059	0.000054
3	0.000033	0.000016	0.000015	0.000008	0.000016
4		0.000001	0.000009	0.000004	0.000002
5		0.000002	0.000004	0.000002	0.000003
6		0.000007		0.00001	0.000008
7		0.000003		0.000004	0.000003
8				0.000003	
9				0.000000727	
10				0.000002	
11				0.000002	
12				0.000003	
13				0.000004	
14				0.000009	
Total area	**0.000061**	**0.000152**	**0.000159**	**0.000180**	**0.000159**

3.3.2 Modelling of InSAR measurements

Theoretical models were developed to explain the deformation fields obtained from the InSAR observations. In particular, models based on solutions of Okada (1985) formulation of dislocation in a homogeneous elastic half space were used. For this purpose, a computer program developed by Tolomei et al. (2003) was used together with a code developed by Luis (2007) to calculate the range change values assuming the same radar line of sight at every pixel. For the purpose of modelling, the fault was assumed to be a simple rectangle divided into small segments (cells or patches) covering the entire length and width of area influenced by interferogram, being the largest deformation field. The initial slip parameters were inferred from wrapped InSAR data: first for January-February (initiation) and subsequently for all other interferograms (growth). During the entire modelling process, the deformation was assumed to be slip along a normal fault, which was inferred from topographic profiles (Figure 3-8).

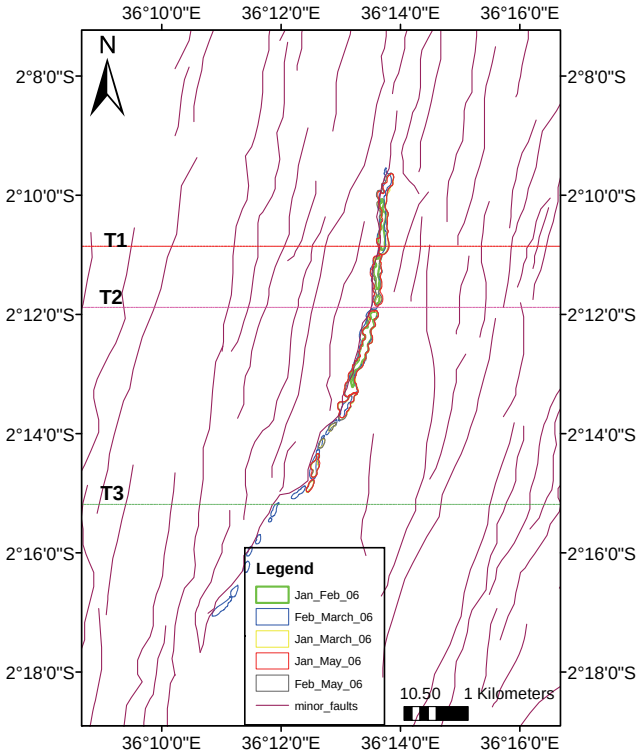

Figure 3-7. Shows outline of the outmost area affected by deformation (i.e. delineated polygons matching outmost lobes) that were used to compute the area shown in Table 3.2. The Traverse line T1, T2 and T3 marks the location along which the topographical profiles along the STRM DEM were extracted as shown Figure 3-8. Notably, the deformation fields remained constant after February-March (i.e. March to May) displacement apart from the isolated and segmented part where deformation fields were possibly obliterated by erosion or atmospheric delays along transmission path.

3.4 Topographical analysis

In order to characterize the relationship between the interferogram and topography, three traverse lines were established: two lines cross the area covered by the five interferograms while the third line covers the segment section with small and isolated displacements, characteristic of February-March deformation (Figure 3-7). It is notable that the deformation was constrained along almost vertical faults, indicating a dip slip displacement. In addition, this deformation is localized within the rift floor (axial zone), characterized by rather gentle slope which precludes possible landslide occurrence.

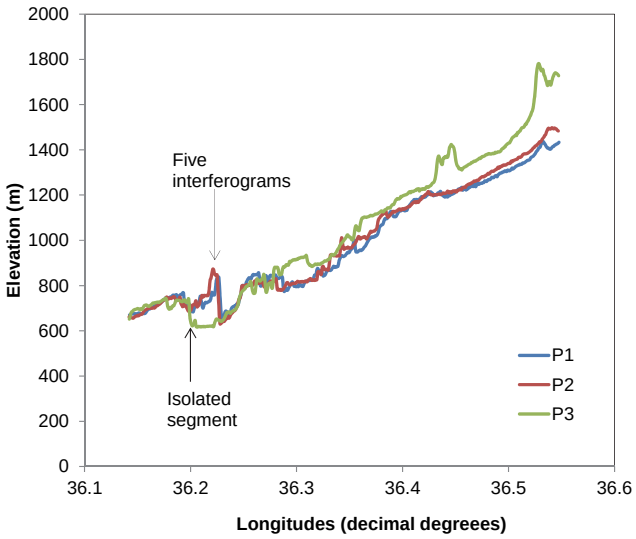

Figure 3-8. Shows the changes in topography across the deformation zone: Profile 1 covers the area of highest spatial displacement for the five interferograms spanning January-June; Profile 2 is across the narrowest displacement zone (partially connecting part) January -June; and Profile 3 traverses the small and isolated segments for February-March interferogram. Note all the displacement occurred along an existing fault line almost dipping at almost 90°. The correlation of the Profiles 1 and 2 discriminates the possible influence of the topography on the deformation fields i.e. both have similar topography but very different amount of deformation.

3.5 Results

The spatial pattern of deformation for the interferogram between January and February 2006 shows tapered elliptically shaped and segmented deformation fields that spread over a distance of ~ 5.9 km along a fault line. The deformed parts attain a maximum slip of 14 mm spread within the segmented fault system. Notably, each segmented unit is broader at its central part and narrow towards the northern and southern edges (Figure 3-2). This entire January-February deformation field was referred to as initiation part of fault reactivation.

The interferogram spanning the period between February and March 2006 (Figure 3-3) shows the most extensive deformation stretching over a distance of ~14.8 km. The deformation unit is dominantly divided into four partially jointed segments that were initially isolated for January-February deformation. Further south, the fringe patterns breakdown into small isolated deformation fields. The four jointed segments attain a length of ~9.8 km,

whereas the isolated segments stretch for about ~5.1 km. The deformation along the jointed segments is marked by complete fringes i.e. 28 mm and that of the isolated segments, similar to January-February interferogram, show half fringes (14 mm). Another notable feature is that the isolated segments show an echelon-shaped deflection from the main fault unit to join other small faults which signifies growth of the fault system.

For the rest of the scenes January-March (Figure 3-3), January-May (Figure 3-4), and February-May (Figure 3-5)) showed similar pattern of deformation to that of February - March but lacking the isolated segment part. This pattern remained remarkably uniform for the subsequent interferogram indicating that the initiated deformation in January – February reached its peak in February-March and remained constant. Indeed, Table 3.2 shows initiation of faulting activity covered a small area in January – February (6.0 x 10-5 km2), this area grew to 1.52 x 10-4 km2 by end of March. The most significant growth was observed between months of February and March (1.8 x 10-4 km2). The months of January-March and March-May indicate equal areas of deformation fields showing that there was no growth during this period. The result from simple elastic modelling shows that the displacement observed from InSAR measurements was as a result of slip of a blind fault oriented in NE-SW direction at depth ranging from 0.5 to 1.5 km and dipping at an angle of about 40° (Figures 3-2c to 3-6c).

A check for possible major earthquake for area affected by deformation from the international earthquake observatories (NEIC, USGS, GFZ, IRIS), showed that there was no single earthquakes from December 2005 to December 2006. However, for year 2007 (marking the seismic crisis period) earthquakes with magnitude as low as 4.2 are recorded in the area to the south.

It not clear why these possible earthquakes associated with earth surface deformation were not recorded by seismic stations but this could partly be due to a poor seismic station configuration in the year 2006 (a more dense configuration was installed in area in the year 2007 i.e. Baer et al. (2008) and Calais et al. (2008) or several earthquakes of small magnitude contributed to the rupture surface between two consecutive ENVISAT ASAR data acquisition (i.e. 35 day repeat pass).

3.6 Estimated earthquake parameters

An estimation of the earthquake parameters associated with the surface deformations observed in the months of January to March 2006 was carried out. In particular, addressing earthquake magnitude. For this purpose,

Kanamori (1977) scalar quantity referred to as seismic moment (Mo), was used as a measure of size of earthquake. The seismic moment is computed from the area of the fault rupture, the average amount of slip, and the force required to overcome the friction binding rocks mass that offset by faulting. The seismic moment is defined as:

Seismic moment (Mo) = μWLD (Equation 3.1)

Where μ is the shear modulus, W is the down-dip width of the rupture; L is the along strike length of the rupture and D is the average slip across the rupture plane. The parameter μ is commonly estimated to be about 3 x 1011 dyne/cm2 (30 GPa) in the crust. A higher value of 7.5 x 1011 dyne/cm2 or (75 Gpa) is estimated for the mantle. All the other dimensional parameters i.e. length, width and slip are computed in cm. To estimate the earthquake magnitude, the seismic moment determined in Equation 3.1 was substituted in Equation 3.2 and moment magnitude computed:

Moment magnitude (Mw)=2/3 LogMo-10.73 (Equation 3.2)

For the January-February deformation the length of rupture surface is 5.9 km, and slippage along the fault plane was 14 mm. The depth was computed to be between 0.5 and 1.5 km, which gives an average of about 1 km. Therefore, the computed seismic moment is about 2.478 x 1022 and the corresponding Moment magnitude is 4.19. For the February-March deformation the length of the rupture surface is 14.8 km and slippage is 28 mm along a 1 km fault plane. The seismic moment is about 1.2432 x 1023 and associated moment magnitude is about 4.66.

3.7 Discussion

The earth's surface deformation was monitored for a period of eight months using sequential interferograms facilitated by favourable acquisition of ENVISAT ASAR images, with 35-days repeat pass. Active deformation occurred within two months (January-March). The deformation that initiated as a small slip (5.9 km) along a normal fault propagated from north to south attaining a length of about 15 km. The non-prevalence of the deformation fields for the segmented part for the period from March to June could possibly be due to obliteration by erosion during long rains common in April-May or due to low resolution of the deformation field (less than a fringe) masked by other noise e.g. atmospheric delays.

Characteristically, the modelled deformation field (this research) initiated from north and propagated south wards in contrast to the deformation

associated with seismic crisis observed later in the year 2007 where slow slip recorded on a normal fault migrated from south to north (Calais et al., 2008). The two sites are located in the same tectonic regime separated by distance of 50 km.

Owing to the long faults and very low earthquake magnitudes prevalent in Kenya Rift, Ibs-von Seht et al. (2001) concluded that the two are uncorrelated, similar to Keir et al. (2006) for Main Ethiopian Rift. However, this study shows that over short temporal scale segment rupture (that involves nucleation and propagation of faulting process) is possibly related to small earthquakes (detection below instruments installed at the time) of low magnitude. Therefore, over repeated reactivation and growth, in longer temporal scale, the fault length and displacement outspans the seismic magnitude characterization. Indeed, segment rupture north of Lake Magadi is related to 1996 seismic crisis (Ibs-von Seht et al., 2001, Atmaoui and Hollnack, 2003, Kuria et al., 2010a), similar to the more recent seismic crisis (July-August 2007) and concomitant segment rupture around Lake Natron (Baer et al., 2008, Calais et al., 2008).

This observation helps to reconcile surface deformation with low seismicity. In addition, the result from simple elastic modelling show that the displacement observed from InSAR measurements was as a result of slip of a blind fault oriented in NE-SW direction at depth ranging from 0.5 to 1.5 km and dipping at an angle of about 40° indicate that first stage of normal faulting discussed by Baer et al. (2008) had actually started earlier. Therefore, a change in stress regime from buried faults (or dyke intrusions) initiates deformation. Subsequently, increase in stress results into fault growth (enlarge deformation field) by linking different fault segments and in the end long sub-parallel fault systems characteristic of actively extending regions are established. However, stress partitioning during an episodic growth (temporal) possibly due to deflection along growing and linking segments diffuses deformation and fault growth ceases as reflected by small and isolated deformation fields to the further south.

The estimates of the earthquake magnitude from the two rupture surfaces and their corresponding amount of slippage using Kanamori (1977) formulation of the seismic moment (So) and moment magnitude (Mw) were made. The earthquake magnitude for 5.9 km rupture surface corresponding to January – February deformation is about 4.19 and that of February – March deformation (14.8 km) amounts to 4.66. It is noteworthy, that whereas the expression for computing seismic moment has been in use for about three decades Kanamori (1977), the estimation of the parameters

(area and slip) used to compute it sourced from structural data are more often been characterized by large errors (Aki and Richards 2002). These errors arise from estimation of the part of the fault that ruptured, the magnitude of slippage along the fault line and width of the fault plane that ruptured, estimated from seismogenic layer. These errors propagate in computation of the final moment magnitude. It is apparent that, the results from the InSAR provides a precise estimation of these parameters and consequently improves the moment magnitude estimation. However, It not clear why these earthquakes associated with earth surface deformation (January – March 2006) were not recorded by seismic stations. This could partly be due to a poor seismic station configuration at the time (a more dense configuration was installed in area in 2007 i.e. (Baer et al., 2008) and (Calais et al., 2008) or several earthquakes of small magnitude contributed to the rupture surface between two consecutive ENVISAT ASAR data acquisition (i.e. 35 day repeat pass). All in all, the 4.19 and 4.66 are typical earthquake magnitudes of the rift floor and mark the earthquake potential of this area.

3.7 Conclusions

These results show a simple faulting mechanism, which is initiated from a small segment. With additional stress, the segments grow to connect or influence other segments and in the end a complex faulting system is established. It is noticeable that the fault nuclear, which was initially a linear segment, forms a flexure i.e. curvilinear shape. The increase in vertical displacement as fault segment grows (depicted by complete fringes) is contemporaneous to longitudinal growth. Therefore, as fault segment grow longitudinally and perpendicular to the minimum compression stress vector, an influence to other segment and fault ensues as reflected by dislocation or segmentation point. Towards south, the offset small fault (from the elongated segment) is seemingly unfavourably oriented with respect to the stress pattern at propagating fault tips and fault growth gradually diminishes or preferably ceases.

In conclusion, the earth surface displacement observed from InSAR measurements and subsequent elastic modelling may be explained by a slip along a blind fault oriented in NE-SW direction at depth ranging from 0.5 to 1.5 km and dipping at an angle of about 40° possibly related to deep seated dyke intrusion. Notably, the NE-SW fault growth is confined along a pre-existing fault and additionally supports E-W extension observed in Chapter 2.

CHAPTER 4

SUBSURFACE CHARACTERISTICS OF ACTIVE FAULTS: INTEGRATED GEOPHYSICAL MAPPING

This chapter is based on:

Kuria, Z.N., Woldai, T., van der Meer, F.D., Barongo, J.O., 2010. Active fault segments as potential earthquake sources: Inferences from integrated geophysical mapping of the Magadi fault system, southern Kenya Rift. J. Afr. Earth. Sci. 57 (4) 345-359. Part II.

and

Kuria, Z.N., Woldai, T., Opiyo_Akech, N. 2010. Imaging saltwater intrusion into coastal aquifers with electrical resistivity tomography at Lamu Island, South Coast Kenya. African Journal of Science and Technology 11 (2) 57-72.

4.1 Introduction

Geophysical exploration techniques have found a wide application in active tectonics. The improvement from 1D to 2D imaging/tomography has allowed a more precise delineation of the fault geometry, mapping faulting intensity, fluid conduits and detection of buried subtle tectonic structures such as fault displacement, folded bedding and weathering profile e.g. (Kuria et al., 2010a, Suzuki et al., 2000, Demanet et al., 2001, Kuria et al., 2010b). As a preliquisite to achieving optimal results, appropriate choice of the technique to apply dictated by geology, desired probe depth, resolution and also on field logistics i.e. topographical ruggedness, vegetation (type and density) is necessary.

Within Kenya Rift, gravimetric measurements in 70s marked the onset of geophysical studies (Wohlenberg, 1975, Fairhead, 1976, Fairhead and Girdler, 1972, Fairhead and Reeves, 1977, Girdler, 1978). This was followed by seismic reflection and refraction in mid 1980s (Achauer et al., 1992, KRISP Working Group Party, 1991) which accelerated in 1990s (Mechie et al., 1997, Keller et al., 1994b). Bouguer anomalies accrue from gravity studies (Birt et al., 1997) reflect low-density, westward dipping zone in the upper mantle to the west of the rift. The seismic studies along the KRISP line crossing the rift indicate low velocity zone within mantle centrally located below the rift i.e rift mantle velocities of 7.8 km/s, which increases to a range from 8.1 to 8.3 km/s on the rift flanks. According to Mechie et al. (1994) the low velocity zone deduced around Lake Magadi becomes anomalous towards the Kenya dome further north attaining respective velocities of 7.6 km/s and 8.0 km/s under rift and its flanks. Both seismic and gravity studies ascribe to presence of rising mantle plume initially inferred by Ebinger (1989). Subsequent work by Simiyu and Keller (2001) construed the upper crustal structure around Lake Magadi area. These studies largely provided regional perspective.

In order to allow for detailed evaluation of the axial rift faults, geophysical investigation was performed using a range of different scales and resolution i.e. resistivity tomography for the detailed shallow investigation, ground magnetics for moderate depths and aeromagnetic for deep investigation (i.e. refining basin structure). The geophysical investigations were coupled with detailed geological and structural mapping, which proved useful for constraining geophysical models. The aim of this integrated geophysical study was to determine the subsurface geometry of active faults, their deformation styles and possible constituents within fault zones (such as fluid, fine sediments) that affect tectonic movement.

In the selection of the study sites, the tectonic development of the Kenya Rift was reviewed as discussed by Baker et al. (1972b) and Smith (1994). They observed that with time there was a north to south rift propagation, and a shift in volcanism from the rift margins towards the axial part of the rift floor. This trend was accompanied by an increase in fault density and a decrease in fault length and displacement (Atmaoui and Hollnack, 2003). Therefore, the recent tectonic activity is mainly concentrated in the axial part of the southern Kenya Rift. Consequently, two study sites were selected along this tectonically active axial zone: one site to the north of Lake Magadi marked by an earthquake swarm activity (Ibs-von Seht et al., 2001) and a several kilometres long well preserved fault zone (caused by a 4.2 magnitude earthquake), and the second site is located south of Lake Magadi close to the location of the hot springs (Figure 4-1), an area of less earthquake activity, targeting 3 active faults (i.e. NE-SW trending faults (F1 and F3) separated by NW-SE fault (F2)) as shown in Figure 4-1.

4.2 Methodology

The methodology adopted in this research was dedicated to establishing fault geometry, characterising faulting activity and determining constituents within local active faults deduced in Chapter 2. The geophysical surveys include ground magnetics and electrical resistivity. The aeromagnetic data was additionally included.

4.2.1 Electrical Resistivity Tomography

Electrical resistivity data were acquired using IRIS Syscal R2 resistivity systems with 72 electrodes (Figure 4-2a). A wenner array configuration with electrode spacing of 5 m was used. The length of a single electrical resistivity tomography (ERT) profile was 360 metres (i.e. 4 cables with 18 take-outs at 5 metres interval). Roll along was performed in order to increase lateral distance of investigation. The maximum depth attained was 65 metres. Two profiles, ERT 1 and 2, were established in the area south Lake Magadi near the hot springs covering a distance of 450 m in E - W direction. Similarly, the other two profiles, ERT 3 and 4 were performed across the ruptured fault zone (in SW-NE and SE-NW direction) in the area north of Lake Magadi. The data were inverted to obtain true resistivities and depths using RES2DINV (Loke and Barker, 1995).

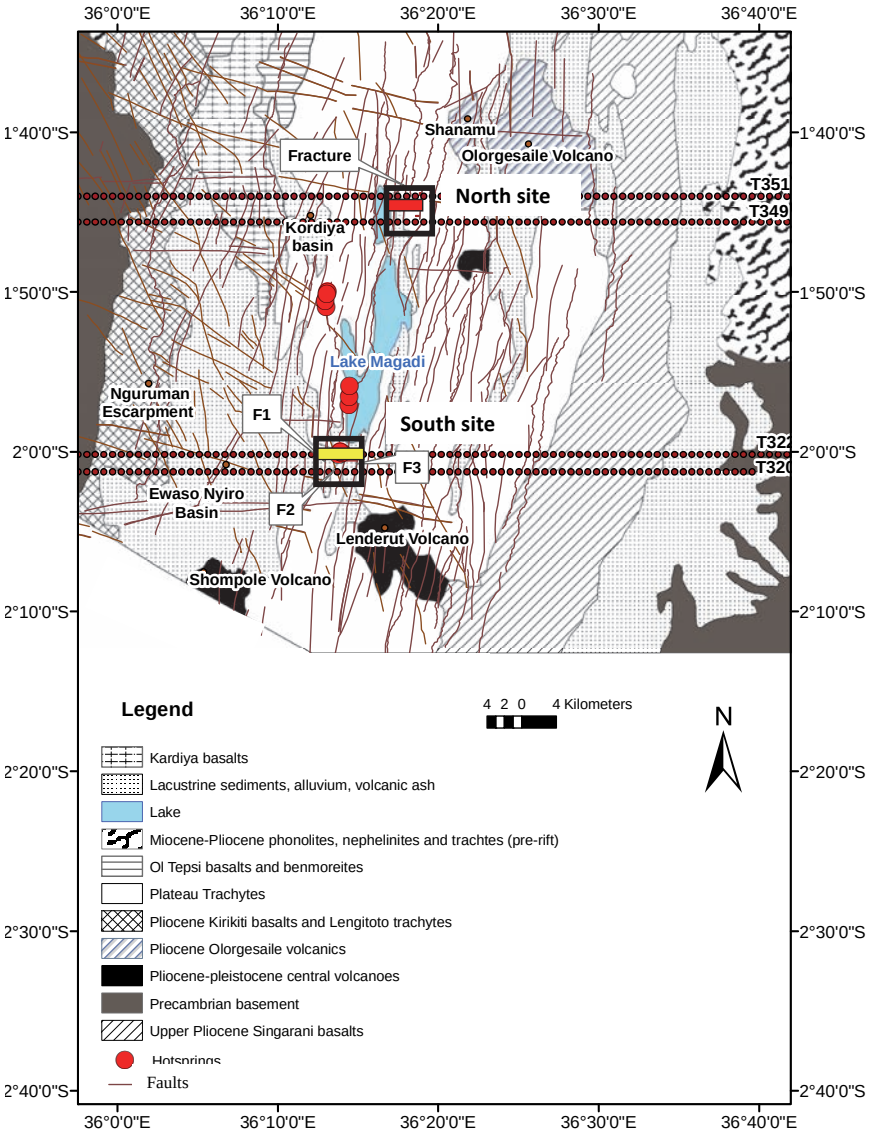

Figure 4-1. Shows lineaments on geological map of Lake Magadi area, south Kenya Rift, developed from ASTER DEM (30-resolution). The lineament trend N-S, dextral NW-SE, strike slip ENE-WSW and sinistral NE-SW. The black boxes to the north and south of Lake Magadi indicate the location of detailed investigations. Yellow patch inside the south black box indicate ground magnetic traverses and ERT profiles and red patch in north black box show location of ERT profiles. Long brown lines labelled T are aeromagnetic flight path lines.

4.2.2 Ground magnetic survey

Ground magnetic measurements were obtained using a proton precession magnetometer (Figure 4-2b), which measures the absolute value of the total magnetic field strength. Four traverses each 2.3 kilometres long running in E - W direction were established. Magnetic data for traverses 1 and 2 were acquired on 19th September 2008 and on 25th September for traverses 3 and 4. The traverses were bounded within two steep fault scarps separated by a monotonously flat terrain. The four traverses 1, 2, 3 and 4 had lateral separations of 55 m, 720 m and 380 m, respectively. The measured points were pre-selected and traced on the ground using an extrex GPS. A base station was selected at the central point, within the four traverses, that was free of any magnetic noise for the purpose of carrying out drift correction due to diurnal effects on the recorded magnetic data (Riddihough, 1971). The inter-station distance was maintained at 25 m intervals and both the magnetic reading and corresponding time observations were made at every station. The observed magnetic data were filtered to remove the drift due to diurnal variations. Noise due to secular change or epoch was considered negligible because the time separation between two base readings was maintained at about one hour.

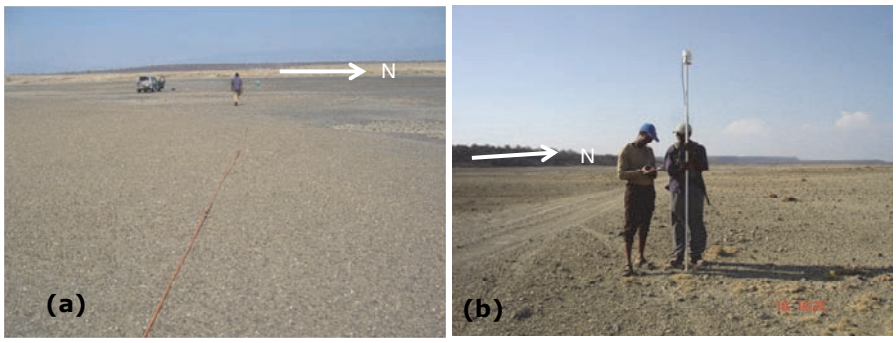

Fig.4-2. Shows examples of geophysical data acquisition in study area using Syscal Resistivity system (a) and Proton precession magnetometer (b).

After correcting for diurnal variations, the next step was to calculate the anomalous geomagnetic field. The background magnetic field was calculated through International Geomagnetic Reference Field (IGRF) 2005 model (a calculated magnetic intensity based on latitudes and longitudes) magnetic field of 33414 nT, inclination of -26.3˚ and declination of 0.002˚. The IGRF values were subtracted from the diurnally corrected observed values to determine the residual geomagnetic field responsible for local geo-magnetic anomaly. The accuracy of the magnetometer reading is + 1nT, while that of the reduced anomalies is + 5nT. The corrected geomagnetic field data were

used as input into 2D Euler deconvolution for quantitative analysis (i.e. the type of the source anomaly and depth to its upper surface) and hence constrain the subsurface geometry along the four traverse lines.

A 2D Euler deconvolution technique (Reid et al., 1990, Cooper, 2006, Cooper, 2008) was used to constrain the subsurface geometry along the traverse lines. Structural Index of 1, 2 and 3 were selected to obtain a 3-dimensional picture of faults for the area enclosed by the four traverse lines.

4.2.3 Aeromagnetic data analysis along profiles

Four aeromagnetic profiles (flight lines 320, 322, 349 and 350) stretching in E – W direction for a distance of about 209 km were extracted from the available database of grid Aeromagnetic data. Two of the profiles covered the area south of Lake Magadi crossing near the hot springs and within the 4 ground magnetic survey traverses. The other two profiles covered the area of earthquake swarm activity and marked with a most recent ruptured fault zone trending NE - SW located to the north of Lake Magadi. Similar to ground magnetic survey, the 2D Euler deconvolution technique was used. The results from IGRF model of the northern profiles were magnetic intensity of 33450 nT, Inclination of -25.613˚ and declination of 0.0675˚. While southern profiles had magnetic intensity of 33414 nT, inclination of -26.3˚ and declination of 0.002˚. All the structural indices were selected for comparison with the ground magnetic survey data. The interpreted models showing pole reduced data, the gradient data and location of magnetic sources are discussed under results. In order to constrain the upper crustal basin structure along the four aeromagnetic profiles structural index 1 (normal fault) was selected and the results compared with the previous works by Simiyu and Keller (1998).

4.3 Results

The results that have been grouped following the description provided under methodology for ease of reference.

4.3.1 Electrical Resistivity Tomography

The 2D resistivity models of the subsurface obtained from the 2D resistivity inversion of the field data traverses are shown in Figures 4-3a,b and Figure 4-3c,d. The most distinct feature retrieved from the inverted process of ERT Profile 1 (Figure 4-3a) is broad inverted funnel-shaped low resistivity zone (0.05 – 0.6 Ωm) delineated over the entire transect and bounded on both ends by a high resistivity body (> 5000 Ωm). The fluid conduit is sub-vertically inclined towards the western side as from a depth of 50 m. Similarly, low resistivity patches characterize the eastern fault boundary (F3)

indicating possibly an older conduit. The eastern fault boundary is vertical indicating activation of strike slip fault as from the depth of 20 m.

The ERT Profile 2 (Figure 4-3b) shows similar geo-electric structure, in terms of the shape and inclination of the faults to that of the Profile 1 (Figure 4-3a): the fault zone within Profile 2 is much narrow (180 m, i.e. between stations 100 and 280 m) compared to that of the Profile 2 (220 m i.e. 100 and 320 m) but characterized by lower resistivity values (i.e. 0.04 compared to 0.2 Ωm). In addition, the area defining the vertical fluid conduit is also very well resolved i.e. consisting of very well delineated geo-electric units. This observation can well be described as probably an increase in temperature of the hot-spring and therefore an increases the conductivity of the fluids.

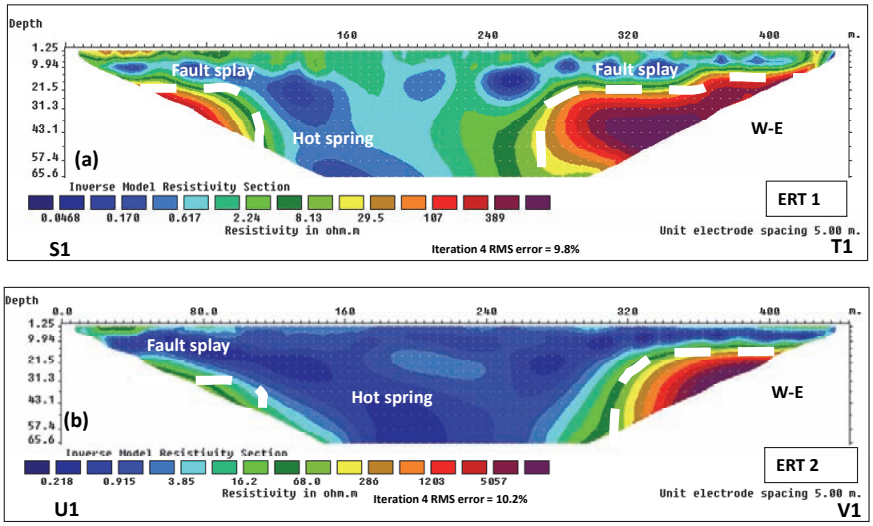

Figure 4-3a,b. Inverse resistivity models of ERT profiles. The labels W1–X1 and Y1–Z1 show the location of the ERT profiles on the corresponding ground magnetic profiles in Figure 4-5. The white broad lines indicate interpreted fault geometry.

The characteristic feature in Figure 4-3(c,d), located north of Lake Magadi, is a sharp vertical high resistivity structure buried by sediments to a depth of about 20 m. The high resistivities are confined in the central part of the rupture. The location of the feature coincided on the ground to the location of the ruptured fault zone, which was probed for a distance of about 60 m due to the difference in orientation of the rupture and ERT profile. This feature is interpreted to be an aperture filled with dry sediments or sheared part of the rock (~70 Ωm). The other poorly developed high resistivity zones to the south and north of the ERT profile are possibly effects of rupturing. A clear

disparity between faults at the north and south sites is the presence or absence of fluids within them.

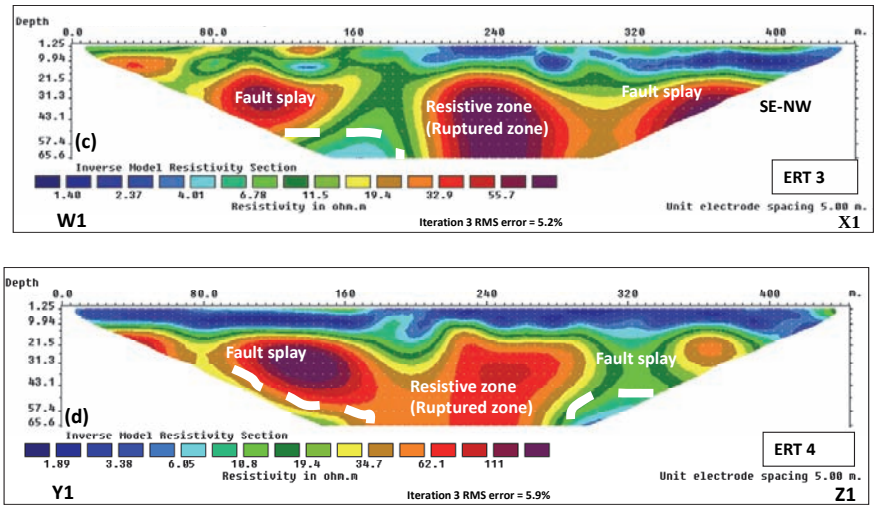

Figure 4-3c,d. Inverse resistivity models of ERT profiles. The labels W1–X1 and Y1–Z1 show the location of the ERT profiles on the corresponding ground magnetic profiles in Figure 4-5. The white broad lines indicate interpreted fault geometry.

4.3.2 Ground magnetic survey

At the south of Lake Magadi site, data was acquired along 4 ground magnetic traverses. The ground magnetic traverses had lateral separations of 55, 720 and 380 m. The aeromagnetic flight line path 320 was selected at the location of ground magnetic traverse 1 which also corresponded with the location of the ERT Profile 1. Similarly, the flight line path 322, ground magnetic traverse 4 and ERT Profile 2 had a common coverage near the location of the hot springs. The results from the 2D Euler deconvolution Profiles 1 - 4 (Figure 4-4) emphasizes fault morphology, faulting activity and fluid inclusion in the fault system.

A 2D deconvolution technique was used to constrain the subsurface fault geometry along the 4 traverse lines: Profile 1 (Figure 4-4a) that stretches over a distance of 2300 m depicts the 3 faults namely F1, F2 and F3 (Figure 4-4a). The profile shows scattered magnetic sources at the location of the three faults, which indicates tectonic movements.

Figure 4-4b shows traverse 2, a profile of highly disturbed magnetic signatures. The F1 zone broadens slightly while F2 is marked only by disturbed signatures indicating tectonically disturbed sediments not saturated

by fluids. The F3 similarly, shows deeper sources (Figure 4-4b). For the miniature faults, the subsidence is present but minimal. The fluid conduit attains a lateral extent of about 150 m and dips towards east at an angle of about 40˚.

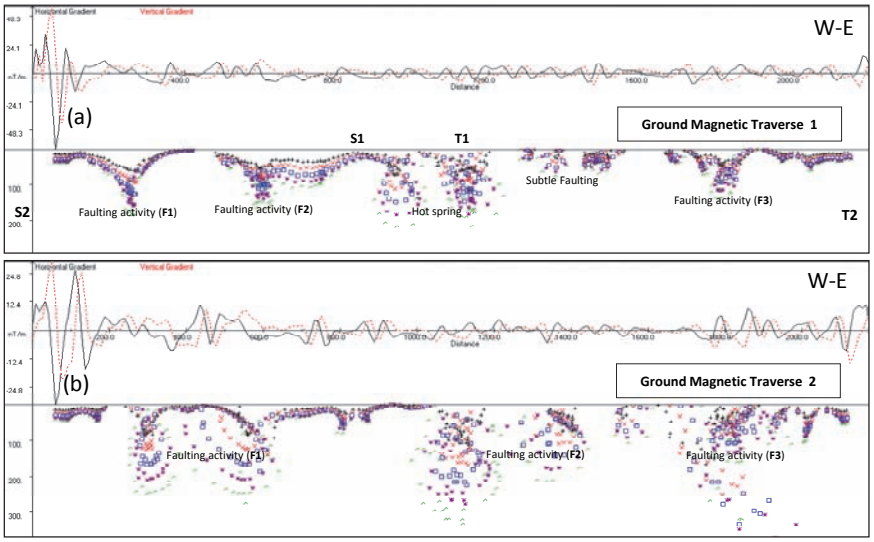

Figure 4-4a,b. 2D deconvolution of the ground magnetic traverses. The symbols indicate structural indices: 1st index (Black +), 2nd index (Red x), 3rd index (Blue□), 4th index (Purple *) and 5th index (Green ^). The labels S2-T2 show the location of the ground magnetic profiles on the corresponding ground aero-magnetic profiles Figure 4-7. For F1, F3 and F3 refer to the text.

The traverse 3 (Figure 4-4c) has no surface manifestation of the hot springs. It has 3 well established faults F1, F2 and F3; F1 and F2 show reduced scattering of the magnetic sources. The F1 indicates minimal disturbance of the magnetic signature, which possibly indicates less movement. The F2 attains a lateral extent less than 25 m but with shallow magnetic sources. The F3 indicates a similar western dip whereas the eastern fault boundary indicates an eastern dip. This could be explained by an intersection of two faults with different orientation. This is supported by the shearing of the magnetic anomalies at the depth of 120 m.

For Profile 4 (Figure 4-4d) F1 has a lateral extent of 250 m (stations 50 - 300 m) and shows magnetic sources to a depth of about 300 m. The magnetic sources are scattered. Two narrow and inclined (at dip angles of about 40˚) subsurface pathways indicate no magnetic sources at depths below 50 m. At the earth surface these points indicated cluster of hot springs, 20 m to the north of the traverse. Another surface manifestation of spring occurs at the

intersection of the F2 and traverse 4. The F2 is marked by an inverted funnel-shaped structure that extends to a depth of about 100 m with a lateral extent of about 50 m. The absence of the magnetic signal could be explained by presence of fluid saturated conduit (fault zone), which in this case has elevated temperatures. The manifestation of the 275 m wide zone with a cluster of hot springs could be explained by widened fault zone near the surface where fluid content within this zone is minimal (Figure 4-4d). Unlike the other two faults, the F3 marking the eastern end of the profile indicates highly disturbed (tectonically) rocks devoid of fluids dipping at an angle of about 45˚ with a lateral extent of about 100 m. From the results of ground magnetic survey, it is apparent that the faulting activity in the area south of Lake Magadi increases in north to south direction and the fluid content in the subsurface decreases in the same direction.

At the site to the north of Lake Magadi the ground magnetic traverses were located within a small open area (<350 m) bounded by very steep dykes on the eastern and western side. The results from this fine grid were only important in mapping the surface geological units and could not be used for probing depths greater than 30 m and have not been discussed further in this context.

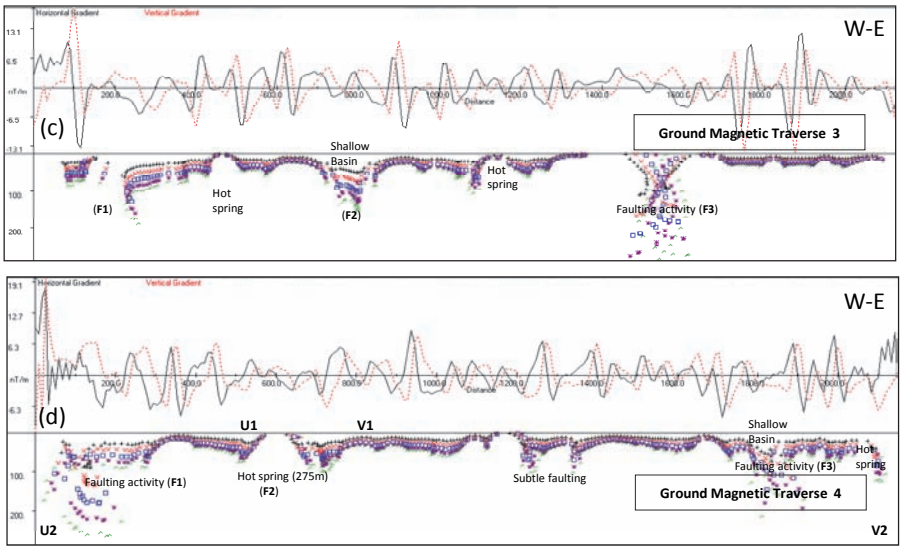

Figure 4-4c,d. 2D deconvolution of the ground magnetic traverses. The symbols indicate structural indices: 1st index (Black +), 2nd index (Red x), 3rd index (Blue□), 4th index (Purple *) and 5th index (Green ^). The labels U2-V2 show the location of the ground magnetic profiles on the corresponding ground aero-magnetic profiles Fig. 4-7. For F1, F3 and F3 refer to the text.

4.3.3 Aeromagnetic profiles

In order to probe increasingly deeper levels into the earth's subsurface two Aeromagnetic profiles; flight line paths 320 and 322 were selected for the area south of Lake Magadi. The results of flight path line 320 (Figure 4-5a) is characterised by 4 distinct trends: 1) western trend is characterized by subtle changes in both the frequency and amplitude of the magnetic signal. The combination of all the structural indices for this western section indicates highly disturbed magnetic signals characteristic of sedimentary zones or highly active fault zones devoid of fluids. The area is underlain by Tanzania Craton, geologically composed of metasediments, metavolcanics, granitoids and other intrusives (Baker, 1958, Shackleton, 1986); 2) high amplitude low frequency zone, which forms a clearly distinct dyke feature that almost reaches the ground surface marks the location of the Nguruman Escarpment (Figure 4-1). The eastern boundary of metasediments and the dyke is interspaced by a down-faulted sedimentary basin (Mara Plains) that attains a thickness of about 4 km. The eastern side of the basin is characterised by a dyke-like structure, whose eastern edge marks the location of Nguruman fault scarp dipping at 60˚ to the east; 3) A very high amplitude trend of positive magnetic anomaly corresponds to about 19 km wide half graben feature, with shallow western part (i.e. 4 km) and a much deep fault guided eastern edge (9 km). This deep edge is characterized by clear absence of the magnetic signal, which indicates presence of fluids at a depth of 9 km and possibly indicate source of the hot springs; and 4) a negative high amplitude and low frequency followed by a low amplitude signal marking the eastern edge of the basin. This 16 km fault zone is geologically composed of Pliocene basalts (Ol Kejo Ngiro Basalts); it marks the eastern boundary of the rift at Magadi area. Within the faulted zone the western bounding faults have marked magnetic sources at a depth of 9 km while the eastern faults attain a depth of 15 km. It was observed that despite the disparity in depth to the bottom of the western and eastern faults within this eastern faulted zone, the magnetic signatures were disturbed at both ends indicating possibly a common tectonic movement. The two parallel eastern rift boundary faults dip at 75˚ to the west, indicating steep inclination than on the western rift boundary at Nguruman scarp.

The flight line 322 (Figure 4-5b) indicates very similar trends in frequency and amplitudes to source of flight line 320 (Figure 4-5a) located 2 km to the south and therefore the architecture of the interpreted subsurface geological features are similar. The notable differences are the: 1) lack of the magnetic signal sources from the basin separating the craton and Nguruman escarpment. The basin on the western side of the dyke indicates some uplift and shearing. However, it is not clear why the magnetic sources between

Nguruman escarpment and the Magadi basin are missing; 2) The second basin (19 km wide at line 320) also indicates uplift at its western boundary and widening in its eastern side with clear shearing at the bottom of the faults. The zone devoid of magnetic sources that was identified as possible source of hot spring is clearly widened along flight line 322. This results tallies with the ground magnetic (Figure 4-4a,b) results that the fluid conduit widens towards the hot springs; and 3) the eastern faulted block indicates some disturbance of the magnetic signatures within the area underlain by basement rocks, this corresponds to a major 35 km long north-south trending fault (Matheson, 1958) that terminates before encountering flight line 320.

Flight line paths 349 and 351 were extracted for the area north of Lake Magadi. The Line 349 (Figure 4-5c) located about 27 km to the north of the line 322 (Figure 4-5a) has similar trends in amplitude and frequencies of the magnetic signals: On the western side of the flight path 349 the feature interpreted as cratonic boundary with the Nguruman escarpment lacks magnetic signatures but its widened. The twisted and uplifted basin at line 322 is either rotated or cut through by very deep faults with magnetic signatures extending to a depth of about 6 km. This indicates active deformation. The dyke feature is narrow but deeply faulted (6 km). The boundary between widened basin and eastern side of the basin indicates highly disturbed magnetic signatures.

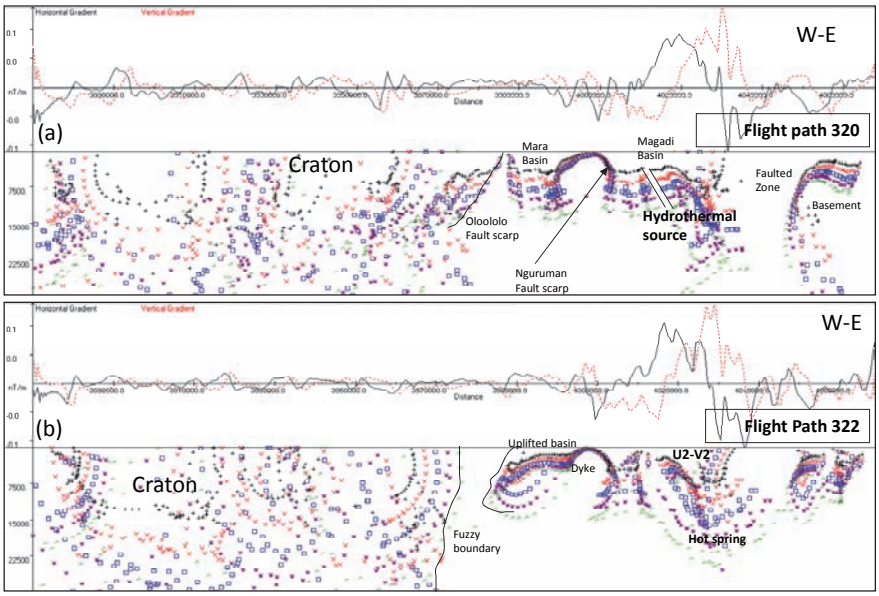

Figure 4-5a,b. Shows 2D deconvolution of the aeromagnetic flight path data 320 and 322. Magnetic sources have been interpreted to a depth of 22.5 km (on the vertical scale). Horizontal scale is AMMP coordinates in meters.

The second basin (19 km wide in line 320) has highly uplifted central parts and a shallow depth of about 2.5 km. The eastern faulted zone is narrow (6 km compared to 16 km at line 320) but has similar dipping angles of 75˚. Unlike at the other locations, the eastern fault zone is characterized by a step fault with magnetic sources at 2.5 km and slightly low angle (65˚) dipping fault on eastern side. The characteristic feature of the line 349 is that it indicates highly disturbed signatures within the entire profile and this could possibly be related to increased tectonic deformation.

The Figure 4-5d (line 351) indicates a cratonic boundary similar to that of flight line 320 i.e. bearing magnetic sources. The basin inter-spacing the boundary between craton and the dyke at the other locations (lines 320, 321, and 349) has been uplifted resulting into a single broad dyke. The basin uplift noted in line 349 for the second basin is much more enhanced at line 351, while its western boundary with the dyke has much reduced signals indicating a deep fault. The eastern fault zone is much wider (12 km) than line 349 and sheared at the bottom similar to line 320. The eastern end indicates a possible rotation or deep faulting followed by 2.5 km deep basement structure. Most significantly, a surface trace of the ruptured zone with depth revealed that the faulting activity occurs at a depth of about 5 km where two differently oriented faults intersect: the low angle eastern fault scarp (65˚

east) and high angle (85˚ west). The tectonic activity is confirmed by the presence of highly disturbed magnetic signatures.

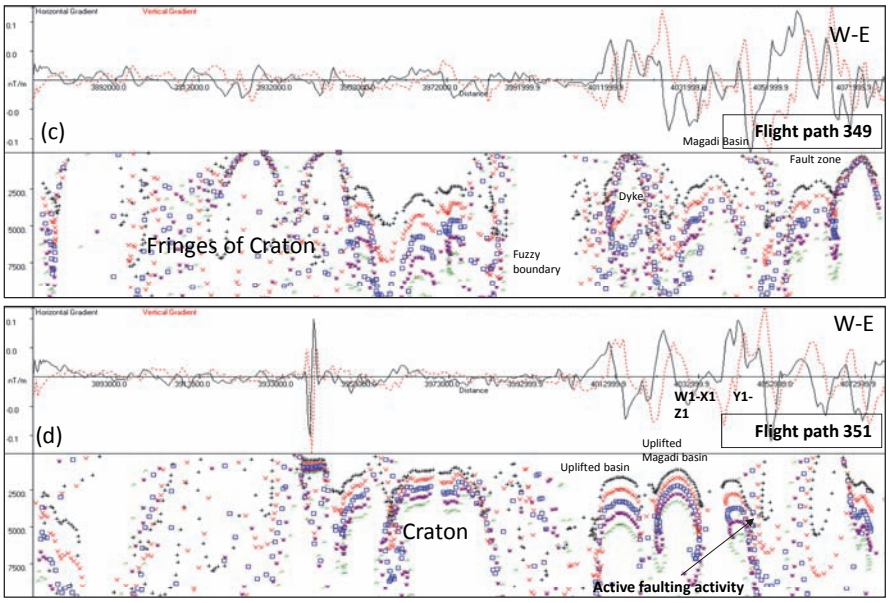

Figure 4-5c,d. 2D deconvolution of the aero-magnetic flight path data 349 and 350. Magnetic sources have been interpreted to a depth of 7.5 km (on the vertical scale) and horizontal scale is AMMP coordinates in meters.

The changes in the upper crustal structure are shown in Figure 4-6a, which is correlated to Figure 4-6b to the south. The basin changes from a well-developed basin structure to a highly rifted domal structure to the north, which indicates active tectonic deformation to north. The magnetic sources were interpreted up to a depth of 15 km to the north compared to 22 km to the south. The loss of magnetism to the north could be related to high heat possibly due to magmatic intrusion.

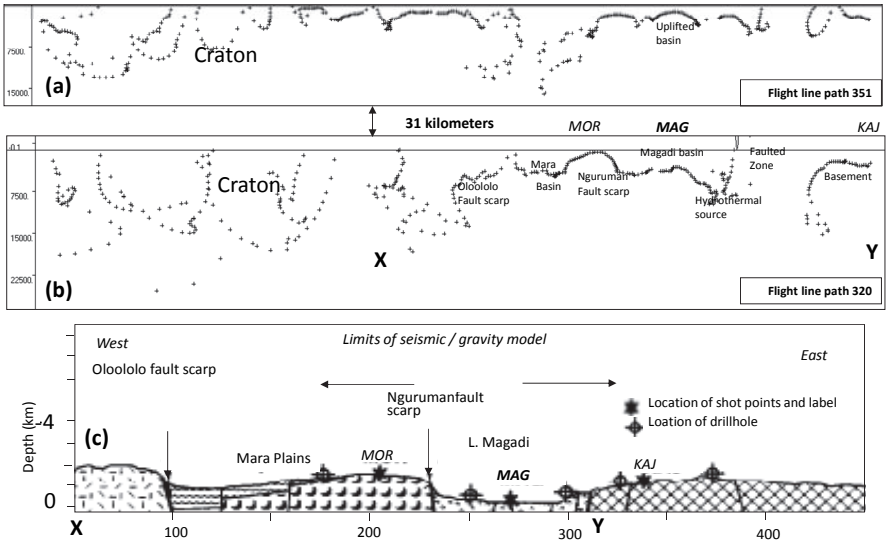

Figure 4-6a,b. Basin architecture deduced from 2D deconvolution of the two aeromagnetic flight paths (320 and 351) is correlated with the previous studies (c). Geological cross-section depicting the shallow structures across the Magadi region of the southern Kenya modified from Simiyu and Keller (1998): the section was compiled from drill hole data and geological reports. The labels X–Y in (b) and (c) show the common areas covered by the two profiles. The basin structure for (b) and (c) is similar indicating a highly correlated interpretation. Magnetic sources for (a) reach a depth of 15 km while that of (b) is 22.5 km indicating possibly magmatic intrusion causing loss of magnetism.

4.4 Discussion

Several geophysical studies have been conducted in the past to locate the suture between the Mozambique Belt and the Tanzania Craton (Nyblade and Pollack, 1992, Tesha et al., 1997, Simiyu and Keller, 1998) without much success. However, in this study the variability in magnetic signatures emanating from the diverse geological compositions of the rocks forming part of the Tanzania Craton (metasediments, metavolcanics, granitoids and other intrusives) provide a distinct boundary with the rocks of the Mozambique Belt that have a characteristic uniform magnetic signature. This provides the first step towards refining the boundary appropriately. A NW-SE trace of isolated low magnetic intensity patches located within a zone of moderate magnetic intensity, in our opinion, marks the location of ANL shear zone (Mathu and Davies, 1996). The moderate magnetic intensity with very small isolated low magnetic anomalies located between the Tanzania Craton and Ngurumani Escarpment provides leads as to the location of reworked rock of Mozambique Belt. This zone has equally been very challenging to define using gravity and seismic methods (Simiyu and Keller, 1998). In addition, this

study supports the interpretation from the gravity profiles across the rift valley in Kenya and Tanzania that contain a gravity low west of the rift valley, a signature from crustal thickening (approx. 5 km) associated with the suture (Nyblade and Pollack, 1992, Tesha et al., 1997, Simiyu and Keller, 1998).

The 2D resistivity models of the subsurface obtained from the 2D resistivity inversion of the four ERT profiles executed at the two sites (south and north of Lake Magadi) provides insights into the subsurface location of the faults; the type of fault (from fault inclination) and the material infilling the faulted zone. The fault zones to the south of Lake Magadi are characterized by very low resistivities (0.05 and 0.2 Ωm) characteristic of hydrothermal-saline conditions (Kuria, et al., 2010b) with a very sharp resistivity contrast with the host rocks. However, to the north the fault zones are characterized by higher resistivities (55-75 Ωm), which indicate reworked or sheared sediments characteristic of active deformation. Based on the nature of the material in the fault zone, it is suggested (in this study) that the fault system delineated to the north of the Lake Magadi (swarm earthquake) support accumulation of stress and therefore becomes a potential source of earthquakes. The increased fluid content in the southern fault zones (conduits of hydrothermal solutions) explains lack of earthquake activity as suggested by Ibs-von Seht et al. (2001). The fluid within the fault zone provides lubrication that affects stress build up and therefore reduces seismicity.

The results from the 4 magnetic profiles, acquired across faults F1, F2 and F3 located south of Lake Magadi, show scattered magnetic sources up to a depth of 200 m. This indicates some on-going faulting activity. However, the fault zone containing fluids (hot springs) lack magnetic sources. The presence of faulting activity supports the results from structural analysis that NE-SW (F1 and F3) and NW-SE (F2) faults are active (Chapter 2).

The 2D inversion of the aeromagnetic data along the area south of the Lake Magadi indicated an upper crustal structure very similar in architecture to the one described by Simiyu and Keller (1998), which includes seismic, gravity and geological data set. The similarity of these two models indicates the reliability of the aeromagnetic data sets for the interpretation of the crustal structure.

The entire basin structure along the aeromagnetic profiles indicates an uplifted, and rotated/twisted Magadi basin to the north and a well- developed basin structure to the south, which is characteristic of active deformation and deep faulting in the north and less activity to the south. This supports works

by Baker (1986) and Smith (1994) who proposed north towards south rift propagation.

At Lake Magadi, the architecture of the asymmetry graben with an intra-rift horst was also clearly defined by the magnetic signature with the western graben attaining a depth of 3.5 km (Simiyu and Keller, 1998), which in this case is about 4 km (Figure 4-6). However, the eastern graben according to interpretation (based on this study) is much deeper (9 km), a zone characterized by a significant break in magnetic signatures at that depth, which is here interpreted as source of the hot springs, which were followed to the earth surface using ground magnetic survey and ERT profiles. To the north, the break in magnetic signature was not observed, instead highly disturbed magnetic signatures characterized the interaction of two different angled faults that indicate possibly a sheared zone (Fenoglio et al., 1995, Telford et al., 1990, Adepelumi et al., 2008). In addition, the morphology of the fault has been better resolved in this study including identification of a possible hydrothermal source which could support the hydrogeological models for hot springs proposed by Eugster (1970) and Eugster (1980). The hot spring source indicating geothermal manifestations do not occur on a regional scale (Martin and Morogan, 1988) and it was found out that they are located on the western deeper part of Magadi basin. This occurrence supports the heat flow considered by (Bailey, 1983) as an expression of focused mantle degassing.

In addition, the 27 km north-south basin structure studied in between the aeromagnetic profiles indicates a variable morphology from a well-defined basin to the south to uplifted, heavily fractured and deformed basin to the north. This kind of deformation according to this study is unlikely to be related to large-scale intrusions in the upper crust similar to findings by Swain et al. (1981); Henry et al. (1990); Keller, et al. (1994a); Birt, et al. (1997) but is undoubtedly related to some magmatic intrusion (Swain, 1992).

The shallow magnetic sources interpreted up to a depth of 15 km to the north compared to 22 km to the south indicate loss of magnetism with depth due to high heat flow (Bailey, 1983) and supports active rifting model due to magmatic intrusion similar to works by Ibs-von Seht et al. (2001); (2008).

4.5 Conclusions

Three different but complementary geophysical techniques comprising of electrical resistivity imaging, ground magnetic survey and aeromagnetic data with different vertical and horizontal resolution were used to define the

subsurface geometry of active faults and deformation styles including features that affect tectonic movement such as fluid inclusions. The study complements the results of the previous papers on: a) mapping subsurface geometry of the seismically active faults (Ibs-von Seht et al., 2001) where only earthquake data was used, now subsurface geometry of the faults has also been determined; and b) works on basin morphology (Simiyu and Keller, 1998), which included data sets from drill hole, geology and seismic refraction. In addition, it provides a combination of techniques which could be used for mapping buried fluid conduits within areas characterized by rocks with high magnetic susceptibility.

The low resistivities (0.05 and 0.2 Ωm) for southern faults indicate hydrothermal-saline conditions, which contrast with the higher resistivities (55-75 Ωm) to the north that show reworked or sheared sediments characteristic of active deformation. Therefore, the presence of fluid explains lack of earthquakes to the south, whereas the resistive materials infilling fault zone support stress build up and becomes a potential earthquake source. In addition, the results from ground magnetic data have revealed faulting activity within active fault zones that do not contain fluids.

The interpretation of the aeromagnetic data indicates that a rotated/twisted Magadi basin to the north and a well-developed basin structure to the south, which is characteristic of active deformation and deep faulting in the north and less faulting activity to the south. This observation support works by Baker (1986) and Smith (1994) who adduced north towards south rift propagation. Additionally, the aeromagnetic results showed major vertical to sub vertical faults (dipping 75-85˚ east or west); a boundary between Tanzania Craton and Mozambique Belt; a refined architecture of the asymmetry graben with an intrarift horst, whose western graben is 4 km deep and eastern graben is much deeper (9 km), with a zone showing significant break in magnetic signatures at that depth, interpreted as source of the hot springs south of Lake Magadi (a location confirmed near surface by ground magnetic and ERT data sets). The shallow magnetic sources to the north of Lake Magadi possibly caused by high heat flow could be explained by presence of magmatic intrusion that supports active rifting model.

The changes in fault morphology, even within a short lateral distance (i.e. 2 km between adjacent flight lines), attest to a very heterogeneous crust and support discretisation of the basin scaled investigations.

CHAPTER 5

CRUSTAL THERMAL REGIME FOR CENTRAL TO SOUTHERN KENYA RIFT: IMPLICATION FOR GEOTHERMAL RESOURCES

This chapter is based on:

Kuria, Z.N., Woldai, T., van der Meer F.D., Barongo, J.O., Noomen, M., Komolafe, A., van der Meijde, M. 2010. Crustal thermal regime for central to southern Kenya Rift: implication for geothermal resources. Accepted: Geothermics; International Journal of geothermal research and its application.

5.1 Introduction

The Paleogene to Recent Kenya Rift belongs to the eastern branch of the great continental East African Rift System (EARS) that stretches over 4000 km from afar Triangle to southern Mozambique. The Kenya Rift forms a classic graben averaging 40-80 km (Kabede, 1989, Baker and Wohlenberg, 1971, Baker et al., 1972a) and is considered as a continental rift in the initial stage of continental breakup (Achauer and Masson, 2002, Chorowicz, 2005). This rift, an intracontinental divergence zone, is superimposed on the eastern margin of the East African plateau and is located close to the boundary of the Tanzanian Craton and the Pan-African Mozambique shear belt (Baker et al., 1972a). To the further south, the classic rift graben dwindles into a broad depression marking the Northern Tanzania Divergence (Macheyeki et al., 2008).

Characteristically, the Kenya Rift has tectonism accompanied by intense volcanism dated Paleogene to Recent (Baker et al., 1971b). The volcanic centres located along the rift include Suswa, Olkaria, Eburru, Menengai, Paka, Silali, Emuruanngogolak, Namarunu and Barrier (Figure 5-1). Most of these volcanic centres had one or more explosive phase including caldera collapse (Baer et al., 2008, Calais et al., 2008, Simiyu, 2010). In addition, the volcanic centres are punctuated with hydrothermal activity (Riaroh and Okoth, 1994) and therefore envisaged to host extensive geothermal systems (Simiyu, 2010). This observation had been affirmed by Cantini et al. (1990) who noted high heat flow regional anomaly characterizing Naivasha trough, and suggested that this anomaly is supported by the occurrence of Olkaria, Suswa and Longonot volcanoes. Other important locations with significant geothermal manifestation in the rift floor include Arus, Lake Bogoria and Lake Magadi (Omenda, 2001).

Currently, geothermal energy is being utilized only from Olkaria field generating (167 MWe), although proven geothermal resource are estimate at 450 MWe (Simiyu, 2010). This indicates that the exploration of the geothermal resources, despite having started in 1970s, is still at youthful stages. Therefore, there is not sufficient understanding of the thermal anomalies and their characterization to geothermal resources along the central to southern Kenya Rift.

Noteworthy, numerous geophysical investigations have been carried in the past with the efforts to constrain crustal structure within the Kenya Rift. These include: delineation of a narrow mantle plume around equator (Fairhead, 1976); establishing a Moho boundary at 35 km within the central rift to 24 km around Lake Turkana e.g. (Prodehl et al., 1994b); constraining

lithospheric structures using gravity measurements e.g. (Swain and Khan, 1977, Swain, 1992, Simiyu and Keller, 1997, Mariita and Keller, 2007) to determining the crustal basin structure of the southern Kenya Rift including the sediment-infill using geology, borehole seismic and gravity measurements e.g. (Simiyu and Keller, 1998, Simiyu and Keller, 2001); Magnetotelluric studies within rift (Rooney and Hutton, 1977), Baringo rift basin (Hautot et al., 2000), southern Kenya rift (Simpson, 2000, Meju and Sakkas, 2007); to seismological studies (Tongue et al., 1992, Young et al., 1991, Ibs-von Seht et al., 2001, Ibs-von Seht et al., 2008). Despite all these efforts thermal structures remains poorly resolved in the area.

A more related approach to characterize the thermal conditions on the rift floor were previous heat measurements within the rift floor that recorded a mean value of 105 ± 51 (sd) mWm^{-2} computed from 15 samples within rift floor (Morgan and Wheildon, 1983, Morgan et al., 1986, Williamson, 1975, Ebinger et al., 1991). For the Mozambique Belt and Tanzania Craton the estimated heat flow values were average of 64 mW m-2 (sd=19 mW m^{-2}; se = 4 mW m^{-2}) and 33 mW m^{-2} (sd=10 mW m^{-2}; se=3 mW m^{-2}) Nyblade (1997) and Nyblade et al. (1990). Estimates of 57 ± 17 mW m^{-2} (using 4 samples) and 39 ± 21 mW m^{-2} (from 10 samples) for eastern and western Kenya Rift shoulders were recorded (Morgan and Wheildon, 1983, Williamson, 1975). Notably, these heat flow measurements are highly variable (as depicted by their error margin), too widely spaced and therefore insufficient to understand their correlation over a wide area involving various tectonic settings.

Despite all these previous approaches, it is apparent that no efforts have been made to characterize geothermal gradient and geo-temperature distributions for the central to southern Kenya Rift from estimates based on Curie isotherms like in other areas e.g. (Shuey et al., 1977, Blakely, 1988, Espinosa-Cardeña and Campos-Enriquez, 2008, Li et al., 2010). This approach is relevant in study area because in areas of high heat flow (as noted at Olkaria geothermal field (Simiyu, 2010)) the depth of the magnetic sources is temperature controlled and Curie isotherm marks such a thermal boundary (Wasilewski and Mayhew, 1992). In line with these observations, this study was carried out with the purpose of determining the Curie point depths, establish whether they represent Curie isotherm or compositional boundaries (using Moho boundary) and interpret them in terms of geothermal potential for the area stretching from central to southern Kenya Rift (Figure 5-1).

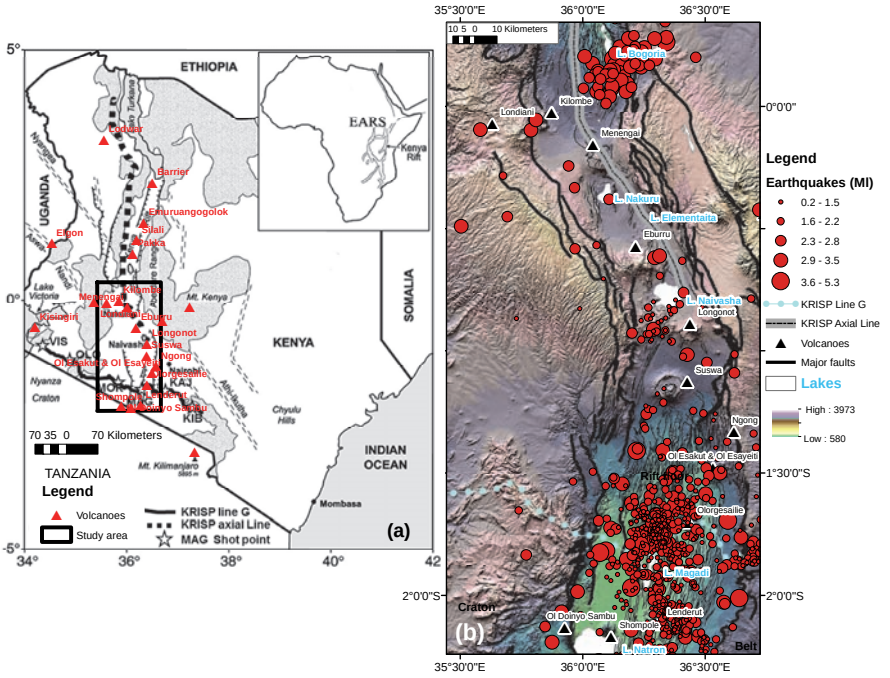

Figure 5-1 (a) Location of the study area, East African Rift System including volcanoes along Kenya Rift and study area marked in bold rectangle (b) SRTM DEM showing tectonic structures marked by rift escarpment. Grey line dotted black marks KRISP axial line and light blue line with rounded markers is traverse of KRISP Line, along which the Moho depth, topography and Curie point depth were extracted and used to plot Figures 5-9a and 5-9b.

5.2 Geology and geothermal manifestation

A detailed review of the geological setting is provided for clear understanding and interpretation of the magnetic anomalies detailed hereafter. The geology of the central to southern Kenya is largely controlled by the tectonic provinces namely Tanzania Craton, Mozambique Belt and upper Cenozoic formations, characterizing the rift floor (Figure 5-2a). In addition, a number of central volcanoes occur within the rift floor marking more localized geology (Baker et al., 1971a).

Geologically, the Tanzania Craton falls under granite-greenstone terranes dated 3.10 to 2.55 Ga comprised of the older Nyanzian group with overlying younger Kavirondian group (Mathu and Davies, 1996). Metavolcanics of the Nyanzian group range from tholeitic basalts (with pillow structures) to calc-alkaline andesites, dacites, rhyolites including pyroclastic agglomerates and tuffs and ashes (Opiyo-Akech, 1988, Ichang'i and MacLean, 1991, Mathu and Nyambok, 1993). The younger group (Kavirondian) consists of basal

conglomerates, greywackes and sandstones with shale and mudstones that occur at the top (Ngecu, 1993).

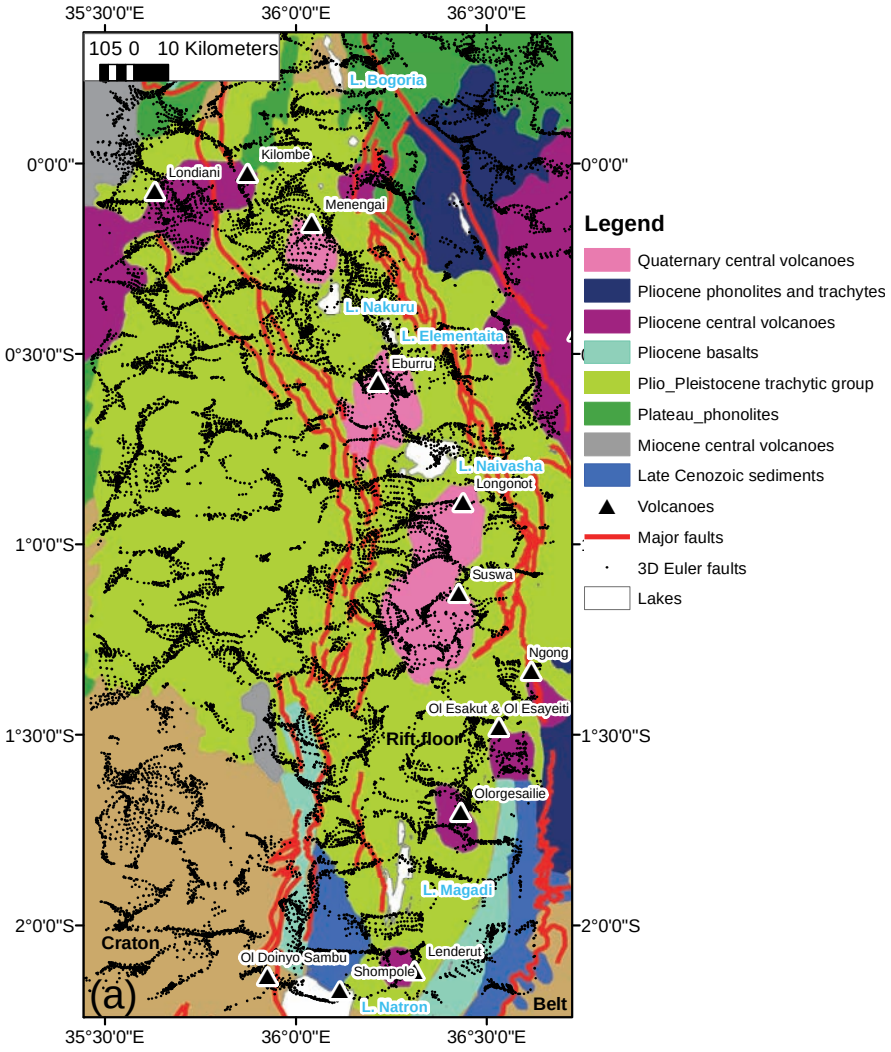

Figure 5-2a. Geological map showing Cenozoic formation (comprised of extensive plains/plateaus and central volcanoes) along rift valley. SW and SE parts mark Tanzania Craton (granite-greenstone terranes) and Mozambique Belt rocks respectively – modified from Baker et al. (1971). Superimposed on the geological map are faults (black linear marks) deduced from 3D Euler deconvolution.

The Mozambique Belt, a Neoproterozoic Mobile belt dating 1.0 – 0.5 Ga (Cahen et al., 1984, Stern, 1994) is comprised of medium to high grade metamorphic rocks i.e. schists, gneisses, migmatites, graniulites, granitoid gneisses and granites. Most of these rocks are re-worked (Simiyu and Keller, 2001). Other common rock types within the belt include amphibolites, serpentinites, quartzites and marbles but the diorites, gabbos and unltramafic are more widely scattered (Mathu and Davies, 1996).

An important structural feature is the NW-SE trending zone of ductile shear known as Anza-Nandi-Loita (ANL) thrusting in the underlying Precambrian basement (Smith and Mosley, 1993). The geological significance of the shear zone is the distribution of the strongly alkaline carbonatitic volcanism along the craton margin (Smith, 1994). It is suggested, from the generation depth for carbonatites, that the lithosphere is about 90 - 100 km of olivine poor nephelinitic and carbonatitic volcanism within East Africa (Wendlandt and Morgan, 1982).

According to (Baker et al., 1971a) the Cenozoic formations are categorized into: 1) extensive formation showing marginal lateral variation comprising plateau and plains, which connotes a fissure or numerous localized eruption centres; 2) central volcanoes with distinct volcanic series (Williams, 1969, Williams, 1970) as shown in Figure 5-2a. Characteristically, the plateau phonolites outcrop on both the western and eastern parts of rift in central Kenya, being the dominant formation around Lake Nakuru. It overlies the Miocene basalts, a formation that stretches further north into Lake Turkana, where it overlies Miocene sediments or Precambrian rocks. In southern Kenya, plateau phonolites form the major (outcropping) geological formation on western part of the rift. The plateau phonolites are dated 11.0 to 13.5 Ma. Mid Pliocene phonolites and trachytes outcrop along outermost boundary fault in the central Kenya Rift about 50 km NW of Lake Bogoria. Further south, the formation is localized along the eastern margin outcropping about 40 km NE of Lake Nakuru and 60 km NE of Lake Magadi. These formations are dated 6 to 7 Ma. Pliocene basalts occur on the down-faulted marginal rift faults in the southern Kenya Rift, Lake Magadi area. To the further north, the formation is overlain by younger volcanics (Baker et al., 1971a) with relatively extended age limits (8.3 to 2.5 Ma). Plio-Pleistocene trachytic group covers almost the entire floor of the central to southern Kenya Rift and along margins of the some central volcano (Baker et al., 1971a). The group consists of lower trachytic tuff which is prominently featured around Lake Nakuru. The upper part of the group comprises Plateau trachytic series of Magadi area (Baker, 1958, Baker, 1963). North of Lake Nakuru this formation stretches to Lake Bogoria area. The lower group is dated 2.5 to 5.0 Ma and

the upper group is within a range from 1.7 to 0.6 Ma. The Quaternary basalts occur in small isolated cones within 250 km east of the rift floor, with linear structures that suggest a fissure control in their evolution. These basalts are dated Late Pleistocene to Holocene age, the precise age determination using radiocarbon dating of the Chyullu Hills basalts is 480 ± 200 years (Saggerson, 1963).

The geology of the Quaternary volcanoes aligned long the rift floor is variable: Suswa consists of basal trachytes overlain by welded ignimbrites with phonolitic lavas and thick pumice forming the upper most geological formation (Riaroh and Okoth, 1994). The caldera floor has fumaroles (highest temperature 96°C) and gas geothermetry that has recorded a temperature of 370°C (Allen et al., 1989). The geology of Longonot is characterized by pyroclastics of trachytic composition (Clarke et al., 1990), notably weak fumarole showings are present (Riaroh and Okoth, 1994). Olkaria is formed of a cluster of numerous steep sided domes (about 80) composed of either lava and pyroclastic or thick lava flows (Clarke et al., 1990). The outcrops comprise of comendite or peralkaline rhyolites. According to Riaroh and Okoth (1994) hot fumaroles, hot and altered ground, silicified pumice and lithic fragments are geothermal markers in Olkaria volcano. Eburru is a Quaternary rhyolite volcano similar to Olkaria. Argillic alteration and fumarole activity mark geothermal activity. Menengai is a product of explosive volcano with trachytic lavas in the crater and pumice, obsidian and scoria forming the rim. It is apparent that the geological composition of the volcanoes is highly variable, certainly causing variable magnetic signatures.

Characteristically, numerous hot springs along the shores of Lake Magadi mark the geothermal activity; the hottest springs (80-90 °C) are located on the northern shores while the other springs attain temperatures of about 32-44°C (Riaroh and Okoth, 1994). On contrary, Lake Bogoria display the spouting stem jet, fumaroles and hot ground indicating relatively increased geothermal activity.

5.3 Aeromagnetic data

The aeromagnetic dataset used in this research is part of the African Magnetic Mapping Project (AMMP) which compiled airborne magnetic data covering most parts of Africa (Barrit, 1993). The aeromagnetic data of the study area was acquired in the year 1987 by Compagnie Générale de Géophysique, a French Seismic Acquisition and Processing Services Company with line spacing of 2 km and flight direction of 90° running in W-E direction at a flying height of 2896 m above mean sea level. Aeromagnetic data was acquired along a total of 241 flight lines (each at 2 km line spacing) and each

flight line covered an average distance of about 148 km i.e. the total area covered was 148 km by 482 km.

In addition, aeromagnetic data was acquired along 16 cross over lines running in N-S direction. The magnetic data was pre-processed by AMMP that included levelling correction and regional field removal (using IGRF model of 1987 with field strength of 33383 nT, Inclination of -35.4°, declination of -1.4° to the south, and 33949 nT, Inclination of -21° declination of -0.13° to the north). It is worth noting that the regional field removal was channel based, meaning that each sampling point was corrected with respect to its geographical location. After correction the magnetic data was gridded at 1 km by 1 km cell size with a projection system of AMMP. For the purpose of this study the database comprising of the 2 km by 2 km was availed by GETECH. Noteworthy, a subset of this database was used to characterize the geology, structure and tectonics of the southern Kenya Rift (Kuria et al., 2010). Once the reliability of this aeromagnetic database was ascertained through the above mentioned study, this more regionalized study was undertaken.

5.3.1 Total magnetic anomalies

The database from GETECH was imported into Oasis Montaj -Geosoft software - (MacLeod et al., 2000) for further processing. A geo-database was automatically generated showing the flight lines, the latitude and longitude coordinates in AMMP projections and geomagnetic anomaly field. The database was then re-projected to local geographic projection (Arc 1960) to facilitate data exchange format with other GIS softwares.

The residual data were interpolated using the minimum-curvature method (Briggs, 1974) on to a 2 km grid and contoured (Figure 5-2b). The essence of retaining the original survey spacing was to avoid overestimation typical of fine grid (i.e. 1 km or even 0.5 km) or underestimation of the anomaly by generalization using a coarse grid i.e. 5 km or more. The minimum curvature as gridding and contouring method was chosen because it models the surface assuming a smooth elastic-like membrane that ensures smallest amount of curvature between points, which construes the anomaly as precise as possible.

Map of the geomagnetic anomaly field (ΔT) of the area covering central to southern Kenya rift Figure 5-2b shows relatively broad and quiet geomagnetic field on south western part marked by mainly negative anomalies with amplitudes of -11 to -27 nT, interpreted as Tanzania Craton (Figure 5-2a). The NW-SE anomaly north of Lake Magadi - marked by light

green colouration with dark blue patches - correspond to the location of the ANL shear zone (Figure 5-1a). At its termination point on the south eastern end the low magnetic anomalies mark the location of the Mozambique Belt with amplitudes of about -45 and -77 nT. Most of the anomalies on the rift floor correlate closely to lithological boundaries: Plio-Pleistocene trachytic group characterizes almost the entire of the rift floor; stretching as a 33 km wide linear structure in SE direction and 20 km SSW. This is marked by the light green colouration on the aeromagnetic map (i.e. -51 and -65 nT). Along the axial rift floor this zone is punctuated by isolated high magnetic intensity that correlates spatially with the location of the three Quaternary central volcanoes (Menengai, Eburru, Longonot- Suswa) covering central to northern area and four Pliocene central volcanoes (Ngong, Ol Esakut - Ol Esayeiti kasut, Olongesailie and Lenderut) south of the study area. The Ol Esakut - Ol Esayeiti kasut, Eburru and Lenderut have very low magnetic intensity (dark blue colour -158 nT). The Menengai, Ngong, Longonot- Suswa and Olongesailie have high magnetic intensity (red +75 nT).

The other central volcanoes include Londiani and Aberdare with intermediate to high magnetic intensity. A small geological unit (measuring 10 km and 18 km), located NE of Menengai Crater separates the Londiani and Aberdares and connotes a possible connection between these formations. The Quaternary basalts are also characterized by moderate to high magnetic intensity located northern and southern parts of the study area. Miocene central volcanoes and alkaline complexes are marked by Tinderet volcanic centre to the NW and a small formation north of the study. Characteristically, the geological boundaries and the magnetic intensity of these formations match closely well and reflect moderate magnetic intensity (largely orange – negative 33.5 nT). Plateau phonolite that occur in the northern area together with a minor outcrop on the western side have low to moderate magnetic intensity (-156 to +58 nT). Therefore, map of the geomagnetic anomaly field (ΔT) can be useful tool for characterizing the lithological boundaries of the areas not easily accessible.

5.3.2 Analytic Signal anomalies

The analytic signal of magnetic data is a mathematical procedure that correctly relocates the amplitude over the magnetic body (source) directly and is not affected by the directions of the earth's magnetic field and magnetization of the body e.g. Nabighian (1972).

In the 3-D case, the analytic signal is given by Roest et al. (1992) as,

$$A(x,y) = \frac{\partial T}{\partial x} i + \frac{\partial T}{\partial y} j + \frac{\partial T}{\partial z} k \qquad \text{(Equation 5.1)}$$

Where i, j and k are the unit vectors in the x, y, z directions respectively. T is the magnetic anomaly. The amplitude function of the analytic signal is

$$| A(x,y) | = \sqrt{\left(\frac{\partial T}{\partial x}\right)^2 + \left(\frac{\partial T}{\partial y}\right)^2 + \left(\frac{\partial T}{\partial z}\right)^2} \qquad \text{(Equation 5.2)}$$

The analytical signal (AS) method was applied to the aeromagnetic anomaly data for central – southern Kenya Rift. The output channel of AS was then gridded using the same grid cell size as the magnetic anomaly (2 km) as shown Figure 5-2c. As expected, the geological contacts between different tectonic provinces on analytic signal are very sharp i.e. the boundary between Tanzanian Craton and rift floor showing a sharp transition from moderate magnetic to high magnetic anomaly, respectively. It is also seen that, the magnetic anomalies become gradually weaker in amplitude but spatially better correlated on the western side (Tanzania Craton), a trend that stretches to the north western corner. This change undoubtedly reflects an increasingly deeper or thicker magnetic crust. In addition, the Tanzanian Craton marked by green colouration with isolated blue shades does not reflect the geological boundary between the cratonic rocks and Plio-pleistocene rocks. Lack of this distinct boundary on magnetic anomaly suggests that Plio-Pleistocene trachytic group possibly flooded on top of the Tanzania Craton.

The rift floor is characterized by moderate magnetic intensity (orange colour) apart from the areas covered by volcanoes. The rift floor is patched with high magnetic intensity zones that correspond to the location of the central volcanic centres. Notably, the variable magnetic intensity anomalies that characterize the volcanic centres in magnetic intensity map are not displayed. This indicates that the variability in the magnetic intensity was a rather surface characterization that could plausibly be explained by degree of weathering. Another most interesting feature is the location of the Pliocene central volcanoes, in particular at the location of the Aberdares. Here a very high magnetic intensity zone (deep red) stretches close to Eburru and Longonot and even further eastwards off the rift zone possibly towards location of Mt. Kenya. This interconnectivity of the Eburru, Longonot and Aberdare tempts inference of a possible common origin.

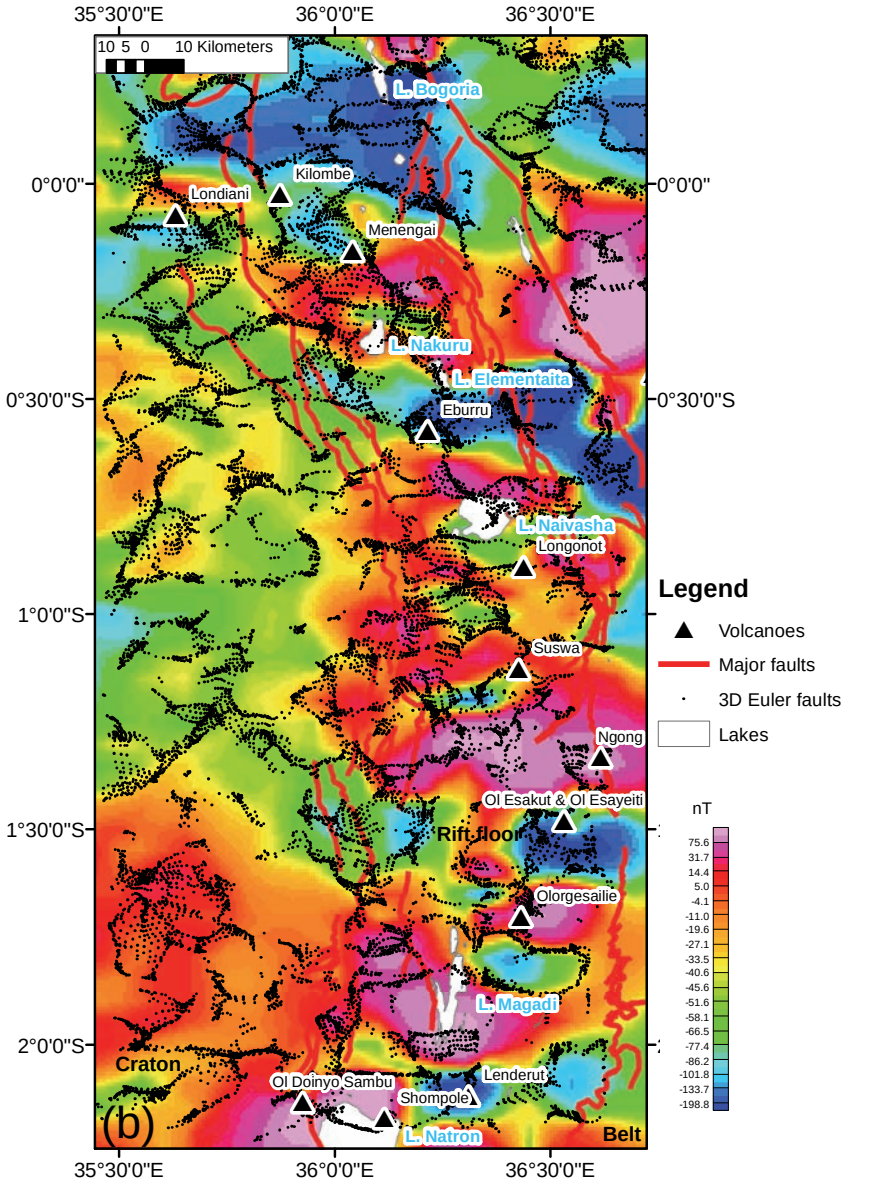

Figure 5-2b. Map of the geomagnetic anomaly field (ΔT) of the area covering central to southern Kenya rift: Tanzania Craton is characterized by relatively quiet geomagnetic field; the rift floor has intensive positive anomalies, which are high frequency sources and patches of low magnetic anomalies mark location of the Mozambique Belt.

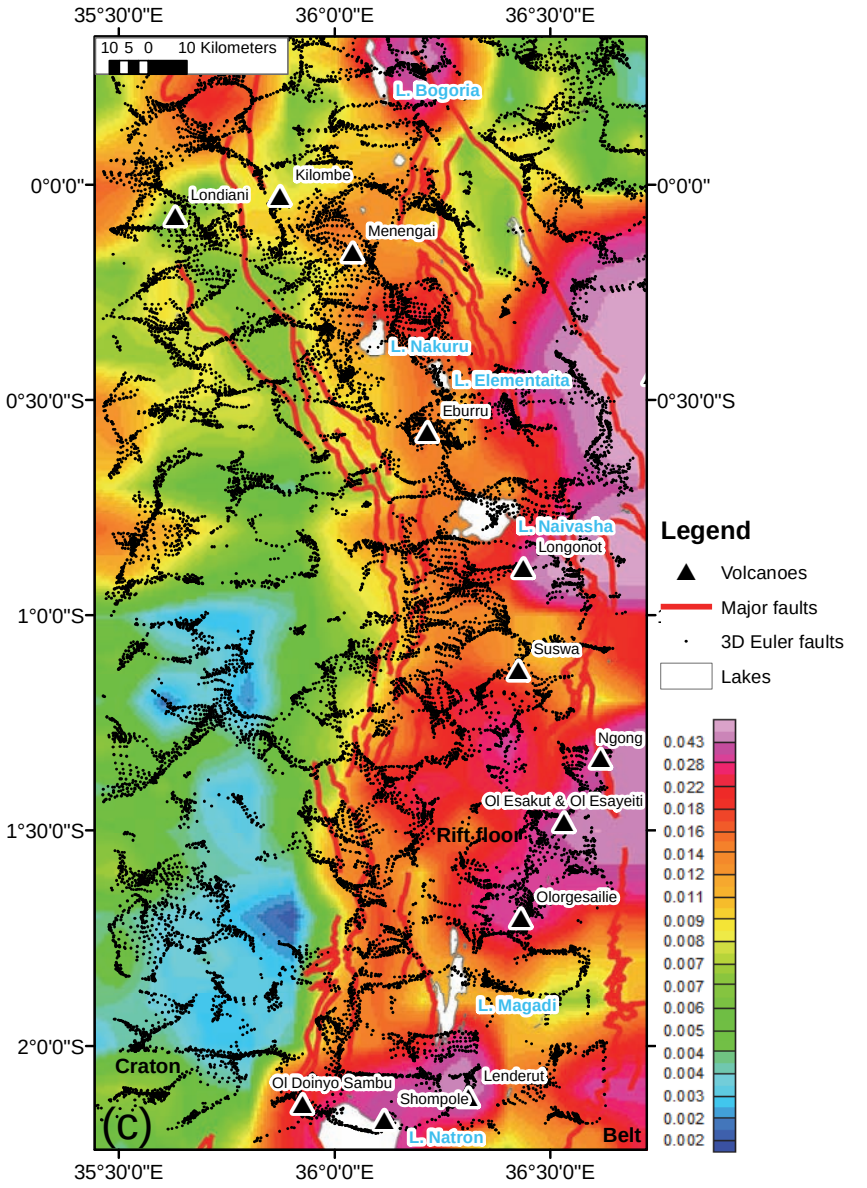

Figure 5-2c. Map of the analytic signal of the total magnetic anomalies (from AMMP 2 km x 2 km cell size) correlated with Tanzania Craton, Mozambique Belt and Rift Valley. Notice the sharp boundaries between these tectonic provinces that define or constrain the three 50 km wide blocks used for radially averaged spectral analysis.

5.3.3 Characterizing magnetic sources

A characterization of the magnetic sources was deemed necessary for optimal selection of the window size and model for spectral analysis detailed in section 5.4. The geological heterogeneity, a result of varied geological terranes (granite-greenstone, metamorphic and volcanic) each with a suite of various rock types and the structural complexity (an interplay of faults, dyke intrusions and volcanoes) all underscore the importance of magnetic source characterization.

Varieties of deconvolution techniques for magnetic source characterization were developed in 1990's and have been in use to-date. These include 3D Euler deconvolution (Reid et al., 1990); 3D analytical signal technique (Roest et al., 1992) later improved by Keating and Pilkington (2004); enhanced analytical technique (Hsu et al., 1998, Hsu et al., 1996); and Source Parameter Imaging method (Thurston and Smith, 1997).

For the purpose of this study, 3D Euler that includes extended Euler deconvolution for 2D structures was used. This methods employs transformation of homogenous functions under rotation and therefore provides multi-depth solutions (Mushayandebvu et al., 2001). A window size of 10 km was selected, which apart from eliminating very small magnetic sources was also equivalent to the moving window for spectral analysis (see section 5.4 below). A depth error estimation of about 15% and structural indices index 1 for the faults were selected. The results are shown in Figures 5-2a, 5-2b and 5-2c.

Generally, the deduced faults are oriented in N-S, NW-SE, E-W to ENE-WSW; and NE-SW similar to what was observed for Lake Magadi area using different techniques (Kuria et al., 2010a). This correspondence gives credibility to the method adopted and reliability of the results obtained. In this context, it is apparent from Figure 5-2a that the faults determined from 3D Euler follows those determined from SRTM DEM (marked major boundary faults) and few of them mimic geological contacts. Interestingly, south western part has very unique magnetic sources both linear and clustered, an area that is characterised by Tanzania Craton and Mozambique Belt rocks. In contrast, within the rift floor most of the linear structures (3D Euler) are buried by volcanic flows (i.e. Pleistocene trachytic group). The characteristic features of Figure 5-2b is that the 3D- Euler linear structures follow the rift morphology as defined by the analytical signal map. Noteworthy, no sources are observed in area of Aberdares and Ngong ranges, an explanation that is not obvious. Figure 5-2c show a very high correspondence of the contacts between the geomagnetic field anomaly and 3D Euler linear structures: at southern

margin Lake Magadi area the contact between the volcanoes and country rock is clearly depicted. A similar observation is made at around Latitude 1°S and Menegai crater area. The location and distribution of the 3D linear structures indicate that there is no preferential direction of the magnetization, a requirement for spectral analysis (see section 5.4).

5.4 Curie point depth estimation

The estimation of the Curie point depth is largely based on a mathematical statistical postulate developed by (Spector and Grant, 1970) that the magnetic anomalies from ensemble of simple sources have their slopes (in logarithms of azimuthally averaged Fourier spectra) related to depth to the top of the ensemble and the spectra also have peak positions on the frequency or wavenumber axis related to the thickness of the magnetic source. The assumption made in this postulation is that all ensemble parameters are uniformly and independently distributed.

Blakely (1995) deduced that in the Fourier domain, the power density spectrum of the observed magnetic field (ΔTxy) is given by:

$$\Phi_{\Delta T}(kx,ky) = \Phi_M(kx,ky)4\Pi^2C_m^2\,|\theta_m|^2\,|\theta_f|^2\exp(-2|k|Zt)(1-\exp(-|k|(Zb-Zt)) \quad \text{(Equation 5.3)}$$

where ΦΔT and ΦM are power density spectra of the observed total field anomaly and magnetization respectively, θm and θf are orientations of magnetization and regional field, Cm is proportionality constant, k is the wave number kx and ky are the wave numbers in the x and y direction), Zt and Zb are respective depths to the top and bottom of the magnetic sources. The radial averages of θm and θf in Equation 5.3 are constants and all other terms are radially symmetric. This 2D power spectrum is averaged within concentric rings about the origin, which transforms Equation 5.3 into 1D spectrum given by:

$$\Phi\Delta T(|k|) = B\exp(-2|k|Zt)(1-\exp(-|k|(Zb-Zt)))2 \quad \text{(Equation 5.4)}$$

where A is a constant that depends on the orientations of magnetization and regional field.

Several methods for estimating Curie point have been developed including; Spectral peak method based on Equation 5.5 (Connard et al., 1983, Blakely, 1995) that states the observed spectral peak is a function of the Zt and Zb.

$$K_{peak} = (\log Zb - \log Zt)/Zb - Zt) \quad \text{(Equation 5.5)}$$

The caveat in this method is that spectral peak is not always observed, as result of uniform magnetization or data windows that are inadequate (Blakely, 1995, Ravat et al., 2007). In addition, the estimation of Zb after estimating Zt is based on trial and error. To partly ameliorate this shortcoming, (Ross et al., 2006, Ravat et al., 2007) developed schemes for forward modelling and inversion methods. After 25 years of using Spector and Grant model, Fedi et al. (1997) introduced a correction factor inherent in Fourier power spectra and manifested as a power-law rate decay approximated to k-2.9 and that is depth independent. The power law exponent arises from an ensemble of magnetized blocks uniformly distributed (Fedi et al., 1997). This correction though not applied in many published papers (Ravat et al., 2007) has tremendously improved depth estimation.

Centroid method is based on the estimation of the depth to the centroid of rectangular parallelepiped sources obtained from slope of an azimuthally averaged frequency-scaled Fourier spectra (dividing spectrum by frequency) with the depth to the top of the sources estimated from the slopes of azimuthally averaged Fourier spectrum (Okubo et al., 1985). The depth to the bottom of the magnetic source is obtained by:

$$Zb = 2Zo - Zt \qquad \text{(Equation 5.6)}$$

Fractal source estimation method is based on fractal or scaling behaviour, where the power spectra is proportional to some power of frequency manifested as k-β (Pilkington and Todoeschuck, 1993, Maus and Dimri, 1995). This is similar to the Fedi et al. (1997) correction described above.

For the purpose of this study the Spector and Grant (1970) model was selected because it supports a wide range of sources i.e. regards block-like sources from statistical ensembles of various sizes and magnetization, and is suitable for representing sources delineated as gross homogenous bodies such as intrusions (Quarta et al., 2000). In addition, the Fedi et al. (1997) correction was applied that does not necessitate the aprior knowledge of ensemble sizes and more importantly it applicable for the uniform magnetization as observed in the study area (see geomagnetic field anomaly map, analytical signal, and magnetic sources). This model contrast purely random sources (Naidu and Mathew, 1998, Naidu, 1968) appropriate for describing a shallow and highly variable magnetization distribution (Quarta et al., 2000).

5.4.1 Selection of window size

The Spector and Grant (1970) Model similar to other Fourier based techniques requires selection of window-blocks on the regional magnetic anomalies. Within each window block the magnetization of the prism ensemble is assumed to be random and not magnetization within each prism. On this basis, the radially-averaged amplitude of the magnetization model are linearized in a logarithmic space at middle to high wavenumber band and low wavenumber bands respectively. To achieve this end, several window sizes (100 km x 100km, 75 km x 75 km, 50 km x 50 km) were tested on geomagnetic field anomaly map, analytical signal map, magnetic sources maps (linear) and geological map. In each case as seen in Figures 5-3a, 5-3b and 5-3c large window sizes of (100 km by 100 km and 75 km and 75 km) sampled regions of disparate geology and/or tectonic province that contradict assumption of random magnetization within each window. A window size of 50 km by 50 km sampled more uniform magnetic sources and therefore was adopted.

A subset of 297 window-blocks was made from geomagnetic field anomaly map in oasis montaj software (Geosoft) each measuring 50 km by 50 km with a step of 10 km along the latitude and longitude. This fine moving step (10 km), which in odds with common 50% window overlap, was chosen to increase spatial resolution and therefore refine the morphology of the bottom magnetic layer with a higher accuracy and provide an independent constrain on the subsurface occurrence of geothermal field. The blocks covered an area of 480 km and 150 km this being area covered by the available dataset.

5.4.2 Spectral analysis

Prior to performing the spectral analysis, the magnetic data was tested for wavelength anomalies, which arise mainly from topography, regional features and magnetic core fields. These would affect Curie point depths estimation. The 2 km grid spaced data of magnetic anomaly of the entire study area (Figure 5-2b), was transformed, computed and analysed as radially averaged log power spectrum. The unfiltered spectrum showed a significant peak at 0.0089 cycles/km. Thereafter the grid data (magnetic anomaly) was filtered using a high pass filter. This filtering distorted the entire spectrum resulting in shallow peak while raising the rest of the spectrum and therefore ignored. The grid data was upward continued at 150, 200 and 250 m using Fourier domain technique (Blakely, 1995). This filtering showed no noticeable effects on the spectrum. Presumably, a flight of 2896 m filtered the high frequencies and more filtering could not improve the spectrum.

Before transforming each of 50 km by 50 km window block to wave number domain (applying the forward FFT), data was detrended to remove the long wavelengths by taking out the first-order surface that best fits the data in a least square sense (Connard et al., 1983) as shown Figures 5-4a and 5-4b. Subsequently, the map data were tapered in order to smooth gradually the intensity to zero at the edges of map data. A 10 point Hamming window was used.

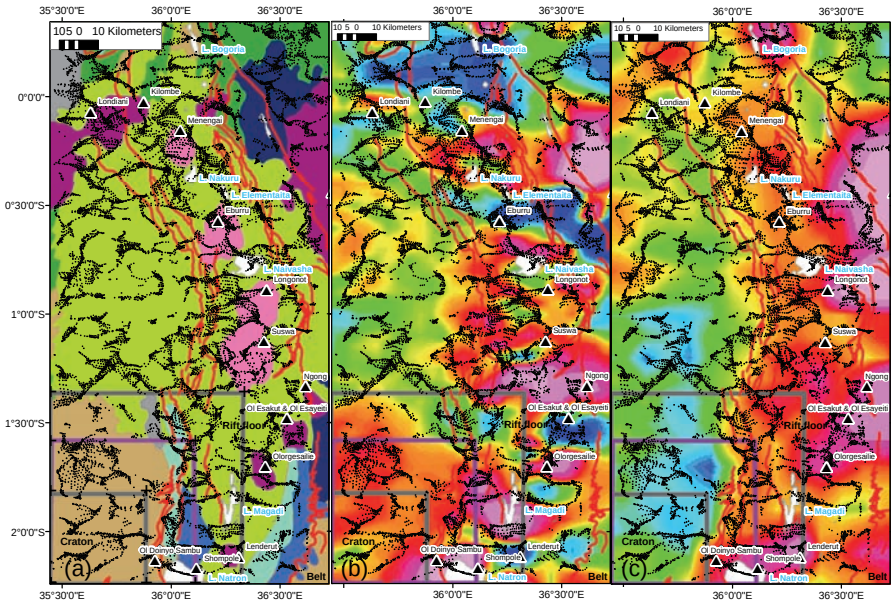

Figure 5-3. shows segments sampled by squared window blocks of 50 km, 75 km and 10 km (three blocks on the south western edge) showing the disparity of (a) geology, (b) geomagnetic anomaly and (c) analytic signal map. Noteworthy, the 50 km window block samples relatively uniform geology and magnetic sources, hence adopted for windowing blocks for spectral analysis. A total of 297 blocks with moving step of 10 km both along the latitudes and longitudes were extracted from geomagnetic anomaly map (b).

From this new grid, 2D DFT transform was computed using the algorithm of Press et al. (2002), and the power spectra calculated. Once the power spectrum is estimated, the next step is to calculate the radial power spectrum. This is a radially averaged 2D spectrum and is estimated by averaging the power spectrum over a set of concentric rings about k=0 with increasing radius (Naidu and Mathew, 1998). Subsequently, the radial power spectrum was normalized with respect to the value of the first harmonic, the natural logarithm calculated, and then new data was transferred to microsoft excel. Frequency scaling of the power spectrum was computed. Prior to

plotting the spectra, the spectrum was filtered by applying the Fedi et al. (1997) correction i.e. both normal radial power spectrum and scaled frequency radial spectrum and subsequently plotted versus wavenumber (Figure 5-5). For the two power spectra i.e. frequency scales and normal power spectrum their gradients were determined by least square regression in the two frequency areas. The bottom depths Zb were calculated using Equation 5.6. This procedure was followed for each of the 297 window-blocks. The calculated Zb were referenced using the centre coordinates of each block. Out of 297 window blocks 181 blocks had significant spectral peaks mostly at either 0.0178 cycles/km or 0.0333 cycles/km. As expected, most of the spectra without peaks sampled areas of variable geology or tectonic province i.e. a combination of either Tanzania Craton and rift volcanics or Mozambique Belt and rift volcanics.

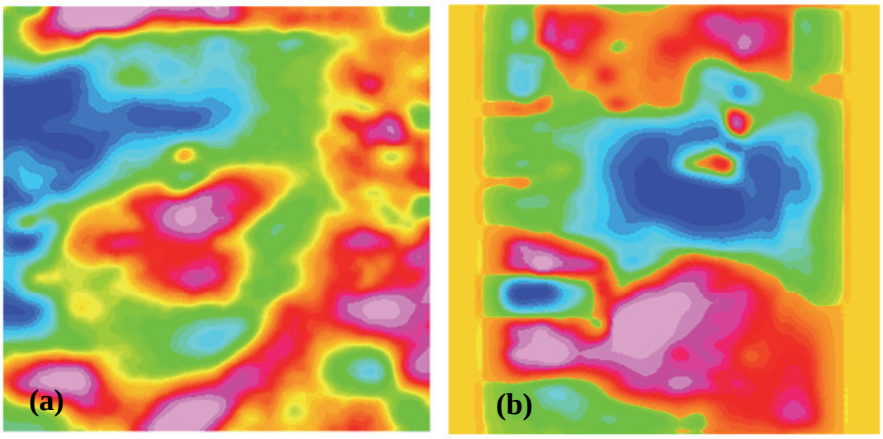

Figure 5-4a. An example of the 50 x 50 km grid extracted from the database for spectral analysis. b) An example of the detrended and tapered grid i.e. smoothened gradually the intensity to zero at the edges of map data. This grid map is used as input for winograd FFT transformation.

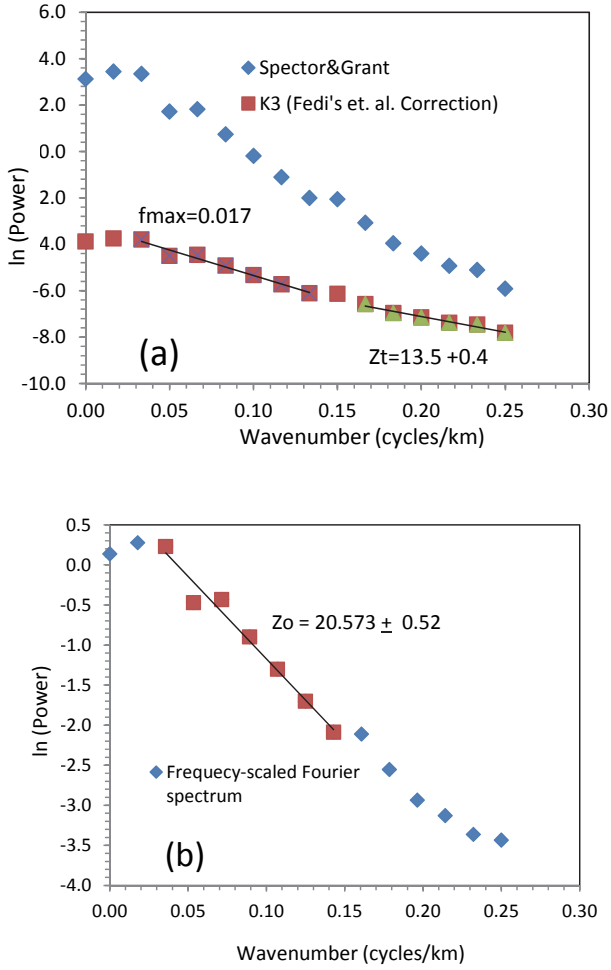

Figure 5-5. Examples of spectra for estimation of the Curie point depth. The blue line in (a) is Spector and Grant (1970) spectrum, a correction of this spectrum using Fedi et al. 1997 correction factor K^{-3} is shown by the red line. The black line is a linear fit by least-square method for the section of the spectrum marked by light green triangles. The depth Zo is found from the slope of radially averaged frequency-scaled power spectrum, black line with red marks (b). The bottom Zb is then obtained from the equation Zb=2Zo-Zt. Notice Zb value of 27.61 and 28.3 for spectral peak and Okubo et al. (1985) respectively for this example.

The results from 297 blocks referenced using their centre coordinates were contoured using minimum curvature with a cell size of 2 km (Figure 5-6). The results show that the rift floor, as marked by major boundary faults, is punctuated by shallow CPDs. The largest shallow CPD anomaly has a width of

37 km (E-W) and length 52 km (N-S) at its longest part and is centered south of Lake Naivasha, stretching between the Longonot and Suswa volcanic centres. This is followed by a NW-SE oriented shallow CPD anomaly beneath Lake Bogoria that is narrower (19 km) but elongated (40 km). The anomaly NW of Lake Magadi and those along the entire western margin of Lake Nakuru mark the small localized anomalies within the rift floor. Surprisingly, a large NW-SE anomaly extends from the western margin of the rift for a distance of about 81 km off the rift floor (approximately latitudes 0.5°S to 1.5°S). Other small anomalies off the rift floor are located west of Lake Magadi and north western part of the study area. The later could possibly be likened to the younger Nyanza rift (Mathu and Davies, 1996) along which nearby volcanic centres of Tinderet and Londiani are located.

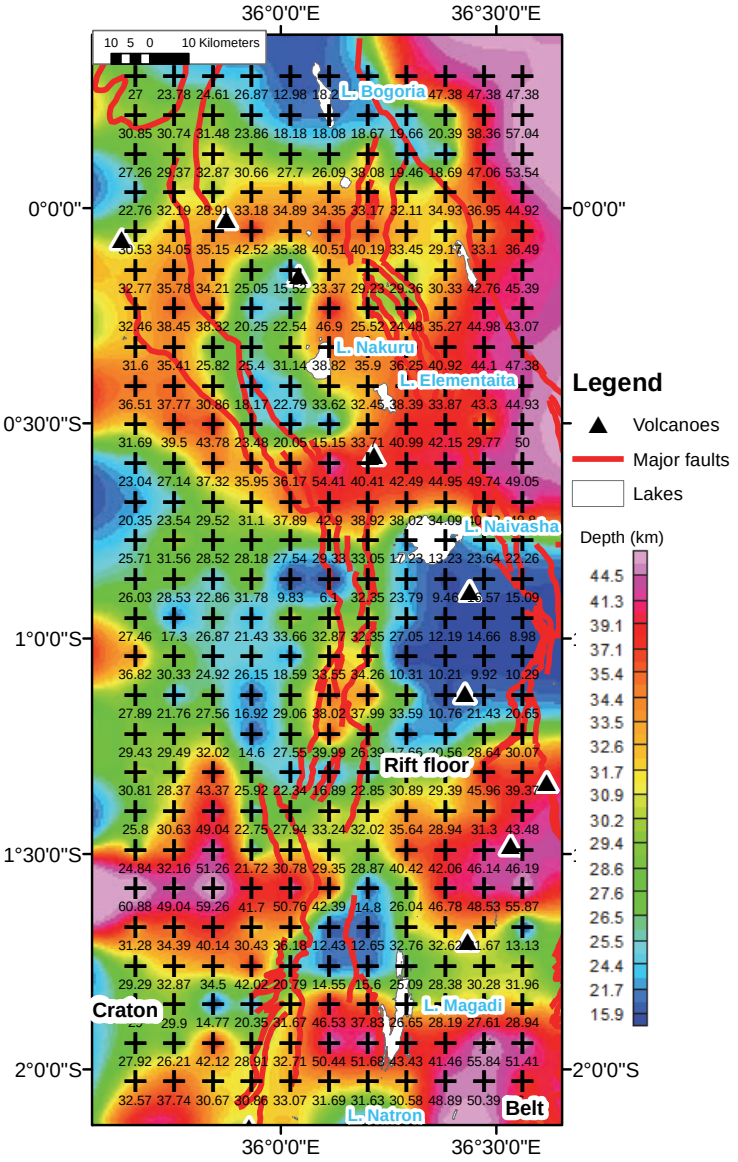

Figure 5.6. Map showing bottom depth (km) of magnetic ensemble synonymous to Curie Point Depth for central to southern Kenya Rift for 297 window blocks as shown with + symbol marking window-centre. Red bold lines mark the rift boundary. Notice the generally thickened magnetic crust punctuated by shallow Curie depths; largest one located south of Lake Naivasha spatially marking location of Olkaria-Longonot-Suswa volcanoes.

The proximity of these shallow CPDs to known volcanic centres possibly indicate active volcanic activity. Deeper sources generally characterize the eastern rift margin between latitudes 0.3°N north and 0.7°S and the isolated segments east, west and partly underlying Lake Magadi at latitudes 1.2°S and 1.6°S. The anomalies east of Lake Magadi correspond to location of ANL shear zone, whereas those to the further north are likened to Mozambique Belt. The western deeper CPD anomalies are possibly part of the Tanzania Craton or its suture boundary with Mozambique Belt. Figure 5-7 shows field evidence of the geothermal manifestation at Olkaria Geothermal field – fumaroles and hot/altered ground surface, Lake Bogoria – jetting geysers and Lake Magadi – hot springs. Coincidently, the magnitude of geothermal manifestations commensurate the CPD estimates i.e. deep CPD at Lake Magadi are characterized by hot springs whereas fumaroles and jetting geysers at Olkaria geothermal field and Lake Bogoria respectively mark shallow CPD.

Figure 5-7. Shows geothermal manifestations at Olkaria geothermal field, jetting geysers of Lake Bogoria, and Hot spring of Lake Magadi (after heavy rains).

5.4.3 Validation of CPD

There is no obvious validation method for CPD, therefore other different techniques were used that provided for cross validation. These include

temperature depth profiles, stable bottom-hole-temperatures (BHT) and steady state geotherms.

5.4.3.1 Temperature-depth profiles

In order to understand the thermal state of the crust probably associated to shallow CPD, two sets of data were used: borehole temperature logging with depth for three boreholes and 93 stable BHT for Olkaria Geothermal field as shown in Figures 5-8a and 5-8b, respectively.

An average temperature-depth log was determined from the three borehole logs, fitted least square regression line and computed a mean global gradient of 52.13°/km (Figure 5-8a). It is noteworthy, that averaging these depth-temperature logs was not an over estimation considering their close proximity i.e. located within a distance of 10 km. This gradient of 52.13°/km, if applied to 14.5 km (average CPD around the boreholes), assuming a constant geothermal gradient, implies somewhat high temperature of 755.9°C. A second regression line was fitted for the upper part of the temperature-depth log (i.e. up to a depth 1 km) that showed a steadily increasing geothermal gradient and close clustering of measured temperature values of the three boreholes. A geothermal gradient of about 39°C/km was obtained, that results into a temperature of 565.5°C at a depth of 14.5 km, which closely approximates 580°C. This temperature gradient that represents the more stable gradient indicates that the estimated CPD is not an overestimation or an underestimation and is therefore considered more representative at least within the rift floor. The unsteady geotherms were affected by circulation of high temperature brines (Wells 908A and 915) and cold water from groundwater hydrogeological systems (well 908).

From the scatter plot of the stable BHT obtained from 97 boreholes (Figure 5.8b), the upper and lower boundaries that confine all the measured BHT were determined. The lower boundary is marked by a gradient of 42.7 °C/km while the upper boundary gradient is 51.6°C/km. The lower limits approximates the average CPD to about 13.7 km while the upper limit falls short to a depth of 7 km, which is shallower by 2 km than the shallowest CPD for Olkaria Geothermal field (estimated at 9 km). The bracketing of the average geothermal gradients with the CPD indicates the validity of the CPD estimates.

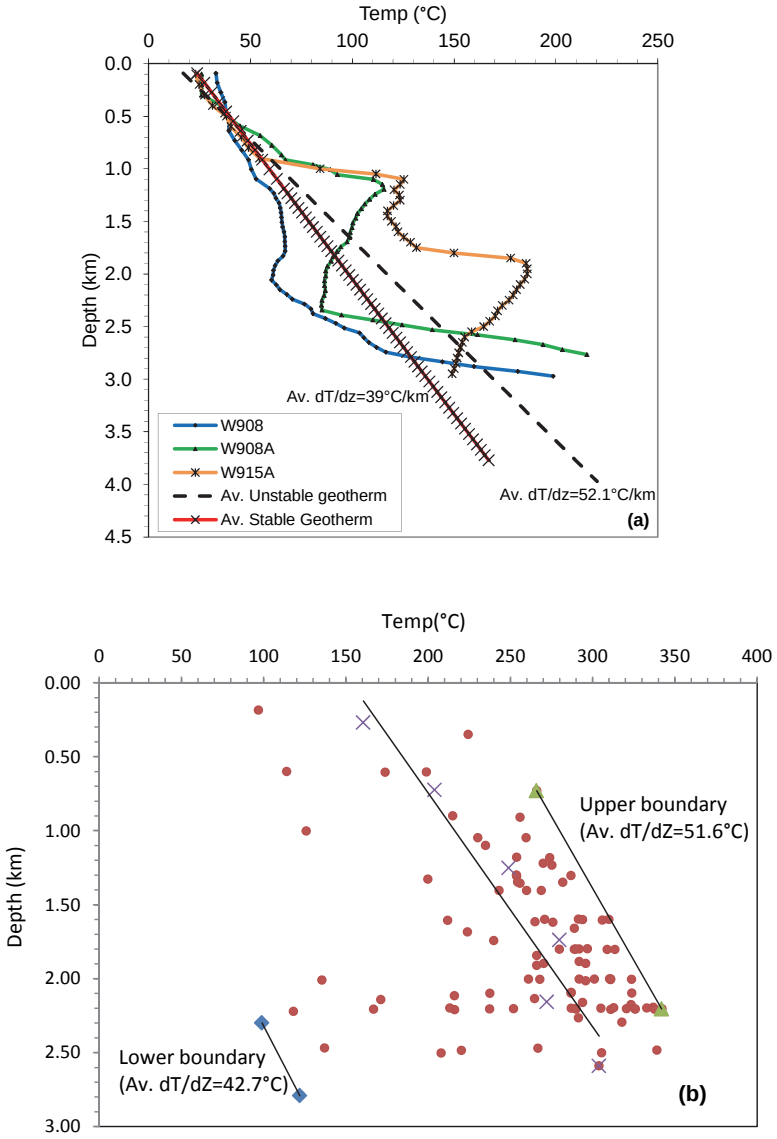

Figure 5-8a. Temperature distribution with depth for 3 boreholes at Olkaria Geothermal field. The upper 1 km depicts the relatively stable geotherm followed by highly irregular temperature distribution with depth, a result of hot brines circulation and cold water systems. Figure 5-8b. Scatter plot of stable-bottom-hole temperatures showing a range of estimated geothermal gradient from 42.7°C/km to 51.2 °C/km similar to that estimations in (a).

5.4.3.2 Steady state geotherms

To better define the crustal thermal structure, steady-state geotherms were calculated by simplifying a thermodynamic modelling problem to a heat conduction problem (Equation 5.7). For the upper crustal zone the heat conduction dominates over the convection because of minor lateral geothermal gradients, high viscosities and conductivities (Li et al., 2010). In this approach, the estimated Curie point depths from magnetic anomalies provide independent and effective constraints on the modelled geothermal field, which cannot be otherwise validated easily other than by surface heat flow. An assumption made is that heat flow within the Mozambique Belt and Tanzania Craton is in a steady state. However, estimates within the rift floor would be influenced by prevalence of transient state.

Steady-state geotherms T(z) were calculated using approach by Turcotte and Schubert (2002) and successfully applied by Albaric et al. (2009) in eastern and western branches of EARS:

$$T(z) = To + \frac{(Qo - Aoe^{-z/b})z}{k} + \frac{Aob^2}{k}(1 - e^{-z/b}) \qquad \text{(Equation 5.7)}$$

Where z is the depth (km), To is the temperature taken from 22°C (from temperature-depth curves), Qo is the surface heat flow (mW m^{-2}), b is a length parameter, and K is the thermal conductivity (W m^{-1} k^{-1}). The heat production exponentially decreases with depth and equal Ao (µW m^{-3}) at the surface.

The geotherms (Figure 5-8c) are calculated with a surface heat production of 2 µW m-3, a value estimated from an average of 8 measurements from Proterozoic rocks made by Chapman and Pollack (1977) and Nyblade et al. (1990). Similar to Albaric et al. (2009), typical values were chosen for the thermal conductivity k and characteristic depth parameter b of 2.5 W m-1 K-1 and 10 km respectively (Fadaie and Ranalli, 1990, Turcotte and Schubert, 2002). Heat flows of 100 mWm-2, 30 mWm-2 and 25 mWm-2 as boundary conditions were used to compute the geotherms (Figure 5.8c). The choice of 25 mWm-2 and 30 mWm-2 respective to the west and east of the southern Kenya Rift was based on global heat flow database from international heat commission (http://www.und.nodak.edu/org).

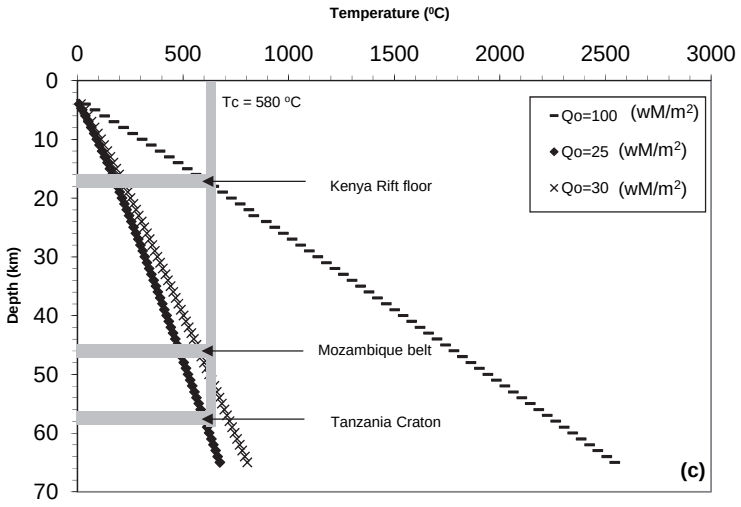

Figure 5-8c. Modelled temperature-depth profiles based on Equation 5.7, notice that at a temperature of 580°C these heat flows correspond to the estimated Curie point depths marked by grey lines.

It is seen from Figure 5-8c that the computed geotherms from the pre-selected heat flows of 100 mWm-2, 30 mWm-2 and 25 mWm-2 intersect with the estimated CPDs at a temperature of about 580°C characteristically defining rift floor, Mozambique Belt and Tanzania Craton. This independent information support the deduced depth to the bottom of the magnetized crust (Figure 5-6) i.e. intersection of the grey horizontal lines (Figure 5.8c) with the determined geotherms at a temperature of 580°C. Using this method, geothermal gradients of about 42.9°C/km and 36.5°C/km were determined using estimates from the CPD of 13.5 km (Olkaria geothermal field near Lake Naivasha) and 15.9 km (Lake Bogoria) at a minimum temperature of about 580°C and are similar to those computed from temperature-depth logs i.e. 39°C/km.

5.5 CPD and Moho depth

In the continental region the Moho marks a magnetic boundary, as the mantle material is non-magnetic and therefore the Curie isotherm should lie either within the crust (shallower than the Moho) or should coincide with the Moho (Wasilewski and Mayhew, 1992). To evaluate relationship between Moho and CPDs and therefore determine if the CPD is a compositional boundary or Curie isotherm, two profiles were selected along KRISP lines (KRISP axial line and KRISP Line G) that traverse the study area (Figures 5-

1). The Moho data were extracted from Keller et al. (1994a) and Mechie et al. (1994) and the ground distances used in their work matched with geographical coordinates using a GIS platform (ArcGIS 10). Using the digitized KRISP traverse lines, the corresponding CPDs were extracted in Geosoft software from the CPD depth map shown in Figure 5-6. A plot all these data sets together with scaled topography (i.e. elevation in km x 10) was made as shown in Figures 5-9a and 5-9b.

The model along the KRISP axial profile line (that follows the rift floor, as shown in Figure 5-1) shows a conspicuous disparity between that CPD and Moho depth (Figure 5-9a); therefore CPD is not a compositional boundary but in this case marks a Curie isotherm depth. In addition, the profile shows three locations of high thermal regime corresponding partly to the location of Olkaria geothermal field on the western margin, a very localized and sharply feature near Menengai crater and generally rising CPD for Lake Bogoria area. Surprisingly, the area between Lake Naivasha and Menegai has subdued dome-shaped Curie point depths that plots below Moho depth. This indicates low geothermal gradient. There seems to be no obvious relationship between topography and other parameters (Moho and CPD).

The model along KRISP Line G - traversing parts of Tanzania Craton, crossing rift floor at Lake Magadi and terminating within Mozambique Belt - contrasts the axial line but still CPD marks a Curie isotherm (Figure 5-9b). On the western margin the CPD is marked by a very sharply westerly dipping edge that on the topographical profile corresponds to the major western rift bounding fault. This deep seated CPD marks location of the Tanzania Craton, a cold thickened shield. The rift floor is characterized by a narrow and localized thermal regime possibly contributing to geothermal manifestations on the earth surface – hot springs (Figure 5-7). Towards the eastern rift margin (marked by the high eastern rift shoulders) CPD assumes a subtle wavy structure indicating marginal thermal variations that possibly are not significant (thermally). It is clearly notable that the KRISP line G traversed the northern most part of Lake Magadi, coincidently along the margin of the local thermal anomaly instead of traversing through it. In addition, a small loop close to Olorgesailie volcano samples part of the ANL shear zone, which explains why the CPDs are subdued compared to those of the axial line.

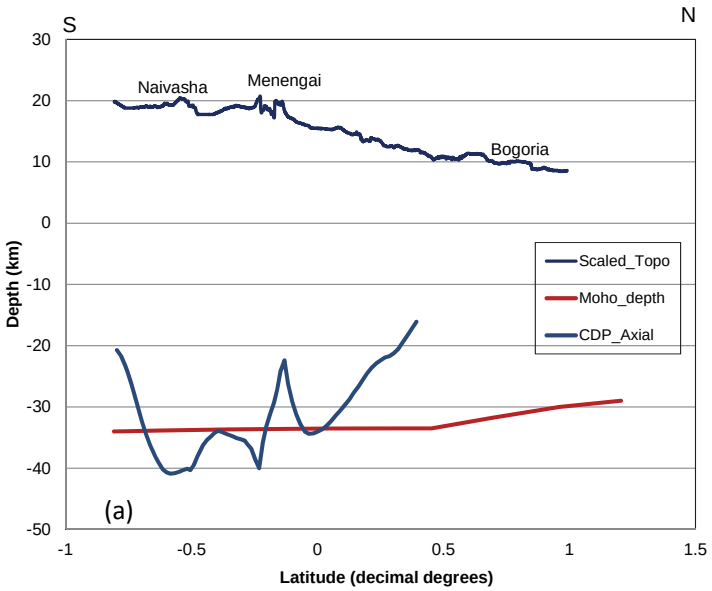

Figure 5-9a. A plot of the Moho depth (km) after Keller et al. (1994), Curie point depth (km), and scaled topography (km X 10) along KRISP axial line (Figures 5-1 and 5-6b).

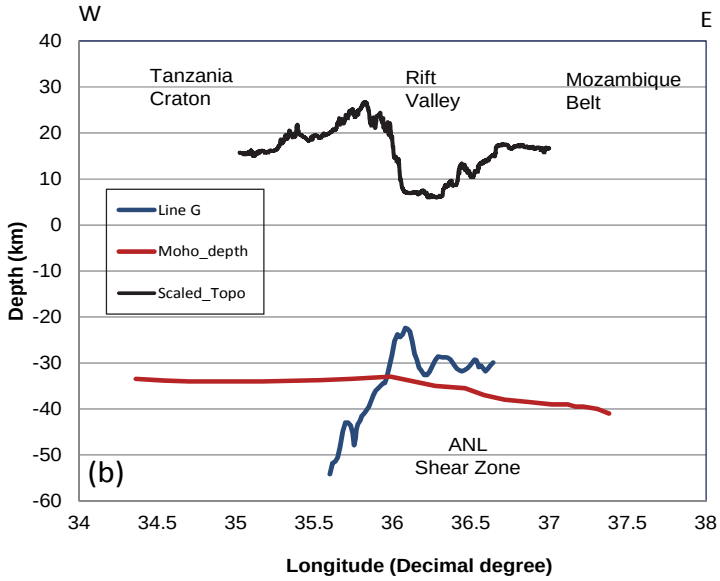

Figure 5-9b. A plot of the Moho depth (km) after Mechie et al. (1994), Curie point depth (km), and scaled topography (km X 10) along KRISP Line G (Figures 1 and 5-6b).

5.6 Discussion

An attempt has been made to construct the thermal structure of the central and southern Kenya Rift by computing the CPD for the first time in area from geomagnetic field anomaly deduced from aeromagnetic data. A choice of the statistical model (Spector and Grant, 1970) that regards block-like sources from statistical ensembles of various sizes and magnetization instead of model established purely random sources (Naidu, 1968) proved suitable in an area as recommended by Quarta et al. (2000). For the purpose of the spectral analysis, trial block sizes of 100 km by 100 km, 75 km by 75 km and 50 km and 50 km were selected. It was found that squared-block with dimensions of 100 km and 75 km sampled regions of disparate geology i.e. green schists terranes of Tanzania craton (Mathu and Davies, 1996) largely composed of metavolcanics and rift floor volcanics. This short coming was ameliorated by choice of the small window-size (50 km). In addition, choice of 50 km by 50 km window-size apart from being in line with the rift floor dimensions estimated to range from 30-60 km wide from seismic data (Kabede, 1989, Baker et al., 1972a), sampled relatively uniform magnetization as shown by geomagnetic anomaly map, analytical signal map, and reflected by geological map. Indeed, small windows have been recommended by Li et al. (2010) for tectonically young and volcanically active area. For example Espinosa-Cardeña and Campos-Enriquez (2008) used a window size of 60 km by 60 km to determine CPD for geothermal area in Cerro Prieto Mexico. The similarity of geological terrain and choice of windows in this study and the previous cases affirms the suitability of the method adopted in estimating CPD. However, choice of very small windows such 9 to 20 km (Dolmaz et al., 2005a) may certainly compromise sampling of long wavelengths part of spectrum.

For the 297 window blocks covering entire study area, over 61% of the blocks attained significant spectral peaks mostly at either 0.0178 cycles/km or 0.0333 cycles/km. Although it has been suggested that lack of well-defined spectral peak could be due to the large wavelength part of the spectrum extending beyond the dimensions of the selected block (Rajaram et al., 2009) or as result of uniform magnetization (Blakely, 1995, Ravat et al., 2007), it is apparent that for this study lack of spectral peaks was caused by highly variable geological formations as shown by geological map, geomagnetic anomaly map, analytical signal map, magnetic source map from 3D Euler. A similar observation was made by Ruiz and Introcaso (2004) in their study at Precordillera Cuyana and Sierra Pampeanas in Argentina who noted that for windows centred in the neighbourhood of lineament and/or different geological terranes their spectra were not clearly defined due sampling different magnetic signatures.

For the purpose of attaining a very high spatial resolution of the undulating morphology of CPDs, a choice of small moving windows at intervals (or steps) of 10 km was made, which contrast the more routine 50% overlap e.g. Rajaram et al. (2009); Ravat et al (2007); Chiozzi, et al. (2005); Stampolidis and Tsokas (2002); Tanaka and Ishikawa (2005); Blakely (1988); Bhattacharyya and Leu (1975). As expected this high sampling offered a continuous and in most cases multiple sampling over the same anomaly thus refining its boundary more precisely. A departure from the routine 50% overlap that disregards the tectonic regime/geological setting is recommended in the future CPD studies.

The results from CPD map (Figure 5-6) show that rift floor (down warped part) is characterized by a series of shallow CPDs with various sizes and shapes. Blakely (1988) noted that thin magnetic crust, as deduced in this study, accounts for tectonically active regions associated with higher heat flow, a notion supported by Rajaram et al. (2009). The largest shallow CPD is located south of Lake Naivasha, possibly associated with Longonot and Suswa volcanoes including Olkaria area. This anomaly that attains a minimum CPD at 9 km in central part and about 20 km at its peripheral margins displays relatively highest degree of geothermal manifestation in the study area (Riaroh and Okoth, 1994). These markers of elevated thermal regime include hot fumaroles, hot and altered ground as also evidenced in Figure 5-7. Indeed, the Olkaria geothermal field, currently under exploitation, is located at the north western margin of this large and possibly highly resourceful geothermal reservoir (shown by the numerous drilled boreholes, Figure 5-1). In addition, the hottest ground temperatures (~93° C) occur within the annular part of Suswa, where fumaroles attain temperatures ranging from 202 to 243°C, which combined with measurable concentrations of methane and hydrogen from fumaroles (Omenda, 2001) attest to a possible geothermal reservoir. Consequently, the CPD indisputably manifest elevated thermal regimes. The other significant (in size) shallow CPD (with an average depth of about 15 km) spatially related to volcanic centres include Menegai that spreads intermittently further south of Lake Nakuru but terminates before reaching Eburru. These slightly deepened CPD indicate subdued geothermal potential. Indeed, according to (Omenda, 2001) these bald lands manifest hot water boreholes, while the floor of Menenagi crater steams on its floor.

The rest of the shallow CPD along the rift floor are associated with axial faults i.e. Lake Bogoria and Lake Magadi. The shallow CPD anomalies located NW of Lake Magadi reach a depth of about 14 km, while those on southern tip of lake attain a depth of about 31 km. Interestingly, hottest springs (80-90 °C)

are located on the northern shores of Lake Magadi while the other springs (south of Lake Magadi) attain temperatures of about 32-44°C (Omenda, 2001, Kuria et al., 2010a). This correspondence of the CPD and thermal regimes manifested by hot spring is certainly not a coincidence. Central to this argument, the Lake Bogoria CPD (about 13 km) manifest steam jets (Figure 5-7) and spouting geysers, hot springs and boiling pools (Omenda, 2001).

The most striking and possibly unexpected CPDs are those located off rift floor, oriented in NW-SE direction past the western margin of the rift bounding faults at latitude 0.5°S and 1.5°S. Whether these features mark buried volcanic centres from which voluminous lava flows were ejected to form plateau and plains is a matter of speculation at the moment. Nevertheless, Baker et al. (1971a) proposed that the lava flows forming plateaus could be sourced from fissures or numerous localized eruption centers, which indicates that these volcanoes may fall under the latter category. All in all, the flooding of the Plio-Pleistocene trachytic group far beyond the western boundary of the rift margin (i.e. more than third of this outcrop) supports Baker et al. (1971a) assertion of volcanic centers. There is no evidence of geothermal manifestation at the moment but the elevated thermal regimes inferred from shallow CPD (6 – 17 km) necessitate immediate further investigation.

A comparison of the Moho depths (Keller et al., 1994a, Prodehl et al., 1997b) with depth to the bottom of magnetic crust from the present study, shows that the bottom of the magnetic crust lies above the Moho depth at three locations within the axial rift zone. These areas represent a thermal boundary rather than a petrological or compositional boundary. However, between Naivasha and Mengai dome-shaped CPD morphology that plot below Moho indicates subdued thermal regime. A much deeper CPD is observed along KRISP line G on the western margin from which a postulation of thickened stable crust (Mathu and Davies, 1996) of low thermal gradient can be inferred. Indeed, Eppelbaum and Pilchin (2006) noted that areas with large CPD mark regions that have low heat flow and low vertical gradient. In this particular area (western termination point of KRISP line G), the CPD is deeply seated far below Moho depth that possibly represent very stable craton. Therefore, depth to the bottom of the ensemble of magnetic sources derived in the present study may be called Curie isotherm depth. However, within the Tanzanian Craton and Mozambique Belt, the depths to the bottom of the ensemble are greater than that of the Moho, which is not strange because Toft and Arkani-Hamed (1992) noted that in some cases the uppermost part of the mantle may be magnetic. These large depths to the bottom of the

magnetic crust observed in these cases can possibly be due to the fact that these regions have low heat flow and low vertical geothermal gradient (Eppelbaum and Pilchin, 2006). The heat flow of and 25 mWm^{-2} and 30 mWm^{-2} are considered representative.

5.7 Conclusions

1. The rift floor, marked by the major boundary faults (down warped part), is characterized by series of shallow Curie depth estimates displaying various sizes and shapes. These are grouped into two categories; those associated spatially with the location of known volcanoes i.e. Longonot-Suswa, Menengai and ologesailie and those associated with axial rift faults i.e. around Lake Bogoria and Lake Magadi (located north west and south of the lake).
2. The another unique category of the CPD are located off the western margin of the rift bounding major faults at about latitude 0.5°S and 1.5°S, unrelated to either major faults or known volcanoes.
3. All the shallow Curie depth estimates are shallower than Moho and therefore they are marked Curie isotherm representing thermal structures.
4. The depth to the Curie isotherm commensurate the degree of geothermal manifestation, particularly within the rift i.e. at Olkaria-Longonot-Suswa with minimum Curie isotherm depth of 9 km has hot fumaroles (202 - 243°C) and hot (~93° C) and altered ground; Lake Bogoria minimum Curie isotherm depth 13 km manifests steam jets, spouting geysers, hot spring and boiling pools; Lake Magadi has two anomalies namely north west with minimum Curie isotherm estimate 14 km with hottest springs (80-90 °C) and south of Lake Magadi a curie isotherm 31 km has hot spring (32-44°C). The floor Menengai crater with minimum Curie isotherm of 15 km shows steaming. In addition, relatively high geothermal gradient of 39 °C/km was estimated from bottom hole temperatures located at Olkaria geothermal field.
5. Although there are no recorded geothermal manifestation of the shallow Curie isotherm located off rift margin (latitude 0.5°S and 1.5°S), their shallow CPD ranging between 6 km and 17 km indisputably manifest elevated thermal regimes - compared to those located within rift floor - indicate very high geothermal potential.
6. The deep CPD (below a depth of 45 km) are inferred to mark locations of thickened crust (Tanzania craton and/or Mozambique belt or even Anza-Nandi-Loita shear zone) characterized by low thermal gradient. Indeed, the estimated heat flow values from steady state geotherms of 25 mWm^{-2} and 30 mWm^{-2} are considered representative.

CHAPTER 6

IMPLICATION OF CURIE POINT DEPTH ON SEISMICITY AND SEISMOTECTONICS

This chapter is based on:

Kuria, Z.N., Woldai, T., van der Meer F.D., Barongo, J.O., Noomen, M., Komolafe, A., van der Meijde, M. 2011. Characterisation of thermal and tectonic structures for central to southern Kenya Rift: Seismotectonic implication. Submitted: Journal of African Earth Sciences.

6.1 Introduction

Thermal structure of the crust determines modes of deformation, depths of brittle and ductile deformation zones, regional heat flow variations, seismicity, subsidence/uplift patterns and maturity of organic matter in sedimentary basins. Indeed, the depth-frequency distribution of the earthquakes has recently been used as proxy for unravelling the rheological properties of the crust and their spatial variations (Albaric et al., 2009). One of the approaches used to study the thermal field structure is the use of the spatial variations in temperature e.g. Trifonova et al. (2009) and references therein. To determine the temperature variations, the primary observable quantity is the heat flow. However, the heat flow measurements are often too widely spaced and often insufficient to understand their correlation over a wide area involving various tectonic settings (Tanaka and Ishikawa, 2005). In particular, within the Kenya Rift information on heat values is scanty (Bailey, 1983, Ebinger et al., 1991, Nyblade, 1997, Nyblade et al., 1990) for mapping regional thermal structures. In order to overcome this limitation, spectral analysis of the magnetic anomaly data makes it possible to estimate Curie point depth which has become synonymous with the depth to Curie temperature e.g. Spector and Grant (1970); Bhattacharyya and Leu (Bhattacharyya and Leu, 1975). This method allows determination of the magnetic layer's bottom which could be either the depth at which ferrogmagnetic minerals pass to a paramagnetic state under the effect of increasing temperature or the depth of compositional change where magnetic rocks are replaced with non-magnetic. The distinction therefore, of these two boundaries (temperature or compositional change) requires independent evidences. All in all, delineating deep magnetic anomalies and then inverting these anomalies offers direct insights into deep magnetic discontinuities possibly connected with seismically active layer that is ultimately associated with regional temperature distribution.

Whereas magnetic spectral analysis has been applied to estimate Curie point depths from many territories in the world such as Japan e.g. Okubo et al. (1989), USA e.g. Blakely (1988), Greece e.g. Stampolidis and Tsokas (2002), Portugal e.g. Okubo et al. (2003), central Europe e.g. Chiozzi, et al. (2005) these work have not received much attention in Africa. In fact, no attempts have been made so far to study the Curie-point depths from magnetic anomalies and their possible links to seismicity distribution.

From the various geophysical works in Kenya Rift, the most remarkable gravity feature is a positive gravity lineation interpreted as a hot mantle intrusion zone, 10–20 km wide, representing the heat source for many geothermal systems in the rift (Cantini et al., 1990). However, there are too

many unknowns and gravity station coverage is too sparse for the results to be unique (Swain, 1992). In addition, KRISP (1991) did not provide overwhelming evidence for the massive intrusion that was originally suggested to explain the axial gravity high yet did provide a velocity section for the upper crust along the axis of the Kenya Rift. Therefore, despite these extensive studies there is still uncertainty on what have caused the gravity anomalies and high velocity zones and how and why they are connected with seismically active belt/zones. In order to bridge this gap, aeromagnetic data is used to determine significant geological structures in the study area (linear and circular i.e. faults and volcanoes) using 3D Euler deconvolution. Subsequently, Curie point depths are estimated to provide insights into thermal structures, whose relationship with linear structures is determined and an inference made on driving mechanism of seismotectonics. In addition, results correlated with known geophysical anomalies (gravity and seismic velocities). In a broader sense, this sheds light on the rifting tectonics in a young continental setting.

6.2 Structural setup and tectonics

The Paleogene to Recent Kenya Rift, a sinuous system consisting of a combination of normal grabens, asymmetric grabens and monoclinally flexed depressions (Baker and Wohlenberg, 1971, Baker et al., 1972a), belong to the eastern branch of the great continental East African Rift System (EARS) that stretches over 4000 km from afar Triangle to southern Mozambique. The Kenya Rift, like the rest EARS, is considered to be in the initial stage of continental breakup (Achauer and Masson, 2002, Chorowicz, 2005). The rift is superimposed on the eastern margin of the East African plateau and is located close to the boundary of the Tanzanian Craton and the Pan-African Mozambique Belt (Baker et al., 1972a). Kenya Rift almost terminates at Northern Tanzania, where it widens into a broad depression and becomes indistinctly defined, a location known as North Tanzanian Divergence that marks a triple junction of the Eyasi, Manyara and Pangani segments (Macheyeki et al., 2008). The study area stretches from central (around Lake Bogoria) to southern Kenya Rift (around Lake Magadi) as shown in Figure 6-1.

On the basis of morphological, structural and volcanic signature, Smith and Mosley (1993) subdivided the Kenya Rift into three segments namely; northern Baringo/Turkana, Aberdare Detachment and southern Magadi/Natron, which are separated by major NW–SE trending ductile shear zones in the underlying Precambrian Basement (Figure 6-1). The southern Kenya Rift segment, in particular, is supposed to have developed on a craton type lithosphere that has been obscured by imbricated thrust slices and

gravitationally collapsed nappes of the Tanzania Craton and the Mozambique belt (Smith, 1994, Simiyu and Keller, 1998). Thus, this pre-existing framework might have influenced and controlled the location and structural geometry of this part of the rift by the reactivation of the Aswa–Nandi–Loita (ANL) shear zone, which is a ductile and brittle NW–SE to NNW–SSE zone bounding Lake Magadi area at its northern limit (Smith and Mosley, 1993).

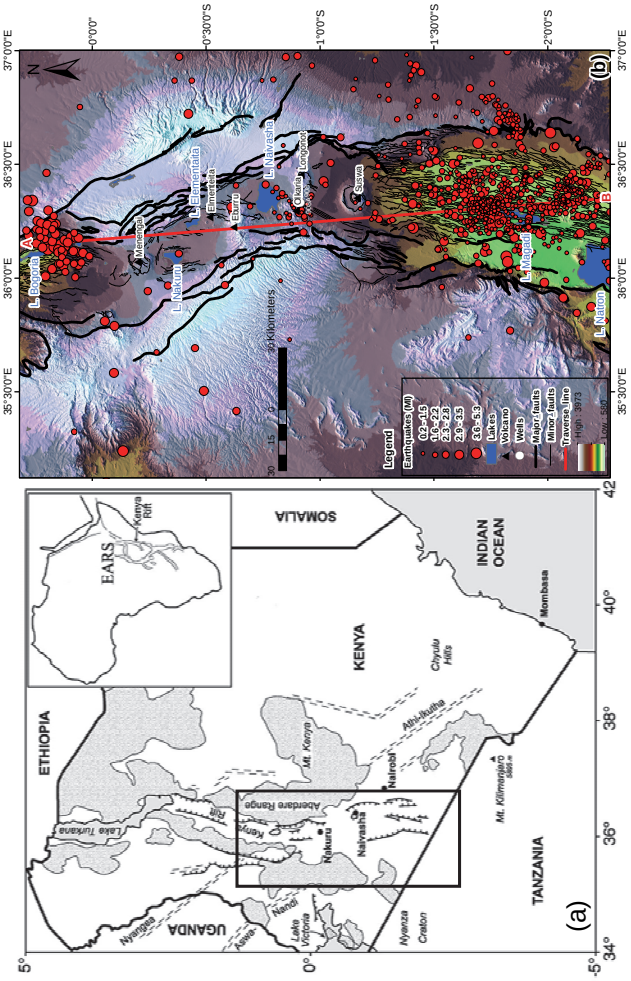

Figure 6-1a. Shows location of Kenya Rift and key features: Aswa–Nandi–Loita shear zone and Aberdare Detachment. Insert is map of Africa showing East African Rift System (EARS) and Kenya Rift. Rectangular block marks location of study area shown in (b). Fig.6-1b. SRTM DEM (solar azimuth 345 and solar elevation 45) showing location of study area, tectonic structures are marked by bold black faults and vast minor faults marking axial rift, major volcanic centres (black triangle), red dots are background seismicity (catalogue from year 1993-1996 and 1999-2001). Red line marks traverse A-B along which the topography, buffer of earthquakes within 25 km and Curie point depths were extracted and used to plot Fig. 6-9.

The crustal structure of the central to southern Kenya Rift is well documented from early gravimetric studies (Fairhead, 1976, Fairhead and Reeves, 1977, Girdler, 1978) to other geophysical studies (KRISP Working Group Party, 1991, Achauer et al., 1992) including vast contribution from seismic refraction-wide-angle reflection experiments (Mechie et al., 1997, Keller et

al., 1994a). The crustal thickness beneath the graben valley is 30 km at latitude 0.5°, but is varied in the western and eastern flanks attaining thickness of 40 km and 35 km respectively (Achauer et al., 1992). Similarly, the shoulders, partly covered by volcanic rocks, are ~2600 m high in the west, ~2000 m in the east. In addition, the sediments and volcanics in the graben are encountered to a depth of 3 km. The rift symmetry is expressed by normal faulting and tilted blocks with two major listic faults and associated roll-over structures (Baker and Wohlenberg, 1971). Accordingly, the regional negative Bouguer anomaly for this area expresses uplift of an asthenospheric body (Fairhead, 1976). Similarly, Keller et al. (1994a) have described a sharply defined lithospheric thinning, with low upper mantle velocities down to depths of over 150 km and alluded that the distinct relative positive residual anomaly in the middle of the graben is due to dyke injection related to reservoirs of magma. Despite the efforts to unravel the crustal structure in this part of the rift several factors play key role; Achauer et al. (1992) outlined the structural attributes that manifest uneven stress distribution, reflecting a heterogeneous crust. These include half grabens of various sizes and polartities, differing displacements and dips on the major faults within rift and the concomitant accommodation zones (King, 1978, Bosworth et al., 1986). In addition, they observed that possible occurrence of intrusions (reflecting variable thermal regime) may affect crustal response to extensional deformation. Therefore, the ardent quest to refine the crustal structure using different approaches and techniques cannot be over emphasized. It was on this premise that this study was proposed focusing on constraining the undulating 3D morphology of thermal structures and their possible tectonic influence for area covering central to southern Kenya Rift.

6.3 Methodology

The methodology used in the study focused on characterizing the geomagnetic field anomaly and the local geology, evaluating the depth of magnetic sources, estimating the Curie point Depths (CPDs) and validating the window-sizes used in spectral analysis, establishing the relationship between earthquake hypocentral distribution and CPD to infer possible driving mechanism of rifting process.

6.3.1 Geomagnetic field anomaly and local geology

For the purpose of characterizing the geomagnetic anomaly and local geology (Figures 6-2a, 6-2b), aeromagnetic data was used. The data covering study area was acquired in the year 1987 by Compagnie Générale de Géophysique, a French Seismic Acquisition and Processing Services Company, being part of the African Magnetic Mapping Project (AMMP) that covered most parts of Africa (Barrit, 1993). These data were acquired at a flight height of 2896 m

above mean sea level with a line spacing of 2 km and flight direction of 90° i.e. running in E-W direction. On average, each flight line covered distance of about 148 km, with entire aeromagnetic data set acquired along 241 flight lines. In addition, aeromagnetic was acquired data along 16 cross-over lines running in N-S direction for the purpose of correcting cross over errors i.e. repeat measurements during E-W and N-S acquisitions. Coincidentally, a total area of 148 km (E-W) by 482 km (N-S) was covered stretching from central to southern Kenya Rift that represents the study area. The magnetic data was preprocessed by AMMP that included levelling correction and regional field removal (using IGRF model of 1987 with field strength of 33383 nT, Inclination of -35.4°, declination of -1.4° to the south, and 33949 nT, Inclination of -21° declination of -0.13° to the north). The regional field removal was channel based (and not the above mentioned declination, inclination and regional field), meaning that each sampling point was corrected with respect to its geographical location. The declination, inclination and regional field are stated for purpose of showing examples of IGRF 1987 model for the study area. Subsequently, a database was built up with a projection system of AMMP. It is worth noting that the quality of these aeromagnetic dataset was confirmed using a subset for the southern Kenya Rift (Lake Magadi area) to characterize the geology, structure and tectonics (Kuria et al., 2010a).

The database from GETECH was imported into Oasis Montaj (Geosoft software) for further processing. The latitude and longitude coordinates in AMMP projections were re-projected to local geographic projection (Arc 1960) to facilitate data exchange format with other GIS softwares. For the purpose of generating geomagnetic anomaly map, the residual data were interpolated using minimum curvature method (Briggs, 1974) on to a 1 km grid and colour contoured using histogram equalization at illumination and declination angles of 45°. The minimum curvature assumes a smooth and a smallest amount curvature between interpolated points, constraining the anomaly precisely. The results were correlated with the local geology.

The analytical signal (AS) method (Roest et al., 1992) was applied to the geomagnetic anomaly data for the study area. According to MacLeod et al. (2000), absolute value of AS is defined as the square root of the squared sum of the vertical and the two horizontal derivatives of the magnetic field. In practice, AS method involves application of a mathematical procedure to correctly relocate the amplitude over the magnetic body (source) directly and is not affected by the directions of the earth's magnetic field and magnetization of the body e.g. Nabighian (1972). After application of AS the results were presented as an additional column in the database, which was

also interpolated using minimum curvature onto a 1 km grid and colour contoured using histogram equalization at illumination and declination angles of 45°. Similar to geomagnetic anomaly, the results were correlated with local geology.

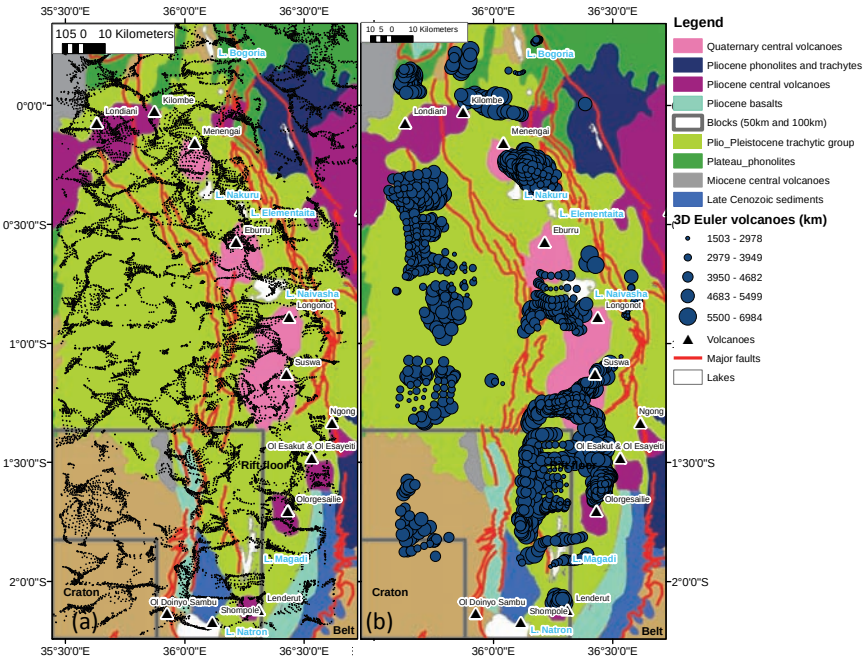

Figure 6-2a and 6-2b. Geological map showing Cenozoic formation (comprised of extensive plains/plateaus and central volcanoes) along rift valley. SW and SE parts mark Tanzania Craton (granite-greenstone terranes) and Mozambique Belt rocks respectively – modified from Baker et al. (1971). Superimposed on (a) are 3D Euler faults marked by linear small black dots and (b) 3D circular structures interpreted as volcanoes deduced from 3D Euler deconvolution (discussed later).

6.3.2 Evaluating depth of magnetic sources

The evaluation of the magnetic sources was important in assessing possible direction of magnetization, a requirement in defining the model for CPD determination using spectral techniques i.e. presence of rift valley would indicate directional magnetization. For the purpose of this study, 3D Euler method was used that includes extended Euler deconvolution for 2D structures that employs transformation of homogenous functions under rotation and therefore providing multi-depth solutions (Mushayandebvu et al., 2001, Reid et al., 1990). A selection of window size of 10 km for faults and 20 km for volcanoes was made. The 20 km length is close to the minimum diameters of the known volcanoes in the study area. It is apparent

that these dimensions also eliminate numerous small magnetic sources that are insignificant for the regional scales considered in spectral analysis. A depth error estimation of about 10% was selected and two types of structural indices; index 1 for the faults and index 3 for rounded structural features related to volcanoes.

6.3.3 Estimating Curie point depths using spectral techniques

The spectral analysis techniques are used to separate influences of different body parameters in the observed magnetic anomaly field as a method of determining CPD. The signal from the top surface of a magnetized body dominates the signal from the bottom at all wavelengths which makes the inverse problem more complicated (Blakely, 1995). However, magnetic data, after the removal of the main field and external currents contains information down to the depth where rocks lose their magnetization either due to compositional or temperature changes e.g. Rajaram, et al. (2009) and references therein. Therefore, analysing the long wavelength part of the magnetic data can provide information about this depth.

There are several methods used to estimate depth at which rocks lose their magnetization from the azimuthally averaged Fourier spectra. A summary from Ravat et al. (2007) include the centroid method (Bhattacharyya and Leu, 1975, Ibrahim et al., 2005), the spectral peak method (Spector and Grant, 1970, Blakely, 1988, Connard et al., 1983, Ross et al., 2006), the power law corrections (Pilkington and Todoeschuck, 1993, Maus and Dimri, 1995, Fedi et al., 1997). In particular, Ravat et al. (2007) obtained best results after applying Fedi et al. (1997) correction – a complete revision of Spector and Grant (1970) statistical model, applicable where models are not random. For noisy data, Odegard and Dickson (2004) suggested that the spectral method may be the only way to determine the depth because the other direct methods have problems dealing with white noise. However, more recent multiscale methods dealing with noise have proved very stable e.g. Fedi (2007).

For the purpose of this study, Spector and Grant model (1970) was used and Fedi et al. (1997) correction applied. This model is based on a mathematical statistical postulate that the magnetic anomalies from ensemble of simple sources have their slopes (in logarithms of azimuthally averaged Fourier spectra) related to the depth to the top of the ensemble and the spectral also have peak positions on the frequency or wavenumber axis related to the thickness of the magnetic source. The assumption is that all ensemble parameters are uniformly and independently distributed. The gist in this combined approach (Spector and Grant model and Fedi et al. correction) is

that prior knowledge of ensemble sizes is not necessary and more importantly it is applicable in area of uniform magnetization as observed in the study area (see geomagnetic field anomaly map, analytical signal). This method contrasts purely random sources (Naidu, 1968) appropriate for describing a shallow and highly variable magnetization distribution (Quarta et al., 2000).

Prior to spectral analysis, the Spector and Grant Model (1970) similar to other Fourier based techniques requires selection of window-blocks on the regional magnetic anomalies. To select the appropriate window size, several window sizes were tested (i.e. 100 km by 100 km, 75 km by 75 km and 50 km by 50 km) by superimposing them on the geomagnetic field anomaly map, analytical signal map, magnetic sources maps. It was observed that 100 km squared window block and that of 75 km sampled highly variable sources making the results geologically insignificant. Therefore, 50 km sized window (which sampled relative uniform anomaly) was adopted as appropriate one. However, for the purpose of completeness spectral analysis was carried out for both 100 km and 50 km window-blocks and their results compared.

A total of 132 squared-window-blocks each measuring 100 km were extracted from geomagnetic field anomaly map in oasis montaj software (Geosoft) gridded on to 2 km cell size. Similarly, a total of 297 squared-window-blocks with a size of 50 km were extracted from the same geomagnetic field anomaly map. All these window-blocks (both for 100 km and 50 km) were sampled with a step of 10 km both in latitude and longitude for the entire 148 km by 482 km area. This fine moving step with 90% overlap of adjacent window-block provided for a very high spatial resolution to constrain accurately the morphology of bottom magnetic crust in area of highly variable tectonic provinces (craton, rift volcanics and Proterozoic mobile belt). Commonly, 50% overlap between adjacent window block is adopted in literature (Blakely, 1988, Okubo et al., 1989, Okubo et al., 2003, Chiozzi et al., 2005).

After constructing the window-blocks, a test on wavelength anomalies, which arise mainly from topography, regional features and magnetic core fields was performed. These would affect CPD estimation. A radially averaged log power spectrum was transformed, computed and analysed for magnetic anomaly covering the entire study area. The unfiltered spectrum showed a significant peak at 0.0089 cycles/km. Several filters were tested i.e. a high pass filter (Okubo et al., 1985), which distorted the entire spectrum (similar to overcorrection of the spectrum in Ravat et al. (2007) resulting into shallow

peak while raising the rest spectrum and therefore this filter was discarded. In addition, the grid data was upward continued at 150, 200 and 250 m using Fourier domain technique (Blakely, 1995). This filtering showed no noticeable effects on the spectrum. It was assumed that a flight of 2896 m possibly filtered the high frequencies and more filtering was inconsequential.

For each of the 50 km and 100 km block, the gridded data was detrended to remove the long wavelengths by taking out the first-order surface that best fits the data in a least square sense (Connard et al., 1983). Then map data was tapered in order to smooth gradually the intensity to zero at the edges of map data using a 10 point Hamming window.

From this new grid, the 2D DFT transform was computed using the algorithm of Press et al. (2002), and the power spectra calculated. Once the power spectrum is estimated, the next step is to calculate the radial power spectrum. This is a radially averaged 2D spectrum and is estimated by averaging the power spectrum over a set of concentric rings about k=0 with increasing radius (Naidu and Mathew, 1998). Subsequently, the radial power spectrum is normalized with respect to the value of the first harmonic, the natural logarithm calculated, and then the new data transferred to microsoft excel. Frequency scaling of the power spectrum was computed. Prior to plotting the spectra, the filter by Fedi et al. (1997) was applied to both normal radial power spectrum and scaled frequency radial spectrum, and subsequently plotted versus wavenumber (Figure 6-3). For the two power spectrum i.e. frequency scales and normal power spectrum their gradients were determined by least square regression in the two frequency areas. The bottom depths Zb were calculated using Equation 6.1 after Okubo et al. (1985). This procedure was followed for each of the 132 squared-window-blocks (100 km) and 297 window- blocks (50 km). The calculated Zb values for each block type (50 km and 100 km) was referenced using the centre coordinates of the respective block and contoured using a cell size of 2 km. The results are presented into maps i.e. CPD for 50 km and 100 km.

$$Zb = 2Zo - Zt \qquad \text{(Equation 6.1)}$$

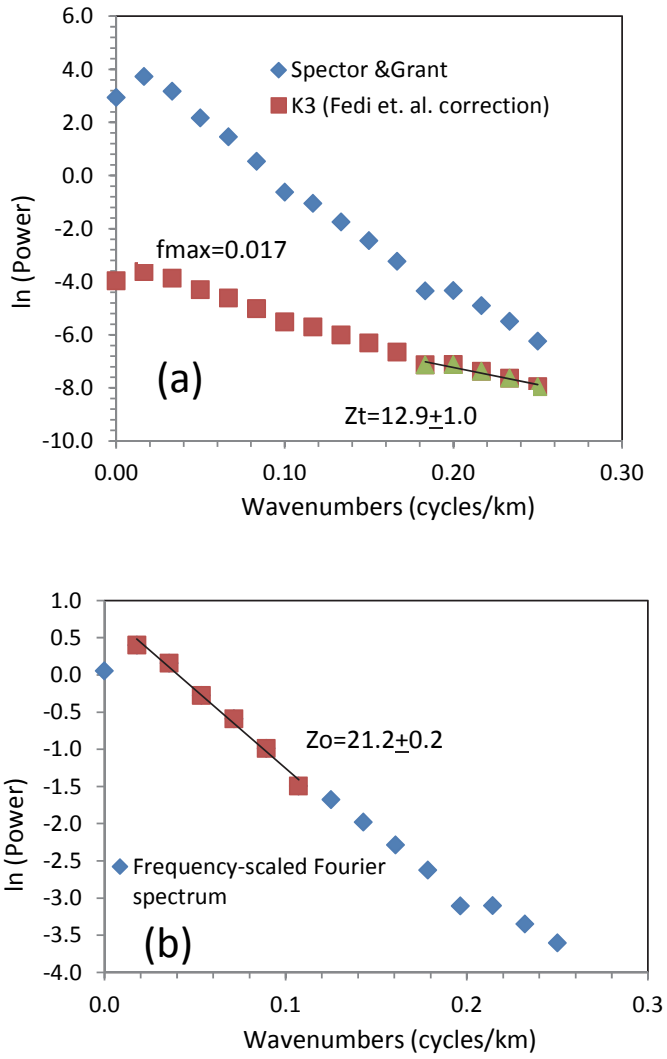

Figure 6-3a and 6-3b. Examples of spectra for estimation of the Curie point depth. The blue line in (a) is Spector and Grant (1970) spectrum, a correction of this spectrum using Fedi et al. 1997 correction factor K^{-3} is shown by the red line. The black line is a linear fit by least-square method for the section of the spectrum marked by light green triangles. The depth Zo is found from the slope of radially averaged frequency-scaled power spectrum, black line with red marks (b). The bottom Zb is then obtained from the equation Zb=2Zo-Zt. Notice Zb value of 29.4 and 29.43 km for spectral peak and Okubo et al. (1985) for this example (Block 100 – see Figure 6.6b).

6.3.4 Evaluating CPD versus window sizes

Using the 50 km and 100 km contoured map (in geosoft grid format) of the CPD, the 50 km grid was subtracted from 100 km grid and "difference grid map" obtained that shows the spatial variation of CPD for the two window-blocks (50 km and 100km). Obviously, the large values in the "difference map" reflect the erroneous magnitude in CPD estimation. On this basis, 6 blocks were selected in the area with largest CPD difference from "difference map", and their corresponding CPD values read from 50 km and 100 km database (i.e. marking same location). Subsequently, temperature with depth was computed for these blocks using Equation 6.2 that was successfully applied by Albaric et al. (2009), where

$$T(z) = To + \frac{(Qo - Aoe^{-z/b})z}{k} + \frac{Aob^2}{k}(1 - e^{-z/b}) \qquad \text{(Equation 6.2)}$$

Where z is the depth (km), To is the temperature taken from 22°C (assumed from earth surface temperature), Qo is the surface heat flow (mW m^{-2}), b is a length parameter, and K is the thermal conductivity (W m^{-1} k^{-1}). The heat production exponentially decreases with depth and equal Ao (µW m^{-3}) at the surface. To calculate the temperature with depth a surface heat production of 2 µW m^{-3}, as estimate from Chapman and Pollack (1977) and Nyblade et al. (1990) was used together with typical values for thermal conductivity k and characteristic depth parameter b of 2.5 $Wm^{-1}K^{-1}$ and 10 km respectively (Fadaie and Ranalli, 1990, Turcotte and Schubert, 2002). The boundary condition for surface heat set at 110 mWm^{-2} being characteristic estimates made by Albaric et al. (2009). The computed temperature with the depth (CPD for 50 km and corresponding 100 km) for 6 blocks was compared with expected temperature of 580 °C. The results are presented in Table 6.1. The estimates made using the 100 km CPD are overestimated compared to the expected 580 °C. This also validates CPD estimates from 50 km squared-window blocks.

6.3.5 Establishing relationship between CPD and earthquake focal depth

The maximum focal depth of earthquakes has long been known to provide fundamental properties of the upper part of the lithosphere, in particular the transition from brittle faulting to plastic flow in the crust, or a change in the frictional sliding process e.g. Sibson (1982). In order to understand the properties of the crust and possibly infer the rifting tectonics, the earthquake focal depth distribution was evaluated and correlated with the CPDs considering that the thermal state (indicated by CPD) and mineral composition of the continental lithosphere are factors controlling the first

order its strength (Chen and Molnar, 1983). For this purpose, earthquake data for period between October 1993 and August 1996 (Hollnack and Stangl, 1998) and between November 1997 and June 1998 (Ibs-von Seht et al., 2001) was used. The original data for the later seismological survey (Ibs-von Seht et al., 2001) was provided courtesy of Ibs-Von Seht, Hannover, Germany. The earthquake data was analyzed using SEISAN program (Havskov, 1997) and applying velocity model derived from the results of the KRISP 1994 experiment (Prodehl et al., 1997b), with mean vp/vs ratio of 1.74. The earthquake locations from the two database are shown in Figure 6-1.

A selection of transects along KRISP line G, KRISP axial line and traverse line A-B was made. Traverse line A-B was selected to characterise the gap between KRISP line G and KRISP axial line. CPD along these traverses were extracted from 50 km grid map in geosoft. Similarly, earthquakes within a buffer zone of 25 km i.e. 12.5 km on either side of the 3 traverse line were also extracted. This 25 km buffer zone was selected to sample adequate number of earthquakes. These two data sets (CPD and earthquake focal depths) were plotted together with scaled topography (i.e. elevation in km multiply by a factor of 10) to display their relationships.

6.4 Results

Several analytical techniques have been employed to unravel the buried geological structures, delineate thermal structures and interpret them in relation to tectonic structures and earthquakes distribution (i.e. focal depth and spatial parameters).

6.4.1 Geomagnetic field anomaly and local geology

The geomagnetic anomaly field (ΔT) of the area covering central to southern Kenya Rift (Figure 6-4a, Figure 6-5b)) shows highly variable magnetic intensities ranging from high positive anomalies (90 nT) to very low negative anomalies (-210 nT) variably distributed in the area: Characteristically, on south western part relatively broad and miniature magnetic intensity of mainly negative anomalies with amplitudes of -11 to -27 nT, mark location of Tanzania Craton. A linear NW-SE oriented trace (marked by light green patched with dark blue colour) truncating the northern limit of Lake Magadi – correspond to ANL shear zone (Kuria et al., 2010a). The NE and SE part with amplitudes of about -45 and -77 nT match the location of Mozambique Belt.

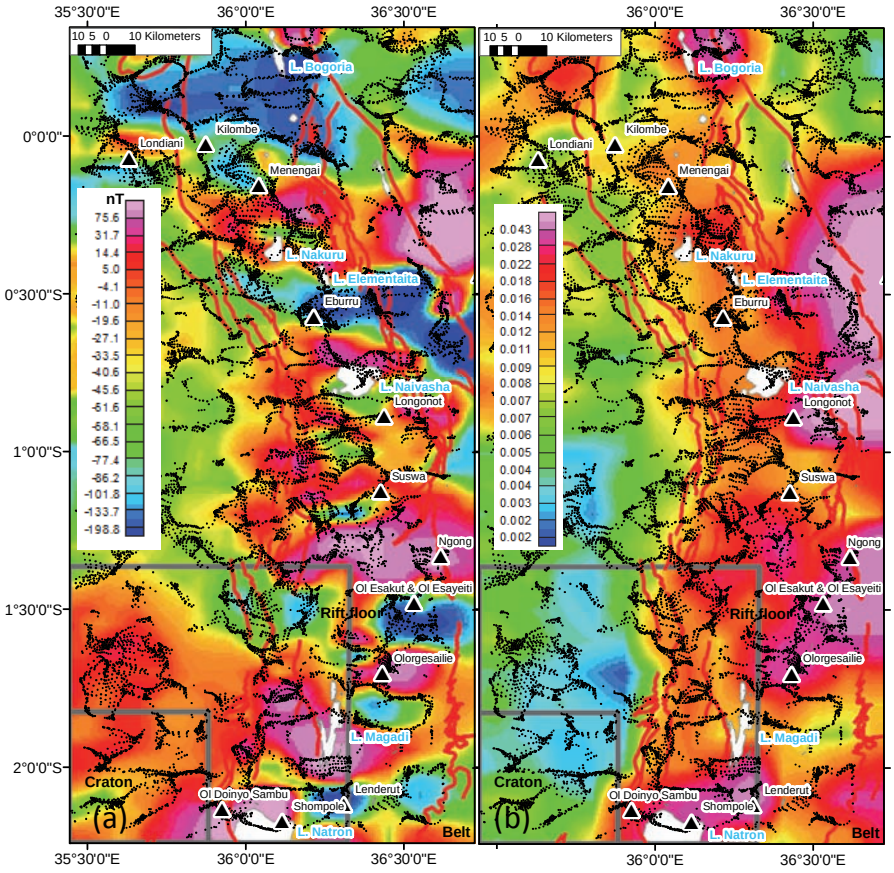

Figure 6-4a. Map of the geomagnetic anomaly field (ΔT) of the area covering central to southern Kenya Rift: Tanzania Craton is characterized by relatively quiet geomagnetic field – several broad mainly negative anomalies are observed on western part. The rift floor has intensive positive anomalies, which are high frequency sources. Patches of low magnetic anomalies mark location of the Mozambique Belt. Figure 6-4b. Map of the analytic signal of the total magnetic anomalies (from AMMP 1km x 1 km cell size) correlated with Tanzania Craton, Mozambique Belt and Rift Valley. Notice the sharp boundaries between these tectonic provinces that define or constrain the three 50 km widow blocks used for radially averaged spectral analysis. Black dots are 3D Euler faults and the grey squared blocks on western corner are 50 km and 100 km showing sampling of different magnetic sources (discussed later).

On the rift floor, there is a fair match of the geomagnetic anomalies and lithological boundaries: the light green colour (-51 and -65 nT) widely spread in the area, particularly on the western part (latitude 1°S) interpreted as Plio-Pleistocene trachytic group. On the axial rift floor, this trachytic group is interspersed by rather isolated high intensity anomalies that correlates spatially with the three Quaternary central volcanoes (Menengai, Eburru, Longonot- Suswa) and four Pliocene central volcanoes (Ngong, Ol Esakut - Ol Esayeiti kasut, Olongesailie and Lenderut) south of the study area. Surprisingly, Ol Esakut - Ol Esayeiti kasut, Eburru and Lenderut have very low magnetic intensity (dark blue colour -158 nT) and Menengai, Ngong, Longonot - Suswa and Olongesailie have high magnetic intensity (red +75 nT). The Quaternary basalts are also characterized by moderate to high magnetic intensity covering northern and southern part of the study area.

The other central volcanoes include Londiani and Aberdare with intermediate to high magnetic intensity, which are interestingly connected by an anomaly of moderate magnetic intensity. Typically, the geological boundaries and the magnetic intensity of Miocene central volcanoes and alkaline complexes are marked by Tinderet volcanic centre to the NW match closely well and reflect moderate magnetic intensity (largely orange – negative 33.5nT). Plateau phonolite (located to the north) have low to moderate magnetic intensity (-156 to + 58 nT). Therefore, map of the geomagnetic anomaly field (ΔT) can be a useful tool for characterizing the lithological boundaries of the areas not easily accessible.

The analytical signal map (Figure 6-4b, Figure 6-5b) depicts sharp contacts allowing a classification from west to east of low, moderate and high magnetic intensities: The boundary between Tanzanian Craton and rift - that stretches from south to almost central Kenya - is very distinct and matches with location of the westerly major rift boundary faults. Along Tanzanian Craton, amplitudes of magnetic anomalies are low with a better spatial correlation that indicates a possibly increasingly deeper or thickened crust. Notably, the magnetic anomalies characteristic of tracytic group are not evident on analytic signal map on this western part. This indicates that the trachytic group forms a relatively thin cover, suggesting possible flooding on top of Tanzanian Craton. The rift floor is characterized by moderate magnetic intensity (orange) apart from the areas characterized by volcanoes that have high magnetic intensities. The distinction of different volcanoes is not vivid on AS, which connotes that the variability in the magnetic intensity (observed in geomagnetic anomaly map) was a rather surface characterization that could plausibly be explained by degree of weathering. Another more interesting feature is the location of the Pliocene central volcanoes, in particular at the

location of the Aberdares. Here, a very high magnetic intensity zone (deep red) stretches close to Eburru and Longonot and even further eastwards off the rift zone possibly towards location of Mt. Kenya - interconnectivity that entice inference to common origin.

6.4.2 Depth of magnetic sources

The map of the linear magnetic sources determined from 3D Euler depicts structures (using structural index 1) oriented in N-S, NW-SE, E-W to ENE-WSW, and NE-SW, which are similar to faults interpreted by Kuria et al. (2010a) for southern Kenya using different techniques. In addition, numerous linear structures follow SRTM DEM and others correspond to geological contacts, which further validates their interpretation. Interestingly, the faults from 3D Euler are not only confined within the rift floor – like those from DEM - but extend to Tanzania Craton and Mozambique Belt though with reduced density (their number and spatial closeness). The dominant structural orientation in areas covered by craton is NE-SW, which surprisingly corresponds to the youngest faults that mark a reactivation of pre-existing structures (Kuria et al. 2010). Other principal structures are NW-SE confined at the central part that could be associated with ANL shear zone. Within the rift floor, the principal structures are NE-SW and NW-SE. The 3D Euler linear structures and geological contacts show a very high spatial correlation at southern margin Lake Magadi area and at around Menengai crater (around Latitude 1°S). Surprisingly, no structures occur at the location of Aberdares and Ngong ranges, an explanation that is not obvious. All in all, the spatial distribution of the 3D linear structures (Figures 6-2a, 6-4a, 6-4b) indicates that there is no preferential direction of the magnetization, a requirement for spectral analysis (see section 6.3.4).

The spatial distribution of the rounded structural features from 3D Euler corresponds to the location of the almost all volcanoes along the rift floor, except for Eburru, Ol Doinyo Sambu and Shombole (Figures 6-2b, 6-5a, 6-5b). Again this correspondence accents the analytical technique and results obtained herein. A more remarkable finding is the location of the similar circular features along a linear trace beyond the western margin of the rift zone (as defined by the major structures). It is possible that these structures are buried volcanic centres (plutonic) and are speculated to be either related to evolution of the rift tectonically or fissure zones along which most of the lavas were emplaced, an observation made for the first time in literature. It is therefore not surprising that the Pliocene trachytic lava flooded most of the Tanzania Craton as noted in section 6.2 (analytic signal).

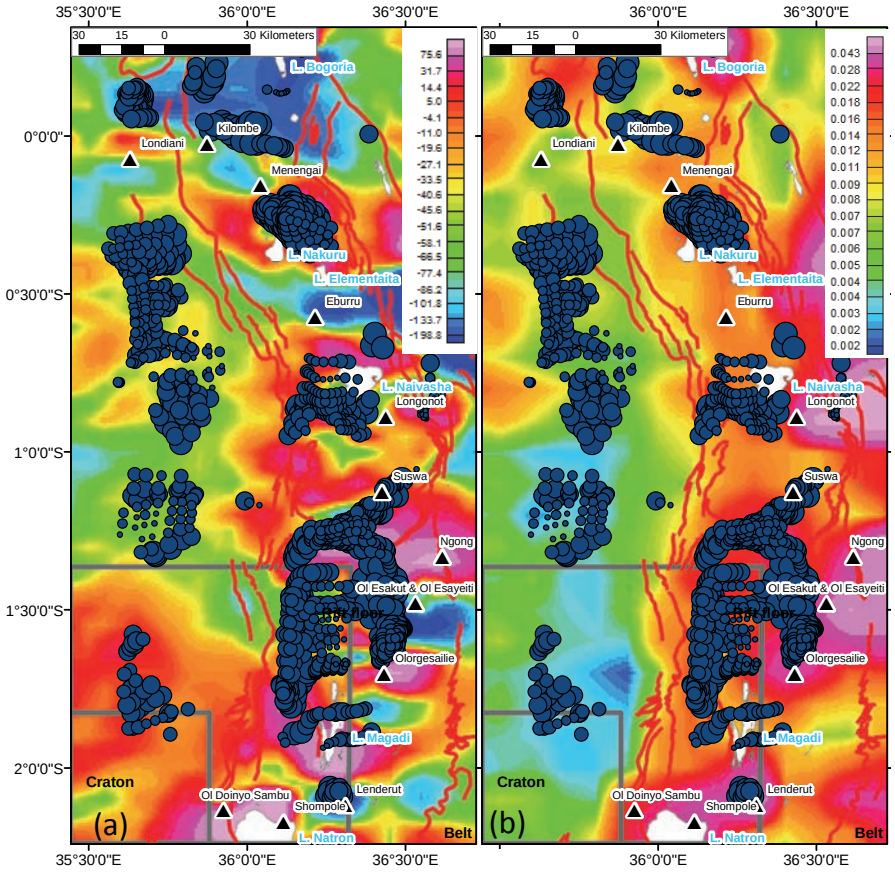

Figure 6-3a and 6.3b similar to Figure 6.2a and 6.2b superimposed in this case with circular features deduced from 3D Euler and interpreted as volcanoes: Those on eastern part are exposed, while those on western are buried.

6.4.3 Estimated Curie point Depths using spectral techniques

The results from the contoured 297 window-blocks (50 km by 50 km) show a thickened magnetic crust (orange to deep red in) interspersed by shallow CPD both within the rift floor and surprisingly beyond the western rift margin at around latitude 0.75° south (Figure 6-6). The largest shallow CPD anomaly (37 km (E-W) and 52 km (N-S)) is centred south of Lake Naivasha stretching between the Longonot and Suswa volcanic centres and attains a shallowest depth at about 9 km. The NW-SE oriented shallow CPD anomaly beneath Lake Bogoria (19 km and 40 km) forms the second largest anomaly. The small sized anomaly within rift floor are located NW of Lake Magadi and along the entire western margin of Lake Nakuru. Interestingly, a large NW-SE anomaly extends from the western margin of the rift for a distance of about

81 km off the rift floor. Noteworthy, these off rift shallow CPD locations correspond spatially to the location of the buried volcanic centers identified from magnetic sources of circular features (Figures 6-2b, 6-5a, 6-5b). Other small anomalies off the rift floor are located west of Lake Magadi and north western part of the study area. The later could possibly be likened to the younger Nyanza rift (Mathu and Davies, 1996) along which nearby volcanic centres of Tinderet and Londiani are located. These shallow CPD correlated to known volcanic centers indicates that these volcanoes are possibly thermally active. Deeper sources generally characterize the eastern rift margin between latitudes 0.3°N north and 0.7°S and the isolated blocks east, west and partly underlying Lake Magadi at latitudes 1.2°S and 1.6°S. The anomalies east of Lake Magadi correspond to location of ANL shear zone, whereas those to the further north are likened to Mozambique Belt. The western deeper CPD anomalies are possibly part of the Tanzania Craton or its suture boundary with Mozambique Belt.

The 132 squared-window-blocks (100 km long) show a dominant shallow CPD anomaly oriented in NW-SE direction between latitudes 0.6°S and 1.5°S with a minimum depth of about 21 km (Figure 6-6b). Other anomalies are located on the NW and SW margin of the study area but are somehow insignificant being outside the grid centre blocks (i.e. products of extrapolation).

The “difference map” i.e. a subtraction of the 50 km grid map from 100 km grid map (Figure 6-6c) show that apart from the shallow CPD anomaly located off the western margin of the rift, all the other shallow CPD anomalies observed in 50 km squared window blocks are masked, indicating that increasing window size masks locally significant sources. Generally, the deep CPD depth on the NW, SE and SW part are retained for the two maps (50 km and 100 km) – marked by blue colour – an indication of small estimation error. It therefore follows that a small window (50 km) is potentially capable of capturing more information from deeper magnetization variations, indeed 50 km window blocks had over 61% significant spectral peak indicating that the depth magnetic ensemble is detectable. The green colour shows a better estimate for central part of the study area and not necessarily within the rift floor, indicating that estimates at the margin are possibly affected by spatial resolution. Therefore, it is conclusive that increasing a window size to capture varied sources from different tectonic regime and/or geological setting masks significantly shallow sources, with subtle effects on spatial resolution except at the margins. Ultimately, an optimum window size increases spatial resolution and captures more sources considerably well.

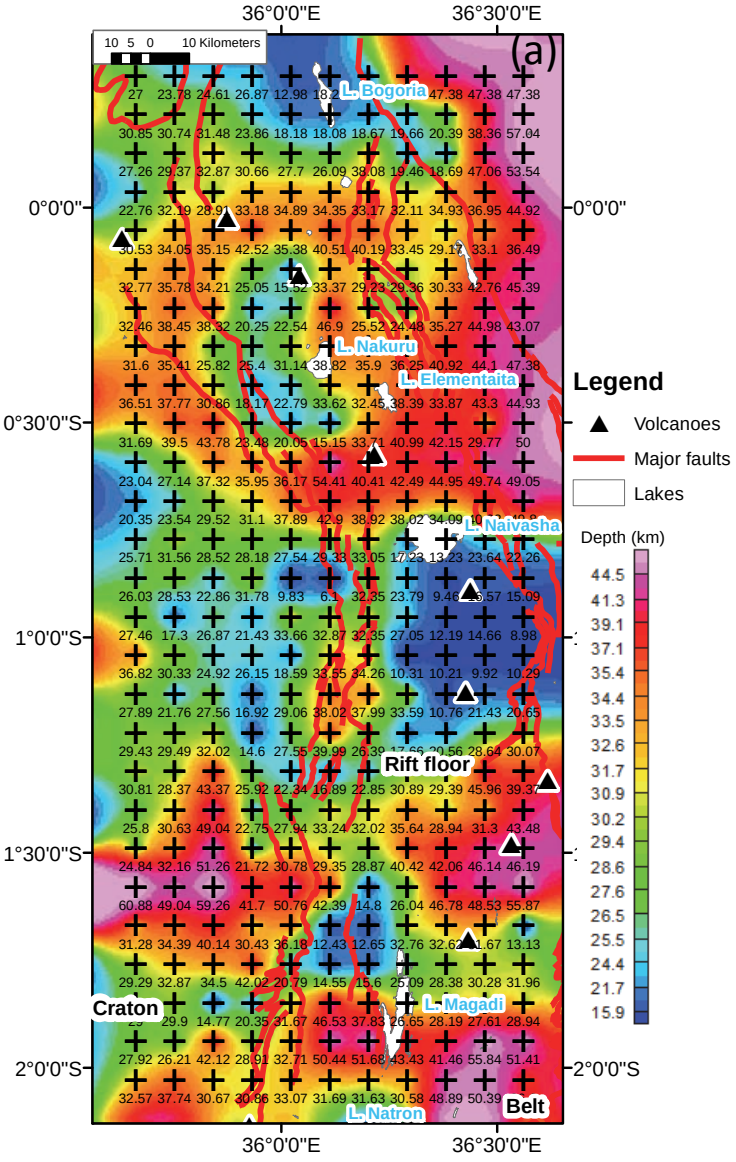

Figure 6.6a. Map showing Curie Point Depths for central to southern Kenya Rift for 297 window blocks (50 km by 50 km) as shown with + symbol marking window-centre. Red bold lines the rift boundary faults. Notice the generally thickened magnetic crust punctuated by shallow Curie depths; largest one located south of Lake Naivasha spatially marking Olkaria-Longonot-Suswa volcanoes.

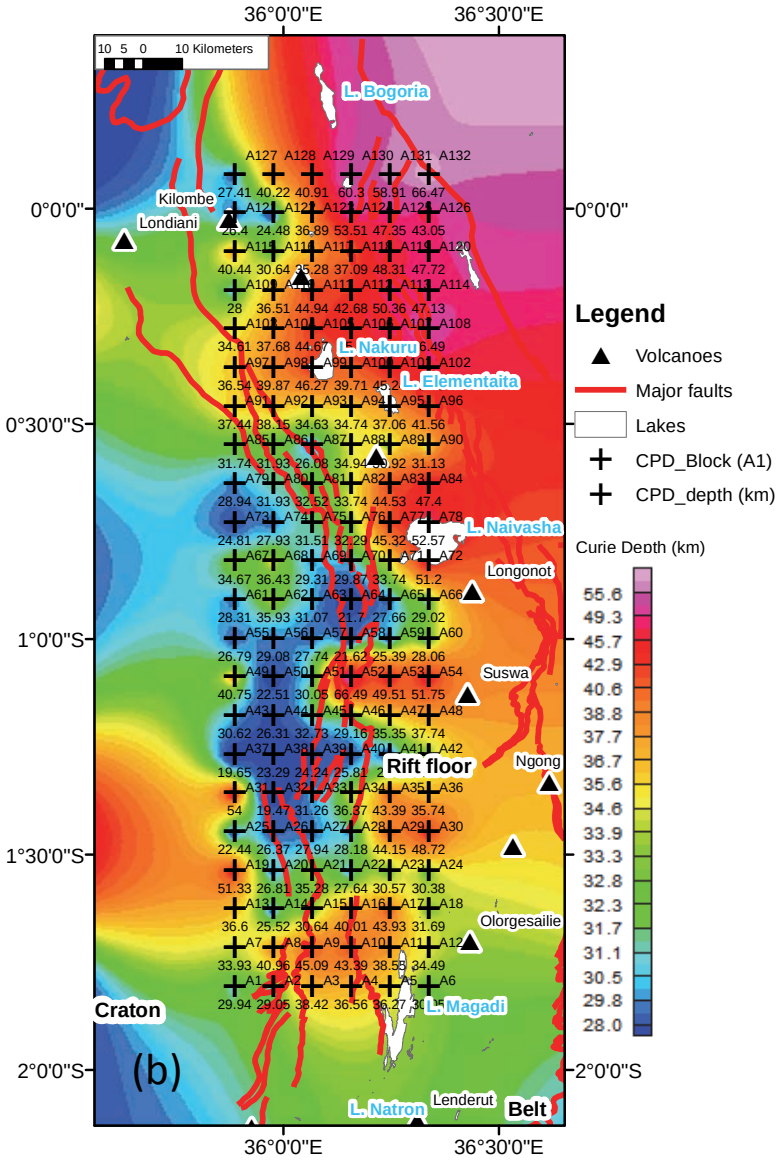

Figure 6.6b. Map showing Curie Point Depths for central to southern Kenya Rift for 132 window blocks (100 km by 100km) as shown with + symbol marking window-centre. Red bold lines mark the rift boundary faults. CDP show dominantly NW-SE direction between latitudes 0.6°S and 1.5°S.

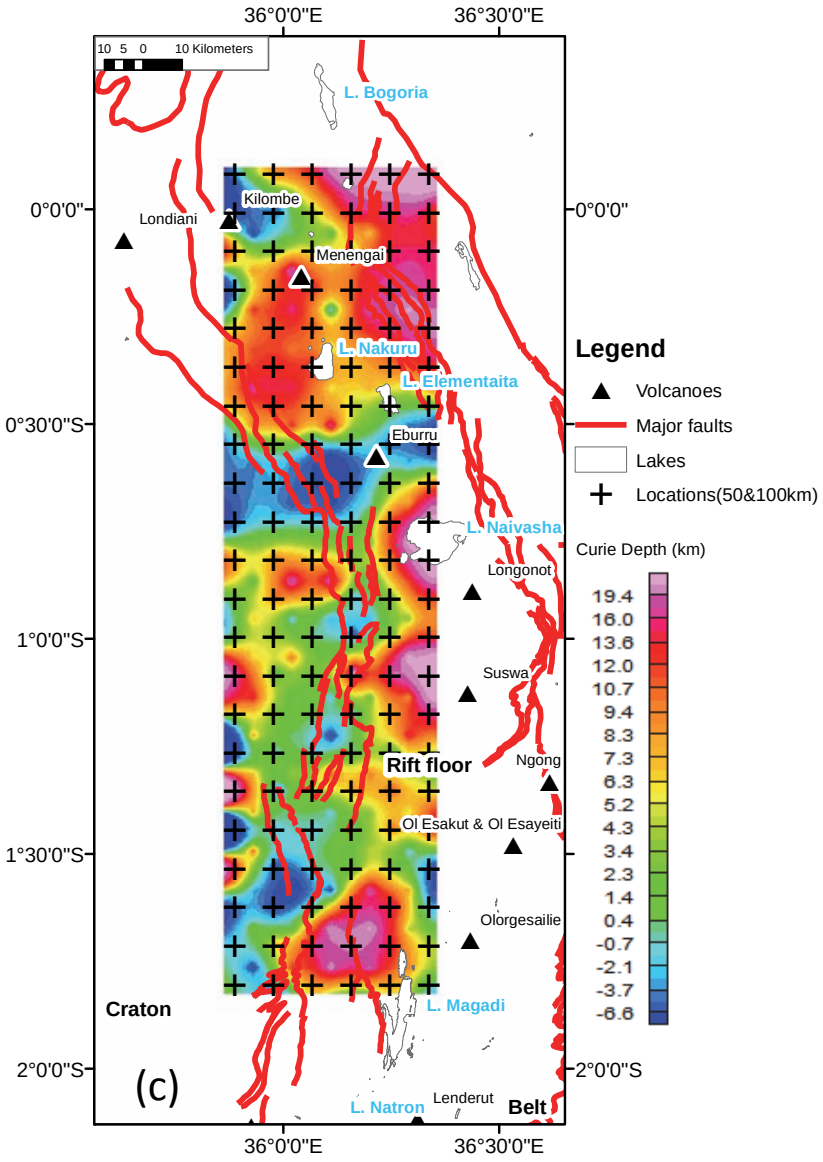

Figure 6-6c. "Difference map", a subtraction of 50 km grid from 100 km grid (using geosoft software). The smallest difference (marked by light green to light blue colour) are located in the central area, where spatial resolution is high compared to the edges. The anomalies marked by buried volcanoes shows a fair approximation. Noteworthy, shallow and significant CPD are masked in 100 km grid as indicated by huge difference at Olkaria-Suswa-Longonot, and Lake Bogoria area.

The results of the 6 blocks selected along window blocks with highest error margin are presented in the Table 6.1. One quickly sees that CPD from 100 km by 100 km window-block are overestimated, while those of 50 km by 50 km are only slightly lower compared to the expected value (580°C). These results additionally validate the CPD estimates.

Table 6.1: Estimated temperature using CPD marking the same location for 100 km and 50 km square window block.

Blocks (100km)	CPD (100km blocks)	Tz (°C) (100km block)	Blocks (50km)	CPD (50km blocks)	Tz (°C) (50km blocks)
A36	35.74	**1594.73**	B119	10.76	**493.16**
A42	31.74	**1418.46**	B130	10.21	**468.94**
A48	37.74	**1682.84**	B141	12.19	**556.18**
A54	51.75	**2299.76**	B152	9.46	**435.91**
A60	28.02	**1254.46**	B163	13.23	**602.03**
A66	29.02	**1298.55**	B174	34.10	**1522.47**

6.4.4 CPD and earthquake focal depth

The 25 km buffer zone (along KRISP line G, KRISP axial line and traverse line A-B) sampled a fair number of earthquakes allowing for correlation between earthquake focal and CPD. The plot of these focal depths along the selected traverse line (Figure 6-7), indicate that they originate from shallow sources with majority occurring at a depth of ~ 10 km. The focal depth distribution of earthquakes shows a clearly defined seismicity cut-off that is spatially variable. The shallow sources occur at Lakes Bogoria, Olkaria – Suswa, and Lake Magadi, locations that correspond spatially to localized shallow CPDs. Whereas the sharp narrow but deepened CPD between Lake Magadi and Olkaria-Suswa is correlated with ease to ANL shear zone – the interpretation of a similar but broadened zone between Olkaria – Bogoria remains aloof (Figure 6-7c). This later part that is largely indifferent is characterized by largely deep CPD that could be likened to a relict Proterozoic root, which is tectonically stable. Noteworthy, the seemingly increased seismicity around Lake Magadi does not commensurate increased tectonic activity but a dense network (von seht 2001) that favoured capturing of more earthquakes. Nevertheless, these results from the correlation of earthquake focal depth and Curie point depth (Figures 6-7a and 6.7c) clearly depicts, for the first time, that deep earthquakes on the rift floor preferentially occur within zones of deep Curie point and in this case specifically mark locations of the Tanzania Craton, Mozambique Belt and ANL shear zone (thickened crustal structure). The presence of these tectonic subsurface structure (thickened crust) is not obvious because it is not reflected on the corresponding topographical profile apart from partly Figure 6-7a (western margin of the rift).

6.5 Discussion

In efforts to advance the understanding of the structural evolution for central and southern part of Kenya Le Turdu et al.(1999) developed a conceptual tectonic model showing normal N-S, the dextral NW-SE and sinistral NE-SW created under E-W extension that was in odds with that of Bosworth and Strecker (1997), which promoted a NW-SE extension. Whereas Atmaoui and Hollnack (2003) supported Bosworth and Strecker (1997), Kuria et al. (2010a) provided detailed evidence for prevalence of structures that supported Le Turdu et al. (1999) model. Notably, Le Turdu et al. (1999) and Kuria et al. (2010a) identified structures for central and southern Kenya Rift respectively, largely using remote sensing techniques. Therefore, the presence of possible buried structures under thick pyroclastic cover (Baker and Mitchell, 1976, Baker and Mitchell, 1984) within the rift remained poorly resolved. Results from this study on linear structures (oriented N-S, NW-SE, NE-SW and E-W) deduced from 3D Euler show predominance of these structures even under thick pyroclastic cover (particularly south of equator to about 1°S), which bridges the gap (Le Turdu et al., 1999, Kuria et al., 2010a) by resolving these buried structures. It worthwhile to note that these buried faults would be difficult to identify otherwise. In addition, the predominance of NE-SW and NW-SE structures even in the area covered by craton (Figure 6-2a,6-4a,b) indicate that they are pre-existing cratonic structures whose genesis possibly dates to pre-rift evolution.

The results from 3D Euler show that the spatial distribution of the rounded structures (interpreted using structural index 3) corresponds to location of 7 volcanoes (Figure 6-2b) on the rift floor with exception of Eburru, Ol Doinyo Sambu and Shombole . According to Baker et al.(1971a) the geology of these volcanoes is as follows: Menengai (trachytic lava); Longonot (Pyroclastic trachyte); Suswa (basal trachyte); Olorgesailie (Olivine basalt); Lenderut (basalt andesite lava); Kilombe (trachytic lava) and Esakut and Ol Esayeiti (basalts). Whereas the geology of the undetected volcanoes is Eburru (rhyolite); Ol Doinyo Sambu (tephrite overlain by fossiliferous sediments) and Shombole (Carbonatite and nephelinite). It is alluded that the magnetic detectability of these volcanoes relates to their mineralogical compositions characterized by low silica content i.e. according to Harvey and Tracy (1996) trachytes consists of alkali feldspars (anothoclase, microcline, orthoclase, sanidine-all being potassium rich and low silica content); phonolites form from a high silica undersaturated melt (with abundant feldpathoids); basalts contain at least 65% feldspar in form of plagioclase. In contrast, high silica content in rhyolite and nephelinite, and high content of carbonates in carbonatite results into low magnetic susceptibility of these undetected volcanoes.

A more remarkable finding using 3D Euler is the location of the buried circular features along a linear trace beyond the western margin of the rift zone (as defined by the major faults) but parallel to the volcanoes identified above. The magnetic sources related to these concealed volcanoes range from a depth 1.5 km – 7 km. It is inferred that these circular features are buried volcanic centres (plutonic) - "possible feeder dykes" - and their geological composition falls under either trachytes, phonolites or basalts similar to volcanoes marking the eastern margin of the rift. It is speculative that they are either related to evolution of the rift tectonically or are fissure zones along which most of the lavas were emplaced: evidenced for the first time in literature. It is therefore not surprising that the Pliocene trachytic lava flooded most of the Tanzania Craton as noted in section 6.2 (analytic signal). This inference is not outrageous because Baker et al. (1971b) suggested that the lava flows forming plateaus could have been sourced from fissures or numerous localized eruption centres, which indicates that this interpretation supports their latter category.

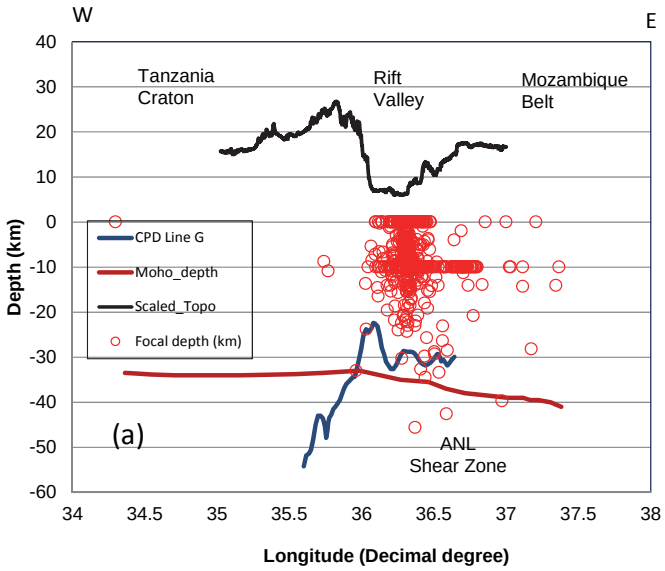

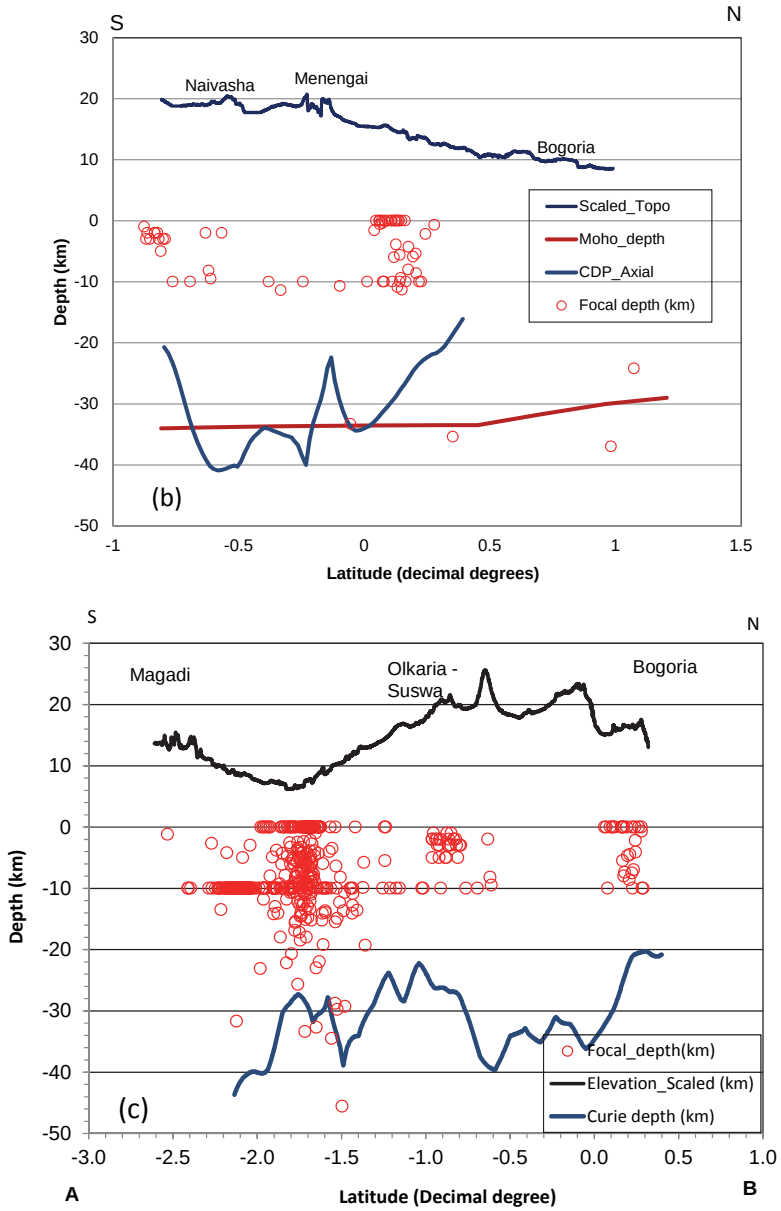

Figure 6-7. Plot of earthquake focal depth distribution versus Curie point depth and scaled Topography (elevation in km x 10) along KRISP Line G (a); KRISP axial line (b) and a traverse line A-B (c). Earthquakes cluster preferentially along (or close to) zones marked by shallow CPD, amid a few outliers. Note: there is no eminent relationship between topography thermal structures.

In estimating depth to the bottom of ensemble of the magnetic sources from the regional aeromagnetic data using spectral analysis, selection of an optimum size of window-block remains one of the challenges towards obtaining reliable results. Noteworthy, there has not been a consensus on the choice of the window size in spite of the numerous research works on spectral analysis on magnetic data. Some have selected very small window sizes varying from 9 to 20 km for example Dolmaz et al. (2005b); 64km by 64km (Espinosa-Cardeña and Campos-Enriquez, 2008); the common window size is 60×90 km to 150×150 km (e.g. Okubo et al. (1985); Dolmaz et al. (2005a) but even much larger window sizes have also been advocated (Chiozzi et al., 2005, Ravat et al., 2007) i.e. 440 km x 440 km to 550 km to 550 km (Rajaram et al., 2009). Therefore, to determine the size of the window-block to use for this case, magnetic sources (linear and circular) were determined, and compared to geology, which is largely dictated by three tectonic provinces (Tanzania Craton, rift volcanics and Mozambique Belt). It was found out a squared window-block of 50 km sampled better distinct magnetic provinces, a requirement advocated for by Tanaka and Ishikawa (2005). However, for the purpose of completeness 100 km squared window blocks were also extracted and analysed, based on observation that large windows potentially capture more information from deeper sources (e.g. Li et al. (2010). The “difference map” (a subtraction of the 50 km grid map from 100 km grid) apart from the shallow Curie depth estimates located off the western margin of the rift at about 0.7 °S, all the other shallow Curie depth estimated in 50 km squared window blocks are masked. It therefore follows that, in this case, increasing window size masks locally significant anomalies. Whereas on the other hand, it is remarkable that the deep Curie depth estimates on the NW, SE and SW part are retained for the two maps (50 km and 100 km). Geologically these areas are covered by Tanzania Craton and Mozambique Belts rocks as also reflected by deep Curie depth estimates. It therefore follows that a 50 km window does not compromise capturing of more information from deeper magnetization variations, which justifies interpretation described hereafter.

The results from the contoured 297 window-blocks (50 km by 50 km) shows for the first time a high resolution of shallow Curie depths are located within the rift floor and surprisingly beyond the western rift margin at around latitude 0.75° south. These Curie depths are spatially associated with volcanic centres both eastern rift margin (exposed on earth surface) and western margin (buried one), an indication that these volcanoes are possibly thermally active. Indeed, the largest shallow Curie depth estimate is located south of Lake Naivasha stretching between the Longonot and Suswa volcanic centres and attains a shallowest depth at about 9 km, and Olkaria

Geothermal Field is located at its north western margin (Omenda, 2001). All the shallow Curie depth estimates: Lake Olkaria –Longonot-Suswa (9-20 km); Lake Magadi (12 – 31 km); Menengai (15 – 20 km); Lake Bogoria (12 – 18 km) including western buried volcanic centers 0.75° south (6 -30 km) are shallower than the estimated Moho depth Figure 6-7 within the axial rift floor (Mechie et al., 1997, Keller et al., 1994b), which indicates they represent a thermal boundary rather than compositional boundary as advanced by Wasilewski and Mayhew (1992). These areas with shallow Curie depth estimates accounts for tectonically active regions associated with higher heat flow, an opinion supported by Rajaram et al. (2009). This provides leads into why the rift floor displays variable tectonism marked by localized swarm earthquake activity i.e. Lake Bogoria (Young et al., 1991); Olkaria-Longonot-Suswa (Hollnack and Stangl, 1998) and Lake Magadi area (Ibs-von Seht et al., 2001). Indeed, Figure 6-7c a traverse line extracted along the rift floor extending from Lake Bogoria and Lake Magadi shows a clearly defined seismicity cut-off that is spatially variable and that correlates with Curie isotherm. This observation also indicates that crust is brittle at these depths (Young et al., 1991, Ibs-von Seht et al., 2001, Albaric et al., 2009).

These earthquakes are of tectonic origin and their depth distributions seem to be temperature controlled. Indeed, Espinosa-Cardeña and Campos-Enriquez (2008) noted in their study of the geothermal field in Cerro Prieto Mexico a marked shallowing of seismicity due to local rise of the Curie isotherm. In this study, it is postulated that cluster of shallow earthquakes and marked shallow Curie isotherm suggest a local rise of magmatic plume, whose size (lateral extent) is defined by 3D morphology of CPD. It is highly unlikely that small magmatic plumes (as defined by narrow lateral extent in CPD map) could support active-model involving asthenospheric upwelling (Baker and Wohlenberg, 1971), it is however apparent that head plume induces conductive heat transfer which affects the rheology and hence accounts for increased seismicity.

On similar note, some earthquakes with focal depths as deep as 40 km have been recorded (e.g. Nyblade and Langston (1995); Ibs-von Seht et al. (2001); Kuria et al. (2010a)). This occurrence of deep earthquakes focal depths along the rift floor in relation to the crustal rheology has been a subject of discussion for a long time (Shudofsky et al., 1987, Fadaie and Ranalli, 1990, Ibs-von Seht et al., 2001, Ibs-von Seht et al., 2008, Albaric et al., 2009). The challenging question of deep earthquakes within the rift floor has largely remained unanswered. Results accrue from this study on correlation of earthquake focal depth and Curie point depth (Figure 6-7) clearly depicts, for the first time, that deep earthquakes on the rift floor

preferentially occur within zones of deep Curie point and in this case specifically mark location of the ANL shear zone (deep crustal structure) at latitude 1.5°S. The presence of this subsurface structure (thickened crust-ANL) is not obvious because it is not reflected on the corresponding topographical profile (Figure 6-7). Surprisingly, a section of the traverse line (Figure 6-7c) between equator and latitude 0.5°S shows, remarkably not even a single earthquake despite being located on the axial rift floor. The CPD of this zone – except the small subdued wavy dome-shape rise - somehow corresponds to those of ANL shear zone at 1.5°S and Tanzania Craton and/or Mozambique Belt at 2.5°S. Whereas it is not clear why no earthquakes are located within this zone, it safe to infer (from its deep CPD) that it represents deep cratonic and/or Proterozoic root.

From the foregoing, it is clear that the tectonic within the rift floor is temperature controlled to a large extent. Indeed, in reference to crustal rheology Albaric et al. (2009) noted that the top most part of brittle-ductile-transition inferred from seismicity peaks in the north Magadi and Bogoria (~10-11km) correlates well to mid-crustal boundary identified by Prodehl et al. (1997a) at ~6.44km s^{-1} and defines where brittle strength equals creep strength. The estimated Curie point depths ~12 km (minimum value northwest of Lake Magadi) and ~12 km (minimum northwest of Lake Bogoria) are slightly deeper than those determined by Albaric et al. (2009) but the non-occurrence of earthquakes below our estimated Curie point depths is not coincidental, leading to an opinion that ductile zone prevails at slightly deeper levels than Curie isotherm. As a whole, it is noted that depths of shallow Curie point depths i.e. less than 20 km characterize magmatic areas with swarm earthquake activity within rift floor (e.g. Young et al. (1991); Ibs-von Seht et. al. (2001) and deeper Curie point depths and deep earthquakes mark non-magmatic areas covered by Tanzania Craton, Mozambique Belt and Aswa Shear Zone (e.g. Shudofsky et al. (1987). These deep CPD generally characterize the eastern rift margin between latitudes 0.3°N north and 0.7°S and the isolated blocks east, west and partly underlying Lake Magadi at latitudes 1.2°S and 1.6°S. The anomalies east of Lake Magadi correspond to location of ANL shear zone, whereas those to the further north are likened to Mozambique Belt. The western deeper CPD anomalies are possibly part of the Tanzania Craton or its suture boundary with Mozambique Belt.

According to Halls et al. (1987), the multiple large magmatic events that cut the Archean Craton and Proterozoic mobile belts in East Africa since ~ 2.5Ga and not only the Cenozoic rifting event, may have been large enough to have intruded and underplated crust. Indeed, Henry (1987) noted, though poorly

constrained, an increase in basement density envisaged as dyke injection extending over the whole width (about 40 km) and down to a depth of 22 km that corresponds to major velocity increase deduced from seismic reflection (KRISP, 1991). Although this has additional been supported by the relative increase of bulk density and seismic velocities in the crust (Julia et al., 2005, Albaric et al., 2009), the morphology of these localized magmatic intrusions (Halls et al., 1987) have remained unmapped.

The above notwithstanding, in efforts to constrain the crustal structure using gravity measurements Baker and Wohlenberg (1971) delineated a narrow magmatic intrusion close the surface at bout equator. On a similar account, Fairhead (1976) delimited a broad dyke intrusion at a about latitude 1.1°S that extends beyond the western margin of the rift. In addition, the most remarkable (gravity feature), a positive gravity lineation interpreted as a hot mantle intrusion zone, 10–20 km wide, representing the heat source for many geothermal systems in the rift was interpreted by Cantini et al. (1990). However, these important results were quashed by Swain (1992) who argued that there are too many unknowns and gravity station coverage is too sparse for the results to be unique (Swain, 1992). Unfortunately, subsequent geophysical measurements by KRISP (1991) did not provide overwhelming evidence for the massive intrusion that was originally suggested to explain the axial gravity high yet did provide a velocity section for the upper crust along the axis of the Kenya Rift - somehow supporting Swain (1992) argument. Therefore, despite these extensive studies there is still uncertainty on what have caused the gravity anomalies and high velocity zones and how and why they are connected with seismically active belt/zones. In efforts to contribute to this long standing debate, two profiles were extracted; one along the equator and the one along latitude 1.1°S following Baker and Wohlenberg (1971) and Fairhead (1976) gravity profiles respectively. The results presented in Figure 6-8 were amazing: The narrow feature delineated by Baker and Wohlenberg (1971) is reflected from the CPD profile with a better lateral resolution but in this case CPD anomaly does no reach the earth surface (instead a maximum depth of 12 km is attained); The other profile (Fairhead, 1976) depicts an extent that is also well construed from the CPD, surprisingly covering the Olkaria-Suswa-Longonot anomaly combined with the buried volcanic centres (feeder dykes), that extend beyond the western margin of the rift. Note that the area between Olkaria-Suswa-Longonot and buried volcanic centre is punctuated by slightly deeper CPD, possibly that could not be resolved by gravity measurements. The similarity between thermal and gravity anomalies is not obvious particularly in cases where anomalies are not resolved using seismic measurements. Nevertheless, these findings validates to some extent the results obtained by Baker and

Wohlenberg (1971) and Fairhead (1976). To resolve this mystery, a very dense seismic reflection and refraction together with high resolution Magnetotelluric survey is recommended. On the account of the similarity of gravity and thermal structures, it is safe to conclude that the shallow Curie depth isotherm mimic magmatic plumes.

In the same perspective, numerous gravity models have been proposed to explain a common anomaly (observed long wavelength Bouguer minimum within rift axis) ranging from lithospheric thinning (Baker and Wohlenberg, 1971), a laterally extensive low density structure stretching 100 km west of rift margin (Fairhead, 1976); rift- and- suture model (Nyblade and Pollack, 1992). All these adduced gravity models failed to recognize the presence of buried volcanic centres "feeder dykes" contributing to different densities west of the rift margin, which is a premise of this present study.

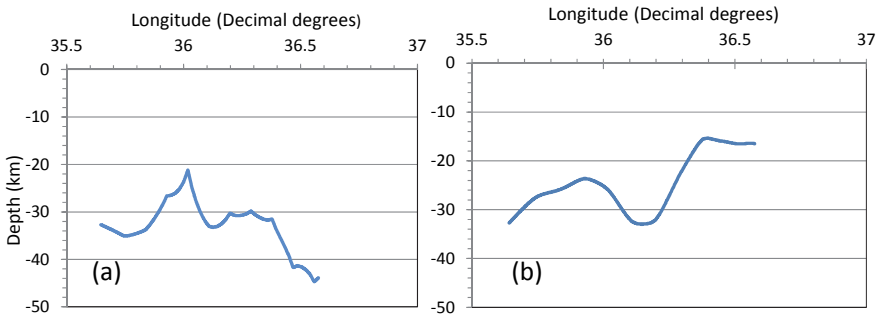

Figure 6-8. Shows CPD along two gravity profiles (a) near the equator along Baker and Wohlenberg (1971) gravity model: Note magma plume (b) along latitude 1.1°S corresponding to the location of broad gravity anomaly (Fairhead, 1976), a moving average along CPD would reproduce the thinned crustal structure (i.e. gravity model produced an average). In addition, (b) shows influence from buried volcanoes off western rift margin (identified in this research).

6.6 Conclusions

Aeromagnetic data covering central to southern Kenya were analysed using 3D Euler deconvolution techniques to map the magnetic sources in the area and interpret them in relation to rifting tectonics. In addition, spectral analysis of Fourier transformed spectra was carried to estimate Curie depths and results were correlated with earthquake focal depth to infer seismotectonics of this region. For purpose of validating and advancing the understanding of the crustal structure the results on Curie depth estimates were compared with other geophysical models.

The results from 3D Euler identified largely buried faults - by thick pyroclastic cover (Baker and Mitchell, 1976, Baker and Mitchell, 1984) - oriented N-S, NW-SE, NE-SW and E-W, which compliments earlier works by Le Turdu et al. (1999) and Kuria et al. (2010a). Remarkably, these buried faults structures would be difficult to identify otherwise. In addition, the predominance of buried faults in area covered by craton (oriented NE-SW and NW-SE) connotes inherited passive fabric in pre-rift evolution that now exerts a strong influence on the rift floor mainly through reactivation (Kuria et al., 2010a).

A more remarkable finding using 3D Euler is the identification for the first time in literature of buried circular structures, referred to as “possible feeder dykes” located beyond the western margin of the rift major faults with sizes similar to their counterpart exposed on the eastern margin. These are inferred to be numerous localized eruption centres through which lava flows were emplaced.

Depths to the bottom of magnetic ensemble using spectral analysis techniques estimates have been constrained better from a squared window size of 50 km compared to that of 100 km. Therefore, it is conclusive that increasing window size masks locally significant anomalies. The estimated CPD mark Curie isotherm that spatially correlates with volcanic centres, both buried and exposed, is an indication that these volcanoes are thermally active. In addition, the morphology of these Curie depth estimates mark target areas for geothermal exploration.

A correlation of the earthquakes (focal depths) to Curie depth estimates along axial rift floor shows that seismicity cut-off is spatially variable and that correlates highly with Curie isotherm. On this account, it is postulated that cluster of shallow earthquakes and marked shallow Curie isotherm suggest a local rise of magmatic plume, whose size (lateral extent) is defined by 3D morphology of CPD. It is highly unlikely that small magmatic plumes (as defined by narrow lateral extent in CPD map) could support active-model involving asthenospheric upwelling (Mohr, 1987). However, it is apparent that head plume induces conductive heat transfer which affects the rheology and hence accounts for increased seismicity. The seismicity cut-off along axial rift floor is spatially variable and correlates highly with Curie isotherm – noting that depth-distribution of these clustered earthquakes seem to temperature controlled – a local rise of magmatic plume is inferred. On contrary, deep earthquakes within rift floor preferentially occur within zones of deep Curie points as evidenced at the location of the ANL shear zone at latitude 1.5°S. The area between equator and latitude 0.5°S with deep CPD

and no single earthquake is inferred to represent deep relict cratonic and/or Proterozoic root.

A relatively close match is observed between gravity models and Curie isotherm, amid minor difference. Whereas further investigation is recommended (using active seismic and magnetotelluric survey), on the account of the similarity of gravity and thermal structures, it is safely concluded that the shallow Curie depth isotherm mimic magmatic plumes.

CHAPTER 7

EFFECT OF DYKE INTRUSION AND FLUIDISED ZONE ON SEISMICITY DISTRIBUTION

This chapter is based on:

Kuria, Z.N., Barongo, J.O., Woldai, T., van der Meer F.D., 2011. Dyke intrusion and fluidized fault zone inferred from magnetotelluric studies at Magadi fault system, southern Kenya implication for seismicity distribution. Submitted: Geophysical Journal International.

7.1 Introduction

Fundamentally, presence of fluids in the rocks whether at intergranular scale (Tullis et al., 1996) or on macro-to-mega fracture scale (Cox, 2002) affects the rheological behaviour of crustal rocks. Consequently, fault zones differ by kinematics, geometry, size, tectonic environment and deformation history (Billi et al., 2003). The fault zones act as conduits linking earth surface to deeper crustal levels (Billi et al., 2007) and to a larger extent support huge volumes of exploitable hydrothermal fluids (Barbier, 2002, Bellani et al., 2004). Simple geometric models on fluid flow suggests that fault terminations, or linkages between fault segments are domains of high fracture density and connectivity, and are therefore likely to localize fluid flow (e.g. Cox et al. (2001); Rowland and Sibson (2004); and Cox (2005)). However, in other instances fault zones act barriers impeding transmission of fluids through them (Caine et al., 1996, Aydin, 2000, Jourde et al., 2002).

On a structural perspective, fault zones are characterized by three main structural components, which include: a fault core in which most of the slip is accommodated; a damage zone characterized by complex fracture networks and minor faults; and a protolith corresponding to the host rock which records only previous (pre-normal faulting) deformation. The amount and distribution of each component depends upon lithology and geologic setting within which the fault has formed (Caine et al., 1996). In contrast, the permeability architecture of a mature fault zone consists of two main components. The damage zones, which has the highest permeability and the fault core, which constitutes a low-permeability sector (e.g. Cox et al. (2001)). Noteworthy, the permeability within these two zones - damage and fault core- is not static but is controlled by a complex evolving fault system both in space and time.

The evolution of the fault zone permeability can be classified into stages according to Caine et al. (1996) namely: (1) the conduit stage, which precedes the development of the fault core. During this initial stage, the progression of fracturing increases the permeability of the fault zone, which behaves as a self-enhancing conduit for fluid flow. Just before the onset of the fault core development, the most evolved sector of the damage zone consists of centimeter-sized quasi-joints. The foliation network ensures a very efficient connectivity and fluid flow. When particle rotation starts, the permeability structure of the fault is disrupted and (2) the evolved stage initiates. Particle rotation and comminution increases the fine-grained matrix within the particle population and dramatically reduce fracture connectivity and permeability. The fault core starts to seal and eventually behaves as a barrier against fluid flow. At this stage, fluid flow is localized in the damage

zone, particularly near the boundary with the fault core where a remnant of the most highly fractured sector is preserved. This ultimately influences stress distribution.

The faulting process (nucleation, propagation or reactivation), a reflection of the tectonic deformation, is closely associated with earthquake nucleation and therefore seismicity of a region. However, the presence of fluids, rarely taken into consideration, weaken the rocks by reducing effective normal stresses across existing faults or induce genesis of micro-cracks and pore interconnectivity leading to new crustal scale shear zones (Wannamaker et al., 2004). It is on this background, that this project was undertaken to identify the disparity in seismicity (Ibs-von Seht et al., 2001, Kuria et al., 2010a) to the north and south of Lake Magadi, southern Kenya Rift, areas located within the same fault system (Figure 7-1). This young tectonic environment experiences on-going extensional deformation and magmatism, which is argued (in this research) to contribute to measurable geophysical anomaly. For this purpose, magnetotelluric (MT) method is used that utilizes naturally occurring electromagnetic (EM) wave (Vozoff, 1972) and collocated transient electromagnetic (TEM) method to image the electrical structure of the earth along two profiles (north and south of the Lake) and use it to explain the observed variability in degree of seismicity as influenced by presence of fluids as shown in Fig.7-1. The results from this study have significant implication in understanding the role of fluids in controlling/influencing seismicity, which has a direct impact on future evolution of the rift systems and associated seismic hazard.

In MT sounding, the EM waves diffuse from a few tens of metres to several tens of kilometres in several cases probing the mantle in respect to high and low frequencies respectively. This makes MT a powerful geophysical tool for imaging subsurface resistivity structure using natural electromagnetic waves. In particular, MT is rendered suitable for imaging presence and distribution of fluids within major fault zone owing to resistivity contrast (i.e. fluid bearing and non- fluid bearing conduits) therein and therefore ideal method for meeting objectives outlined above. Whereas this method has been applied to many tectonically active regions in the world (e.g. Unsworth et al. (2000); Wannamaker et al. (2004)) examples in Africa include Rooney and Hutton (1977), Bailey et al. (2000), Hautot et al. (2000), Simpson (2000), Sakkas et al. (2002), Weckman et al. (2003), Mekkawi et al. (2005), and Meju and Sakkas (2007).

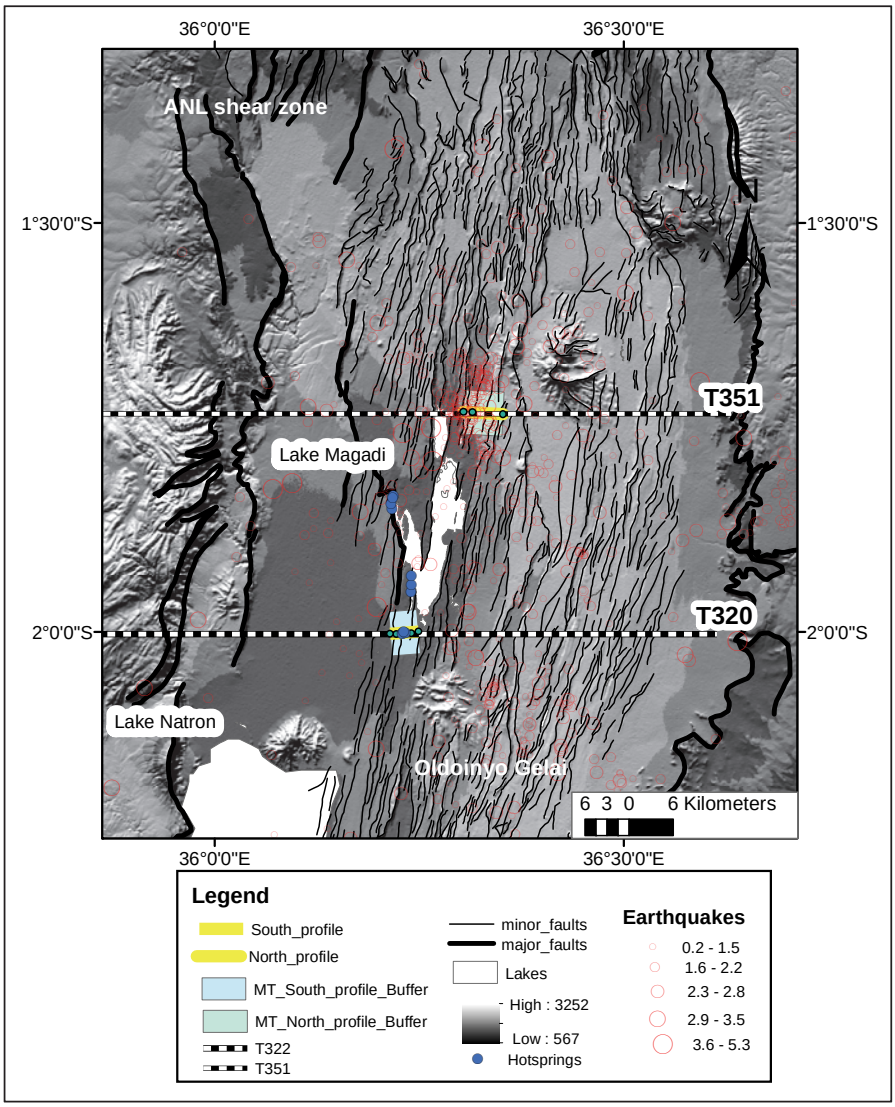

Figure 7-1. Location of the study area (SRTM - Shaded relief) – notice high density of faults and increased seismicity within axial rift zone. The black line with white dots labelled T351 and T320 mark the location aeromagnetic flight lines along which faults (deduced from magnetic sources) and earthquakes are correlated in Figure 7-8.

7.2 Tectonic evolution of the rift system

The evolution of the rift system dates back to the East African Orogeny, a product of Neoproterozoic orogenesis (Stern, 1994) involving accressionary and amalgamation of east and west Gondwana (Shackleton, 1986, Shackleton, 1993, Shackleton, 1996, Stern, 1994). Among other belts, the Proterozoic Mozambique Belt is a part of this orogeny. The western margin of Mozambique Belt in southern Kenya and Northern Tanzania is bordered by Archean Tanzania Craton, a boundary along which Cenozoic rifting and magmatism evolved (Bosworth, 1987, Smith, 1994) to form part of Kenya Rift. However, the presence of crystalline rocks on both the western and eastern part of the rift (Simiyu and Keller, 2001) complicates the precise localization of the boundary between Mozambique Belt and Tanzania Craton.

Structurally, the Kenya Rift is a part of the eastern branch of the continental scale East African Rift System (EARs) shown in Figure 7-1. This eastern branch stretches from Afar triple junction and straddles through Ethiopia, whilst the western branch circumvents Lake Victoria thorough Uganda, Rwanda, Burundi, Tanzania, Malawi and terminates further south into Mozambique (Chorowicz, 2005). The East African Plateau is a characteristic feature of elevated relief lying between eastern and western rift branches and on which Lake Victoria is located (Bechtel et al., 1987). At the central part of Kenya Rift (i.e. 2°N to 2°S) lies the Kenya Dome (~300 – 400 km wide topographic high) superimposed on the fringe of the plateau, an area where the rift has markedly uplifted shoulders e.g. Baker and Wohlenberg (1971).

Several model for the evolution of the Kenya Rift have been adduced ranging from extension of the lithosphere by pure shear (Baker and Wohlenberg, 1971), through extension by simple shear (Bosworth, 1987) to diapiric upwelling of an asthenolith (Mohr, 1987). The current geophysical data support the active model of rifting and indicate the presence of an asthenospheric diapir or plume beneath the central part of the Kenya Rift and at the base of the lithosphere, which is undergoing a pure shear extension. Seismic refraction images (Green et al., 1991) show small-degree melts rising from the plume to the base of the crust as consequence of the thermal weakening of the overlying lithosphere. Seismic tomography data (Anderson et al., 1992), crustal thickness variations (KRISP Working Group Party, 1991) and Moho topography (Pointing and Maguire, 1990) point to the underplating of ultramafic and mafic accumulations at the crust-mantle boundary. This high-velocity layer (6.8 to 7.1 km/s) rises to more than 10 km at the centre of Kenya dome and may be a zone of maximum thickness of the cumulates (Macdonald, 1994).

In asserting active modelling, some authors like Campbell and Griffiths (1990) suggest that the thermal anomaly may be a small convective cell. Using the areal extent of the uplift and of the initial volcanism, Campbell and Griffiths assumed a diameter of 100-150 km for the initial plume beneath the Gregory Rift. Heat flow data (Wheildon et al., 1994), which reflect the thermal processes in active faulting, indicate that the floor of the Kenya Rift shows neatly higher heat flow than the shoulders, and that there is a strong spatial association between high heat flow site, Quaternary volcanism, faulting and hydrothermal manifestations along the rift axis (Chapter 5 and 6).

On geological evolution, Kenya Rift is characterized by extensive volcanic activity. According to Morley (1992), rift related magmatic activities started in northern Kenya in Oligocene. Subsequently, these magmatic activities propagated southwards - preferentially bounded within the rift proper and its western flank – and is still an on-going process (Williams, 1978, Calais et al., 2008, Baer et al., 2008). In Late Miocene times, large basaltic fields began to develop on the eastern flank of the rift with Quaternary volcanism confined to rift and eastern flank (Baker, 1986, Karson and Curtis, 1989). Three volcanoes located in south Kenya rift attest to this volcanic activity namely Ologorgesailie, Lenderut (2.5 Ma) and Shompole (2.0 Ma). The geology of Lake Magadi area according to Baker (1958); (1963) is characterized by metamorphic rocks, the Plio-Pleistocene volcanics and Holocene to Recent Lake and fluvial sediments.

7.3 Magnetotelluric and Transient electromagnetic studies

7.3.1 Data acquisition

Magnetotelluric (MT) data were acquired using three sets of 5-channel data acquisition systems, commonly referred to as MTU-5A, from Phoenix Geophysics Ltd. – Canada. The MTU-5A system acquires MT data in frequencies ranging from 400 Hz to 0.0000129 Hz, making it suitable for both shallow and deeper earth investigations. Together with MTU unit, induction coils and 100 m long grounded electric dipoles were used in acquiring MT measurements. The recording array comprised of two perpendicular horizontal components (i.e. magnetic north-south and east-west) of magnetic fields on the ground surface and a vertical magnetic field component using induction coil magnetometers. The MT electric dipoles loops were arranged in a cross configuration of non-polarizing CdCl2 electrodes buried in wet clay and spaced at 100 m. The cables, where necessary, were buried to minimize the effects of spurient voltage likely to arise from wind induced oscillations.

MT soundings were acquired along two profiles within axial rift floor: one covering the area south of Lake Magadi near the hot springs, while the second profile was performed across the ruptured fault zone in the area north of Lake Magadi, commonly characterized by high seismic activity (Figure 7-1). Five soundings were performed on the southern part along ~ 7.5 km traverse line and three soundings covered ~ 11 km segment in the northern area (e.g. Figure 7-2a). The average station spacing is 1 km along the southern transect and 1.5 to 3 km for the northern part. The disparity in spacing of the sounding stations, particularly to the north, was hampered by rugged topography and accessibility. However, the adopted sounding spacing is still adequate for resolving shallow features defined by short wavelengths. Simultaneous recordings of MT data from several sites were synchronized using GPS clocks: On the first-day 2 MT sets acquired data simultaneously, while on the second day all the 3 MT sets were installed in the southern area. In the north, MT data were acquired simultaneously by only two MT units. This synchronous data acquisition by different MTU systems proved suitable for identifying noisy data.

TEM soundings were performed at the same area as MT i.e. MT station was centrally placed within a 150 m squared sided loop of TEM array (Figure 7-2b). This TEM-MT approach provided for probing the same geological formations, which is necessary for accurate static correction (Meju, 1996). The TEM equipment set (a product of Zonge Engineering Co.) comprised of transmitter (GGT-3 with a maximum loop current of 12 amps), transmitter controller (XMT-16), data logger (GDP 16 - a three channel unit), receiver coil (TEM/3-with receiver moment of 10000 m2) and voltage regulator (VR-1). The power source was from a 5 Hp Honda generator. For each TEM sounding, a central-loop and a single-loop configuration with a 150 m sided square transmitter was used. Prior to data acquisition, the receiver and transmitter controller were synchronized (in-phase) using a high precession crystal clock, which ensured that voltage was measured by the receiver only after the transmitter was turned off (i.e. only transient responses of the ground to inductive energization were measured). A half-duty square wave current was transmitted at frequencies of 16, 4 and 2 Hz. Logarithmically spaced sampling gates were used i.e. 16 Hz having 25 gates starting at 34.14 μs to 12.18 ms; 4 Hz had 31 sampling gates 36.14 μs to 48.42 ms and 2 Hz had 34 gates starting at 84.18 μs to 96.85 ms. At each repetition rate, several repeated transients were stacked and stored in a memory cache inside the data logger and were transferred to a personal computer for processing.

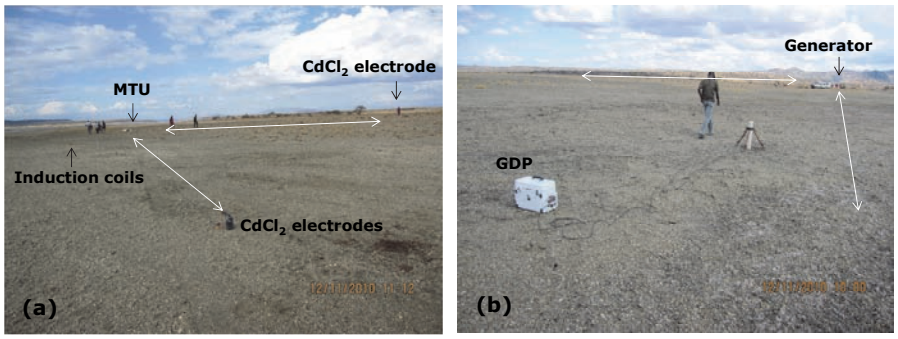

Figure 7-2. Field set-up for MT data acquisition (a) and TEM (b). In (a) The MTU is centrally placed with the electrodes installed perpendicularly to induction coils as shown by double-edged white arrows. In (b) the white double-edged white arrows mark part of the 150 m long square sided loop.

7.3.2 Data analysis

The MT time series data acquired by MTU-5A units were downloaded onto PC and displayed using a synchro time series viewer software with acronym SyncTSV that allows for graphical representation of the raw time-series data, deriving the power spectra from the time series data and determining coherence between orthogonal channels. Fourier transforms were determined from the raw time series data using a program SSMT2000 provided by the Phoenix Geophysics-Canada (Phoenix Geophysics, 2003). The cross powers were stored in files and could be displayed graphically using the program, MTU editor. The stored files were then converted to industry-standard EDI format for further geophysical analysis and interpretation using WinGLink from Geosystems.

The results showing a combined plot of orthogonal apparent resistivity and phase versus frequency plots are of good quality (Figure 7-3). However, two plots: one to the south (MS4) and one to the north (MN3) indicated a high density of large error bars, particularly for the lower frequencies. Whereas this could be attributed to the closer proximity of the high tension power lines and close proximity to human settlement for MN3, the noise at MS4 could possibly be due to electrode noise having been set early in the day when it was still very hot.

Standard tensorial techniques were used to process the MT data (Egbert and Booker, 1986). The output of the impedance tensor elements were used to compute the apparent resistivities, phases, azimuths, polar diagrams, induction arrows and skew (Groom and Bahr, 1992). The apparent resistivities for TE (xy) and TM (yx) measurement directions were obtained.

The TEM data that comprised of average stacks from GDP-16, were used to construct 1D models (apparent resistivity with depth). These models were used for static shift correction (dielectric distortions) of all the MT data. The data 1D TEM models fitted very well to the MT data for high frequency (Figure 7-4) as expected.

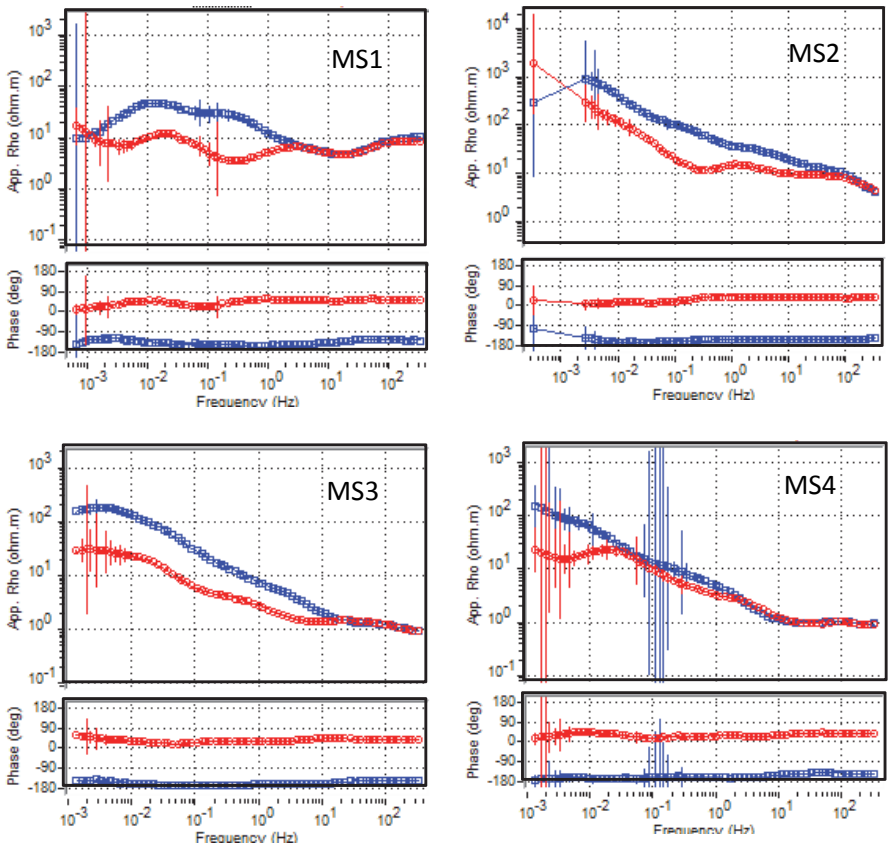

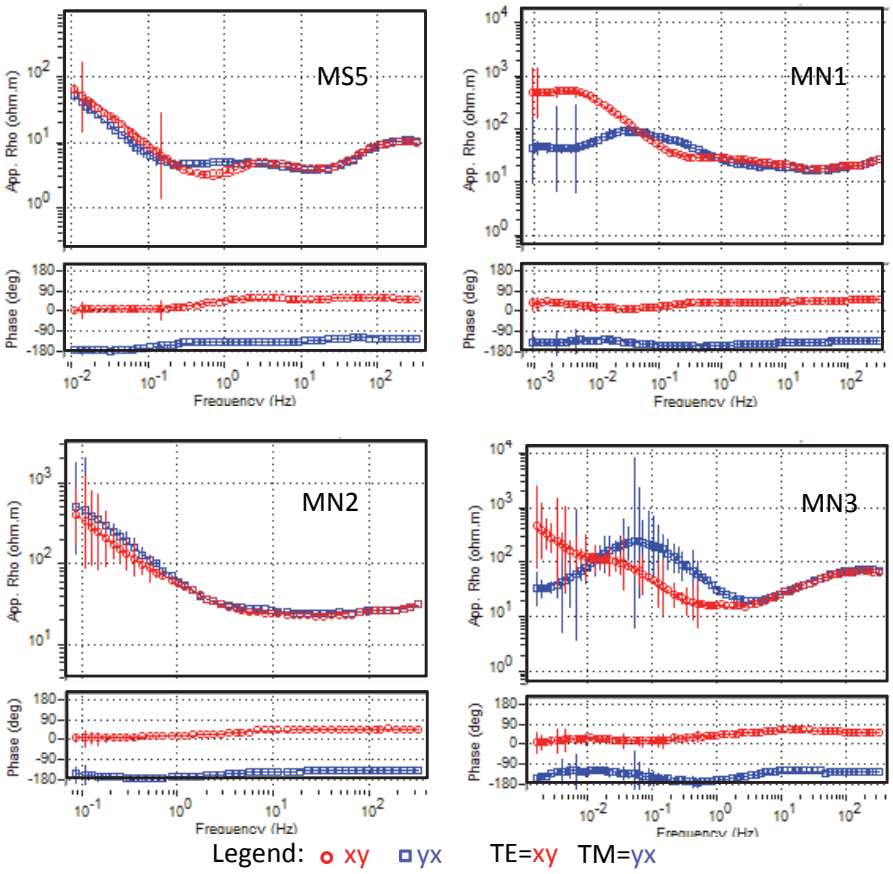

Figure 7-3. A combined plot of the observed apparent resistivity and phase with response of 2D model (line plot within the markers) for TE and TM mode. The larger error bars are noted at a frequency band of about 10^{-1} for MS4 and MN3 stations. Note: MS denotes MT for south profile and MN for north profile.

7.3.3 Two-dimensional MT data inversion

Prior to carrying out the 2D inversion of the statically corrected MT data along the two pre-selected MT profiles (north and south), a test on strike direction of the geoelectric structure and the orientation of survey traverses was performed. The two MT profiles, oriented in approximately EW direction, run almost perpendicular to the regional strike N-S, with the northern oriented a few degrees to the NE, as correspondingly reflected by the MT profile. A decomposition technique was used to assess the dimensionality of the data (Groom and Bailey, 1989). The results (Figure7-5a and 7-5b) indicate that at frequency band 10^{3} to 10^{-1} Hz the average strike is about N4°E and N15°W along north and south profile, which is close to strike

direction of the Magadi fault system with its sinuous character (Kuria et al., 2010a). Therefore, the electrical strike is close to the geological strike of the Magadi fault system. The impedance skew values (Swift, 1967) for all the site are less than 0.2 and below for frequency band between 103 and 1 Hz (Figure 7-5c,d). However, at lower frequencies (10^{-1} to 10^{-3} Hz) the skew becomes higher indicating a possible 3D geoelectric structure at deeper levels. The largely uniform strike and considerably low skew values at frequency band ranging from 10^{3} to 1 Hz support a 2D inversion and interpretation of the MT data.

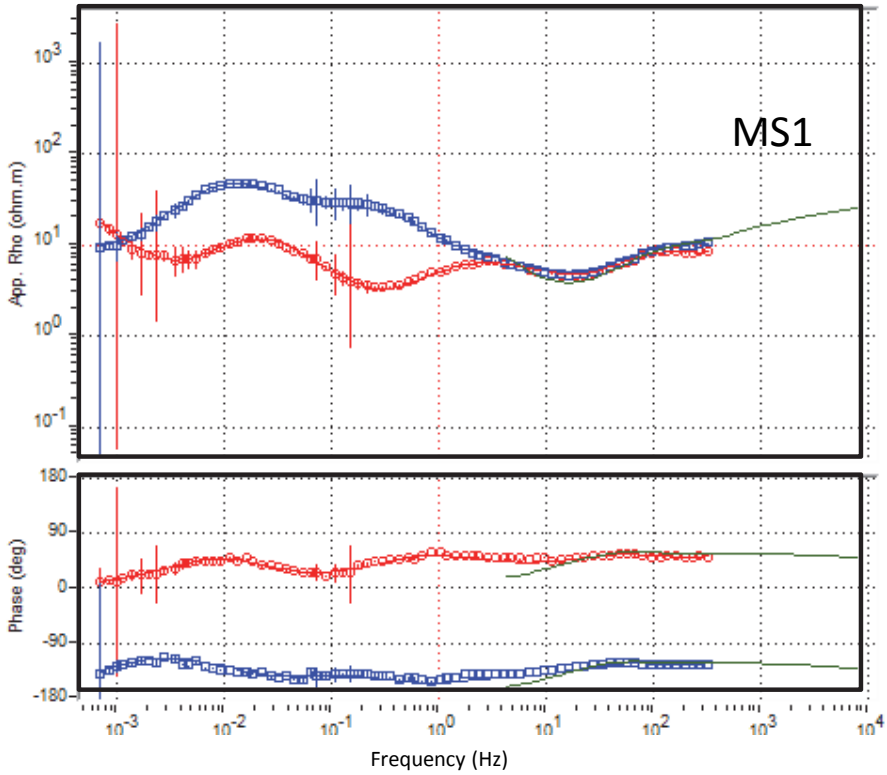

Figure 7-4. Typical static shift using the central-loop 1D TEM model (the smooth light green line) that fits reasonably well for the high frequency component of both TE and TM data. The shift factor was 1.79 and 1.35 for TE and TM respectively.

In addition, assessment of the induction arrows (Parkinson, 1983) – a ratio of vertical to horizontal magnetic fields from MT data – was carried out. Normally, these induction arrows indicate the degree of lateral conductivity variations in the ground by being orthogonal to and point towards anomalous current concentration hosted by a dominant conductive structural feature

(Jones and Price, 1970). The intensity of these current concentration anomalies is proportional to the size (length) of induction arrow. It is noteworthy, that induction arrows of Lake Magadi area are very small and do not define any significant trend at all frequencies (Figures 7-5e and 7-5f) indicating that all MT stations are located on a significant conductive anomaly.

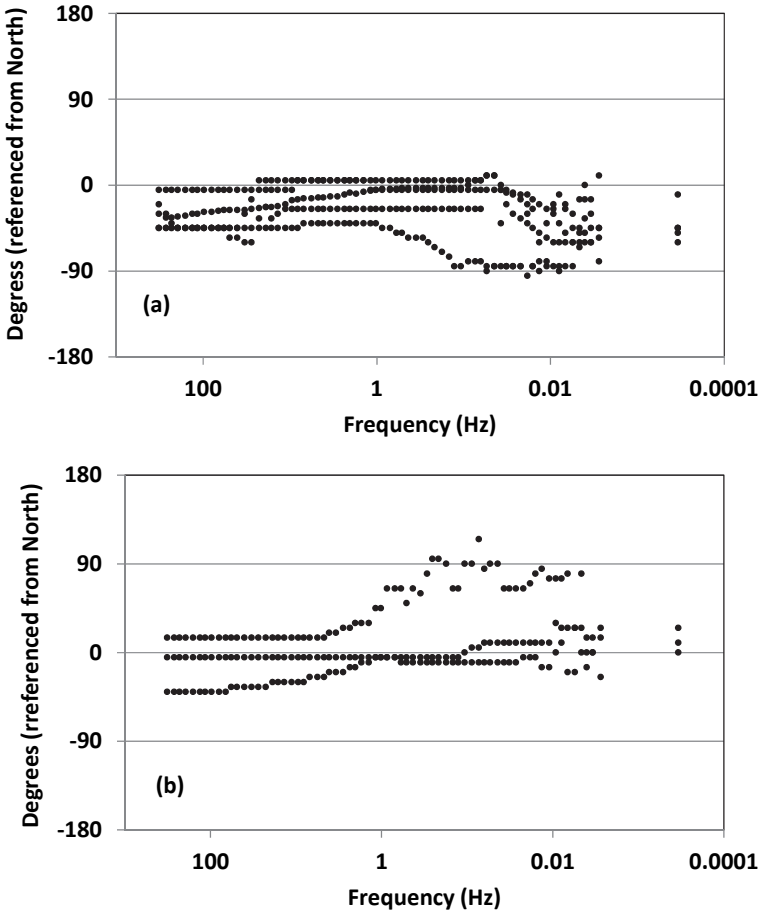

Figure 7-5. A conformity test of MT data for 2D inversion and interpretation. (a) and (b) strike direction of the geoelectric structure (N4°E and N15°W) perpendicular to the profile line.

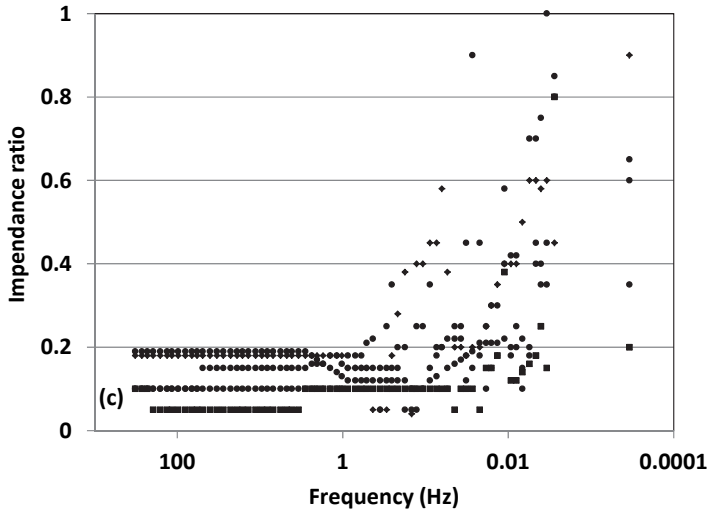
1
0.8
0.6
0.4
0.2
0
Impendance ratio
(c)
100
1
0.01
0.0001
Frequency (Hz)

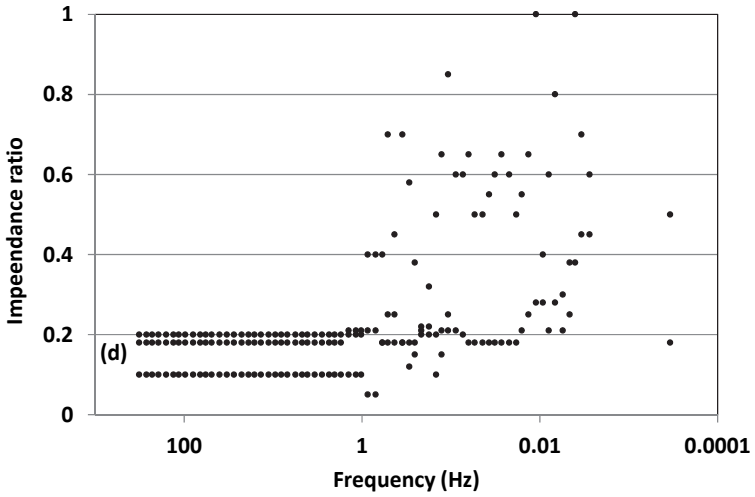
1
0.8
0.6
0.4
0.2
0
Impeendance ratio
(d)
100
1
0.01
0.0001
Frequency (Hz)

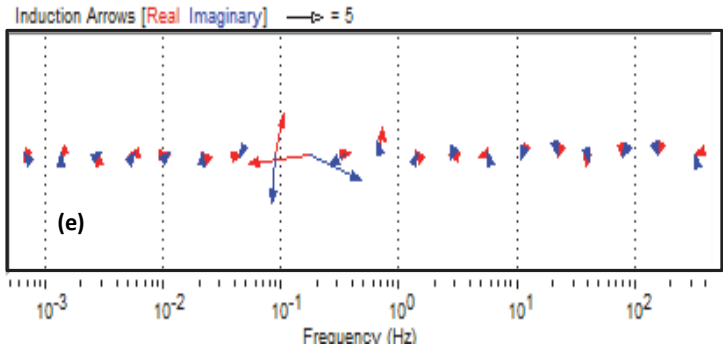
Induction Arrows [Real Imaginary] = 5
(e)
10-3
10-2
10-1
100
101
102
Frequency (Hz)

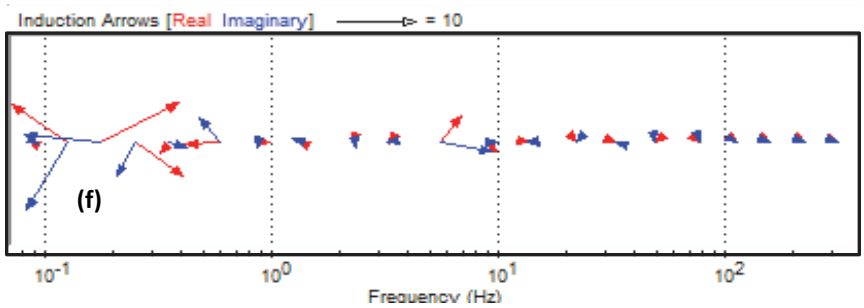

Figure 7-5. A conformity test of MT data for 2D inversion and interpretation c) and (d) Impedance skew values plot less than 0.2 for frequency 10^3 to 1 Hz supporting 2D structure at lower frequency a 3D structure prevails. (e) and (f) are examples of graphical plot of real and imaginary induction arrows for MS3 (south profile) and MN2 (north profile) respectively. The imaginary components are more sensitive to shallow induced features (hence more variable) and real components are more sensitive to regional features. Notably the induction arrows are very small and not definitive of any preferred orientation indicating MTU unit placed on top of the conductor.

7.3.3.1 MT Pseudo-sections

A plot of the pseudo-sections of the apparent resistivity as a function of frequency for both TE (xy) and TM (yx) directions along northern and southern profile are shown in Figure 7-6. The southern profile shows a very highly resistive feature that stretched at frequency band 103 to 1 Hz and covers stations MS3, MS4 and MS5 below, which a dome shaped low resistivity zone (1 - 4 Ωm) prevails. In contrast, the zone between station MS1 and MS2 is characterized by a low resistivity structure that stretches across all the frequency bands (10^3 to 10^{-2} Hz). This feature is oriented in NE - SW for frequency band 10^{-1} - 10^{-3} Hz and deflects to NW-SW for lower frequencies. Interestingly, the two low resistivity features at low frequencies (i.e. dome-shaped and zonal) are separated by a resistivity band of about 20 Ωm. The northern profile shows a gradual decrease in resistivity from highs of about 500 to 100 Ωm at frequency band ranging from 103 to 1 Hz. At lower frequencies (deeper levels), the resistivities decrease to 1 - 20 Ωm except at station MN3 (Rho TE) where a resistive body seems to intrude.

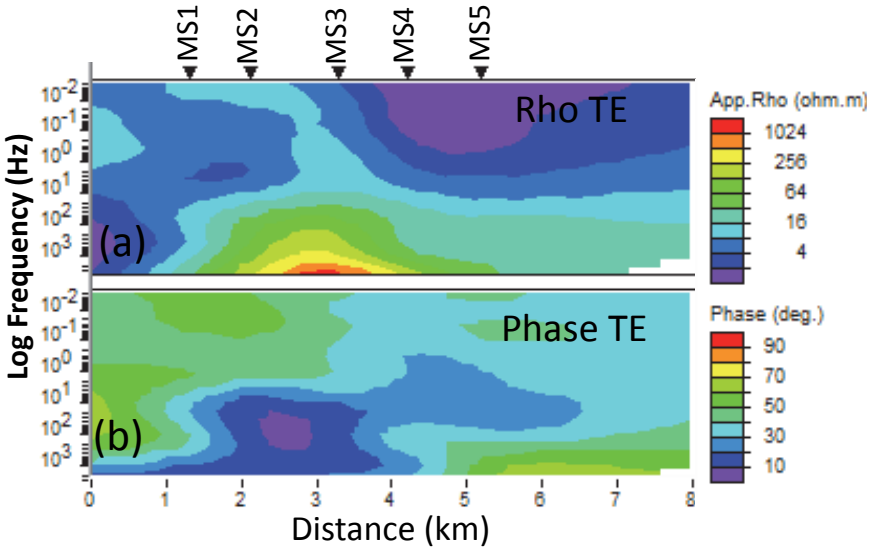
MS1
MS2
MS3
MS4
MS5
Rho TE
Phase TE
(a)
(b)
Log Frequency (Hz)
Distance (km)
App.Rho (ohm.m)
1024
256
64
16
4
Phase (deg.)
90
70
50
30
10

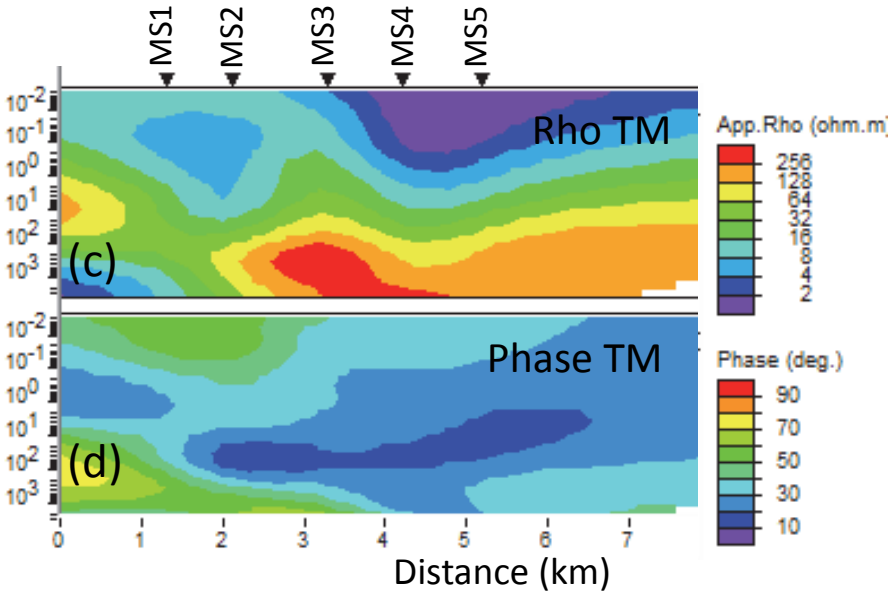
MS1
MS2
MS3
MS4
MS5
Rho TM
Phase TM
(c)
(d)
Distance (km)
App.Rho (ohm.m)
256
128
64
32
16
8
4
2
Phase (deg.)
90
70
50
30
10

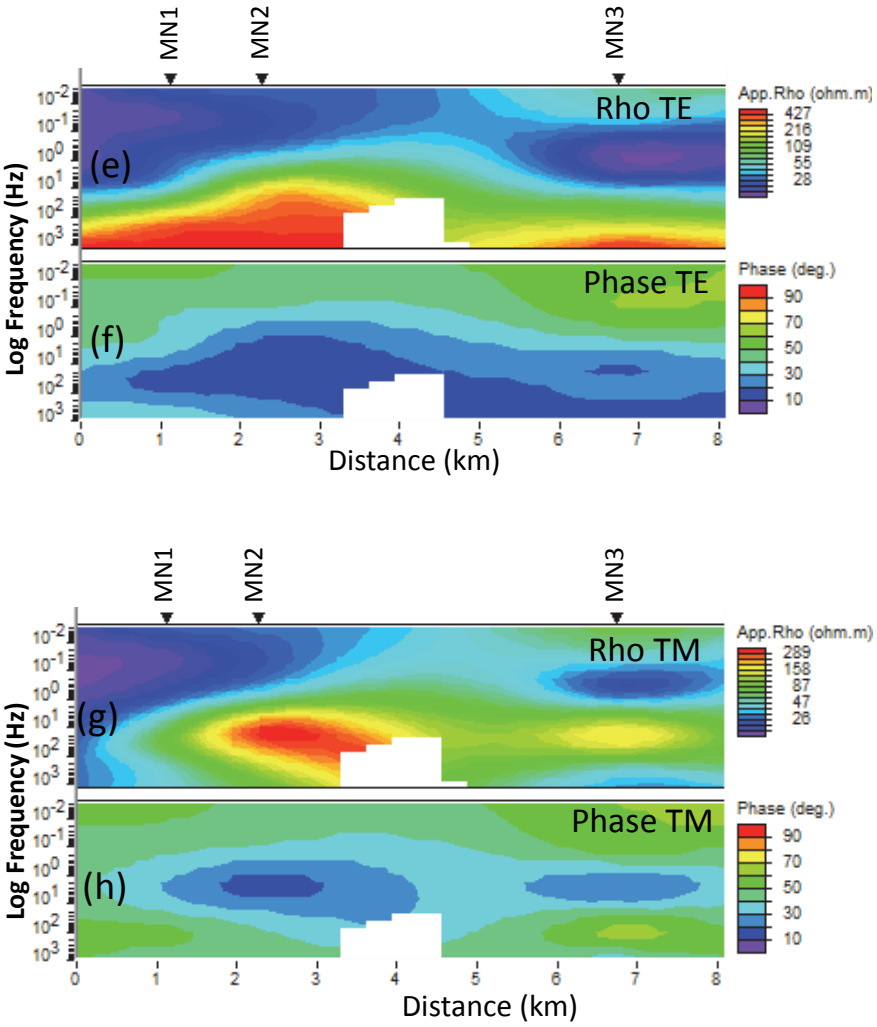

Figure 7-6. Pseudo-sections of apparent resistivity and phase as a function of frequency for both TE and TM directions along south and north profiles with MT stations labelled MS and MN respectively. Figures. a, b, e, f show apparent resistivity and phase for TE mode data where electric currents flow parallel to the fault. Figures. c, d, g, h illustrate apparent resistivity and phase for TM mode data where electric currents flow across the fault.

7.3.3.2 Two dimensional model results

Prior to 2D modelling, 1D models were constructed using a linearized inversion scheme e.g. Marquardt (1963). Subsequently, using parameters obtained from the 1D modelling, the MT data was analysed using a 2D inversion scheme (Rodi and Mackie, 2001).

The MT data was inverted jointly for both TM and TE (i.e. inverted TM mode apparent resistivity and phase data, inverted TE mode apparent resistivity and phase data and inverted frequency transfer functions). An error floor of 5% was used for both apparent resistivity and phase during inversion, an error threshold of 10% for apparent resistivity and 5% for phase, a regularized smoothing operator tau (τ) of 3 and a normalized root-mean square error of 1.5 (Rodi and Mackie, 2001) as threshold of misfit (i.e. error for termination of inversion exercise). During the inversion process smoothing was allowed with depth. A plot of the computed response of the model and the field data is shown in Figure 7-3. (i.e. TE and TM models). The RMS misfits were 3.48 and 2.24 for south and north inverted 2D models respectively (see Figures 7-7a and 7-7b).

The depth of probe for the south and north 2D models was about 45 km this being largely the depth supported by 2D models, a depth below which 3D geoelectric structure prevails. The geoelectric model of the profile south of Lake Magadi (Figure 7-7a) shows a characteristically very conductive structural feature (less than 4 Ωm i.e. purplish) at depth between 11 and 45 km confined to the western side of the profile, with a 10 km thick (i.e. 22 and 32 km) zone that branches westwards. This very conductive axis is surrounded by conductive material (4 - 8 Ωm i.e. deep blue colour) that extends to a shallow depth of about 6 km. This very conductive zone was inferred to be a melt and the surrounding material to be fluidized conduit zone. At the depth between 3 and 6 km, the conduit becomes narrow (about 2 km) and also increases in resistivity further to a range of 8 - 32 Ωm. At shallow depth (below 1 km) the resistivity not only drops sharply to 1 Ωm but also becomes laterally extensive, covering the entire profile except for a very small segment west of the profile. The east of the profile is characterized by gradually increasing resistivities from 32 to 2048 Ωm that can be attributed to presence of induced hydrofractures (i.e. leaks from main conductive) and resultant weathering. This scenario is also observed on the western side from a depth of 1 to 5 km, but here resistivities are higher than 8000 Ωm.

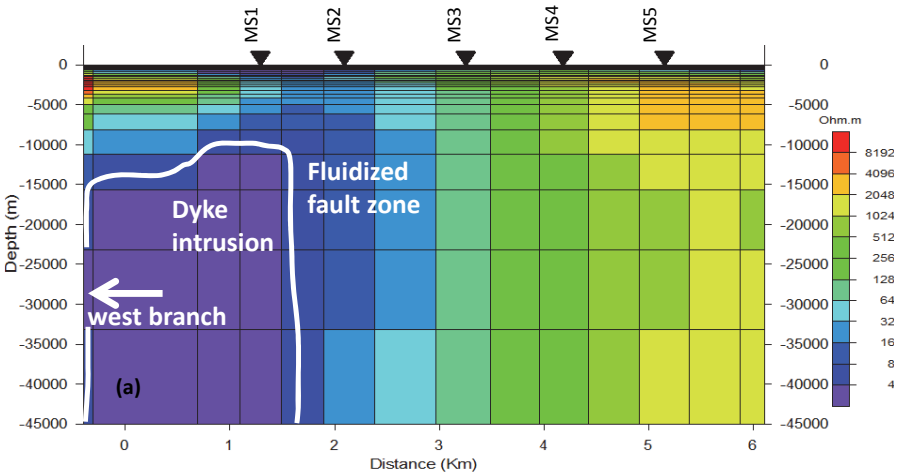

Figure 7-7a. 2D inverted electrical resistivity models along the southern profile near the location of the hot springs. The RMS misfit is 3.48. No earthquake was sampled within a buffer zone 3 km (and even 4 km) along the southern transect, which indicates possible influence of fluids on earthquake nucleation process.

The northern profile (Figure 7-7b) depicts a similar faulted architecture to that of the south profile. However, the resistivities are considerably higher: the most conductive zone, about a km wide, has resistivities ranging from 32 – 64 Ωm and stretches from a depth of ~ 33 km to 45 km; A more resistive zone (64 - 128 Ωm) attains a thickness of about 10 km (~23 - ~33 km); a depth ranging from 15 - ~ 23 km has a fairly resistive zone (128 - 1024 Ωm); ultimately the weathered and fractured zone (1024 - 2048 Ωm) reaches its shallowest depth ~ 11 km. A very resistive rock mass, with possibly only miniature fractures, indicates prevalence of rather compact and massive conditions (2048 – 4096 Ωm) at depth ranging between 5 – 11 km. This possibly forms the cap rock for this area, impeding flow of fluids. Towards the earth surface, the conductivities change rather abruptly dropping to a range of 4 - 64 Ωm at the depth between 1- 2 km. A low resistivity zone (16 - 64 Ωm) characterizes the entire profile at depth ranging from 0.5 – 1 km and thickens on both the eastern and western ends. A very highly resistive zone (~2,000 – over 8,000 Ωm i.e. orange to deep red) that wedges out with depth in eastern direction at a depth ranging from 2.5 to 34 km possibly marks the compact and massive crystalline rock mass. This could be a probe within the ANL shear zone. Generally, all other parts of the profile largely indicate varying degree of weathering characteristic of fault zones with no fluid. The location of the station MN2 coincides with location a several

kilometres long well preserved fault zone caused by a 4.2 magnitude earthquake (Ibs-von Sent et al., 2001).

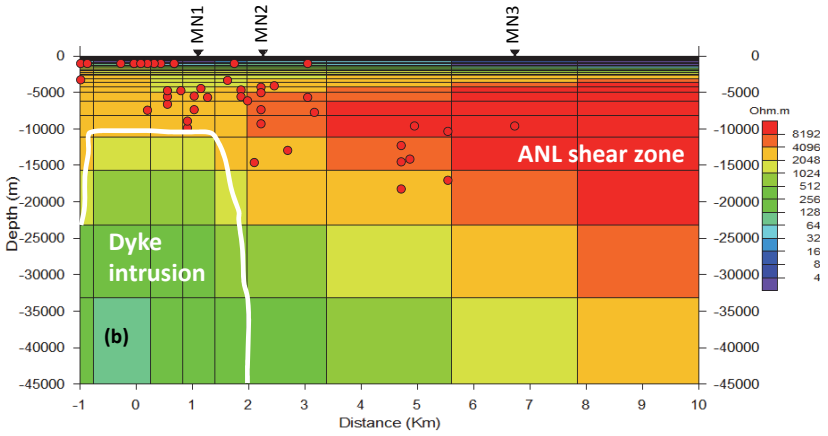

Figure 7-7b. 2D inverted electrical resistivity models along the northern profile within the area of swarm earthquake activity. The RMS misfit 2.24 is slightly lower than southern profile. The Red dots denote earthquake hypocentres within a buffer zone of 3 km. Note the highly conductive zone at depth ~ 33 – 45 km that correlates spatially with preferential occurrence of shallow earthquakes; earthquakes cut-off depth at 9 km and the weathered/fractured zone up to 11 km manifest dyking process. The wedging out of the more resistive rock mass from central towards easten end marks gentle E-dip of the suture zone (rift and ANL shear zone).

7.4 MT 2D sections and earthquake focal depth

Earthquakes foci within a buffer zone (3 km) defined along the two MT traverses (north and south of Lake Magadi) were projected on the geoelectric 2D models of MT sections (Figure 7-7b). These earthquakes were extracted from catalogues for period between October 1993 and August 1996 (Hollnack and Stangl, 1998) and between November 1997 and June 1998 (Ibs-von Seht et al., 2001, Kuria et al., 2010a), as shown in Figure 7-1. The selection of the earthquake data from an all-inclusive earthquake database, and not only the recent events, underscores the importance of each earthquakes in providing fundamental properties of the lithosphere, in particular the transition from brittle faulting to plastic flow in crust or change in the frictional sliding process (Sibson, 1982).

Surprisingly, no earthquake was selected within a buffer zone of 3 km along the southern profile, even after the buffer was increased to 4 km. It was realized that increasing the buffer zone to 5 km for ~ 7.5 km long section would be an overestimation or too much generalisation of the crustal

properties. This feature was attributed to presence of fluids within the fault zone mapped as a highly conductive zone on the western end of the profile.

For the northern profile earthquake foci are preferentially clustered within shallow crustal levels, below a depth of 10 km, and localized within a stretch of ~ 3 km on western side of the section, which indicates dyking process. However, a few earthquakes are located at the central part of the profile within more compact and resistive rocks (~ 2000 – 4000 Ωm), which are also ideally brittle.

7.5 Discussion

The 2D MT response of the southern area can reasonably be attributed to a deep conductor (~ 1 – 4 Ωm) that extends vertically at depths ranging from 11 - 45 km, surrounded by sub-vertical zone of relatively conductive material (4 - 8 Ωm). Near the earth surface, the low resisitivity characterize almost the entire transect. The relatively conductive material can be construed to represent fault zone in-filled with crustal fluids possibly of magmatic origin. These fluids which possibly change in composition at a depth ranging from 3 to 6 km (i.e. marked by increased resistivity) reach the earth's surface and augment the Lake Magadi water of similar conductivity. Whereas the low resistivity within the conduit is indicative of hypersaline brines, the narrow and very highly conductive zone (~ 1 – 4 Ωm) reaching a depth of 11 km towards earth surface possibly mark water undersaturated crustal melts that possibly signify dyking process. Similar observations were made in Central Great Basin of Nevada U.S.A. an area characteristic of regional extension (Wannamaker et al., 2004). Mckenzie (1978) noted that extension rifting concomitantly cools the crust and re-absorbs original fluids. Therefore, to generate a conductor at deeper levels (like 11 km in this case) requires basaltic underplating, crystallization and fluid exsolution a phenomenon noted by Wannamaker et al. (2004). Indeed, Bailey (1983) noted that high heat flow along the axial rift was a result of focused mantle degassing, which is viewed (in this case) as a major driving force of upward fluid migration. Therefore, a melt manifested as a narrow dyke is inferred to characterize the area. Indeed, Roex et al. (2001) noted from a detailed geochemical analysis that lavas of south Kenya Rift floor have magma type composition bearing mantle plume signatures, an evidence that upwelling mantle plays a role in the initiation of the rift tectonics. This mantle plume is constrained as a dyke from results from this study.

It is noticeable from Figure 7-1 and as earlier mentioned by Ibs-von Seht et al. (2001); (2008); Kuria et al. (2010a) that seismicity south of Lake Magadi is markedly lower compared to that of the northern region. A projection of

earthquakes within a buffer zone of 3 and even 4 km along southern MT profile, surprisingly, never sampled any earthquake. Ibs-von Seht et al. (2001) attributed this reduced seismicity to increased micro crack porosity. Whereas Ibs-von Seht and others argument may be valid, the absence of the earthquakes within this transect is explained as a result of fluids contained therein. These fluids results into reduced mechanical strength and inability to allow stress build-up as observed by Unsworth et al. (2000) along San Andreas fault at Parkfield, California. Therefore, the fluidized fault zones of low-strength accommodate deforming stress. Indeed, high conductivities would be a result of high temperature fluids (hypersaline brines) that reach the earth surface as hot springs (Kuria et al., 2010a), or melting caused by exsolution of crystallizing and underplating crustal rocks. The decrease in resistivity within the fluidized zone at depth ranging from 3 - 6 km could either be attributed to lowering in temperature as fluid ascend within colder and shallow crustal rocks or mixing of recharge sourced from meteoric water (Eugster, 1970) with magmatic water.

A projection of the earthquake hypocentres along the magnetic section for the southern profile (Fig. 7-7b) shows that earthquake are localized within a linear listic structure extending to a depth of 25 km, which marks lower brittle domains of middle crust. A comparison of this zone with 2D MT profile shows that it corresponds to the more resistive section on the eastern side of the fluidized conduit. However, on the eastern side the low resistivity zone persists. Smith et al. (1989) noted that such seismicity is as a result of stress build due to crustal columnar pressures. Therefore, the seismicity is confined within area outside the low resistivity regime, which is interpreted to represent fluidized and altered zone (marginally weathered) of reduced mechanical strength and thus incapable of supporting significant stress internally, as noted by Wannamaker et al. (2004) elsewhere.

The resistivity structures along the northern profile indicate moderately conductive volcanic rock section that is fundamentally disrupted by intrusion on the western deeper parts of the profile. These rocks show an increase in conductance at depth ranging from 15 to 33 km, which becomes even more pronounced below this depth attaining a minimum of ~ 16 Ωm. This is attributed to intrusive heating. Interestingly, a moderate resistive but narrow zone attains a shallow depth of up to 11 km to the earth's surface along the area of swarm earthquake activity. It is along this area that Ibs-von Seht et al. (2001) noted that hypocentres of the earthquake cluster were not only shallow but exhibited a sharp cut-off at a depth ~ 9 km. The same is noted in Figure 7-7b. From this correspondence (moderate conductive zone and focal depth cut-off), it is tempting to infer that conductor is either fluid or a melt

that has a triggering role in nucleation of earthquakes. Indeed, the plot of the magnetic sources, used to define subsurface fault morphology, shows no magnetic sources below a depth of 8 km. A projection of earthquake hypocentres along this magnetic profile (Figure 7-8b) shows a plot along fault zone. It is therefore plausible that the steep normal faults of the brittle crustal domain stretch to ductile regime and enhance permeability through extensive fissuring. These deep seated fissured zones then provide for fluids with lithospheric pressure sourced from ductile regime to ascend to lower crustal scale faults and reduce effective normal stress. Minor stress fluctuations are expected to channel these fluids upward to induce a major seismic event as observed by 4.2 magnitude earthquake (Kuria et al., 2010a, Atmaoui and Hollnack, 2003, Ibs-von Seht et al., 2001) at the location of MT station MN2 (i.e. MTU unit was place on the fracture zone – a result of this earthquake).

A very large segment of high resistive rocks towards the east of the profile may signify a probe within the crystalline deep rooted rocks of the ANL shear zone, a complex zone of brittle and ductile shear (Smith and Mosley, 1993). The depth of the ANL shear zone has not yet been identified (Meju and Sakkas, 2007) but is noted to be below 45 km (reliable extent of 2D maximum probed depth in this study). It is worthwhile to note that although the margin between rift and ANL shear on the MT profile seems to be reasonably well defined, the orientation of the E-W profile and the NW-SE strike of ANL shear zone need to put into consideration. All in all, the wedging out of the high resistive and compact rock on the eastern side of the northern profile - interpreted as ANL shear zone - indicate an eastward dip consistent with Shackleton's (1986) E-dipping suture at the western margin of the Mozambique Belt. The low resistivity at depth ranging from 0.5 km to 1 km and characterizing almost entire profile, though prominent on the eastern and western ends, possibly mark deep aquifers with increased clay or saline content (Kuria et al., 2010b).

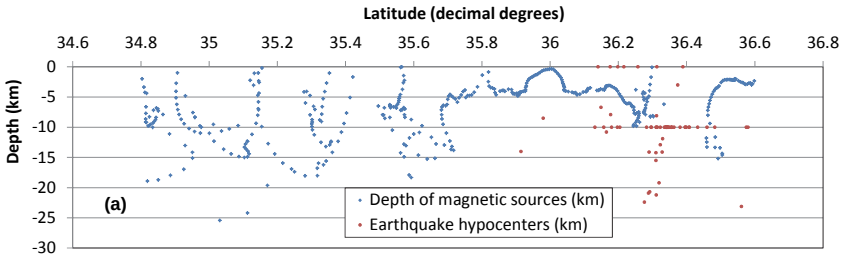

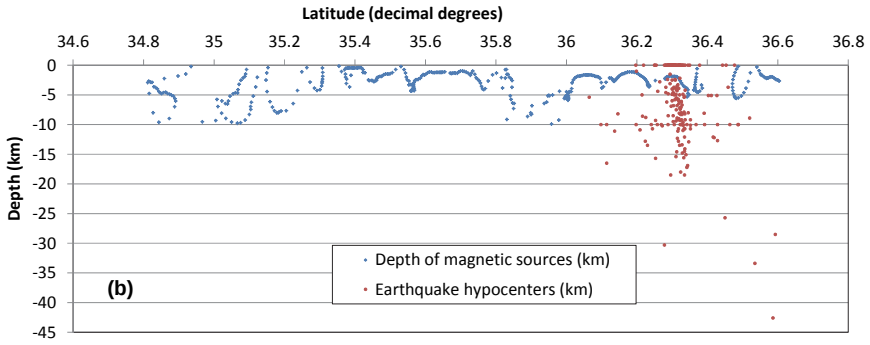

Figure 7-8. Profiles of the magnetic sources (blue dots) determined from 2D Euler deconvolution along flight lines showing fault morphology (for details see Kuria et al., 2010). The red dots denote earthquake focal depth sampled from a 6 km wide buffer zone along the flight lines. Notably, earthquake activity is concentrated along the rift axial zone. For south profile (a) – flight line 320 - the deep earthquakes display a listic structure a common feature with normal faults but devoid of magnetic sources. North profile (b) - flight line 351- the magnetic sources show similarly shallow magnetic sources and shallow earthquake focal depth within axial zone but increasing linear trend in earthquake depth eastwards marking probe within ANL shear zone or relict cratonic root.

The 3D seismic tomography (Achauer and Masson, 2002) evidenced a steep-walled low velocity zone, interpreted as a narrow asthenospheric wedge, which broadens below a depth 100 km. Together with the density-velocity contrast Achauer and Masson concluded that partial melts are contained in the upper mantle, reflected by low velocity diapiric signatures. It is plausible that the narrow high conductivity zones (in this study) represent feeder dyke supporting emplacement of partial melts.

7.6 Conclusion

From our study the following conclusions can be drawn:

1. Low resisitivity conductors that occur as sub-vertical corridor towards the earth's surface along the southern profile represent melt expressed as dyke with fluidized fault zones. The fluids sourced from ductile domains inhibit stress build up by reducing effective normal stress.
2. Confinement of the seismicity outside the low resistivity regime along the south profile represent zone of reduced mechanical strength incapable of supporting significant stress internally.
3. The correspondence of moderate conductive zone (~11 km) and focal depth cut-off (9 km) along the northern profile leads to inference that the conductor is either fluid or a melt that has a triggering role in nucleation of earthquakes

4. Extensional deformation as a rifting process enhances increased permeability that supports transmission of high pressure lithospheric fluid from ductile domain to the steep normal faults of the brittle crust. Minor stress perturbation disperses the fluids upwards to induce earthquake particularly north of Lake Magadi.
5. The sustained permeability zones within fluidized zone that lends them imaged with MT method compels an opinion that such copious fluids are sourced from upwelling mantle.
6. High conductivity zones though of variable resistivities (i.e. ~ 1 Ωm in the south compared to ~ 50 Ωm in north) are interpreted as feeder dykes supporting emplacement of partial melts.
7. Wedging-out of the high resistive feature east of the northern profile marks the east dipping suture of ANL shear zone.
8. Although the depth of the ANL shear zone has not been established, this study indicates that it is below 45 km. This depth is based on maximum probe depth for the 2D MT inversion, a depth below which 3D model prevails.

CHAPTER 8

SYTHESIS

8.1 Introduction

This chapter focuses on the integration of the key outputs from the preceding chapters, highlighting the key scientific contribution in this project. A brief description of the geological structures in the southern Kenya Rift is provided showing an update of the previous works. Subsequently, the tectonic forces prevailing in this extensional rifting regime are elucidated, which bridges the gap on neotectonic development. In addition, two profiles located north and south of Lake Magadi show the interrelationships between different geophysical models (magnetic sources from 2D Euler deconvolution, Curie point depths (CPD), Magnetotelluric (MT) and electrical resistivity imaging/tomography (ERT)). The integration of these geophysical models with "snap-shots" that monitor fault nucleation, growth and linkage using synthetic aperture radar interferometry (InSAR) techniques within a specified timescale provides not only the most robust approach in modelling the processes that drive seismotectonics but also help to infer tectonic evolution coupled with a prognosis of earthquake potential.

8.2 Seismically active structures (faults, fractures)

A systematic study on the active faults - as earthquake generating structures - to determine their spatial and density distribution was carried out. Using a combination of the ASTER images and ASTER DEM, earthquake epicentral distribution and 3D Euler deconvolution linear structures were delineated. Subsequently, a detailed field campaign was undertaken to confirm interpreted lineaments particularly from satellite images, establish their cross-cutting relationships and obtain structural data (i.e. strike and dip).

Earlier works that are central to understanding southern Kenya Rift, showed occurrence of normal, strike slip and oblique faulting in central and northern Kenya Rift (Doser and Yarwood, 1991, Strecker and Bosworth, 1991). In addition, Strecker and Bosworth (1991) deduced a clockwise change in stress field in the central part of the rift. The extension direction interpreted to have been oriented ENE-WSW during Miocene, later rotated to E-W in early Pleistocene then NW-SE during Quaternary times (Bosworth et al., 1992). More recent structural studies by Atmaoui and Hollnack (2003) at southern Kenya Rift, Lake Magadi area, support the Strecker and Bosworth (1991) and Bosworth et al. (1992) clockwise rotation of the extension direction.

The results from structural studies (Chapter 2) based on substantial field evidence identified four sets of faults with different age and deformational styles (Figure 2-2, Chapter2), namely (in a chronological sequence): normal

N-S; dextral NW-SE; strike slip ENE-WSW and sinistral NE-SW. The previous studies did not recognize the existence of the sinistral oblique NE-SW trending faults which were created to counterbalance the NW-SE faults. Noteworthy, the NW-SE and NE-SW structures are reactivation of the pre-existing structures. In addition, the NW-SE lineaments are closely linked to ASWA-Nandi-Loita (ANL) shear zone – a highly fractured zone of massive quartizitic Precambrian rocks (Smith and Mosley, 1993). NNW striking lineament are distributed to the north of Lake Magadi and delimited to its southern margin. ENE-WSW structures are normal to the regional trend of the rift and affect both Tertiary volcanics of the rift floor and Precambrian rocks of Nguruman region. The lineament density is high along volcanoes (Oldoinyo Sambu, Shompole, and Lenderut) to the south of Lake Magadi. However, to the north lineament density decreases between Loita hills and Ologesaile volcano. NE-SW structures do not continue south of Lake Magadi but the NW-SE persists on the south eastern part of the lake marking the propagation of the ANL in that direction. These structural interpretation, that reflects spatial and density distribution of faults and fractures, supports an E-W rift extension and therefore, bridges the gap in opinion on neotectonic extension of rift suggested by earlier authors.

The results from the focal mechanism solutions derived from analysis of well-located earthquakes using first motion P-polarities are presented using “beachballs” and discussed in Chapter 2 (Figure 2-7). An almost uniform spatial distribution of earthquakes used for this analysis was selected to characterize orientation and sense of slip as shown by the 22 “beachballs”, whose location mark patch of the fault that slipped. Distinctly, the orientation of the fault planes depicted by the “beachballs” tallies with orientation of the faults, deduced from ASTER DEM and ASTER image, described above. These orientations marking all directions (E-W, N-S, NE-SW and NW-SE) attest to the fact that most of faults on the axial rift floor are active. The dominant strike of the fault planes ranges between 10-20°, with steep P-axes and almost horizontal T-axes, which indicates that NE-SW oriented normal faults are actively deforming under E-W extension.

8.3 InSAR studies

In order to validate the E-W extension direction deduced from the structural studies (Chapter 2) and provide evidence for spatial strain distribution with its temporal constrain, an area (100 km by 100 km) south of Lake Magadi continuously monitored for a period of eight months. For this purpose, ENVISAT ASAR images with a 35-day repeat pass, 3-pass and 4-pass radar interferometry analysis technique were used. This technique has not been applied in monitoring faulting activity. Fundamentally, mapping of the

faulting activity not only provides clues on spatial distribution and intensity of hazard (earthquake) but also provides insights that explain intertwinement of discontinuous deformation of faults in the upper crust as a results of more continuous flow in the lower part of the lithosphere e.g. Jackson (1999) premise on which this work was proposed.

The faulting activity along normal faults, organized as sub-parallel systems (Chorowicz, 2005), is not uniformly distributed over entire period of extension. Characteristically, permanent or recurrent faulting activity shifts from one fault system to another making their temporal evolution more difficult (Goldsworthy and Jackson, 2001). Consequently, the fault zone architecture – a product of the faulting activity - becomes both temporary and spatially variable. Methods used to map this variability include geological approach (Yielding et al., 1997), branching of fault during evolution (Childs et al., 1996), fault and linkage (Cartwright et al., 1995) and local changes in stress environment (Sibson, 1986). In all these approaches, understanding of strain distribution (both on temporal and spatial scale) during faulting activity and its relationship to the regional stress field remains poorly resolved.

The results from interferogram of January-February 2006 show an NE-SW oriented but segmented deformation unit (~5.9 km long), with a high slippage (14 mm) spread over the entire fault scarp (200 m) that marks initiation of faulting process. Subsequent deformation (February-March 2006) joined the initially isolated segments (i.e. growth) becoming laterally extensive (~14.8 km) with increased slippage (i.e. 28 mm). Towards the termination point, the fringes breakdown into small isolated segments defining propagation direction. Noteworthy, the isolated segments for the January – February deformation show an echelon-shaped deflection from the main fault to join other small faults providing for further growth and linkage of the fault system. The other interferograms between March and August showed no deformation but were very useful for intrinsically validating the January to March deformation, which would be difficult to validate otherwise. The deformation area increased from 6.0×10^{-5} km^2 (in January-February) to 1.8×10^{-4} km^2 by the end of March. Elastic modeling using Okada (1985) formulation of the interferogram defined a typically blind fault slip at a depth of 0.5 – 1.5 km dipping at 40°. Baer et al. (2008) described a similar normal faulting from 2007 seismic crisis that hit Lake Natron area located 50 km south of the study site (this project). It therefore, follows that the first normal faulting episode discussed by Baer et al. (2008) had actually started earlier in the study area. From this study, it is fair to conclude that a change in stress regime from buried faults (or dyke intrusions) initiated deformation. It is now evidenced (from this study) that normal faults within the axial zone

are evolving through small scale slip movement which through reactivation and propagation cumulatively results into large vertical displacements. From the foregoing, it is clear that the principal active structure in southern Kenya Rift is youngest NE-SW trending fault driven possibly by dyke intrusion, which provides overwhelming evidence to E-W rift extension direction.

An estimation of the earthquake potential from the two rupture surfaces and their corresponding amount of slippage using (Aki and Richards, 2002) formulation of the seismic moment (So) and moment magnitude (Mw) was made – see Chapter 3. The earthquake magnitude for 5.9 km rupture surface corresponding to January – February deformation is about 4.19 and that of February – March deformation (14.8 km) amounts to 4.66. It not clear why these earthquakes associated with earth surface deformation were not recorded by seismograph stations but this could partly be due to a poor seismic station configuration at the time (a more dense configuration was installed in area in 2007 i.e. (Baer et al., 2008) and (Calais et al., 2008) or several earthquakes of small magnitude contributed to the rupture surface between two consecutive ENVISAT ASAR data acquisition (i.e. 35 day repeat pass). All in all, the 4.2 and 4.7 is a typical earthquake magnitude of the rift floor and marks the earthquake potential of this area.

8.4 Integrated geophysical models

A plot of integrated geophysical models was made along the traverse lines T320 and T351, located south and north of Lake Magadi respectively. Moho depths were obtained from Keller et al. (1994a) and Mechie et al. (1994) along KRISP line G by marching the relative distance used in their work with geographical coordinates using a GIS platform (ArcGIS 10). CPD were extracted from CPD map in Geosoft software (Chapter 5). For earthquakes, a buffer zone of 6 km was created and earthquakes within this (6 km) zone clipped. All these data sets were plotted together with scaled topography (i.e. elevation in km x 10) from SRTM DEM as shown in Figure 8-1.

For geophysical model along traverse line T320, the CPD are slightly shallower than Moho within the rift zone, marked by saddle shaped structure but deeper on both eastern and western parts of the rift. On the western flank, the CPD is gentle but dips steeply on the eastern side (characteristic of a zone with no magnetic sources from 2D Euler). The earthquake focal depths cover a wide lateral extent and are concentrated at a depth of 10 km, below which a characteristically linear and narrow zone of deepening earthquakes persists and corresponds to the steeply dipping CPD (western margin). Notably, the deep earthquakes plot at the crest of CPD, a subtle zone that is shallower than Moho. The magnetic sources defining the

subsurface character of the faults shows a deepened basinal structure, a location immediately south of Lake Magadi and marks a slight offset from the CPD crest. The earthquake hypocenters plot on the eastern fault bounding the basin. To the further east, the magnetic sources wedge out as linear trace following the CPD boundary.

The Moho marks a magnetic boundary because the mantle materials are non-magnetic (Wasilewski and Mayhew, 1992). If a CPD lies above the Moho it represents a Curie isotherm and if it corresponds to the Moho it marks a compositional boundary. The CPD plot slightly shallower than Moho within the rift zone and therefore represents a Curie isotherm, with low enthalpy. However, on the western flanks of the rift, CPD is almost corresponding to Moho but then rise gradually. In contrast, the eastern rift margin had CPD deeper than Moho, which indicates that upper most part of the mantle may be magnetic (Toft and Arkani-Hamed, 1992). In addition, these rift flank areas with deep CDP possibly have low heat flow and low vertical geothermal gradient (Eppelbaum and Pilchin, 2006).

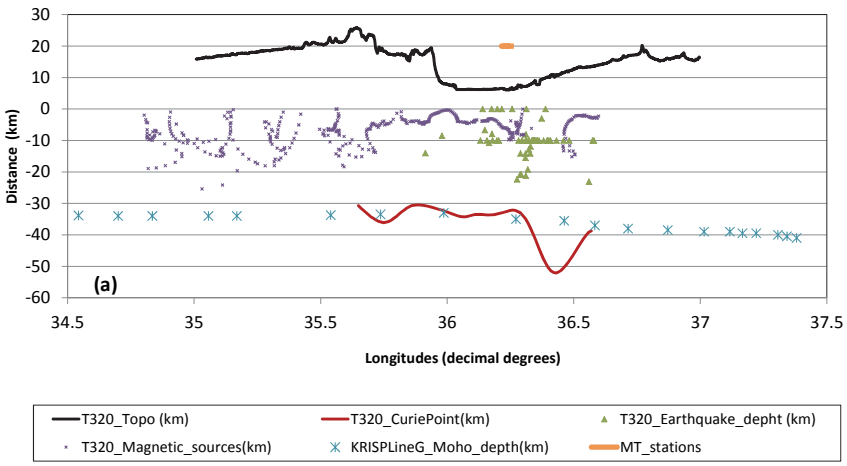

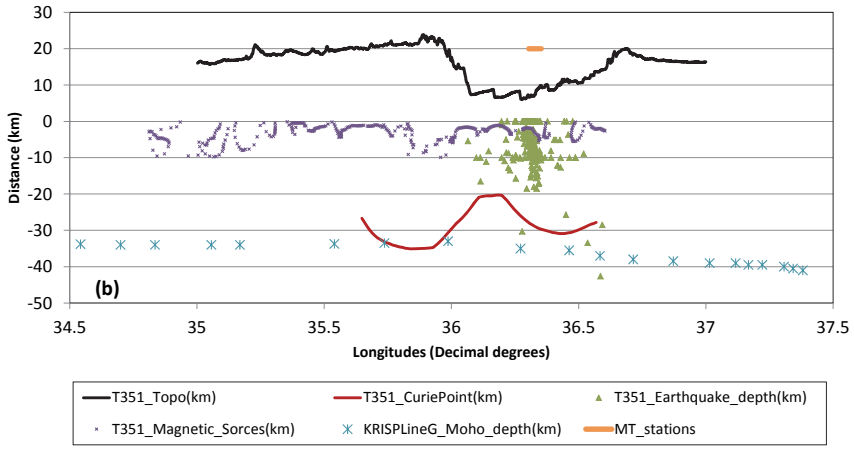

Figure 8-1. Integrated geophysical models showing interrelationships between Magnetic sources (mapping fault morphology), CPD and Moho depth (displaying thermal anomalies), and earthquake focal depth (marking seismogenic zone). (a) Geophysical model along traverse T320 located south of Lake Magadi. (b) Geophysical model along T351 located north of Lake Magadi. Note the reduced seismicity and shallow CPD for the southern profile and an increased seismicity particularly along a linear deepened zone and deep CPD for northern profile. Location of T320 and T351 is shown in Fig. 7-1.

A zoom-in into the part of the integrated geophysical model that correspond with the area covered by the MT section (Figure 8-2) shows a unique correspondence of shallowest CPD, fairly scattered magnetic sources at a depth ~ 5 km and almost complete absence of earthquakes (except two at extreme ends of the profile) along profile T320 (south Lake Magadi - Figure 8.2a). On the MT profile this zone is marked by a very highly conductive material (~ 1 Ωm) to a depth of ~11 km. This zone is interpreted as partial melt marking a thin dyke (~1-2 km) and the exsolution from this melt inhibit stress buildup by reducing effective normal stress. The circulation of the high temperature fluids, as noted from the hot springs along this profile, provides evidence that the tensional fractures supporting fluid flow are connected with deep faults linked to crustal heat sources (Dunkley et al., 1993).

On contrary, geophysical model along traverse line T351 (north of Lake Magadi) shows CPD deeper than Moho with marginally elevated central section (Figure 8-1b). The earthquakes are concentrated along a narrow linear zone reaching a depth ~ 9 km, a depth below which the earthquakes scatter but follow, at subdued level, the linear trace of CDP particularly on the eastern part. There is a generalized cluster of earthquakes along a laterally extensive zone at a depth of 10 km. The magnetic sources within the

rift form cyclic three dome shaped features with the eastern margin almost mimicking the architecture of southern basin. The occurrence of the CPD below Moho indicates that upper mantle is magnetic but more importantly that this area is characterized by low heat flow and low vertical geothermal gradient (Eppelbaum and Pilchin, 2006).

A comparison between the integrated geophysical model and MT section shows moderately conductive zone reaching a depth of about 11 km that is capped by a very resistive rock mass (2048 – 4098 Ωm) as shown in Figure 8-3. Near the earth surface, the resistive cap rock is weathered to a depth of ~ 5 km, therefore the resistive rock attains only a thickness ~ 6 km. Earthquakes show a cut-off depth ~9 km on the western end, with a gradually increasing depth attaining a maximum at a depth of ~18 km. It is notable that the earthquakes plot preferentially along the more resistive (brittle) zones. The conductive zone up to a depth of 11 km is interpreted as a melt. The extensive stress, as rifting process, subjects the steep normal faults (defined dome shaped features) to high pressured lithospheric fluids sourced from the ductile regime. The upward dispersion of these fluids as a result of minor stress perturbation encounters the resistive cap rocks and induces stress into the brittle upper crustal rocks, which is not thick enough (~ 6 km) to absorb a lot stress and therefore minor swarm earthquakes occur.

A very highly resistive body on the eastern flank along the northern profile that increase in thickness at an angle of ~ 45° is possibly an inherited cratonic or Proterozoic root marking ANL shear zone (Tesha et al., 1997, Meju and Sakkas, 2007). This shear zone is characterized by deep earthquakes, a low heat flow and low vertical geothermal gradient as noted in Chapter 6, which explains deep seated CDP.

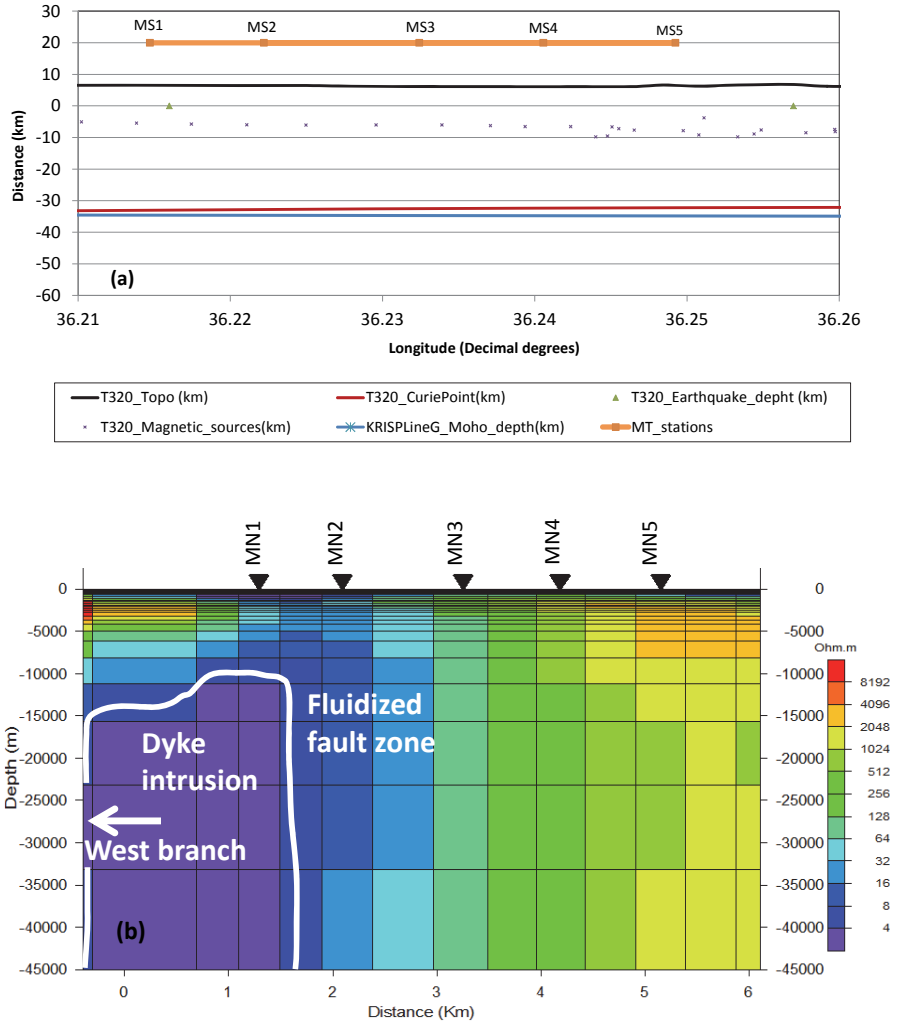

Figure 8-2. A comparison of the integrated geophysical model (a) and Inverted 2D MT model (b) along profile south of Lake Magadi. Note shallow CPD, laterally and linearly scattered magnetic sources (~5km), and almost complete absence of earthquakes for integrated model (a) and correspondingly this western zone is characterized by a vertical low conductivity zone (~1Ωm) reaching a depth of 11 km (b), interpreted as a partial melt. The more resistive zones on the eastern end are characterized by increased and randomly scattered magnetic sources indicating onset of faulting activity.

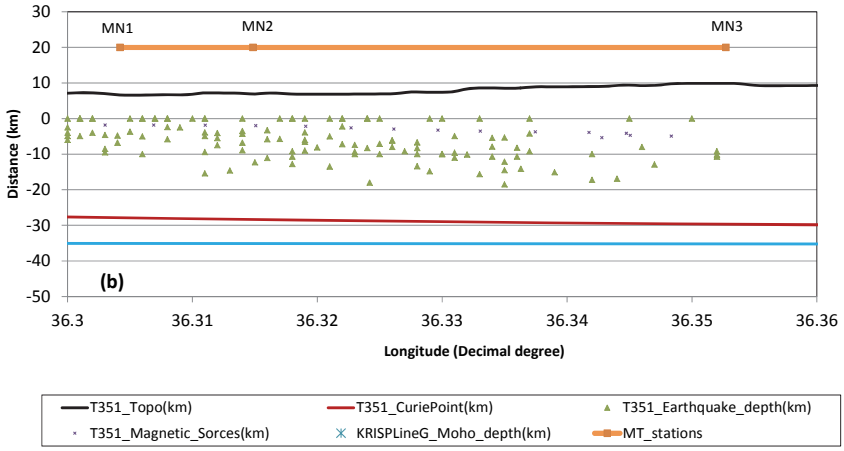

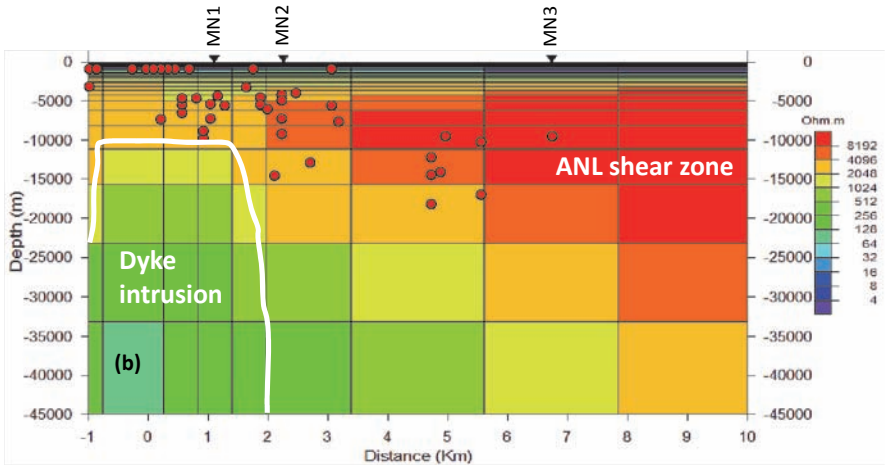

Figure 8-3. A comparison of the integrated geophysical model (a) and Inverted 2D MT model (b) along profile north of Lake Magadi. Note the deep CPD depth, deep Moho (but shallower than CPD), shallow earthquakes on the western end but an increasingly deepening earthquakes eastwards. On MT eastern corresponds with a moderate conductor on the western side, interpreted as dyke intrusion. Earthquakes are confined within the more brittle. Deeper CPD than Moho low heat flow and low vertical geothermal gradient further east indicates a E-dipping ANL shear zone with relatively deep earthquakes.

8.5 Conclusions

The primary motivation of studying the seismotectonics of the southern Kenya Rift was to provide understanding on the intertwinement of surface structural features (i.e. faults) and earth subsurface dynamical process(es) in

the realm of earthquake potential. In addition, an evaluation of the geothermal resources was also performed. This entailed use of a suite of remote sensing and geophysical techniques. Apart from deviating from the traditional earthquake hazard assessment, it is apparent that this (thesis) approach focuses on modelling process(es) associated with earthquake generation and distribution. In so doing, the close connection between earthquake and faulting mechanics – displayed by fault nucleation, growth and interaction – as products of the same dynamical process is emphasized. The ultimate goal being to identify the driving mechanism of faulting process and earthquake generation in a young continental rift setting.

- **To establish spatial and density distribution of active extensional structures including their geometry and trends and their implication to earthquakes distribution.**

The structural framework of the Magadi fault system is defined by four sets (Figure 2-2 in Chapter 2). According to their cross cutting relationship with respect to the oldest include: normal N-S; dextral NW-SE; strike slip ENE-WSW and sinistral NE-SW. The previous studies did not recognize the existence of the sinistral oblique NE-SW trending faults which were created to counterbalance the NW-SE faults. Noteworthy, the NW-SE and NE-SW structures are reactivation of the pre-existing structures. In addition, the NW-SE lineaments are closely linked to ASWA-Nandi-Loita (ANL) shear zone – a highly fractured zone of massive quartizitic Precambrian rocks (Smith and Mosley, 1993).

NNW striking lineament are distributed to the north of Lake Magadi and delimited to its southern margin. ENE-WSW structures are normal to the regional trend of the rift and affect both Tertiary volcanics of the rift floor and Precambrian rocks of Nguruman region. The lineament density is high along volcanoes (Oldoinyo Sambu, Shompole, and Lenderut) to the south of Lake Magadi. However, to the north lineament density decreases between Loita hills and Ologesaile volcano. NE-SW structures do not continue south of Lake Magadi but the NW-SE faults persist on the south eastern part of the lake marking the propagation of the ANL in that direction.

The results accrue from this study are in odd with those of Strecker and Bosworth (1991) who advocated a NW-SE neotectonic extension from their work in central Kenya Rift by assuming the NW-SE structures as direction of extension; and Atmaoui and Hollnack (2003) who argued an E-W to ESE-WNW neo-tectonic extension for the Lake Magadi area by assuming the NW-SE dextral movement is localized based on (possibly) inadequate field data. Both views failed to recognize the existence of the sinistral oblique slip NE-

SW trending faults that were created under an E-W extension to counterbalance NW-SE fault. The results from this study are highly consistent with the rift development model of central Kenya Rift proposed by Le Turdu et al. (1999). According to the current study (this thesis) the model at the onset of the rifting tectonics the rift experienced normal faulting under E-W extension. Subsequently, a tectonic change reactivated pre-existing structures creating dextral NW-SE, strike slip ENE-WSW and sinistral NE-SW faults under E-W extension.

- **To determine migration and propagation of the extension throughout the Magadi rift basin and relate it to the entire Kenyan rift.**

Most studies on the migration and propagation of the extension are based on fault growth, which incorporates nucleation and linkage of fault segments (Segall and Pollard, 1980, Trudgill and Cartwright, 1994, Le Turdu et al., 1999, Le Gall et al., 2000). For this purpose, structural geometry of faults including their displacements and lengths are characterized. Whereas this method has been widely used, the temporal growth history of the fault system cannot be quantified or determined equivocally. For this study (this thesis) SAR interferometry technique was used to resolve structural geometry of an evolving fault system as well as providing equivocally temporal constrain throughout the entire monitoring period.

The results show that fault nucleation began along NE-SW existing fault between the months of January and February 2006. This onset deformation field was defined by isolated, tapered elliptically shaped segments characterized by a high slippage (14 mm) spread along dip slip (width 200 m) of a normal fault. Each isolated segment was separated from the next by a zone of locally minimum or no slippage at all. The entire slippage surface covered an area of ~ 6.0×10^{-5} km^2. This deformation (January – February) was referred as initiation of a faulting process. The subsequent deformation marking growth and linkage stretched over a distance of ~ 14.8 km and covered an area of 1.8 x 10-4 km2 i.e. 300% growth. The deformation joined the initially isolated segments (January-February). Further south the deformation fields breakdown into small isolated segments defining propagation direction. The slippage along the joined segments increased to 28 mm but the isolated ones attained only 14 mm. The isolated segments show an echelon-shaped deflection along the main fault to join others small faults marking the linkage of the fault system. There was no detectable deformation observed in the next 6 months monitoring period after February-March deformation.

- **To deduce the magnitude of the surface deformation in the Magadi area (ground deformation detection) and relate it to potential earthquakes**.

The simple elastic modeling of the InSAR results showed that the deformation was caused by a ~ 56 mm slippage at depth of 0.5 to 1.5 km along 40° dipping blind fault. An estimation of the earthquake potential from the two rupture surfaces and their corresponding amount of slippage using (Aki and Richards, 2002) formulation of the seismic moment (So) and moment magnitude (Mw) was made – see Chapter 3. The earthquake magnitude for 5.9 km rupture surface corresponding to January – February deformation is about 4.19 and that of February – March deformation (14.8 km) amounts to 4.66. It not clear why these earthquakes associated with earth surface deformation were not recorded by seismograph stations but this could partly be due to a poor seismic station configuration at the time (a more dense configuration was installed in area in 2007 i.e. (Baer et al., 2008) and (Calais et al., 2008) or several earthquakes of small magnitude contributed to the rupture surface between two consecutive ENVISAT ASAR data acquisition (i.e. 35 day repeat pass). All in all, the 4.2 and 4.7 is a typical earthquake magnitude of the rift floor and marks the earthquake potential of this area.

It is highly unlikely that that such a deformation would be caused regional scale extensional forces and therefore a dyke provides a feasible explanation. These findings provide overwhelming evidence that the mechanism of the deformation is driven by E-W extension along the youngest faults (NE-SW), which is indeed an on-going process localized along existing faults i.e. reactivation process. The propagation direction is north-south. This is consistent with earlier works by Baker and Wohlenberg (1971a) and Smith (1994) who noted that the age of the rift initiation as well as volcanism suggest a north towards south rift propagation. In addition, this work bridges the gap on extensional direction for central Kenya proposed by Le Turdu et al. (1999).

Noteworthy, the observed deformation (InSAR) is not confined along the ANL shear zone (otherwise it would be localized within the dextral slip faults oriented in NW-SE direction) or near the Kenya dome but occurs close to the Tanzanian Craton. From this study, the regime of the on-going crustal deformation is localized within a small area, i.e. less than 15 km long, which lead to a hypothesis that the rifting process could possibly be taking place within small discrete domains that join (through growth and linkage) to form a regional scale rift system. This is supported by Le Gall et al. (2000) who noted that lava flows when subjected to tensile stress break along columnar joints, these being zones of minimum tensile strength. Merging of small

fissures, scaled down to columnar joints, results into growth of major fractures (Anders and Wiltschko, 1994, Angelier et al., 1997). Ultimately, through coalescence of small scale fractures, regional scale faults are established. The fact that normal faults are products of reactivated deep pre-existing discontinuities (Pohn, 1981, Anders and Wiltschko, 1994, Cloke et al., 1997, Higgins and Harris, 1997), zones along which on-going deformation is localized attest to this hypothesis. It is worthwhile to note that prevalence of the joints does not necessary signify nucleation points of the normal faulting but mark zones of minimum tensile strain (Le Gall et al., 2000).

- **To map and quantify the thermal gradients as possible driving mechanism of the rifting process as well as geothermal indicators.**

It well understood that temperature is major factor controlling the mechanical strength of rocks (Sibson, 1982, Pasquale et al., 1999). Therefore, to understand thermally controlled processes, CPD were determined from aeromagnetic data using spectral analysis techniques for central to southern Kenya Rift (Chapter 5, Figure 5-6b). Indeed, the undulating morphology as deduced from spatial distribution of CPD could provide insights into seismogenic behaviour and geodynamic evolution in rifting tectonics (Li et al., 2010). These CPD together with their spatial variation were mapped for the first time along Kenya Rift.

The results from CPD show that rift floor (down warped part) is characterized by a series of shallow CPDs with various sizes and shapes. The largest shallow CPD is located south of Lake Naivasha possibly associated with Longonot and Suswa volcanoes including Olkaria area. This anomaly that attains a minimum CPD at 9 km in central part and about 20 km at its peripheral margins displays relatively highest degree of geothermal manifestation in the study area (Riaroh and Okoth, 1994). These markers of elevated thermal regime include hot fumaroles, hot and altered ground as also evidenced in Figure 5-7. Indeed, the Olkaria geothermal field, currently under exploitation, is located at the north western margin of this large and possibly highly resourceful geothermal reservoir (shown by the numerous drilled boreholes, Figure 5-1). In addition, the hottest ground temperatures (~93° C) occur within the annular part of Suswa, where fumaroles attain temperatures ranging from 202°C to 243°C, which combined with measurable concentrations of methane and hydrogen from fumaroles (Omenda, 2001) attest to a possible geothermal reservoir. Consequently, the CPD indisputably manifest elevated thermal regimes. The other significant (in size) shallow CPD (with an average depth of about 15 km) spatially related to volcanic centers include Menegai that spreads intermittently further south of

Lake Nakuru but terminates before reaching Eburru. These slightly deepened CPD indicate subdued geothermal potential. Indeed, according to (Omenda, 2001) these bald lands manifest hot water boreholes, while the floor of Menenagi crater steams on its floor.

The rest of the shallow CPD along the rift floor are associated with axial faults i.e. Lake Bogoria and Lake Magadi. The shallow CPD anomalies located NW of Lake Magadi reach a depth of about 14 km, while those on southern tip of lake attain a depth of about 31 km. It is remarkable that hottest springs (80-90 °C) are located on the northern shores of Lake Magadi while the other springs (south of Lake Magadi) attain temperatures of about 32-44°C (Omenda, 2001, Kuria et al., 2010a). This correspondence of the CPD and thermal regimes manifested by hot spring is certainly not a coincidence. Central to this argument, the Lake Bogoria CPD (about 13 km) manifest steam jets (Figure 5-7) and spouting geysers, hot springs and boiling pools (Omenda, 2001).

The most striking and possibly unexpected CPDs are those located off rift floor oriented in NW-SE direction past the western margin of the rift bounding faults at latitude 0.5°S and 1.5°S. There is no evidence of geothermal manifestation at the moment but the elevated thermal regimes inferred from shallow CPD (6 – 17 km) necessitate immediate further investigation. The location of the buried volcanoes (determined from 3D Euler) underscores the importance of additional investigation. Noteworthy, Fairhead 1976 construed a gravity model running these volcanoes (using techniques of the day) as shown in Figure 6-8 but these results were quashed by Smith (1972). It is most likely that the volcanoes had an influence on the gravity anomaly; however their occurrence (off western rift margin) would be a remote possibility to have been thought about based on current structural and tectonic setting of the rift.

A plot was made of CPD extracted along the KRISP axial and Line G (crossing the rift at Lake Magadi) and compared them with Moho depths (Keller et al., 1994a, Mechie et al., 1994) see Figures 6-7. The CPD along axial rift are shallower than Moho depth (~33 to ~35 km) indicating that CPD is a thermal boundary (Curie isotherm) rather than a compositional boundary. However, along line G the CPD are deeper than moho depths at location of the Tanzania Craton and Mozambique Belt but shallower within the rift, similar to axial line. The occurrence of CPD below Moho was observed by Toft and Arkani-Hamed (1992) and they concluded that in some cases uppermost part of mantle may be magnetic, a conclusion made also draw for this area. In addition, the large depths to the bottom of the magnetic crust (CPD)

observed can possibly be due to the fact that these regions have low heat flow and low vertical gradient (Eppelbaum and Pilchin, 2006). Conversely, the zones of shallow CPD characterize zone of high heat flow (e.g. Blakely (1988) in a given region and therefore the three isolated zone of shallow CPD mark the thermally active zones. In addition, earthquakes were clipped within a 25 km buffer zone along the KRISP axial line and line G and were compared with the CPD along the same line. It is observed that swarm earthquake activity (cluster) occur in areas with marked local rise of Curie isotherm while deeper earthquakes on the rift floor preferentially occur within zones of deep Curie point characterized by thickened crustal structure (Aswa shear zone) and other inherited cratonic or Proterozoic roots. Seismic cut-off depths occur slightly above estimated Curie isotherm depth. From results of the CPD, Moho and earthquakes, it is reasonable to conclude that the isolated zones with shallow CPD mark magmatic plumes, and that the movement of or within these intrusions cause shallow earthquakes, at least, along these zone reflecting rifting tectonics.

Using temperature-depth profiles from Olkaria Geothermal Field, a geothermal gradient of about 39°C/km was estimated, which when correlated to CPD results into a temperature of 565.5°C at a depth of 14.5 km, which is slightly lower than the 580°C. This temperature gradient that represents the more stable gradient indicates that the estimated CPD is not an overestimation or an underestimation and is therefore more representative at least within the rift floor. The unsteady geotherms were affected by circulation of high temperature brines and cold water from groundwater hydrogeological systems.

To furnish details on fault architecture and its associated seismicity within Lake Magadi rift basin, MT and TEM sounding were performed along two profiles located north and south Lake Magadi. The 2D MT models were compared with CPD and earthquake focal depths (Figures 8-1). Southern profile showed a typically ~ 1-2 km wide sub vertical conductor (largely 1-4 Ωm at deeper levels) stretching from the earth surface to a depth below 45 km and surrounded by highly weathered rock mass (4-8 Ωm). This conductive zone was characterized by shallowest CPD, a break in magnetic source (indicating high heat flow) and complete absence of earthquakes. The very highly conductive zone (~ 1 Ωm) reaching a depth of 11 km to the earth surface was interpreted as partial melt representing a thin dyke whereas the surrounding conductive zones were interpreted as magmatic fluids, a result of exsolution from the melt. These fluids reaching the earth surface as hot springs inhibit stress build up by reducing effective normal stress. The more resistive zones to the further east support minimal seismic activity being

zones incapable of supporting significant stress internally. On contrary, the northern profile shows a moderate to a resistive zone ~1 - 2 km wide reaching a depth of about 11 km that is capped by a very resistive (2048 – 4098 Ωm) rock mass ~ 6 km thick. A swarm of earthquake focal depths plot within this moderately conductive zone and show a clear cut-off at a depth ~9 km. However, away from conductive zone, earthquakes plot preferentially along more resistive (brittle) zones. The moderately conductive zone is interpreted as dyke that triggers nucleation of earthquakes at shallow and more resistive (brittle) zones to a depth of ~ 9 km (also observed by Ibs-von Seht et al. (2001); (2008). It is inferred that the extensive stress, as rifting process, subjects the steep normal faults to high pressured lithospheric fluids sourced from the ductile regime. The upward dispersion of these fluids as a result of minor stress perturbation encounters the resistive cap rocks and induces stress into the brittle upper crustal rocks, which is not thick enough to absorb a lot stress and therefore swarm earthquakes occur. This explains the increased seismicity in this area. On the other hand, the resistive rock mass inclined at an angle of ~ 45° at the eastern end of the northern profile and characterized by both deep earthquakes and deep CPD marks location of ANL shear zone. This evidence attest to the fact that dyke intrusion is the main driving mechanism of the rifting process and presence of fluids (and the pressures therein) influences the seismicity.

Bibliography

ACHAUER, U., MAGUIRE, P. K. H., MECHIE, J. & GREEN, W. V. 1992. Some remarks on the structure and geodynamics of the Kenya Rift. *Tectonophysics,* 213**,** 257-268.

ACHAUER, U. & MASSON, F. 2002. Seismic tomography of continental rifts revisited: from relative to absolute heterogeneities. *Tectonophysics,* 358, 17-37.

ADEPELUMI, A. A., AKO, B. D., AJAYI, T. R., OLORUNFEMI, A. O., AWOYEMI, M. O. & FALEBITA, D. E. 2008. Integrated geophysical mapping of the Ifewara transcurrent fault system, Nigeria. *Journal of African Earth Sciences,* 52**,** 161-166.

AKI, K. & RICHARDS, P. G. 2002. Quantitative seismology (2nd ed. ed.), University Science Books.

ALBARIC, J., DÉVERCHÈRE, J., PETIT, C., PERROT, J. & LE GALL, B. 2009. Crustal rheology and depth distribution of earthquakes: Insights from the central and southern East African Rift System. *Tectonophysics,* 468, 28-41.

ALLEN, D. J., DARLING, W. G. & BURGESS, W. G. 1989. Geothermics and hydrogeology of the southern part of the Kenya Rift Valley with emphasis on the Magadi-Nakuru area. *Br. Geol. Surv. Res. Rep.,* SD/89/1.

ANDERS, M. K. & WILTSCHKO, D. V. 1994. Microfracturing, paleostress and the growth of faults. *J. Struct. Geol.,* 16**,** 519–538.

ANDERSON, D. L., TOSHIRO, T. & ZHANG, Y. 1992. Plate tectonics and hot spots: The third dimension. *Nature,* 256**,** 1645-1651.

ANGELIER, J., BERGERAT, F., DAUTEUIL, O. & VILLEMIN, T. 1997. Effective tension-shear relationships in extensional fissure swarms, axial rift zone of northeastern Iceland. *Journal of Structural Geology,* 19, 673-685.

ATMAOUI, N. & HOLLNACK, D. 2003. Neotectonics and extension direction of the Southern Kenya Rift, Lake Magadi area. *Tectonophysics,* 364, 71-83.

AYDIN, V. 2000. Fractures, faults and hydrocarbon entrapment, migration, and flow. *Marine and Petroleum Geology,* 17, 797-814.

BAER, G., HAMIEL, Y., SHAMIR, G. & NOF, R. 2008. Evolution of a magma-driven earthquake swarm and triggering of the nearby Oldoinyo Lengai eruption, as resolved by InSAR, ground observations and elastic modeling, East African Rift, 2007. *Earth and Planetary Science Letters,* 272, 339-352.

BAILEY, D., WHALER, K. A., ZENGENI, T., JONES, P. C. & GWAVAVA, O. 2000. A magnetotelluric model of the Mana Pools basin, northern Zimbabwe. *J. Geophys. Res.,* 105, 11185– 11202.

BAILEY, D. K. 1983. The chemical and thermal evolution of rifts. *Tectonophysics,* 94, 585-597.

BAKER, B. 1986. Tectonics and volcanism of the southern Kenya Rift Valley and its influence on rift sedimentation. *Geological Society London Special Publications,* 25, 45.

BAKER, B., WILLIAMS, L., MILLER, J. & FITCH, F. 1971a. Sequence and geochronology of the Kenya rift volcanics. *Tectonophysics,* 11, 191-215.

BAKER, B. H. 1958. Geology of the Magadi Area. *Report Geological Survey of Kenya.*

BAKER, B. H. 1963. Geology of the South of Magadi. *Report Geological Survey of Kenya.*

BAKER, B. H. & MITCHELL, J. G. 1976. Volcanic stratigraphy and geochronology of the Kedong-Olorgesailie area and the evolution of the South Kenya Rift Valley. *J. Geol. Soc. London,* 132**,** 467-484.

BAKER, B. H. & MITCHELL, J. G. 1984. Stratigraphy, geochronology and volcano-tectonic evolution of the Kedong-Naivasha-Kinangop region, Gregory Rift Valley, Kenya. *J. Geol. Soc. London,* 141**,** 1057-1070.

BAKER, B. H., MOHR, P. A. & WILLIAMS, L. A. J. 1972a. Geology of the Eastern Rift System of Africa. *The Geological Society of America, Special paper* 136**,** 67

BAKER, B. H., MOHR, P. A. & WILLIAMS, L. A. J. 1972b. Geology of the Eastern Rift System of Africa. *The Geological Society of America, Special paper* 136**,** 1-67.

BAKER, B. H., WILLIAMS, L. A. J., MILLER, J. A. & FITCH, F. J. 1971b. Sequence and geochronology of the Kenya rift volcanics. *Tectonophysics,* 11, 191-215.

BAKER, B. H. & WOHLENBERG, J. 1971. Structure and evolution of the Kenya Rift Valley. *Nature,* 229, 538-542.

BARBIER, E. 2002. Geothermal energy and current status: An overview. *Renew. Sust. Energ. Rev,* 6, 3-65.

BARRIT, S. D. 1993. The African Magnetic Mapping Project. *ITC Journal,* (1993-2), 121-131.

BECHTEL, T. D., FORSYTH, D. W. & SWAIN, C. J. 1987. Mechanisms of isostatic compensation in the vicinity of the East African Rift Kenya. *Geophys. J. R. Astor. Soc.,* 90, 445-465.

BELLANI, S., BROGI, A., LAZZAROTTO, A., LIOTTA, D. & RANALLI, G. 2004. Heat flow, deep temperatures and extensional structures in the Larderello Geothermal Field (Italy): constraints on geothermal fluid flow. *Journal of Volcanology and Geothermal Research,* 132, 15-29.

BHATTACHARYYA, B. & LEU, L. 1975. Analysis of magnetic anomalies over Yellowstone National Park: mapping of Curie point isothermal surface for geothermal reconnaissance. *Journal of Geophysical Research,* 80, 4461-4465.

BILLI, A., SALVINI, F. & STORTI, F. 2003. The damage zone-fault core transition in carbonate rocks: implications for fault growth, structure and permeability. *Journal of Structural Geology,* 25, 1779-1794.

BILLI, A., VALLE, A., BRILLI, M., FACCENNA, C. & FUNICIELLO, R. 2007. Fracture-controlled fluid circulation and dissolutional weathering in sinkhole-prone carbonate rocks from central Italy. *Journal of Structural Geology,* 29, 385-395.

BIRT, C. S., MAGUIRE, P. K. H., KHAN, M. A., THYBO, H., KELLER, G. R. & PATEL, J. 1997. The influence of pre-existing structures on the evolution of the southern Kenya Rift Valley -- evidence from seismic and gravity studies. *Tectonophysics,* 278, 211-242.

BLAKELY, R. J. 1988. Curie temperature isotherm analysis and tectonic implications of aeromagnetic data from Nevada. *Journal of Geophysical Research,* 93, 817–832.

BLAKELY, R. J. 1995. Potential theory in Gravity and Magnetic applications, Cambridge University Press, Australia.

BOSWORTH, W. 1985. Geometry of propagating continental rifts. *Nature,* 316**,** 626–627.

BOSWORTH, W. 1987. Off-axis volcanism in the Gregory rift, east Africa: Implications for models of continental rifting. *Geology,* 15, 397.

BOSWORTH, W., LAMBIASE, J. & KEISLER, R. 1986. A new look at the Gregory's Rift: The Structural Style of the continental rifting. *EOS*, 576-578.

BOSWORTH, W. & STRECKER, M. R. 1997. Stress field changes in the Afro-Arabian rift system during the Miocene to Recent period. *Tectonophysics,* 278, 47-62.

BOSWORTH, W., STRECKER, M. R. & BLISNIUK, P. M. 1992. Integration Of East African Paleostress and Present-Day Stress Data: Implications For Continental Stress Field Dynamics. *Journal of Geophysical Research,* 97 11,851-11,865.

BRIGGS, I. C. 1974. Machine contouring using minimum curvature. *Geophysics,* 39, 39-48.

BUNGUM, H. & NNKO, A. A. 1984. Seismicity and tectonics of the Stiegler's Gorge area, Tanzania. *Journal of Geophysical Research,* 89, 1874-1889.

CAHEN, L., SNELLING, N. J., DEHAL, J. & VAIL, J. R. 1984. The Geochronology and Evolution of Africa, Clarendon Press, Oxford.

CAINE, J., EVANS, J. & FORSTER, C. 1996. Fault zone architecture and permeability structure. *Geology,* 24, 1025.

CALAIS, E., D'OREYE, N., ALBARIC, J., DESCHAMPS, A., DELVAUX, D., DEVERCHERE, J., EBINGER, C., FERDINAND, R. W., KERVYN, F., MACHEYEKI, A. S., OYEN, A., PERROT, J., SARIA, E., SMETS, B., STAMPS, D. S. & WAUTHIER, C. 2008. Strain accommodation by slow slip and dyking in a youthful continental rift, East Africa. *Nature,* 456, 783-787.

CAMPBELL, I. & GRIFFITHS, R. 1990. Implications of mantle plume structure for the evolution of flood basalts. *Earth and Planetary Science Letters,* 99, 79-93.

CANTINI, P., CATALDI, A. & PINNA, E. 1990. Gravity study of the structure of Suswa volcano and basement in the Kenya Rift. *Geothermics,* 19, 367-384.

CARTWRIGHT, J. A., TRUDGILL, B. D. & MANSFIELD, C. S. 1995. Fault growth by segment linkage: an explanation for scatter in maximum displacement and trace length data from the Canyonlands Grabens of SE Utah. *Journal of Structural Geology,* 17, 1319-1326.

CHAPMAN, D. S. & POLLACK, H. N. 1977. Heat flow and heat production in Zambia: Evidence for lithospheric thinning in central Africa. *Tectonophysics,* 41, 79-100.

CHEN, W.-P. & MOLNAR, P. 1983. Focal depths of intracontinental and intraplate earthquakes and their implications for the thermal and mechanical properties of the lithosphere. *J. Geophys. Res.,* 88, 4183-4214.

CHILDS, C., NICOL, A., WALSH, J. J. & WATTERSON, J. 1996. Growth of vertically segmented normal faults. *Journal of Structural Geology,* 18, 1389-1397.

CHIOZZI, P., MATSUSHIMA, J., OKUBO, Y., PASQUALE, V. & VERDOYA, M. 2005. Curie-point depth from spectral analysis of magnetic data in central-southern Europe. *Physics of The Earth and Planetary Interiors,* 152, 267-276.

CHOROWICZ, J. 2005. The East African rift system. *Journal of African Earth Sciences,* 43, 379-410.

CLARKE, M. C. G., WOODHALL, D. G., ALLEN, D. & DARLING, G. 1990. Geological, volcanological and hydrogeological controls on the occurrence of geothermal activity in the area surrounding Lake Naivasha Kenya. *British Geological Survey Research Paper, report to the Ministry of Energy, Kenya.*

CLOKE, I., MOSS, S. & CRAIG, J. 1997. The influence of basement reactivation on the extensional and inversional history of the Kutai Basin, East Kalimantan, SE Asia. *Journal of the Geological Society,* 154, 157.

CONDIE, K. 1997. Plate tectonics and crustal evolution, Butterworth-Heinemann.

CONNARD, G., COUCH, R. & GEMPERLE, M. 1983. Analysis of aeromagnetic measurements from the Cascade Range in central Oregon. *Geophysics,* 48, 376-390.

COOPER, G. R. J. 2006. Obtaining dip and susceptibility information from Euler deconvolution using the Hough transform. *Computers & Geosciences,* 32, 1592-1599.

COOPER, G. R. J. 2008. Euler Deconvolution with Improved Accuracy and Multiple Different Structural Indices. *Journal of China University of Geosciences,* 19, 72-76.

COWIE, P., SCHOLZ, C. H., EDWARDS, M. & MALINVERNO, A. 1993. Fault strain and seismic coupling on mid-ocean ridges *Journal of Geophysical Research* 98, 17 911–17 920.

COX, S. 2002. Fluid flow in mid-to deep crustal shear systems: Experimental constraints, observations on exhumed high fluid flux shear systems, and implications for seismogenic processes. *Earth Planets and Space,* 54, 1121-1126.

COX, S., KNACKSTEDT, M. & BRAUN, J. 2001. Principles of structural control on permeability and fluid flow in hydrothermal systems. *Reviews in Economic Geology,* 14, 1–24.

COX, S. F. 2005. Coupling between deformation, fluid pressures and fluid flow in ore-producing hydrothermal systems at depth in the crust. *Economic Geology,* 100th Anniversary Volume, 1-35.

CROSSLEY, R. 1979. Structure and volcanism in the S. Kenya rift. in:Geodynamic Evolution of the Afro-Arabian Rift System. Accademia Nazionale Dei Lincei, Rome.

DEMANET, D., RENARDY, F., VANNESTE, K., JONGMANS, D., CAMELBEECK, T. & MEGHRAOUI, M. 2001. CASE HISTORY-The use of geophysical prospecting for imaging active faults in the Roer Graben, Belgium. *Geophysics,* 66, 78-89.

DÉVERCHÈRE, J., PETIT, C., GILEVA, N., RADZIMINOVITCH, N., MELNIKOVA, V. & SAN'KOV, V. 2001. Depth distribution of earthquakes in the Baikal

rift system and its implications for the rheology of the lithosphere. *Geophysical Journal International,* 146, 714-730.

DOLMAZ, M., USTAOMER, T., HISARLI, Z. & ORBAY, N. 2005a. Curie Point Depth variations to infer thermal structure of the crust at the African-Eurasian convergence zone, SW Turkey. *Earth Planets and Space,* 57, 373-383.

DOLMAZ, M. N., HISARLI, Z. M., USTAÖMER, T. & ORBAY, N. 2005b. Curie Point Depths Based on Spectrum Analysis of Aeromagnetic Data, West Anatolian Extensional Province, Turkey. *Pure and Applied Geophysics,* 162**,** 571-590.

DOSER, D. & YARWOOD, D. 1991. Strike-slip faulting in continental rifts: examples from Sabukia, East Africa (1928), and other regions. *Tectonophysics,* 197, 213-224.

DUNKLEY, P. N., SMITH, M., ALLEN, D. J. & DARLING, W. G. 1993. The geothermal activity and geology of the northern sector of the Kenya Rift Valley. *British Geological Survey Research Paper,* SC/93/1.

EBINGER, C. 1989. Tectonic development of the western branch of the East African rift system. *Geological Society of America Bulletin,* 101, 885.

EBINGER, C., PETIT, C. & BUROV, E. 2002. Causes and consequences of lithospheric extension: the ups and downs of continental rifts. *Special Publication - SEPM,* 73, 11-24.

EBINGER, C. J., KARNER, G. D. & WEISSEL, J. K. 1991. Mechanical strength of extended continental lithosphere: Constraints from the Western Rift System, East Africa. *Tectonics,* 10, 1239-1256.

EGBERT, G. D. & BOOKER, J. R. 1986. Robust estimation of geomagnetic transfer functions. *Geophys. J. R. Astron. Soc,* 87, 173-194.

EPPELBAUM, L. V. & PILCHIN, A. N. 2006. Methodology of Curie discontinuity map development for regions with low thermal characteristics: An example from Israel. *Earth and Planetary Science Letters,* 243, 536-551.

ESPINOSA-CARDEÑA, J. M. & CAMPOS-ENRIQUEZ, J. O. 2008. Curie point depth from spectral analysis of aeromagnetic data from Cerro Prieto geothermal area, Baja California, México. *Journal of Volcanology and Geothermal Research,* 176, 601-609.

EUGSTER, H. 1970. Chemistry and origin of the brines of Lake Magadi, Kenya. *Mineral, Soc. Am., Spec.,* Pap. 3, 213- 235.

EUGSTER, H. Year. Lake Magadi, Kenya, and Its Precursors. *In:* NISSENBAUM, A., ed. Hypersaline Brines and Evaporitic Environments, 1980. Elsevier Science & Technology, 195-232.

FADAIE, K. & RANALLI, G. 1990. Rheology of the lithosphere in the East African Rift System. *Geophysical Journal International,* 102, 445-453.

FAIRHEAD, J. D. 1976. The structure of the lithosphere beneath the Eastern rift, East Africa, deduced from gravity studies. *Tectonophysics,* 30, 269-298.

FAIRHEAD, J. D. & GIRDLER, R. W. 1972. The seismicity of the east african rift system. *Tectonophysics,* 15, 115-122.

FAIRHEAD, J. D. & REEVES, C. V. 1977. Teleseismic delay times, Bouguer anomalies and inferred thickness of the African lithosphere. *Earth and Planetary Science Letters,* 36, 63-76.

FAIRHEAD, J. D. & STUART, G. W. 1982. The seismicity of East African Rift System and comparison with other continental rifts. *Tectonophysics,* 133, 277-285.

FALORNI, G., TELES, V., VIVONI, E. R., BRAS, R. L. & AMARATUNGA, K. S. 2005. Analysis and characterization of the vertical accuracy of digital elevation models from the Shuttle Radar Topography Mission. *J. Geophys. Res.,* 110, F02005.

FEDI, M. 2007. DEXP: A fast method to determine the depth and the structural index of potential fields sources. *Geophysics,* 72, I1-I11.

FEDI, M., QUARTA, T. & DE SANTIS, A. 1997. Inherent power-law behavior of magnetic fieldpower spectra from a Spector and Grant ensemble. *Geophysics,* 62, 1143–1150.

FENOGLIO, M. A., JOHNSTON, M. J. S. & BYERLEE, J. D. 1995. Magnetic and electric fields associated with changes in high pore pressure in fault zones: Application to the Loma Prieta ULF emissions. *J. Geophys. Res.,* 100, 12951-12958.

GIRDLER, W. 1978. Comparison of the East African rift system and the Permian Oslo rift. *In:* RAMBERGI.B. & NEUMANN, E.-R. (eds.) *Tectonics and Geophysics of Continental Rifts.* Reidel, Dordrecht.

GLOAGUEN, R., MARPU, P. R. & NIEMEYER, I. 2007. Automatic extraction of faults and fractal analysis from remote sensing data. *Nonlinear Processes in Geophysics* 14, 131–138.

GOLDSTEIN, R. M. & WERNER, C. L. 1998. Radar interferogram filtering for geophysical applications. *Geophys. Res. Lett.,* 25, 4035-4038.

GOLDSWORTHY, M. & JACKSON, J. 2001. Migration of activity within normal fault systems: examples from the Quaternary of mainland Greece. *Journal of Structural Geology,* 23, 489-506.

GREEN, W. V., ACHAUER, U. & MEYER, R. P. 1991. A three-dimensional seismic image of the crust and upper mantle beneath the Kenya rift. *Nature,* 354, 199-203.

GRIMAUD, P., RICHERT, J., ROLET, J., TIERCELIN, J., XAVIER, J., MORLEY, C., COUSSEMENT, C., KARANJA, S., RENAUT, R. & GUERIN, G. 1994. Fault geometry and extension mechanisms in the central Kenya Rift, East Africa. A 3D remote sensing approach. *Bulletin de la Centre de Recherches Exploration–Production Elf-Aquitaine,* 18, 59–92.

GROOM, R. & BAHR, K. 1992. Corrections for near surface effects: decomposition of the magnetotelluric impedance tensor and scaling corrections for regional resistivities: a tutorial. *Surveys in Geophysics,* 13, 341-379.

GROOM, R. & BAILEY, R. 1989. Decomposition of magnetotelluric impedance tensors in the presence of local three-dimensional galvanic distortion. *Journal of Geophysical Research,* 94, 1913-1925.

HALLS, H., BURNS, K., BULLOCK, S. & BATTERHAM, P. 1987. Mafic dyke swarms of Tanzania interpreted from aeromagnetic data. *In:* HALLS, H. C. & FAHRIG, W. F. (eds.) Mafic Dyke Swarms*.* Geological Assn of Canada.

HARVEY, R. & TRACY, R. J. 1996. Petrology, 2nd edition, Freeman.

HAUTOT, S., TARITS, P., WHALER, K., LE GALL, B., TIERCELIN, J. J. & LE TURDU, C. 2000. Deep structure of the Baringo rift basin (Central Kenya) from three-dimensional magneto-telluric imaging: implications for the rift evolution. *J. Geophys. Res.,* 105, 23493- 23518.

HAVSKOV, J. 1997. *The SEISAN Earthquake Analysis Software for IBM PC and SUN, Ver. 6.0.*, Institute of Solid Earth Physics, University of Bergen, Norway.

HENRY, W. J., MECHIE, J., MAGUIRE, P. K. H., KHAN, M. A., PRODEHL, C., KELLER, G. R. & PATEL, J. 1990. A Seismic Investigation of the Kenya Rift Valley. *Geophysical Journal International,* 100, 107-130.

HIGGINS, R. & HARRIS, L. 1997. The effect of cover composition on extensional faulting above re-activated basement faults: results from analogue modelling. *Journal of Structural Geology,* 19, 89-98.

HOLLNACK, D. & STANGL, R. 1998. The seismicity related to the southern part of the Kenya Rift. *Journal of African Earth Sciences,* 26, 477-495.

HSU, S., COPPENS, D. & SHYU, C. 1998. Depth to magnetic source using the generalized analytic signal. *Geophysics,* 63, 1947–1957.

HSU, S., SIBUET, J. C. & SHYU, C. 1996. High-resolution detection of geologic boundaries from potential field anomalies: an enhanced analytic signal technique. *Geophysics,* 61, 373–386.

IBRAHIM, A., HALIL, I. K. & ALI, K. 2005. Curie-point depth map of Turkey. *Geophysical Journal International,* 162, 633-640.

IBS-VON SEHT, M., BLUMENSTEIN, S., WAGNER, R., HOLLNACK, D. & WOHLENBERG, J. 2001. Seismicity, seismotectonics and crustal structure of the southern Kenya Rift—new data from the Lake Magadi area. *Geophysical Journal International,* 146, 439-453.

IBS-VON SEHT, M., PLENEFISCH, T. & KLINGE, K. 2008. Earthquake swarms in continental rifts -- A comparison of selected cases in America, Africa and Europe. *Tectonophysics,* 452, 66-77.

ICHANG'I, D. W. & MACLEAN, W. 1991. Archaean volcanic facies in the Migori segment, Nyanza greenstone belt, Kenya: stratigraphy, geochemrstry and mineralisation. *Journal African Earth Sciences,* 13, 277-290.

JACKSON, J. 1999. Fault death: a perspective from actively deforming regions. *Journal of Structural Geology,* 21, 1003-1010.

JONES, F. W. & PRICE, A. T. 1970. The perturbations of alternating geomagnetic fields by conductivity anomalies. *Geophys. J. R. Astron. Soc.,* 20, 317-334.

JOURDE, H., FLODIN, E., AYDIN, A., DURLOFSKY, L. & WEN, X. 2002. Computing permeability of fault zones in eolian sandstone from outcrop measurements. *AAPG bulletin,* 86, 1187.

JULIA, J., AMMON, C. J. & NYBLADE, A. A. 2005. Evidence for mafic lower crust in Tanzania, East Africa, from joint inversion of receiver functions and Rayleigh wave dispersion velocities. *Geophysical Journal International,* 162, 555–569.

KABEDE, F. 1989. *Source parameters and tectonic implications of selected earthquakes in Afar depression of Ethiopia neighbouring regions.* PhD Thesis, University of Uppsala.

KAMPUNZU, A. & MOHR, P. 1991. Magmatic Evolution and Petrogenesis in the East African Rift System. *Magmatism in extensional structural settings: the Phanerozoic African Plate*, 85.

KANAMORI, H. 1977. The energy release in great earthquakes. *J. Geophys. Res.,* 82, 2981–2876.

KARSON, J. & CURTIS, P. 1989. Tectonic and magmatic processes in the eastern branch of the East African rift and implications for

magmatically active continental rifts. *Journal of African Earth Sciences (and the Middle East),* 8, 431-453.

KEATING, P. & PILKINGTON, M. 2004. Euler deconvolution of the analytic signal and its application to magnetic interpretation. *Geophysical Prospecting,* 52, 165-182.

KEIR, D., EBINGER, C. J., STUART, G. W., DALY, E. & AYELE, A. 2006. Strain accommodation by magmatism and faulting as rifting proceeds to breakup: Seismicity of the northern Ethiopian rift. *J. Geophys. Res.,* 111, B05314.

KELLER, G. R., MECHIE, J., BRAILE, L. W., MOONEY, W. D. & PRODEHL, C. 1994a. Seismic structure of the uppermost mantle beneath the Kenya rift. *Tectonophysics,* 236, 201-216.

KELLER, G. R., PRODEHL, C., MECHIE, J., FUCHS, K., KHAN, M. A., MAGUIRE, P. K. H., MOONEY, W. D., ACHAUER, U., DAVIS, P. M., MEYER, R. P., BRAILE, L. W., NYAMBOK, I. O. & THOMPSON, G. A. 1994b. The East African rift system in the light of KRISP 90. *Tectonophysics,* 236, 465-483.

KELLER, R. G., KHAN, A. M., MORGANC, P., WENDLANDT, R., BALDRIDGE, S. W., OLSEN, K. H., PRODEHL, C. & BRAILE, L. 1991. A comparative study of the Rio Grande and Kenya rifts. *Tectonophysics,* 197, 355-371.

KIANJI, G. K. 2003. *Investigation on the seismicity of Kenya using the university of Nairobi seismic network.* M.Sc. Thesis, University of Nairobi.

KING, B. C. 1978. Structural evolution of the Gregory rift valley. *In:* BISHOP, W. W. (ed.) *Geological Background to Fossil Man. Geol. Sot. London.*

KRISP WORKING GROUP PARTY 1991. Large-scale variation in lithospheric structure along and across the Kenya rift. *Nature,* 354, 223-227.

KURIA, Z. N., WOLDAI, T., MEER, F. D. V. D. & BARONGO, J. O. 2010a. Active fault segments as potential earthquake sources: Inferences from integrated geophysical mapping of the Magadi fault system, southern Kenya Rift. *Journal of African Earth Sciences,* 57, 345-359.

KURIA, Z. N., WOLDAI, T. & OPIYO-AKECH, N. 2010b. Imaging saltwater intrusion into coastal aquifers with electrical resistivity tomography at Lamu Island, south coast Kenya. *African Journal of Science and Technology, Science and Engineering Series,* 11, 57-72.

LAST, R. J., NYBLADE, A. A., LANGSTON, C. A. & OWENS, T. J. 1997. Crustal structure of the East African Plateau from receiver functions and Rayleigh phase velocities. *Journal of Geophysical Research,* 102, 469–483.

LAY, T. & WALLACE, T. C. 1995. *Modern global seismology*, Academic Press San Diego, California.

LE GALL, B., NONNOTTE, P., ROLET, J., BENOIT, M., GUILLOU, H., MOUSSEAU-NONNOTTE, M., ALBARIC, J. & DEVERCHÈRE, J. 2008. Rift propagation at craton margin.: Distribution of faulting and volcanism in the North Tanzanian Divergence (East Africa) during Neogene times. *Tectonophysics,* 448, 1-19.

LE GALL, B., TIERCELIN, J. J., RICHERT, J. P., GENTE, P., STURCHIO, N. C., STEAD, D. & LE TURDU, C. 2000. A morphotectonic study of an extensional fault zone in a magma-rich rift: the Baringo Trachyte Fault System, central Kenya Rift. *Tectonophysics,* 320, 87-106.

LE TURDU, C., TIECELIN, J. J., RICHERT, J. P., ROLET, J., XAVIER, J. P., RENAUT, R. W., LEZZAR, K. E. & COUSSEMENT, C. 1999. Influence of pre-existing oblique discontinuities on the geometry and evolution of extensional fault patterns: evidence from the Kenya rift using SPOT imagery. *In:* MORLEY, C. K. (ed.) *Geoscience of Rift Systems – Evolution of East Africa.* AAPG Studies in Geology.

LI, C.-F., SHI, X., ZHOU, Z., LI, J., GENG, J. & CHEN, B. 2010. Depths to the magnetic layer bottom in the South China Sea area and their tectonic implications. *Geophysical Journal International,* 182**,** 1229-1247.

LOKE, M. H. & BARKER, R. D. 1995. Least-square deconvolution of the apparent resistivity pseudo-sections. *Geophysics,* 60**,** 449–523.

LUIS, J. F. 2007. Mirone: A multi-purpose tool for exploring grid data. *Computers & Geosciences,* 33**,** 31-41.

MACDONALD, R. 1994. Petrological evidence regarding the evolution of the Kenya Rift Valley. *Tectonophysics,* 236**,** 373-390.

MACHEYEKI, A. S., DELVAUX, D., BATIST, M. D. & MRUMA, A. 2008. Fault kinematics and tectonic stress in the seismically active Manyara-Dodoma Rift segment in Central Tanzania-Implications for the East African Rift. *Journal of African Earth Sciences,* 51**,** 163-188.

MACLEOD, I. N., JONES, K. & DAI, T. F. 2000. 3-D Analytic Signal in the Interpretation of Total Magnetic Field Data at Low Magnetic Latitudes. *Research papers Geosoft Inc.*

MAGUIRE, P. K. H. 1988. The crustal structure of the East Africa through Earthquake seismology*.* P.hD Thesis, University of Durham.

MAGUIRE, P. K. H. & LONG, R. E. 1976. The Structure on the Western Flank of the Gregory Rift (Kenya). Part I. The Crust. *Geophysical Journal of the Royal Astronomical Society,* 44**,** 661-675.

MARIITA, N. O. & KELLER, G. R. 2007. An integrated geophysical study of the northern Kenya rift. *Journal of African Earth Sciences,* 48**,** 80-94.

MARQUARDT, D. W. 1963. An algorithm for least-squares estimation of nonlinear parameters. *J. Soc. Ind. Appl. Math.,* 11**,** 431-441.

MARTIN, F. R. & MOROGAN, V. 1988. Partial melting of fenitized crustal xenoliths in the Oldoinyo Lengai carbonatitic volcano, Tanzania: reply. *American Mineralogist* 73**,** 1468–1471.

MASSONNET, D. & FEIGL, K. L. 1998. Radar interferometry and its applications to changes in the Earth's surface. *Reviews of Geophysics,* 36**,** 441–500.

MATHESON, F. J. 1958. Geology of Kajiado Area. *Geological Survey of Kenya.*

MATHU, E. M. & DAVIES, T. C. 1996. Geology and the environment in Kenya. *Journal of African Earth Sciences,* 23, 511-539.

MATHU, E. M. & NYAMBOK, I. Year. A re-evaluatron of the geology and tectonics of the granitoid plutons around Kakamega town. Western Kenya. *In:* OPIYO-AKECH, N., ed. Proceedings of the 5th Conference on the Geology of Kenya, 1993 UNEP/UNESCO, Nairobi. 63-68.

MAUS, S. & DIMRI, V. 1995. Potential field power spectrum inversion for scaling geology. *J. Geophys. Res.,* 100, 12605-12616.

MCCALL, G. J. H. 1957. The Menengai caldera, Kenya colony. *20th international Geological Congress,* Section 11, 55-69.

MCKENZIE, D. 1978. Some remarks on the development of sedimentary basins. *Earth and Planetary Science Letters,* 40, 25-32.

MECHIE, J., KELLER, G., PRODEHL, C., KHAN, M. & GACIRI, S. 1997. A model for the structure, composition and evolution of the Kenya rift. *Tectonophysics,* 278, 95-119.

MECHIE, J., KELLER, G. R., PRODEHL, C., GACIRI, S., BRAILE, L. W., MOONEY, W. D., GAJEWSKI, D. & SANDMEIER, K. J. 1994. Crustal structure beneath the Kenya Rift from axial profile data. *Tectonophysics,* 236, 179-200.

MEJU, M. 1996. Joint inversion of TEM and distorted MT soundings: Some effective practical considerations. *Geophysics,* 61, 56-65.

MEJU, M. & SAKKAS, V. 2007. Heterogeneous crust and upper mantle across southern Kenya and the relationship to surface deformation as inferred from magnetotelluric imaging. *Journal of Geophysical Research,* 112, B04103.

MEKKAWI, M., SCHNEGG, P., ARAFA-HAMED, T. & ELATHY, E. 2005. Electrical structure of the tectonically active Kalabsha Fault, Aswan, Egypt. *Earth and Planetary Science Letters,* 240, 764-773.

MOHR, P. 1987. Structural style of continental rifting in Ethiopia: reverse decollements. *EOS,* 68, 721-736.

MOLNAR, P. & AGGARWAL, Y. P. 1971. A microearthquake survey in Kenya. *Bulletin of the Seismological Society of America,* 61, 195-201.

MORGAN, P. 1983. Constraints on rift thermal processes from heat flow and uplift. *Tectonophysics,* 94, 277-298.

MORGAN, P., SEAGER, W. & GOLOMBEK, M. 1986. Cenozoic thermal, mechanical and tectonic evolution of the Rio Grande rift. *Journal of Geophysical Research,* 91, 6263-6276.

MORGAN, P. & WHEILDON, J. 1983. Constraints on rift thermal processes from heat flow and uplift. *Tectonophysics,* 94, 277-298.

MORLEY, C. K., WESCOTT, W. A., STONE, D. M., HARPER, R. M., WIGGER, S. T. & KARANJA, F. M. 1992. Tectonic evolution of the northern Kenyan Rift. *Journal of the Geological Society,* 149, 333-348.

MOUGENOT, D., RECQ, M., VIRLOGEUX, P. & LEPVRIER, C. 1986. Seaward extension of the East African Rift. *Nature,* 321, 599-603.

MUSHAYANDEBVU, M. F., VAN DRIEL, P., REID, A. B. & FAIRHEAD, J. D. 2001. Magnetic source parameters of two-dimensional structures using extended Euler deconvolution. *Geophysics,* 66, 814-823.

NABIGHIAN, M. N. 1972. The analytic signal of two-dimensional magnetic bodies with polygonal cross-section: its properties and use for automated anomaly interpretation. *Geophysics,* 37, 507-517.

NAIDU, P. 1968. Spectrum of the potential field due to randomly distributedsources. *Geophysics,* 33, 337-345.

NAIDU, P. S. & MATHEW, M. P. 1998. Analysis of geophysical potential fields: a digital signal processing approach. *In:* PRABHAKAR, S. N. & MATHEW, M. P. (eds.) *Advances in Exploration Geophysics.* Elsevier.

NGECU, W. M. Year. Stratigraphv and sedimentology of the Archaean Greenstone Belt of Western Kenya. *In:* OPIVO-AKECH, N., ed. Proceedings of the 5th Conference on the Geology of Kenya, 1993 UNEP/UNESCO, Nairobi., 57-62.

NYBLADE, A. 1997. Heat flow across the East African plateau. *Geophysical Research Letters,* 24, 2083-2086.

NYBLADE, A., BIRT, C., LANGSTON, C., OWENS, T. & LAST, R. 1996. Seismic experiment reveals rifting of craton in Tanzania. *EOS Transactions,* 77, 517.

NYBLADE, A. & LANGSTON, C. 1995. East African earthquakes below 20 km depth and their implications for crustal structure. *Geophysical Journal International,* 121, 49-62.

NYBLADE, A. A. & POLLACK, H. N. 1992. A gravity model for the lithosphere in western Kenya and northeastern Tanzania. *Tectonophysics,* 212, 257-267.

NYBLADE, A. A., POLLACK, H. N., JONES, D. L., PODMORE, F. & MUSHAYANDEBVU, M. 1990. Terrestrial heat flow in East and Southern Africa. *J. Geophys. Res.,* 95, 17,371–17,384.

ODEGARD, M. E. & DICKSON, W. G. 2004. Depth to basement using spectral inversion of magnetic and gravity data: application to Northwest Africa and Brazil. *SEG Int'l Exposition and 74th Annual meeting,10-15 October.* Denver, Colorado.

OKADA, Y. 1985. Surface deformation due to shear and tensile faults in a half space. *Bulletin of Seismological Society of America,* 75**,** 1135–1154.

OKUBO, Y., GRAF, R. J., HANSEN, R. O., OGAWA, K. & TSU, H. 1985. Curie point depths of the island of Kyushu and surrounding areas, Japan. *Geophysics,* 50**,** 481–494.

OKUBO, Y., MATSUSHIMA, J. & CORREIA, A. 2003. Magnetic spectral analysis in Portugal and its adjacent seas. *Physics and Chemistry of the Earth, Parts A/B/C,* 28**,** 511-519.

OKUBO, Y., TSU, H. & OGAWA, K. 1989. Estimation of Curie point temperature and geothermal structure of island arcs of Japan. *Tectonophysics,* 159**,** 279-290.

OLSEN, K. H., BALDRIDGE, S. W. & CALLENDER, J. F. 1987. Rio Grande rift: an overview. *Tectonophysics,* 143**,** 119-139.

OMENDA, P. A. 2001. An update on the status of geothermal resource exploration and development in Kenya, Proceedings, Commercial development of geothermal power projects in Kenya (unpubl.).

OPIYO-AKECH, N. 1988. Geology and geochemistry of the late Archaean greenstone belt association*. Maseno area, Kenva.* Ph. D. dissertation, University of Lercester, UK.

PARKINSON, W. D. 1983. Introduction to Geomagnetism, Scottish Academic Press, Edinburgh.

PASQUALE, V., VERDOYA, M. & CHIOZZI, P. 1999. Thermal state and deep earthquakes in the Southern Tyrrhenian. *Tectonophysics,* 306**,** 435-448.

PHOENIX GEOPHYSICS 2003. *V5 System* 2000MTU/MTU-A User Guide, Phoenix Geophysics, Ltd, Toronto.

PILKINGTON, M. & TODOESCHUCK, J. P. 1993. Fractal magnetization of continental crust. *Geophys. Res. Lett.,* 20**,** 627-630.

POHN, H. A. 1981. Joint spacing as a method of locating faults. *Geology,* 9**,** 261-285.

POINTING, A. & MAGUIRE, P. 1990. A seismic velocity model for the upper mantle in northern Kenya derived from teleseismic earthquake data. *Journal of African Earth Sciences,* 11**,** 391-399.

PRESS, H. W., TEUKOSKY, S. A., VETTERELING, W. T. & FLANNERY, B. P. 2002. *Numerical recipes in Fortran, The Art of Scientific Computing, Second edition*, Cambridge University Press.

PRODEHL, C., FUCHS, K. & MECHIE, J. 1997a. Seismic-refraction studies of the Afro-Arabian rift system--a brief review. *Tectonophysics,* 278, 1-13.

PRODEHL, C., JACOB, A. W. B., THYBO, H., DINDI, E. & STANGL, R. 1994a. Crustal structure on the northeastern flank of the Kenya rift. *Tectonophysics,* 236**,** 271-290.

PRODEHL, C., KELLER, G. R. & KHAN, M. A. 1994b. Crustal and Upper Mantle Structure of the Kenya Rift. *Tectonophysics,* 236, 483.

PRODEHL, C., RITTER, J. R. R., MECHIE, J., KELLER, G. R., KHAN, M. A., JACOB, B., FUCHS, K., NYAMBOK, I. O., OBEL, J. D. & RIAROH, D. 1997b. The KRISP 94 lithospheric investigation of southern Kenya -- the experiments and their main results. *Tectonophysics,* 278, 121-147.

QUARTA, T., FEDI, M. & DE SANTIS, A. 2000. Source ambiguity from an estimation of the scaling exponent of potential field power spectra. *Geophysical Journal International,* 140, 311-323.

RAJARAM, M., ANAND, S. P., HEMANT, K. & PURUCKER, M. E. 2009. Curie isotherm map of Indian subcontinent from satellite and aeromagnetic data. *Earth and Planetary Science Letters,* 281, 147-158.

RAVAT, D., PIGNATELLI, A., NICOLOSI, I. & CHIAPPINI, M. 2007. A study of spectral methods of estimating the depth to the bottom of magnetic sources from near-surface magnetic anomaly data. *Geophysical Journal International,* 169, 421-434.

REID, A. B., ALLSOP, J. M., GRANSER, H., MILLETT, A. J. & SOMERTON, I. W. 1990. Magnetic interpretation in three dimensions using Euler deconvolution. *Geophysics,* 55, 80-91.

RIAROH, D. & OKOTH, W. 1994. The geothermal fields of the Kenya rift. *Tectnophysics,* 236, 117-130.

RIDDIHOUGH, R. P. 1971. Diurnal corrections to magnetic surveys – An assessment of errors*. *Geophysical Prospecting,* 19, 551-567.

RODI, W. & MACKIE, R. L. 2001. Nonlinear conjugate gradients algorithm for 2D magnetotelluric inversions. *Geophysics,* 66, 174-187.

ROEST, W. R., VERHOEF, S. J. & PILKINGTON, M. 1992. Magnetic interpretation using the 3-D analytic signal. *Geophysics,* 57, 116 -125.

ROEX, A., SPÄTH, A. & ZARTMAN, R. 2001. Lithospheric thickness beneath the southern Kenya Rift: implications from basalt geochemistry. *Contributions to Mineralogy and Petrology,* 142, 89-106.

ROGERS, J. 1993. A History of the Earth, Cambridge Univ Pr.

ROONEY, D. & HUTTON, V. 1977. A magnetotelluric and magnetovariational study of the Gregory Rift Valley, Kenya. *Geophys. J. R. Astron. Soc.,* 51, 91-119.

ROSS, H. E., BLAKELY, R. J. & ZOBACK, M. D. 2006. Testing the use of aeromagnetic data for the determination of Curie depth in California. *Geophysics,* 71, L51-L59.

ROWLAND, J. & SIBSON, R. 2004. Structural controls on hydrothermal flow in a segmented rift system, Taupo Volcanic Zone, New Zealand. *Geofluids,* 4, 259-283.

RUIZ, F. & INTROCASO, A. 2004. Curie point depths beneath Precordillera Cuyana and Sierras Pampeanas obtained from spectral analysis of magnetic anomalies. *Gondwana Research,* 7, 1133-1142.

RYKOUNOV, L., SEDOV, V., SAVRINA, L. & BOURMIN, V. J. 1972. Study of microearthquakes in the rift zones of East Africa. *Tectonophysics,* 15, 123-130.

SAGGERSON, E. P. 1963. Geology of the Simba-Kibwezi area. *Geological Survey of Kenya Report.*

SAHRAOUI, H. O., HASSAINE, B. & SERIEF, C. 2006. Radar Interferometry with Sarscape Software. Shaping the Change Photogrammetry and Remote Sensing PS 5.8, XXIII FIG Congress Munich, Germany.

SAKKAS, V., MEJU, M., KHAN, M., HAAK, V. & SIMPSON, F. 2002. Magnetotelluric images of the crustal structure of Chyulu Hills volcanic field, Kenya. *Tectonophysics,* 346, 169-185.

SCHOLZ, C. H. 1990. The mechanics of earthquakes and faulting, Cambridge University Press, USA

SCHOLZ, C. H. & CONTRERAS, J. C. 1998. Mechanics of continental rift architecture. *Geology,* 26, 967-970.

SCHOLZ, C. H., DAWERS, N. H., YU, Y.-Z., ANDERS, M. H. & COWIE, P. A. 1991. Fault growth and fault scaling laws: Preliminary results. *Journal of Geophysical Research,* 98, 21 951–21 961.

SEARLE, R. C. 1970. Evidence from Gravity Anomalies for Thinning of the Lithosphere beneath the Rift Valley in Kenya. *Geophysical Journal of the Royal Astronomical Society,* 21, 13-31.

SEGALL, P. & POLLARD, D. 1980. Mechanics of discontinuous faults. *Journal of Geophysical Research,* 85, 4337-4350.

SENGÖR, A. & BURKE, K. 1978. Relative timing of rifting and volcanism on Earth and its tectonic implications. *Geophysical Research Letters,* 5, 419-421.

SHACKLETON, R. 1996. The final collision zone between East and West Gondwana: where is it? *Journal of African Earth Sciences,* 23, 271-287.

SHACKLETON, R. M. 1986. Precambrian collision tectonics in Africa. *Geological Society, London, Special Publications,* 19, 329-349.

SHACKLETON, R. M. 1993. Tectonics of the lower crust: A view from the Usambara Mountains, NE Tanzania. *J. Struct. Geol.,* 15, 663-671.

SHAH, E. 1986. The seismicity of Kenya. PhD. thesis, University of Nairobi.

SHUDOFSKY, G., CLOETINGH, S., STEIN, S. & WORTEL, R. 1987. Unusually deep earthquakes in East Africa: constraints on the thermo-mechanical structure of a continental rift system. *Geophys. Res. Lett,* 14, 741-744.

SHUDOFSKY, G. N. 1985. Source mechanisms and focal depths of East African earthquakes using Rayleigh-wave inversion and body-wave modelling. *Geophysical Journal of the Royal Astronomical Society,* 83, 563-614.

SHUEY, R., SCHELLINGER, D., TRIPP, A. & AL, L. 1977. Curie depth determination from aeromagnetic spectra. *Geophysical Journal of the Royal Astronomical Society,* 50, 75-101.

SIBSON, R. 1982. Fault zone models, heat flow, and the depth distribution of earthquakes in the continental crust of the United States. *Bulletin of the Seismological Society America* 72, 151–163.

SIBSON, R. H. 1986. Brecciation processes in fault zones: Inferences from earthquake rupturing. *Pure and Applied Geophysics,* 124, 159-175.

SIMIYU, S. 2010. Status of geothermal exploration in Kenya and future plans for Its development. Proceedings World Geothermal Congress 2010 Bali, Indonesia, 25-29 April 2010.

SIMIYU, S. M. & KELLER, G. R. 1997. An integrated analysis of lithospheric structure across the East African plateau based on gravity anomalies and recent seismic studies. *Tectonophysics,* 278, 291-313.

SIMIYU, S. M. & KELLER, G. R. 2001. An integrated geophysical analysis of the upper crust of the southern Kenya rift. *Geophysical Journal International,* 147, 543-561.

SIMIYU, S. M. & KELLER, R. G. 1998. Upper crustal structure in the vicinity of Lake Magadi in the Kenya Rift Valley region. *Journal of African Earth Sciences,* 27, 359-371.

SIMPSON, F. 2000. A three-dimensional electromagnetic model of the southern Kenya Rift: Departure from two dimensionality as a possible consequence of a rotating stress field. *Journal of Geophysical Research,* 105, 19321.

SMITH, M. 1994. Stratigraphic and structural constraints on mechanisms of active rifting in the Gregory Rift, Kenya. *Tectonophysics,* 236, 3-22.

SMITH, M. & MOSLEY, P. 1993. Crustal heterogeneity and basement influence on the development of the Kenya Rift, East Africa. *Tectonics,* 12, 591-606.

SMITH, R., NAGY, W., JULANDER, K., VIVEIROS, J., BARKER, C. & GANTS, D. 1989. Geophysical and tectonic framework of the eastern Basin and Range-Colorado Plateau-Rocky Mountain transition. *Geophysical Framework of the Continental United States, Mem. Geol. Soc. Am,* 172**,** 205-233.

SMITH, W. C. 1931. A Classification of some Rhyolites, Trachytes, and Phonolites from part of Kenya Colony, with a Note on some Associated Basaltic Rocks. *Quarterly Journal of the Geological Society,* 87, 212-258.

SNOKE, J. A., MUNSEY, J. W., TEAGUE, A. G. & BOLLINGER, G. A. 1984. A program for focal mechanism determination by combined use of polarity and SV-P amplitude ratio data, Earth quake notes.

SPECTOR, A. & GRANT, F. S. 1970. Statistical models for interpreting aeromagnetic data. *Geophysics,* 35, 293-302.

STAMPOLIDIS, A. & TSOKAS, G. N. 2002. Curie Point Depths of Macedonia and Thrace, N. Greece. *Pure and Applied Geophysics,* 159, 2659-2671.

STERN, R. 1994. Arc-Assembly and Continental Collision in the Neoproterozoic African Orogen: Implications for the Consolidation of Gondwanaland. *Annual Review of Earth and Planetary Sciences,* 22, 319-351.

STRECKER, M. R., BLISNIUK, P. M. & EISBACHER, G. H. 1990. Rotation of extension direction in the central Kenya Rift. *Geology,* 18, 299-302.

STRECKER, M. R. & BOSWORTH, W. 1991. Quaternary Stress-Field change in the Gregory Rift, Kenya. *EOS,* 72, 21-22.

SUESS, E. 1891. Die BrÛche des östlichen Africa. *In:* CHOROWICZ, J. (ed.) The East Africa rift system*.* J. Africa Earth Sciences.

SUZUKI, K., TODA, S., KUSUNOKI, K., FUJIMITSU, Y., MOGI, T. & JOMORI, A. 2000. Case studies of electrical and electromagnetic methods applied to mapping active faults beneath the thick quaternary. *Engineering Geology,* 56, 29–45.

SWAIN, C. J. 1992. The Kenya rift axial gravity high: a re-interpretation. *Tectonophysics,* 204, 59-70.

SWAIN, C. J. & KHAN, M. A. 1977. Kenya: a catalogue of gravity measurements. Geol. Dept., Univ. Leicester.

SWAIN, C. J., KHAN, M. A., WILTON, T. J., MAGUIRE, P. K. H. & GRIFFITHS, D. H. 1981. Seismic and gravity surveys in the Lake Baringo-Tugen Hills area, Kenya Rift Valley. *Journal of the Geological Society,* 138, 93-101.

SWIFT, C. M. A. 1967. A magnetotelluric investigation of an electrical conductivity anomaly in the South-western United States. Ph.D. Thesis, MIT.

TANAKA, A. & ISHIKAWA, Y. 2005. Crustal thermal regime inferred from magnetic anomaly data and its relationship to seismogenic layer thickness: The Japanese islands case study. *Physics of The Earth and Planetary Interiors,* 152, 257-266.

TELFORD, W. M., GELDART, L. P., SHERIFF, R. E. & KEYS, D. A. 1990. Applied Geophysics, Cambridge University Press.

TESHA, A. L., NYBLADE, A. A., KELLER, G. R. & DOSER, D. I. 1997. Rift localization in suture-thickened crust: Evidence from bouguer gravity anomalies in northeastern Tanzania, East Africa. *Tectonophysics,* 278, 315-328.

THURSTON, J. B. & SMITH, R. S. 1997. Automatic conversion of magnetic data to depth, dip, and susceptibility contrast using the SPI (TM) method. *Geophysics,* 62, 807-813.

TOBIN, D. G., WARD, P. L. & DRAKE, C. L. 1969. Microearthquakes in the Rift Valley of Kenya. *Geological Society of America Bulletin,* 80, 2043-2046.

TOFT, P. B. & ARKANI-HAMED, J. 1992. Magnetization of the Pacific Ocean Lithosphere Deduced From Magsat Data. *J. Geophys. Res.,* 97, 4387-4406.

TOLOMEI, C., ATZORI, S., SALVI, S. & DOUMAZ, F. 2003. DIMOT: a GIS tool for modelling surface displacement due to fault dislocation. Technical Report INGV n°17, 27.

TONGUE, J. A., MAGUIRE, P. K. H. & YOUNG, P. A. V. 1992. Seismicity distribution from temporary earthquake recording networks in Kenya. *Tectonophysics,* 204, 71-79.

TRIFONOVA, P., ZHELEV, Z., PETROVA, T. & BOJADGIEVA, K. 2009. Curie point depths of Bulgarian territory inferred from geomagnetic observations and its correlation with regional thermal structure and seismicity. *Tectonophysics,* 473, 362-374.

TRUDGILL, B. D. & CARTWRIGHT, J. A. 1994. Relay ramp forms and normal fault linkages - Canyonland National Park. *Utah. Bull. Geol. Soc. Am.,* 106, 1143-1157.

TULLIS, J., YUND, R. & FARVER, J. 1996. Deformation-enhanced fluid distribution in feldspar aggregates and implications for ductile shear zones. *Geology,* 24, 63.

TURCOTTE, D. L. & SCHUBERT, G. 2002. Geodynamics, Second Edition, Cambridge, UK.

UNSWORTH, M., BEDROSIAN, P., EISEL, M., EGBERT, G. & SIRIPUNVARAPORN, W. 2000. Along strike variations in the electrical structure of the San Andreas Fault at Parkfield, California. *Geophysical Research Letters,* 27, 3021-3024.

VOZOFF, K. 1972. The magnetotelluric method in the exploration of sedimentary basins. *Geophysics,* 37, 98.

WANNAMAKER, P., CALDWELL, T., DOERNER, W. & JIRACEK, G. 2004. Fault zone fluids and seismicity in compressional and extensional environments inferred from electrical conductivity- The New Zealand Southern Alps and U. S. Great Basin. *Earth Planets and Space,* 56, 1171-1176.

WASILEWSKI, P. J. & MAYHEW, M. A. 1992. The moho as a magnetic boundary revisited. *Geophys. Res. Lett.,* 19, 2259-2262.

WECKMANN, U., RITTER, O. & HAAK, V. 2003. A magnetotelluric study of the Damara Belt in Namibia: 2. MT phases over 908 reveal the internal structure of the Waterberg Fault/Omaruru Lineament. *Phys. Earth Planet. Inter,* 138, 91-112.

WENDLANDT, R. F. & MORGAN, P. 1982. Lithospheric thinning associated with rifting in East Africa. *Nature,* 298, 734-736.

WHEILDON, J., MORGAN, P., WILLIAMSON, K., EVANS, T. & SWANBERG, C. 1994. Heat flow in the Kenya rift zone. *Tectonophysics,* 236, 131-149.

WILLIAMS, L. 1978. Character of Quaternary volcanism in the Gregory rift valley. *Geological Society London Special Publications,* 6, 55.

WILLIAMS, L. A. J. 1969. Volcanic associations in the Gregory rift valley, East Africa. *Nature,* 224, 61-64.

WILLIAMS, L. A. J. 1970. The volcanics of the Gregory rift valley, East Africa. *Bulletin of Volcanology,* 34, 439-465.

WILLIAMSON, K. H. 1975. Terrestrial Heat Flow Studies in Kenya. Ph.D, Univ. London.

WOHLENBERG, J. 1975. The structure of the lithosphere beneath the East African Rift zones from interpretation of Bouguer anomalies. *Afar Depression of Ethiopia*, 125.

YIELDING, G., FREEMAN, B. & NEEDHAM, D. T. 1997. Quantitative fault seal prediction. *American Association of Petroleum Geologists Bulletin* 81, 897–917.

YOUNG, P. A. V., MAGUIRE, P. K. H., LAFFOLET, N. & D'A EVANS, J. R. 1989. Implications of the distribution of seismicity near Lake Bogoria in Kenya rift. *Geophysical Journal of the Royal astronomical Society,* 105, 665-674.

YOUNG, P. A. V., MAGUIRE, P. K. H., LAFFOLEY, N. D. A. & EVANS, J. R. 1991. Implications of the distribution of seismicity near Lake Bogoria in the Kenya Rift. *Geophysical Journal International,* 105, 665-674.

ZEBKER, H. A., WERNER, C. L., ROSEN, P. A. & HENSLEY, S. 1994. Accuracy of Topographic Maps Derived from ERS-1 Interferometric Radar. *IEEE Transactions on Geoscience and Remote Sensing,* 32, 823–835.

Summary

The earth surface is characterized by actively deforming domains that evolve with time into beautiful landforms, particularly within Kenya rift system. These include a sinuous system of grabens, flexed depressions, series of volcanoes to uplifted rift shoulders. In addition, the rift also hosts vast geothermal resources - as manifested on the earth surface. The potential of these geothermal resources remains aloof. Regrettably, these active zones/domains also host numerous hazards, the typical one being the earthquakes. Whereas these features (landforms, geothermal manifestation, earthquakes etc) may seem obvious, the geological processes behind remains largely unknown.

This study was formulated with a global scientific objective of examining and understanding active faults and how they relate with earthquakes (seismotectonics). The specific objectives include: establishing spatial and density distribution of active extensional structures including their geometry and trends and their implication to earthquakes distribution; determining migration and propagation of the extension throughout the Magadi rift basin and relate it to the entire Kenya Rift; deducing magnitude of the surface deformation in the Magadi area (ground deformation detection) and relate it to potential earthquakes; and mapping/quantifying thermal gradients as possible driving mechanism of the rifting process.

Using a suite of remote sensing and geological field mapping techniques, the spatial and density distribution of the active faults was elucidated. This was largely important in deciphering the fault geometry and trends, in particular, their linkage to regional stress distribution. In addition, the fault density certainly provides prognosis of areas prone to earthquakes.

Once a model was established on the types of faults (based on their orientation) and their deformational styles (based sense of movement), an evidence of the prevalent deformation (extension direction) was necessary. This was in part essential in understanding the concept of rift migration and propagation (implication for earthquake distribution), commonly studied under the subject matter of fault growth through nucleation and linkage in structural geology. For the purpose of this study as well as addressing caveats in structural geology approach, remote sensing techniques, using interferometric synthetic aperture radar (InSAR) provided both spatial (area affected by deformation) as well as temporal constrain on faulting activity. This was achieved by monitoring continuously (35 – day satellite repeat pass) for a period of eight months covering an area of 100 km by 100 km (single scene) and determining the magnitude of deformation between two radar

acquisitions. The areas affected and style of deformation was clearly resolved, and also a link to the driving mechanism of deformation inferred through simple modeling techniques.

From the foregoing, it apparent that a charactserisation of the surface fault parameters was achieved. However, as mentioned earlier underpinning geological process or phenomenon associated with faulting activity is deemed even more necessary. In light of this, a study was formulated to assess the intertwinement of the deep and surface earth processes in the realm of seismotectonics. In a practical sense, a detailed evaluation of the axial fault (seismically more active zone) using geophysical survey techniques was performed. The choice of geophysical survey methods adopted in this research was careful made to address different scales and resolutions i.e. resistivity tomography for the detailed shallow investigation, ground magnetics for moderate depths and aeromagnetic for deep investigation (i.e. refining basin structure). The geophysical investigations were coupled with detailed geological and structural mapping, which proved useful for constraining geophysical models. The results accrue from this study apart from reviewing the geology, allowed for interpretation of the fault 2D geometry (i.e. depth and angle of dip), intensity of faulting activity (from scattering of magnetic signatures) to constituents in the faults that affect its deformation (fluids).

It was noted that thermal structures had an influence on the faulting activity. Therefore, using temperature as parameter for thermal mapping, several approaches were adopted. One was to use the aeromagnetic data and determine the depth to the bottom of the magnetic crust appropriately referred to as magnetic ensemble. At these depths, the rocks lose their ferromagnetism due to temperature. It therefore follows that mapping the bottom morphology of the magnetic ensemble would indirectly reflect the geo-temperature distribution allowing for characterization of geothermal gradient. After the choice of the appropriate model (supporting distribution of magnetization), the depths of magnetic ensemble synonymous with Curie point depths and their spatial distribution were determined. The results indicate shallow Curie isotherm depth that locally commensurate the geothermal manifestation. On establishing the driving mechanism, these localized Curie isotherm interpreted as mantle plume were indeed small to support large-scale rifting process. However, at localized scale the mantle plume (inferred from Curie isotherm) induces conductive heat transfer which affects the rheology and hence accounts for increased seismicity. Indeed, a deep mapping of the fault architecture using a collocated Magnetotelluric (MT) and Transient Electromagnetic survey (TEM) provided evidence for dyke

intrusion and presence of copious fluids (high concentration of brines-emplaced as hot spring) within the faulted domains. In the end, all objectives were clearly accomplished.

Samenvatting

Het aardoppervlak wordt gekenmerkt door actieve deformatie zones, die met het verstrijken van de tijd leiden tot schitterende landvormen, zeker in de Keniaanse riftvallei. Kenmerkende vormen voor een extensie zone zijn een kronkelend stelsel van slenken, glooiende depressies, het voorkomen van vulkanen, en hoge kliffen aan de randen van de spreidingszone. De riftvallei is tevens rijk aan geothermische bronnen, welke zich manifesteren aan het aardoppervlak. Het potentieel van deze bronnen wordt vooralsnog niet gebruikt. Helaas is er in dit soort actieve spreidingszones ook de dreiging van verscheidene natuurrampen, met name aardbevingen. Hoewel al deze kenmerken (landschapsvormen, geothermische activiteit en aardbevingen) duidelijk zijn, worden achterliggende geologische processen veelal niet begrepen.

Dit onderzoek had als hoofddoel het verkrijgen van begrip van actieve breuksystemen, en het kunnen relateren van deze breuksystemen aan aardbevingen (seismotektoniek). De specifieke doelen van dit onderzoek bestonden uit: Het vaststellen van de ruimtelijke dichtheidsverdeling van structuren die kenmerkend zijn voor extensie, zoals de vorm en richting, en de invloed op de aardbeving verdeling; het vaststellen van migratie en propagatie van de extensie in de Magadi riftvallei, en dit relateren aan de gehele Keniaanse riftvallei; het meten van de hoeveelheid deformatie aan het aardoppervlak in de Magadi vallei, en dit relateren aan potentiele aardbevingen; en tenslotte het kwantificeren en karteren van geothermische gradiënten, als zijnde een mogelijk mechanisme achter de extensie.

Door gebruik te maken van aardobservatie technieken en geologische kartering in het veld, konden locaties en dus ruimtelijke dichtheid van actieve breuken bepaald worden. Dit was niet alleen van belang voor het ontcijferen de breuk geometrie en de oriëntatie, maar in het bijzonder ook voor het relateren van breukvoorkomens aan de regionale spanning verdeling. Met de opgedane kennis over ruimtelijke dichtheid van breuken bleek het mogelijk om een prognose te maken welke gebieden gevoelig zijn voor aardbevingen.

Wanneer een model eenmaal vastgesteld was aan de hand van het type breuk (gebaseerd op oriëntatie) en de stijl van deformatie (gebaseerd op bewegingsrichting), was het nodig om de overheersende deformatie (richting

van extensie) vast te stellen. Dit was van belang om het concept achter migratie en propagatie van een spreidingszone (en daarmee de implicatie voor aardbevingsvoorkomens) te begrijpen, hetgeen gewoonlijk beschreven wordt in structurele geologie als breuk groei door middel van verbinding van nuclei. In het belang van dit onderzoek, maar ook om tegemoet te kunnen komen aan bovengenoemde tekortkomingen in structurele geologie, werd gebruikt gemaakt van aardobservatie, interferometrie van radar met synthetische apertuur (InSAR), voor het bepalen van de ruimtelijke verspreiding van gebieden getroffen door deformatie als ook de tijdsduur van breuk activiteit. Dit werd bereikt door een gebied van 100 bij 100 kilometer te observeren gedurende een periode van 8 maanden (met een herhaling elke 35 dagen) en de hoeveelheid deformatie aan het aardoppervlak te meten. De getroffen gebieden en stijl van deformatie konden duidelijk herleid worden, en ook de samenhang met het mechanisme achter de deformatie kon worden afgeleid door middel van eenvoudig modeleren.

Uit het voorgaande wordt duidelijk dat een karakterisatie van breuken aan het aardoppervlak gemaakt kon worden. Zoals echter al eerder vermeld, is het begrip van het geologische mechanisme achter deze breukactiviteit van groot belang. Er werd daarom een onderzoek geformuleerd om de verstrengeling van diepe on ondiepe processen in de ondergrond in termen van seismotectoniek te bestuderen. In de praktische zin bestond dit uit een gedetailleerde evaluatie van de breuk as (een gebied met verhoogde seismische activiteit) door middel van geofysische metingen. Deze metingen werd zorgvuldig gekozen bij de verschillende schaalgroottes van observatie. Weerstand tomografie werd bijvoorbeeld gebruikt voor gedetailleerde studie van de ondiepe ondergrond, magnetische metingen in het veld voor gemiddelde diepte, en gevlogen magnetische metingen voor de diepe ondergrond.

De geofysische metingen werden gecombineerd met een gedetailleerde structureel geologische kartering, hetgeen nuttig bleek om de geofysische modellen van randvoorwaardes te voorzien. De resultaten die uit dit onderzoek naar voren komen geven, naast een overzicht van de geologie, mogelijkheid tot een interpretatie van een 2-dimensionale breuk oriëntatie (bijvoorbeeld diepte en de hoek van het breukvlak), van intensiteit van breukactiviteit (door diffusie van magnetische kenmerken), en van de

bestandsdelen in een breuk die bepalend zijn voor de deformatie (vloeistoffen).

Uit het onderzoek kon worden opgemaakt dat thermische structuren invloed hadden op de breukactiviteit. Temperatuur werd daarom gebruikt voor thermisch karteren, waarbij verscheidene methodes gebruikt werden. Een daarvan was het gebruik van gevlogen magnetische data, waarbij de diepte tot de bodem van de magnetische korst bepaald werd. Op deze dieptes verliezen gesteentes hun ijzer-magnetische eigenschappen als gevolg van verhoogde temperatuur. Het karteren van de morfologie van de bodem van de magnetische korst geeft een indirecte representatie van de temperatuur in de ondergrond, die weer herleid kan worden tot een geothermische gradiënt. Met de keuze van een toepasselijk model (dat de verdeling van magnetisaties ondersteund) kon de dikte van de magnetische korst, gelijk de diepte van de Curie temperatuur, bepaald worden. De resultaten laten een ondiepe Curie isotherm zien die plaatselijk samenvalt met geothermische expressies. Bij het bepalen van het achterliggende mechanisme bleek dat plaatselijke Curie isothermen, geïnterpreteerd als mantel pluimen, te klein waren om het mechanisme achter een grootschalig spreiden van de korst te zijn. Echter, op kleine schaal veroorzaken de mantel pluimen (afgeleid van de Curie isothermen) conductief warmte transport, hetgeen de reologie beïnvloed en dus verantwoordelijk kan zijn voor seismische activiteit. Bij het karteren van de breuk architectuur in de diepe ondergrond door het samenvoegen van magnetotellurische (MT) en tijd-domein electromagnetische (TEM) metingen, leverde dan ook inderdaad bewijs voor een dijk intrusie en de overvloedige aanwezigheid van vloeistoffen (met een hoge concentratie van zouten, bestaande als warme bron) binnen de breukzones.

Hiermee zijn uiteindelijk alle doelstellingen van dit onderzoek behaald.

Name: **Kuria**, Zacharia Njuguna

Date of Birth: 12th February, 1971

Address: University of Nairobi, P.O.
Box 30197 – 100, Nairobi, Kenya.

Email: Kuria@itc.nl; zkuria@uoni.ac.ke; kuriazack@yahoo.com

Tel: +254-254 020 4449004

Working Experience

1. 2002 – Todate: Lecturer at the University of Nairobi, Department of Geology. Also works for Comprehensive Nuclear Test Ban Treaty Organisation (CTBTO).
2. 1999-2002: Senior hydrogeologist, Groundwater Survey (K) Ltd. Nairobi.
3. 1998 – 1999: Hydrogeologist, Ministry of Environment. Head of Groundwater Section and Deputy District Water Officer, Kisumu District.

Educational Qualification

1. 2007 – : PhD on sandwich construction between University of Twente (Faculty - International institute for Geo-information Science and Earth Observation (ITC) and University of Nairobi (Department of Geology).
2. 1998 – 2001: MSc. In applied Geophysics – University of Nairobi (Scored grade "A" in all course units).
3. 1990 – 1995: BSc. In Geology – University of Nairobi (First Class Honours Degree).

Other Educational training

1. Trained on InSAR data analysis during ESA SAR Toolbox Fringe 2009 Workshop (Rome, Italy).
2. Trained on Electrical Resistivity Tomography under MAWARI Project (Nakuru, Kenya – 2009).
3. Trained on seismology, seismic data analysis, hazard assessment and risk mitigation at Potsdam, Germany (October 2005).
4. Trained on seismology, seismic data analysis, hazard assessment and risk mitigation at Helwan Institute, Cairo, Egypt (1995).
5. Trained on use of high resolution Quickbird Sattellite Imagery and GIS at Regional Centre for mapping Resources for Development (June 2004).
6. Trained on application of geophysics to continental shelf research at UNEP Nairobi (March 2006).

Author's Publication:

Thesis/Dissertation

1. Kuria, Z.N. 2001. Hydrogeology of Lake Nakuru drainage basin, using electrical resistivity survey. M.Sc. Thesis, University of Nairobi, Kenya.
2. Kuria, Z.N. 1994. Geological Mapping of Makweni (Kibwezi Area) and Kitui (Ikutha Area) Districts. B.Sc. Dissertation, University of Nairobi, Kenya

Published Journal articles

1. Kuria, Z.N., Woldai, T., Barongo, J.O., van der Meer F.D. Active fault segments as potential earthquake sources: inferences from integrated geophysical mapping of the Magadi fault system, southern Kenya Rift. Journal of African Earth Sciences 57, 345-359.
2. Kuria, Z.N., Woldai, T., Opiyo_Akech, N. 2010. Imaging saltwater intrusion into coastal aquifers with electrical resistivity tomography at Lamu Island, South Coast Kenya. African Journal of Science and Technology 11 (2) 57-72.

Accepted Journal articles

1. Kuria, Z.N., Woldai, T., van der Meer F.D., Barongo, J.O., Noomen, M., Komolafe, A., van der Meijde, M. Crustal thermal regime for central to southern Kenya Rift: implication for geothermal resources. Submitted: Geothermics; International Journal of geothermal research and its application.
2. Kodikra, G.L., Woldai, T., van Ruitenbeek, J.A., Kuria, Z.N., van der Meer, F., Shepherd, K.D., van Hummel, G.J. Spectral remote sensing of evaporate minerals and associated sediments in Lake Magadi area, Kenya. Submitted: International Journal of Applied Earth Observation and Geoinformation.

Submitted Journal articles

1. Kuria, Z.N., Woldai, T., van der Meer, F.D., Barongo, J.O. Fault growth through nucleation and interaction at Lakes Magadi-Natron area, south Kenya rift: inferences from repeat pass radar interferometry, Submitted: International Journal of Digital Earth.
2. Kuria, Z.N., Woldai, T., van der Meer F.D., Barongo, J.O., Noomen, M., Komolafe, A., van der Meijde, M. Characterisation of thermal and tectonic structures for central to southern Kenya Rift: Seismotectonic implication. Submitted: Journal of African Earth Sciences.

3. Kuria, Z.N., Barongo, J.O., Woldai, T., van der Meer F.D. Dyke intrusion and fluidized fault zone inferred from magnetotelluric studies at Magadi fault system, southern Kenya implication for seismicity distribution. Submitted: Geophysical Journal International.

Project reports

Kuria has compiled over 100 technical reports (since 1998) on various projects from geophysical works carried out in Kenya, South Sudan and Somalia. Ten (10) of these reports are list below as examples:

1. Kuria, Z.N. 2010. Geological, electrical resistivity and seismic refraction survey for Karura hydro power plant, Mbeere-Mwingi Districts for Earthview Geoconsult Ltd.
2. Kuria, Z.N. 2010. Geological survey at four bridge sites along Mulot – Muhuru Bay roads for Mangat I.B. Patel and Partners.
3. Kuria, Z.N. 2009. Groundwater resource assessment, detailed groundwater investigation and well-field design (10 boreholes) for Delmonte Ltd.
4. Kuria, Z.N. 2009. Assessment of groundwater (aquifers) along Shella Water Catchment area, Lamu Island for National Museums of Kenya.
5. Kuria, Z.N. 2008. Hydrogeological and Geophysical investigations, five (5) sites and Conditions assessment (5 boreholes) in Dinsor District, **Somali** (ADRA Somali).
6. Kuria, Z.N. 2008. Hydrogeological and Geophysical investigations, thirty (30) sites Kapoeta North and South, Eastern Equatorial Southern **Sudan** for AAR Japan and Drilling Services International.
7. Kuria, Z.N. 2007. Hydrogeological and Geophysical investigations, fifteen (15) sites in Awoda Payam, Aweil Centre County Bahr El Ghazal, **Sudan** for Medair, Kenya**.**
8. Kuria, Z.N. 2004. Geophysical investigation of the soil profile along 50 kilometer section between Sondu Miriu power station and Kisumu sub-station for Surtech Ltd. and KENGEN.
9. Kuria, Z.N. 2003. Evaluation of community water supply for Baringo North (Belgium Technical Cooperation) and Formulation of second phase of Baringo community water supply (Belgium Technical Cooperation.
10. Kuria, Z.N. 2001. Report on groundwater potential and Well siting, Nakuru North Wellfield, Nakuru District for NWC&PC/ Mangat Patel.

ITC Dissertation List

http://www.itc.nl/Pub/research_programme/Graduate-programme/Graduate-programme-PhD_Graduates.html